

**NONLINEAR OPTICAL PROPERTIES OF SELECTED LASER DYES
INVESTIGATED USING PHOTOACOUSTICS, FLUORESCENCE
AND STIMULATED SCATTERING**

REJI PHILIP

**THESIS SUBMITTED
IN PARTIAL FULFILMENT OF THE REQUIREMENTS
FOR THE DEGREE OF
DOCTOR OF PHILOSOPHY**

**DEPARTMENT OF PHYSICS
COCHIN UNIVERSITY OF SCIENCE AND TECHNOLOGY
COCHIN - 682 022
INDIA**


1993

CERTIFICATE

Certified that the work presented in this thesis entitled "NONLINEAR OPTICAL PROPERTIES OF SELECTED LASER DYES INVESTIGATED USING PHOTOACOUSTICS, FLUORESCENCE AND STIMULATED SCATTERING" is based on the original work carried out by Mr. Reji Philip under my guidance at the Department of Physics, Cochin University of Science & Technology, Cochin - 682 022, and that no part thereof has been included in any other thesis submitted previously for the award of any degree.

Cochin - 682 022
April 5, 1993





Dr. Jacob Philip
Professor of Physics

DECLARATION

Certified that the work presented in this thesis entitled "NONLINEAR OPTICAL PROPERTIES OF SELECTED LASER DYES INVESTIGATED USING PHOTOACOUSTICS, FLUORESCENCE AND STIMULATED SCATTERING" is based on the original work done by me under the guidance of Dr. Jacob Philip, Professor, Department of Physics, Cochin University of Science & Technology, Cochin - 682 022, and that no part thereof has been included in any other thesis submitted previously for the award of any degree.

Cochin - 682 022
April 5, 1993


Reji Philip

PREFACE

Nonlinear optics is a fast growing branch of Physics that finds different applications in various disciplines of science and Technology. The advent of lasers which could provide strong, tunable and monochromatic radiation gave thrust to the growth of nonlinear optics which was in its infancy in the sixties. Many new phenomena have been discovered, which are novel enough to modify man's understanding of nature.

This thesis is the result of our attempts to comprehend in better detail two of the above mentioned nonlinear phenomena, namely multiphoton absorptions and stimulated scattering occurring in organic media. Laser dyes have been chosen for detailed studies considering their fundamental importance as complex organic fluorophores and their commercial importance in dye lasers. The thesis is arranged in seven chapters to accommodate all major aspects of the underlying theory and details of the experiments conducted.

The first chapter discusses the theoretical framework of two techniques adopted for carrying out the present investigations - pulsed photoacoustics and antistokes fluorescence (PA and ASF respectively). For the sake of completeness we outline the RG theory in brief along with the theory of pulsed PA generation. The luminescence properties of organic dye solutions and their lasing characteristics are discussed. An introduction to nonlinear optical phenomena is given, and the theory of second harmonic generation and multiphoton absorptions is presented.

In the second chapter, details of the photoacoustic and fluorescence instrumentation adopted for performing the present experiments are given. A liquid PA cell and a PZT transducer chamber have been fabricated for the present studies. The efficiency of this acoustic detection system is checked by means of a novel experiment in which the spatial beam profile of a pulsed Nd:YAG laser has been

recorded using the PA technique. Details of a pulse preamplifier, designed and fabricated for amplifying PA signals generated by weakly absorbing media is given. Essential aspects of fluorescence instrumentation also are presented in this chapter.

Chapter Three gives an account of the studies carried out in the laser dye DCM. The investigation of multiphoton absorptions taking place in DCM at a typical pump wavelength of 532 nm has been carried out by means of Photoacoustics. In DCM the $S_0 \rightarrow S_1$ transition matches with the 532 nm pump wavelength. It is known that in dyes, all higher excited states S_n ($n > 1$) have a strong tendency to relax nonradiatively to the S_1 level, prior to the $S_1 \rightarrow S_0$ fluorescence. The probability for $S_n \rightarrow S_0$ radiative emission is very low even though it exists. Thus if by strong $S_0 \rightarrow S_1$ optical pumping a few molecules are excited to one of the S_n levels, there are two ways for detecting such molecules : either by observing the weak antistokes fluorescence ($S_n \rightarrow S_0$) or by observing the strong $S_n \rightarrow S_1$ nonradiative transitions. The potential advantages of the latter method are clearly demonstrated in this chapter. Solution samples of DCM taken in the solvents dimethylformamide and ethylene glycol + benzyl alcohol have been prepared in the concentration range of 10^{-3} to 10^{-6} moles/lt. and the behaviour of the nonlinear PA signal as a function of the pump laser power has been studied in all the concentrations. The occurrence of higher order absorptions is obvious from the obtained data. The results have been analyzed to give a measure of nonlinear absorption coefficient in each sample.

The same samples have been optically excited by 1060 nm radiation available from the present Nd:YAG laser, and PA as well as ASF signals are recorded. In this case the PA technique fails to give an indication of the excitations to S_1 and S_2 levels, because of the strong background resulting from overtone absorptions in the solvents. However, weak $S_1 \rightarrow S_0$ ASF is observed in this case which reveals the occurrence of nonlinear absorptions taking place in the system. The ASF spectra are recorded in each sample and the results are analyzed.

Details of similar investigations carried out in the dye cresyl violet (CVP) are given in chapter Four. CVP is taken in two solvent systems, namely methanol and methanol:water. The results are discussed in sufficient detail.

Chapter Five contains details of the experiments performed to observe stimulated Raman and Brillouin scattering (SRS and SBS) in dilute dye solutions. Rhodamine 6G dissolved in acetone at various low concentrations are taken as the samples here. Because of the competing fluorescence process, stimulated scattering disappears above a certain concentration. Asymmetry in forward-backward scattering, optical pulse narrowing and phase conjugation property of the backscattered beam are investigated. The effect of the presence of a fluorescing impurity, viz. Rhodamine 6G on the behaviour of SRS from a pure solvent like acetone is discussed.

Chapter Six presents the results of parametric studies carried out on the characteristics of broadband laser action in dye solutions. Initially samples are taken in a test tube purposefully to avoid cavity oscillations to a good degree, but still we have observed the occurrence of amplified spontaneous emission. Further experiments are conducted with the samples taken in a cuvette, permitting oscillations to occur in the broadband resonator formed by the polished end faces of the cuvette. Dependence of the emission on parameters like the cavity length, concentration, pump power etc. have been investigated.

Chapter Seven summarizes the contents of the thesis. A general overview of the work is presented. The various advantages and disadvantages of the PA and ASF techniques in investigations of higher order absorptions, as revealed from the present studies, are mentioned.

Part of the results obtained from the above investigations have been published/accepted for publication as the following journal papers. The remaining results are communicated/being communicated for publication.

- (1). Characteristics of two-photon absorption in methanol solutions of Rhodamine 6G using laser induced pulsed photoacoustics
Reji Philip, P Sathy, VPN Nampoore, Jacob Philip and CPG Vallabhan
J. Phys. B : At. Mol. Opt. Phys., 25, 155 (1992)
- (2). Observation of two photon absorption in Rhodamine 6G using photoacoustic technique
P.Sathy, Reji philip, VPN Nampoore and CPG Vallabhan
Optics communications, 74 (5), 313 (1990)
- (3). Fluorescence quantum yield of Rhodamine 6G using pulsed photoacoustic technique
P.Sathy, Reji philip, VPN Nampoore and CPG Vallabhan
Pramana, J. Phys., 34, 585 (1990)
- (4). Effect of a fluorescing impurity on the characteristics of stimulated Raman scattering from acetone
P.Sathy, Reji Philip, VPN Nampoore and CPG Vallabhan
Pramana, J. Phys., 38, 673, (1992)
- (5). An experimental set-up for the study of pulsed laser induced acoustic signals in condensed matter
Reji Philip, P.Sathy, VPN Nampoore, Jacob Philip, and CPG Vallabhan
J.Acoust.Soc.Ind., 16, 223 (1988)
- (6). Beam profile characterization of a high energy pulsed laser using photoacoustic technique
Reji philip, P.Sathy, VPN Nampoore and CPG Vallabhan
J.Acoust.Soc.Ind.,17, 332 (1989)
- (7). Characteristics of Photoacoustic signal from methanol solutions of the laser dye Rhodamine 6G
Reji Philip, P.Sathy, VPN Nampoore, Jacob Philip and CPG Vallabhan
J.Acoust.Soc.Ind., 18, 11 (1990)
- (8). Dependence of laser-induced ultrasonic pulse amplitude in dye solutions on concentration
P.Sathy, Reji Philip, VPN Nampoore and CPG Vallabhan
Journal of Pure and Applied Ultrasonics, 13, 24 (1991)

- (9). Photoacoustic observation of two photon processes in the laser dye Rhodamine 6G
P.Sathy, Reji Philip, VPN Nampoori, Jacob Philip and CPG Vallabhan
Proceedings of the National seminar on lasers in Engineering and Medicine, Nov.-Dec. 1989, Trivandrum, pp. 120-123
- (10). Optical pulse compression and phase conjugation by stimulated scattering in organic media
Reji Philip, P Sathy, VPN Nampoori, Jacob Philip and CPG Vallabhan
Proceedings of the National symposium on Antennas and Propagation, Dec.29-31 (1992), CUSAT, Cochin
- (11). Laser induced nonlinear fluorescence from dyes
P Sathy, Reji Philip, VPN Nampoori and CPG Vallabhan
Proceedings of the National Laser symposium, Feb.17-19, (1993), IIT, Madras, pp.235-237
- (12). Stimulated Raman scattering from Benzene and Benzene-acetone mixture
T Ramachandran, Reji Philip, P Sathy, VPN Nampoori and CPG Vallabhan
Proceedings of the National Laser symposium, Feb.17-19, (1993), IIT, Madras, pp.208-209

Accepted for publication

- (1). Design of a preamplifier for amplification of pulsed photoacoustic signals detected by a piezoelectric transducer
Reji Philip, Johny Isaac and Jacob Philip
(J.Acoust.Soc.Ind.)
- (2). Characteristics of the photoacoustic signal at the lasing threshold of the laser dye Rhodamine 6G
P.Sathy, Reji Philip, VPN Nampoori and CPG Vallabhan
(J.Acoust.Soc.Ind.)

CONTENTS

	Page No.
CHAPTER 1 INTRODUCTION	1
PART I - PHOTOACOUSTIC SPECTROSCOPY	2
1.1a Brief history of PAS	3
1.1b General theory of the PA effect in condensed media : The CW excitation case	4
1.1c Direct PA generation by pulsed photoacoustics	10
1.1d Theory for PA generation in strongly absorbing opaque liquids	19
1.1e Saturation effects in photoacoustics	22
PART II - FLUORESCENCE SPECTROSCOPY	22
1.2a Absorption of light	23
1.2b Fluorescence emission	31
PART III -INTRODUCTION TO NONLINEAR OPTICAL PHENOMENA	37
1.3a The nonlinear optical susceptibility tensor	37
1.3b Second harmonic generation	39
1.3c Two-photon processes	43
1.3d Time evolution and time dependent perturbations	44
PART IV - PROPERTIES OF LASER DYES	50
1.4a General properties of organic dyes	50
1.4b Absorption of light by organic dyes	53
1.4c Deactivation pathways for excited dye molecules	56
1.4d Environmental effects	59
PART V - INVESTIGATION OF NONLINEAR ABSORPTIONS BY PHOTOACOUSTICS AND FLUORESCENCE	62
1.5a Nonlinear Fluorescence from dye solutions	63
1.5b Generation of Photoacoustic signals in dye solutions	66
References	68

CHAPTER 2 INSTRUMENTATION

2.1 Instrumentation for Photoacoustics	72
2.2 The present PA experimental set up	81
2.3 Instrumentation for Fluorescence	89
2.4 The present fluorescence set up	99
2.5 Instrumentation for Stimulated scattering and Optical phase conjugation	103
2.6 Common instruments used	103
2.7 Laser beam profile analysis by photoacoustics	106
References	110

CHAPTER 3 HIGHER ORDER ABSORPTIONS IN DCM

3.1 Introduction	111
3.2 Absorption and Fluorescence properties	113
3.3 Investigations by Photoacoustics	113
3.4 Investigations by Fluorescence	127
3.5 Conclusions	135
References	136

CHAPTER 4 HIGHER ORDER ABSORPTIONS IN CRESYL VIOLET

4.1 Introduction	137
4.2 Absorption and Fluorescence properties	139
4.3 Investigations by photoacoustics - Results and discussion	139
4.4 Investigations by Fluorescence - Results and discussion	151
4.5 Conclusions	157
References	158

**CHAPTER 5 STIMULATED RAMAN AND BRILLOUIN SCATTERING
FROM DYE SOLUTIONS**

5.1	Introduction	159
5.2	Electromagnetic treatment of Stimulated Raman scattering	162
5.3	Stimulated Brillouin scattering	169
5.4	Optical phase conjugation by stimulated scattering	172
5.5	Anomalous experimental results in SRS	175
5.6	Experimental	177
5.7	Results and discussion	178
5.8	Conclusions	187
	References	192

CHAPTER 6 GENERATION OF BROAD BAND LASER PULSES FROM DYES

6.1	Evolution of the dye laser	194
6.2	Practical dye laser configurations	196
6.3	Theory of a simple dye laser	202
6.4	Design of the broadband resonator	204
6.5	Pump power dependence of the emission	207
6.6	Concentration tuning of the dye laser wavelength	207
6.7	Energy transfer and double band lasing in dye mixtures	208
6.8	Conclusions	221
	References	222

CHAPTER 7 GENERAL CONCLUSIONS 225

CHAPTER 1

INTRODUCTION

This thesis presents the results of the spectroscopic investigations carried out on the nonlinear optical properties of selected organic laser dyes. The techniques used for these investigations are mainly photoacoustic and fluorescence spectroscopies. This introductory chapter discusses all these aspects - techniques, properties and materials - in somewhat detail. The chapter is divided into five parts: the first two and the fifth for techniques, the third for the properties investigated and the fourth for the materials studied. The essential principles and theoretical details which form the necessary background for the latter chapters are outlined here.

PART I

PHOTOACOUSTIC SPECTROSCOPY

In its broadest sense, spectroscopy can be defined as the study of the interaction of radiation with matter. Because of its versatility, range and nondestructive nature, optical spectroscopy remains a widely used and most important tool for investigating and characterizing properties of matter. Conventional optical spectroscopies tend to fall into two major categories : the first one involves the study of optical photons that are transmitted through the material of interest whereas the second involves the study of light that is scattered or reflected from the material. Almost all conventional optical methods are variations of these two basic techniques. It should be noted that these techniques preclude the detection and analysis of those photons that have undergone an absorption, or annihilation by interaction with the material, even though this process is often the one of most interest to the investigator.

Optical spectroscopy is invaluable and successful in studies on reasonably clear media such as solutions, crystals and specularly reflective surfaces. There are, however, several instances where conventional reflection and transmission techniques fail : very weakly absorbing media, opaque media, highly light scattering materials such as powders, amorphous solids, gels, smears, suspensions etc. are some of them. Over the years various techniques have been developed for the optical investigation of highly light scattering and opaque materials, the most common of which are diffuse reflectance [1], attenuated total reflection and internal reflection spectroscopy [2] and Raman scattering [3]. All these techniques have proven to be very useful, yet each is useful only over a small wavelength range, and the data obtained are often difficult to interpret.

During the past few years, another optical technique has been developed to investigate the optical properties of those materials that are unsuitable with the conventional transmission or reflection methodologies. This technique, called photoacoustic spectroscopy or PAS, is different from the conventional techniques mainly in that even though the incident energy is in the form of optical photons, the

interaction of these photons with the material under investigation is studied not through the subsequent detection and analysis of some of the photons, but rather through a direct measure of the energy absorbed by the material as a result of its interaction with the photon beam. In a typical experiment the sample is illuminated with an intensity modulated monochromatic radiation. If any of the incident photons are absorbed by the sample, internal energy levels within the sample are excited. Upon subsequent de-excitation of these energy levels, all or part of the absorbed photon energy is transformed into heat energy through nonradiative de-excitation processes. In a gas this heat energy appears as kinetic energy of the gas molecules, while in a solid or liquid it appears as vibrational energy of ions or atoms. In PAS we measure this internal heating of the sample. Hence PAS is clearly a form of optical spectroscopy. Usual temperature sensors such as thermistors and thermopiles, though simple and efficient, have several inherent disadvantages for being used in PAS in terms of sensitivity, detector risetime and the speed at which measurements can be made. A more appropriate method is the measurement of heat production through volume and pressure changes produced in the sample or in an appropriate transducing material in contact with the sample.

1.1a. Brief History of PAS

The discovery of the photoacoustic effect in 1880 by Alexander Graham Bell was rather accidental. While experimenting with his 'photophone' he found that chopped sunlight, when focused on solid substances such as Selenium, produced an acoustic signal [4]. These signals were often audible if a hearing tube was used. Following Bell, John Tyndall [5] and Wilhelm Roentgen [6] also demonstrated the PA effect in various gases. In attempting to account for the effect, Bell conjectured that adsorbed gases were responsible for PA generation in dark, spongy solids such as lampblack. However, the hypotheses of Mercadier [7] and Preece [8], in which the periodic heating and cooling of the gas layer adhering the solid surface being irradiated was considered, came closest to the modern explanation of PA effect). After the initial flurry of interest generated by Bell's original work, experimentation with the PA effect apparently ceased. The effect was considered only as an interesting curiosity without any

great scientific value. Furthermore, in those days the PA experiments were difficult to perform and quantitate, primarily because they required the investigator's ear to be the signal detector!

The PA effect lay completely dormant for nearly 50 years until the advent of the microphone. In 1938 Viengerov [9] reported the use of PA effect for a gas analyzer system. By 1948 gas analyzers with a differential cell configuration, based on the design of Luft [10] became commercially available. These analyzers could measure ppm levels of CO_2 in N_2 . De-excitation and energy transfer processes also were studied in gases in the 1940 s by PA technique. Measurement of the vibrational lifetimes of gaseous molecules by PA was first proposed by Gorelik [11] and carried out by Slobodskaya [12]. After the advent of lasers, there was a strong thrust on PA spectroscopy, and numerous studies were performed in gases, liquids and solids. The growth of PAS was further accentuated by the development of new techniques like PA Raman spectroscopy, Doppler free PA spectroscopy etc, with the result that it has become one of the most powerful tools of scientific analysis of our times.

1.1b. General theory of the PA effect in condensed media : The CW excitation case

The primary source of a photoacoustic signal from a condensed sample, as measured by the gas-microphone method, arises from the periodic heat flow from the sample to the surrounding gas with the subsequent change in the gas pressure within the cell. Since the acoustic signals generated in the sample are not "directly" observed in the gas-microphone technique, it is often treated as an "indirect" PA generation method. A general theory for the PA effect in condensed media was first formulated by Rosencwaig and Gersho [13,14]. This theory, now commonly referred to as the RG theory, shows that in the gas-microphone measurement of a PA signal, the signal depends both on the generation of an acoustic pressure disturbance at the sample-gas interface and on the transport of this disturbance through the gas to the microphone. The generation of the surface pressure disturbance depends in turn on the periodic temperature of the sample-gas interface. The RG theory derives exact expressions for this temperature, while it considers the transport of the disturbance in

the gas in an approximate heuristic manner, which is, however, valid for most experimental conditions. Later refinements of the RG theory treat the transport of the acoustic disturbance in the gas more exactly, using Navier-Stokes equations [15-17]. The basic results of the RG theory have not been changed by these improvements; however, they are able to account for observed deviations from the RG theory at very low frequencies and at frequencies near the cell resonances.

In the following section we outline a simplified version of the salient features of the RG theory.

1.1b1. Theory of indirect PA generation by "thermal piston"

In general, indirect PA generation requiring acoustic detection in a coupling fluid in contact with the sample does not provide as high a sensitivity as the direct PA generation for detecting weak absorptions. However, indirect PA generation is very valuable for the opposite case of weak absorption, ie, when the optical absorption is so strong that no light passes through the sample.

A simple case of indirect PA generation is shown in Fig.1.1. Let a laser beam of radius r , modulated at frequency f , be incident on the sample of thickness l in a cylindrical cell of radius R and coupling gas thickness l_g . Let the optical absorption coefficient of the sample be α at the excitation wavelength, and the optical absorption length be $\mu_a = 1/\alpha$. The modulated component of the laser-induced heating is distributed over a diffusion length μ_s given by

$$\mu_s = [D_s / (\pi f)]^{1/2} \quad (1.1)$$

where D_s is the thermal diffusivity of the sample ($D_s = k_s/\rho C$ where k_s is the thermal conductivity, ρ the density and C the specific heat). We assume that the optical wavelength and the modulation frequency are so chosen that μ_s is shorter than l and μ_a , as indicated in case (a) in fig.1.2. Let the intensity of modulated laser beam be represented by

$$I(t) = \frac{1}{2} I_0 (1 + \sin 2\pi ft) \quad (1.2)$$

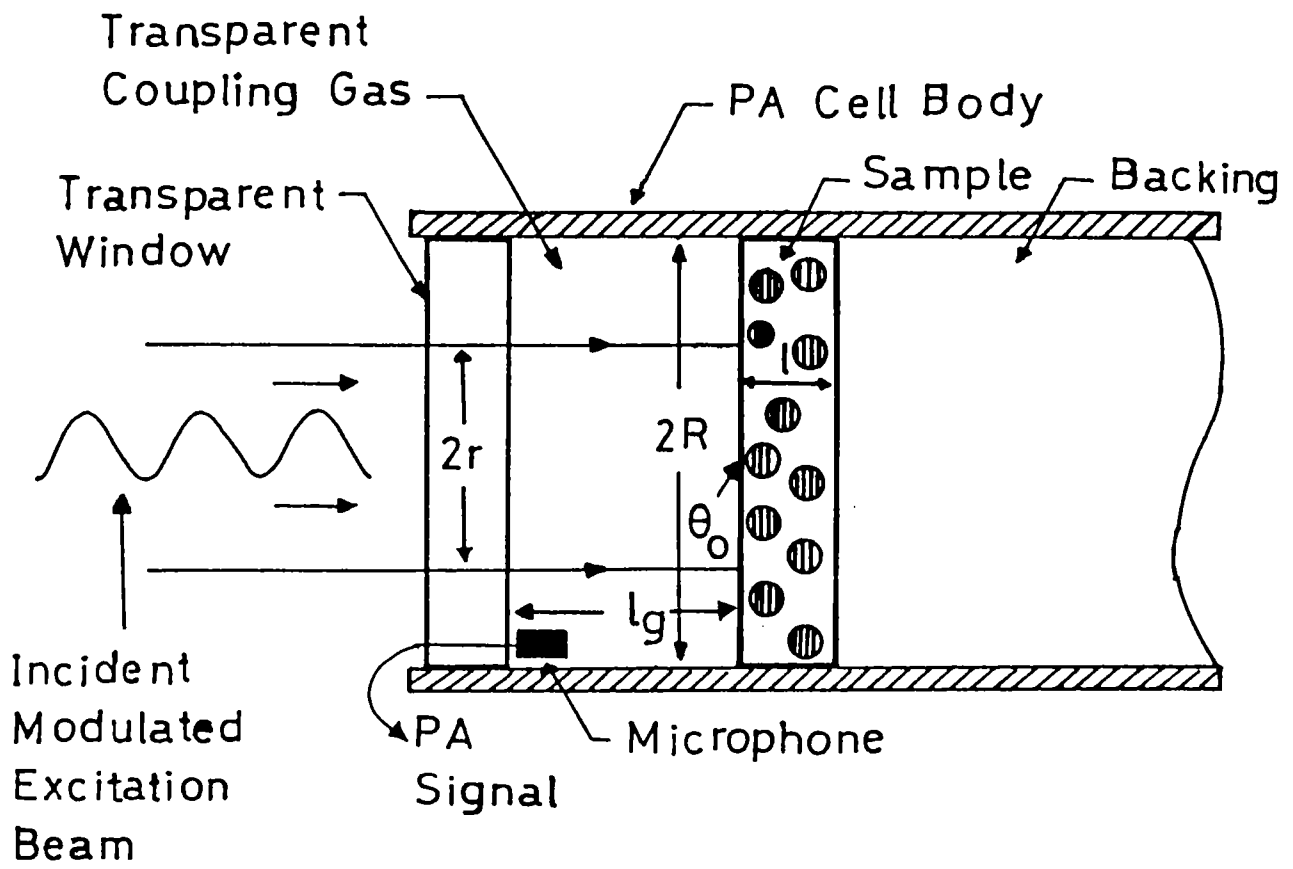


Fig.1.1 : A simple case of indirect PA generation.

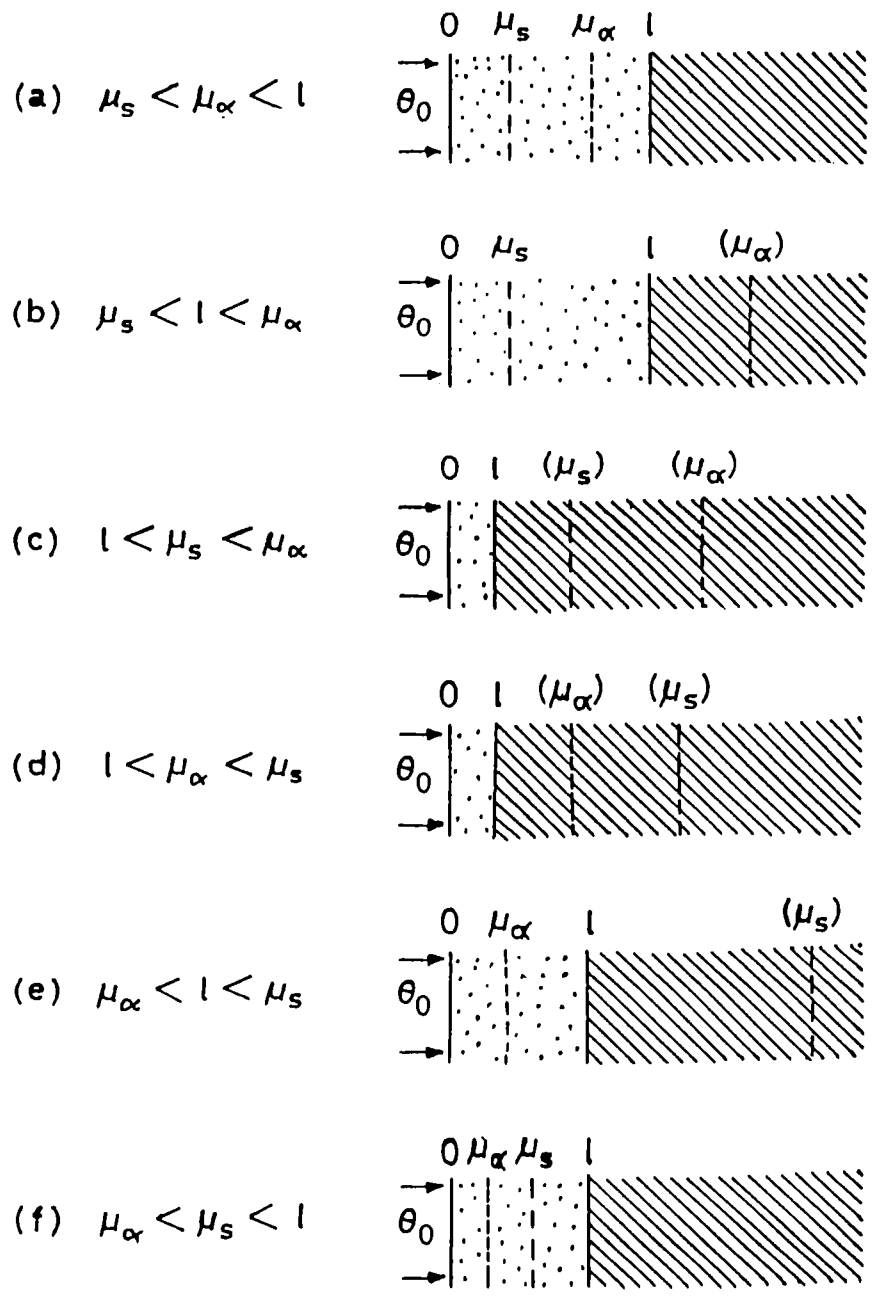


Fig.1.2 : Various possible cases of "thermal piston" PA generation, depending on the relative magnitudes of μ_s , μ_α and l . θ_0 is the amplitude of the temperature oscillation at the sample surface in contact with the coupling gas. The dotted area indicates the sample in contact with the coupling gas on the left and the backing material (shaded) on the right. When μ_s or μ_α is larger than l , the location of μ_s or μ_α is indicated, assuming that the backing has the same thermal diffusivity and optical absorption coefficient as the sample.

The "active" heat produced within the diffusion length μ_s , which is the depth in communication with the coupling gas, is only a fraction μ_s/μ_α of the power input, which is absorbed over a depth μ_α . The equation for heat conduction applied to the geometry of Fig.1.2(a) can be written as follows:

$$\begin{aligned} & (\text{thermal conductivity}) \times (\text{thermal gradient}) = \\ & (\text{thermal power within diffusion length}), \end{aligned}$$

which means

$$k_s (\theta_0/\mu_s) \approx I_0 (\mu_s/\mu_\alpha) \quad (1.3)$$

Thus

$$\theta_0 \approx I_0 \frac{\alpha \mu_s^2}{k_s}, \quad (1.4)$$

where k_s is the sample conductivity, $\alpha = 1/\mu_\alpha$, and θ_0 is the amplitude of the temperature variation on the sample surface, which is thermally coupled to an active volume V_{act} of the gas, given by

$$V_{act} \approx \pi r^2 s_g, \quad (1.5)$$

where

$$s_g = \begin{cases} \mu_g & \text{for } l_g > \mu_g, \\ l_g & \text{for } l_g < \mu_g. \end{cases} \quad (1.6)$$

Here, μ_g is the thermal diffusion length of the gas medium. Using the ideal gas law, the amplitude δV of the volume change of V_{act} is

$$\delta V = V_{act} \theta_0 / T, \quad (1.7)$$

where T is the absolute temperature. Now the volume fluctuation δV causes a pressure fluctuation δP at the microphone. Assuming the adiabatic pressure-volume relation, we have

$$\delta P = \gamma P \delta V/V_0, \quad (1.8)$$

where γ is the ratio of specific heats and V_0 is the total cell

volume, given by

$$V_0 = \pi R^2 l_g + V_r, \quad (1.9)$$

where V_r is the residual volume in the PA cell [18,19]. From the above equations we obtain the PA amplitude δP as

$$\delta P \approx \frac{\gamma P s_g r^2}{T(R^2 l_g + V_r/\pi)} \theta_0 \approx \frac{\gamma P s_g r^2 I_0}{T(R^2 l_g + V_r/\pi)} \frac{\alpha \mu_s^2}{k_s}. \quad (1.10)$$

Equation 1.10 indicates that the PA magnitude is proportional to the sample absorption coefficient α ; thus the normalized PA signal $\delta P/I_0$, measured for a range of excitation wavelength λ , can provide the absorption spectrum $\alpha(\lambda)$. The main advantage is that spectra of totally opaque or highly light scattering materials can now be measured.

The other cases of indirect PA generation indicated in Fig.1.2 correspond to other permutations of the magnitudes of the three lengths characterizing the sample, namely, μ_s , μ_α , and l . The sample is assumed to be mounted on a thick substrate or backing material of thermal conductivity k_b and thermal diffusion length μ_b . However, the substrate properties are only important for cases (c), (d) and (e). The only differences among the various cases of fig.1.2 are the equations of heat conduction; the other equations governing indirect PA generation (equations 1.5 to 1.9) are the same for all the cases. The first factor of Eqn.1.10 is invariant for various cases, whereas the second factor varies in accordance with the heat conduction equations. These semiquantitative results obtained by intuitive arguments are in agreement with the RG theory, where the phase factor of the PA signal also is calculated. The phase factor corresponds to the time lag of the PA signal with respect to the excitation modulation.

1.1b2. Other causes of indirect PA generation

Besides the thermal piston source discussed above, there are other mechanisms also for indirect PA generation, ie optical excitation of a specimen causing sound generation in an adjacent fluid. These mechanisms include surface vibrations, gas evolution and

bending of plate specimens as indicated in Fig.1.3 which are activated only under favourable circumstances. A discussion of these effects can be found in Tam [20] and references therein.

1.1b3. Experimental verification of the RG theory

One of the most obvious and important predictions of the RG theory is that the photoacoustic signal is linearly proportional to the power of the incident photon beam, irrespective of the sample or cell geometry. So it is possible to construct optical power meters based on the PA effect, and several of these have been described by various authors [21-23]. The variation of the PA signal amplitude as a function of sample thickness and modulation frequency for thin polymer films has been found to obey the RG theory except at very low modulation frequencies such as 10 Hz [24]. Wetsel and McDonald [17] have shown that the chopping frequency dependence of the PA signal is in agreement with the RG theory, and the predicted PA saturation has been demonstrated in aqueous solutions of the dye Methylene blue by McClelland and Kniseley [25].

1.1c. Direct PA generation by Pulsed Photoacoustics

As we have seen above, the "conventional" technique of PA spectroscopy utilizes a gas phase microphone that senses the heating and cooling of a gas layer in thermal contact with the sample of condensed matter which is being irradiated by a chopped light beam. However, this technique for condensed sample relies on inefficient thermal diffusion into a gas surrounding the sample, and can be viewed actually as a photothermal [26] technique and not a photoacoustic one, since the acoustic signal generated in the sample plays only a minor role. Hence this technique has an inherently low sensitivity [27-29] and is often only useful for observing absorptions typically exceeding 1%. The low coupling efficiency can be partially compensated for, however, by the use of high efficiency gas-phase microphones. Some reports point out that improvements in the sensitivity are possible by using piezoelectric transducers in contact with solid samples [27] or liquid samples [28], but these authors still have used cw light beams chopped at low audio frequencies.

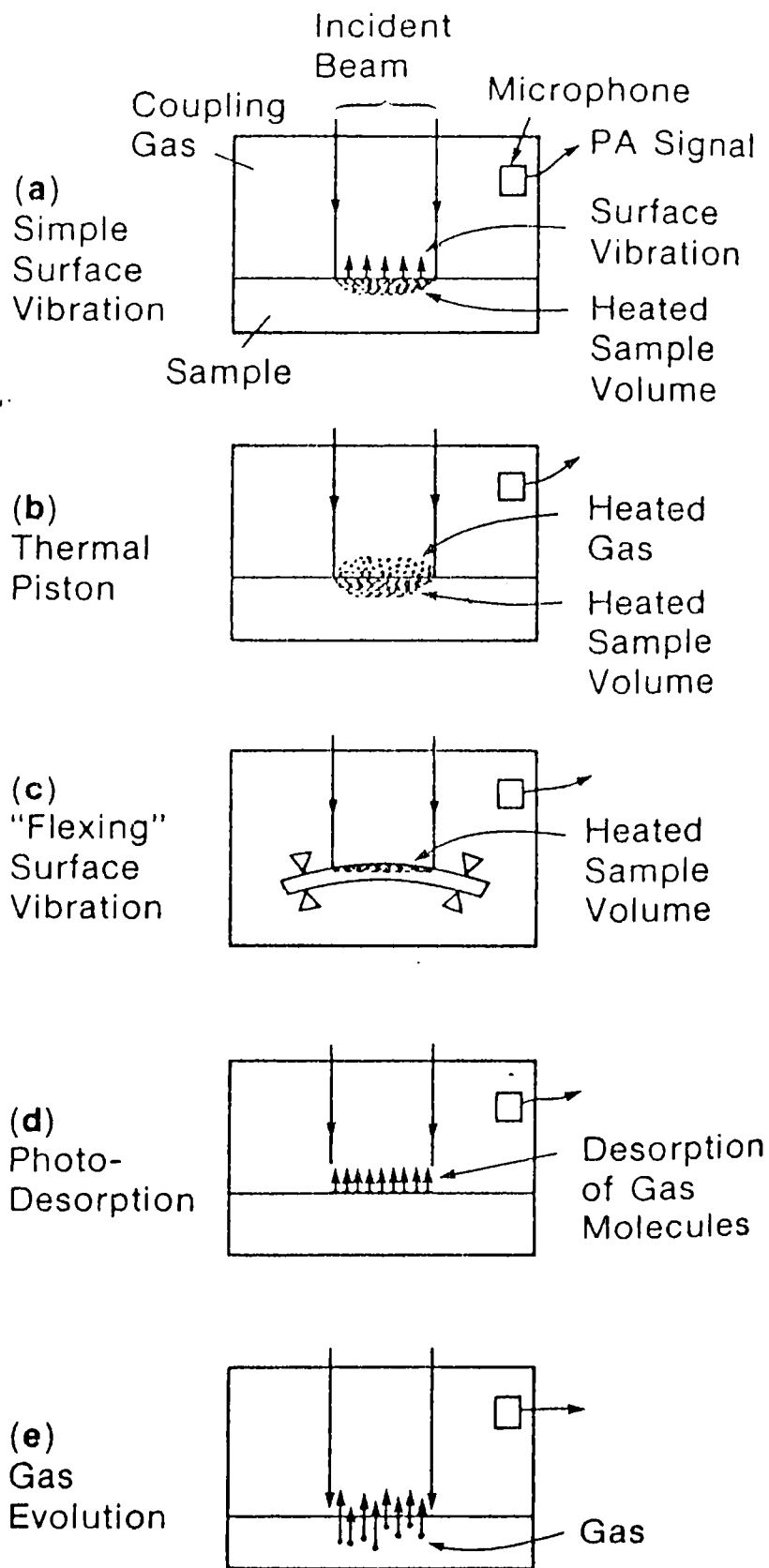


Fig.1.3 : Various possible causes of indirect PA generation other than the thermal piston source.

Attempts to use a pulsed laser source instead of cw modulation method seems to have been undertaken for the first time by Bonch-Bruevich et al [30]. However, the potential of pulsed PA spectroscopy has been brought out and demonstrated by the pioneering work of Patel and Tam, and the several experiments conducted by them are discussed in two excellent review papers [20,31]. They have shown that pulsed PA spectroscopy technique, involving the use of pulsed lasers, a piezoelectric transducer in direct contact with the sample, and gated detection can have very high detection sensitivities. This technique is truly photoacoustic in character, because the original acoustic pulse generated in a condensed sample is directly detected by a piezoelectric transducer, where good acoustic impedance matching also is ensured. The unique capability of pulsed photoacoustics (PPA) in spectroscopy is reflected in experiments carried out to (a) determine unambiguously the visible absorption spectra of liquid H₂O and D₂O, (b) reveal the absorption profiles of high vibrational overtones in 'transparent' organic liquids, (c) observe the absorption spectra of micron-thick liquid films and powder films, etc. [31]. For example, these authors could record the spectral profiles of the sixth, seventh and eighth harmonics of C-H stretch in benzene and estimate the absolute absorption coefficients by PPA. They could measure absorption coefficients as small as 10⁻⁶ to 10⁻⁷ cm⁻¹, with an S/N ratio of 1, using a laser pulse energy of ≈ 1 mJ. The pulse repetition frequency was 10 sec⁻¹ and integration (averaging) time was 1 sec. Studies prior to these observations by thermal lensing spectroscopy [32], wavelength modulation spectroscopy [33] and long-pathlength spectroscopy utilizing liquid-filled hollow optical fibres [34] could record only up to the sixth harmonic absorption profile.

The factors that affect and limit the ultimate sensitivity of PPA technique include (a) Optical absorption signals from windows, (b) scattering of light from the bulk of the liquid being absorbed by the transducer and (c) electrostriction. The signals arising from the first two can be minimized by the choice of low-loss windows, reduction of scattering impurities in the liquid and an appropriate time gating of the acoustic signals observed from the piezoelectric transducer. Time gating is very important since scattered light travels at the velocity of light in the medium while the acoustic signal generated in the bulk travels at the acoustic velocity in the

medium. Thus the bulk acoustic signal will be delayed as compared to the acoustic signals generated from scattered light. On the other hand for the case of acoustic signals resulting from optical absorption by the windows, the acoustic pulse arrives after that originating from the sample.

The acoustic pulse generated due to electrostriction processes in the laser-irradiated region is, however, of similar form arising from the bulk absorption, and hence there is no reasonable way in which the two can be distinguished. The use of short-laser pulse durations (giving rise to high optical intensities and correspondingly high electric fields) will accentuate the effects of electrostriction. It can be shown that the absorption coefficient α_1 at which the photoacoustic signal and the acoustic signal due to the electrostrictive effect become equal is inversely proportional to the diameter of the laser spot size [31]. For a laser pulse width of 70 ns and beam spot size ≈ 3 mm one can estimate $\alpha_1 \approx 6 \times 10^{-8} \text{ cm}^{-1}$, and if the pulse width is longer, say 1 μs , then α_1 becomes $\approx 4 \times 10^{-9} \text{ cm}^{-1}$. Further, there is no (or only very weak) dependence of the electrostriction pulse on laser wavelength. Hence, even the $4 \times 10^{-9} \text{ cm}^{-1}$ level does not represent a limitation on the smallest absorption coefficient that can be measured using PPA spectroscopy if the material being studied has a wavelength dependent absorption. Subtraction of a constant background signal as large as a factor of 10 to 100 times that corresponding to a well defined peak can easily be done electronically. However, such extreme situations will be encountered rather rarely in actual practice, even though those are the occasions where the utility of PPA will most clearly be demonstrated.

1.1c1. Semiquantitative theory for small laser radius and weak absorption

The theoretical treatment for this special case is illustrated by first considering a simplified version of pulsed PA generation. The excitation pulse is considered small enough so that thermal diffusion is negligible (this usually means that the excitation pulse is much shorter than 1 ms). Consider a long cylindrical irradiated region with small radius R_s (Fig.1.4a), ie, $R_s < v\tau_L$, where v is the sound

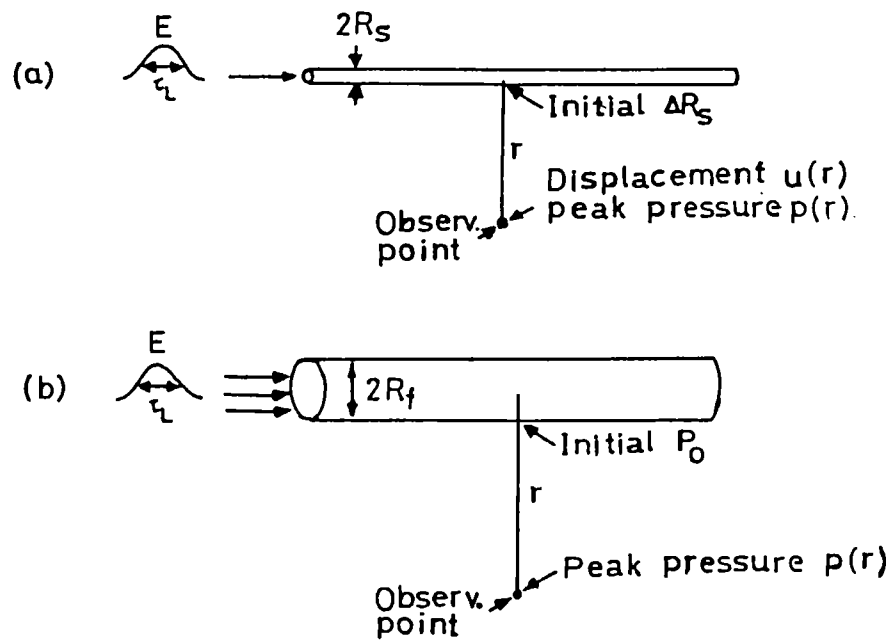


Fig.1.4 : Pulsed PA generation for weak absorption in an infinite medium. (a) laser beam radius R_S smaller than $v\tau_L$, (b) laser beam radius R_S larger than $v\tau_L$.

velocity in the medium and τ_L is the laser pulse width. The initial expansion ΔR of the "source" radius R immediately after the laser pulse is given by [20]

$$\pi(R + \Delta R)^2 l - \pi R^2 l = \beta V_1 \Delta T, \quad (1.11)$$

with the temperature rise just after the laser pulse being

$$\Delta T = \frac{E\alpha l}{\rho V_1 C_p}, \quad (1.12)$$

where l is the length of the PA source (assumed long), β is the expansion coefficient, $V_1 = R^2 l$ is the source volume, E is the laser pulse energy, α is the absorption coefficient (with $\alpha l \ll 1$), ρ is the density, and C_p is the specific heat at constant pressure. It may be noted that R is *not* equal to the illuminated radius R_s , since equations 1.11 and 1.12 are valid just after the laser pulse, when the active source volume has expanded to a larger radius $v\tau_L$ due to acoustic propagation. Thus we should put $R = v\tau_L$. Combining the above two equations and assuming $\Delta R \ll R$, which is true in all cases we are considering, we have

$$\Delta R = \frac{\beta E\alpha}{2\pi \rho C_p v\tau_L} \quad (1.13)$$

The peak displacement $U_s(r)$ at the observation point, at distance r from the PA source (for $r \ll l$), varies as $r^{-1/2}$ because of conservation of acoustic energy, as described by Landau and Lifshitz [35]. For a cylindrical acoustic wave we have

$$U_s(r) = \Delta R (R/r)^{1/2} = \frac{\beta E\alpha}{2\pi \rho C_p (v\tau_L r)^{1/2}} \quad (1.14)$$

The peak acoustic pressure $P_s(r)$ at position r is related to the acoustic displacement $U_s(r)$ by

$$P_s(r) \approx v\rho U_s(r)/\tau_L. \quad (1.15)$$

Substituting equation 1.14 into 1.15, we obtain the peak PA pressure observed at r for small source radius as

$$P_s(r) \approx \frac{\beta E \alpha v^2}{2\pi C_p (v\tau_L)^{3/2} r^{1/2}} \quad (1.16)$$

1.1c2. Semiquantitative theory for large laser radius and weak absorption

The opposite case of a large laser radius, ie, $R_f > v\tau_L$ (Fig.1.4b) can be treated as follows. A large radius means that the heated volume does not have time to expand isobarically immediately after the laser pulse; instead a pressure pulse P_0 is produced at the cylinder surface immediately after the laser pulse. P_0 is given by [20]

$$P_0 = \rho v^2 \beta \Delta T = \frac{\rho v^2 \beta E \alpha}{\pi R_f^2 \rho C_p} \quad (1.17)$$

where ρv^2 is the bulk modulus of the medium and eqn.1.17 is obtained from the consideration that the stress P_0 and the strain $\beta \Delta T$ are related by the bulk modulus. Again, the peak acoustic pressure $P_f(r)$ for the cylindrical wave scales as $r^{-1/2}$, so that

$$P_f(r) = P_0 (R_f/r)^{1/2} = \frac{\beta v^2 E \alpha}{\pi R_f^{3/2} C_p r^{1/2}} \quad (1.18)$$

Equation 1.18 is seen to be basically the same as Eqn.1.16, except that the effective source radius $v\tau_L$ in the small laser radius case is replaced by the actual radius R_f in the large laser radius case. It might be noted here that alternate theoretical treatments of the problem [36,37] indicate different dependences on R_f and r , but all results give pressure amplitudes proportional to $\beta v^2 E \alpha / C_p$. A comparison of equations 1.16 and 1.18 shows that

$$P_f(r)/P_s(r) \approx (v\tau_L/R_f)^{3/2} < 1, \quad (1.19)$$

which shows that a large source radius produces a weaker PA pulse than a small source radius, all other conditions being identical. This is intuitively appealing, since for the large-radius case, the contributions from different positions in the source do not add up coherently because of the long acoustic transit time across the diameter.

1.1c3. Rigorous theory of PA generation by thermal expansion and electrostriction

Theories of PA generation by a thermal expansion mechanism have been developed by White [38], Gournay [39], Hu [40], Liu [41] and others. Theories of PA generation by thermal expansion and electrostriction have been developed by Bechuk et al [42], Brueck et al [43], Lai and Young [44], and Heritier [45]. Here we briefly outline Lai and Young's theory for the weak absorption case (ie, line PA source). The basic equations for PA generation are the equation of motion

$$\rho \ddot{\mathbf{u}} = - \nabla p \quad (1.20)$$

and the equation of expansion

$$\nabla \cdot \mathbf{u} = - \frac{p}{\rho v^2} + \beta T - \frac{\gamma I}{2nc_L \rho v^2}, \quad (1.21)$$

where $\mathbf{u}(r,t)$ is the acoustic displacement at distance r from the axis of the PA cylindrical source, $p(r,t)$ is the acoustic pressure, T is the temperature rise due to the laser pulse of intensity $I(r,t)$, γ is the electrostrictive coefficient, n is the refractive index of the medium, and c_L is the velocity of light in a vacuum. Taking the second time derivative of Eqn.1.21 we get

$$\frac{1}{\rho v^2} \frac{\partial^2 p}{\partial t^2} + \nabla \cdot \ddot{\mathbf{u}} = \beta \ddot{T} - \frac{\gamma}{2nc_L \rho v^2} \frac{\partial^2 I}{\partial t^2} \quad (1.22)$$

substituting Eqn.1.20 into Eqn.1.22 and also using

$$\ddot{T} = \frac{\alpha \dot{I}}{\rho C_p}, \quad (1.23)$$

where thermal diffusion is neglected (when laser pulse duration is much shorter than thermal diffusion time), we get the following inhomogeneous wave equation for the acoustic pressure:

$$\left[\frac{1}{v^2} \frac{\partial^2}{\partial t^2} - \nabla^2 \right] p = \left[\frac{\alpha \beta}{C_p} \frac{\partial}{\partial t} - \frac{\gamma}{2nc_L v^2} \frac{\partial^2}{\partial t^2} \right] I \quad (1.24)$$

The solution of Eqn.1.24 may be simplified by introducing a potential function $\phi(r,t)$ that satisfies the following reduced wave equation:

$$\left[\frac{1}{v^2} \frac{\partial^2}{\partial t^2} - \nabla^2 \right] \phi = I(r,t). \quad (1.25)$$

Equations 1.24 and 1.25 imply the following. The acoustic pressure p can be written as the sum of a thermal expansion term p_{th} and an electrostriction term p_{el} , given by

$$p_{th} = \frac{\alpha \beta}{C_p} \frac{\partial \phi}{\partial t}, \quad (1.26)$$

and

$$p_{el} = - \frac{\gamma}{2nc_L v^2} \frac{\partial^2 \phi}{\partial t^2}, \quad (1.27)$$

with

$$p = p_{th} + p_{el} \quad (1.28)$$

Equations 1.26 and 1.27 have the following two important implications. First, p_{el} is proportional to the time derivative of p_{th} , ie,

$$p_{el} \propto dp_{th}/dt. \quad (1.29)$$

Hence, whenever p_{th} is at a peak, p_{el} passes through a zero. Thus the effect of p_{el} can be minimized by using a boxcar integrator to detect the PA signal, with the boxcar gate set at t_1 with a suitable gate width. Second, the peak magnitudes $|p_{el}|$ and $|p_{th}|$ are related by

$$\frac{|p_{el}|}{|p_{th}|} \approx \frac{\gamma C_p}{2nc_L v^2 \alpha \beta} \frac{1}{\tau_a}, \quad (1.30)$$

where τ_a is the width of the laser pulse. If we put $\tau_a = 1 \mu s$ and substitute values for the other parameters in Eqn.1.30 for typical liquids like water or ethanol, we conclude that

$$\frac{|p_{el}|}{|p_{th}|} < \frac{10^{-5}}{\alpha}, \quad (1.31)$$

where α is expressed in cm^{-1} . Hence for common liquids at room temperature the electrostrictive pressure is small compared to the thermal expansion pressure, unless α is smaller than 10^{-5} cm^{-1} . However, even in this low absorption case, the electrostrictive pressure effect can be suppressed, for example by a factor of 100, by suitably setting the boxcar gate for detection as discussed above [44]

The solution of equations 1.25 and 1.26 to obtain the pressure profile $p_{th}(r,t)$ due to thermal expansion has been carried out by several authors. The simplest case is for an infinitely long and narrow pulsed PA source produced by a pulsed laser beam with instantaneous energy $E(t)$ given by

$$E(t) = \frac{E_0}{\pi^{1/2} \tau_L} e^{-(t/\tau_L)^2} \quad (1.32)$$

where E_0 is the total energy. Patel and Tam [31] have found the solution to this simplest case to be

$$P(r,t) = - \frac{v \beta \alpha E}{\pi(\pi^{1/2}) C_p \tau_L^3} \int_{-\alpha}^{t-r/v} \frac{t' e^{-(t'/\tau_L)^2} dt'}{[v^2(t-t')^2 - r^2]^{1/2}} \quad (1.33)$$

(Note: PA source is referred to as "broad" or "narrow" depending on whether $v\tau_L$ is respectively smaller or larger than the excitation beam waist ω_0).

1.1d. Theory for PA generation in strongly absorbing and opaque liquids

The thermoelastic generation of spherical or plane acoustic waves in strongly absorbing liquids has been investigated by various authors [46-49]. The generation of plane acoustic waves in strongly absorbing liquids by pulsed laser irradiation can be well described by an analytical model which takes the temporal shape of the laser pulse into account. Under certain assumptions (homogeneous, isotropic and inviscous medium, neglect of heat diffusion, rate of thermal expansion small compared with sound speed) we can start with the wave equation [49]

$$\nabla^2 p - \frac{1}{c_o^2} \frac{\partial^2 p}{\partial t^2} = \frac{-\beta}{C_p} \frac{\partial H}{\partial t} \quad (1.34)$$

where p is the generated pressure amplitude, c_o the sound speed, β the thermal expansion coefficient and C_p the specific heat at constant pressure of the liquid while $H(x,y,z,t)$ is the density of the electromagnetic energy absorbed and converted to heat in unit time.

Suppose the laser pulse shape be approximated by the equation

$$f(\theta) = \begin{cases} 0 & \text{for } \theta < 0 \\ \theta^3 \exp[3(1-\theta)] & \text{for } \theta \geq 0 \end{cases} \quad (1.35)$$

where $\theta = t/t_R$ is the time normalized by the risetime t_R of the laser pulse. We consider the regime of surface heating, ie, the generation of plane acoustic waves, which implies $2a \gg 1/\alpha$ where $2a$ is the laser beam diameter and α the absorption coefficient of the liquid at the laser wavelength. We further assume that the absorption length $1/\alpha$ is much shorter than the sound propagation distance during the laser pulse duration τ_L , ie, $(\alpha)^{-1} \ll c_o \tau_L$. This means that this model is generally applicable to long laser pulses as long as the heat diffusion during τ_L can be neglected which usually implies $\tau_L \ll 1$ ms. Under these conditions the peak acoustic pressure p^{\max} for a free boundary and rigid boundary are respectively given by

$$p_f^{\max} \propto \frac{\beta I_o}{\alpha t_R C_p} \quad (1.36)$$

for the free surface, and

$$p_r^{\max} \propto \frac{\beta I_o c_o}{C_p} \quad (1.37)$$

for the rigid surface. Here I_o is the laser pulse intensity. The case of free and rigid boundaries are depicted in Fig.1.5. According to these equations the PA amplitudes are independent of the absorption coefficient α for the regime of rigid boundary, and for the case of a free surface it is inversely proportional to α . Thus in the free surface case, absorption spectra can be measured for opaque liquids. Indirect PA technique based on RG theory also allows spectroscopic

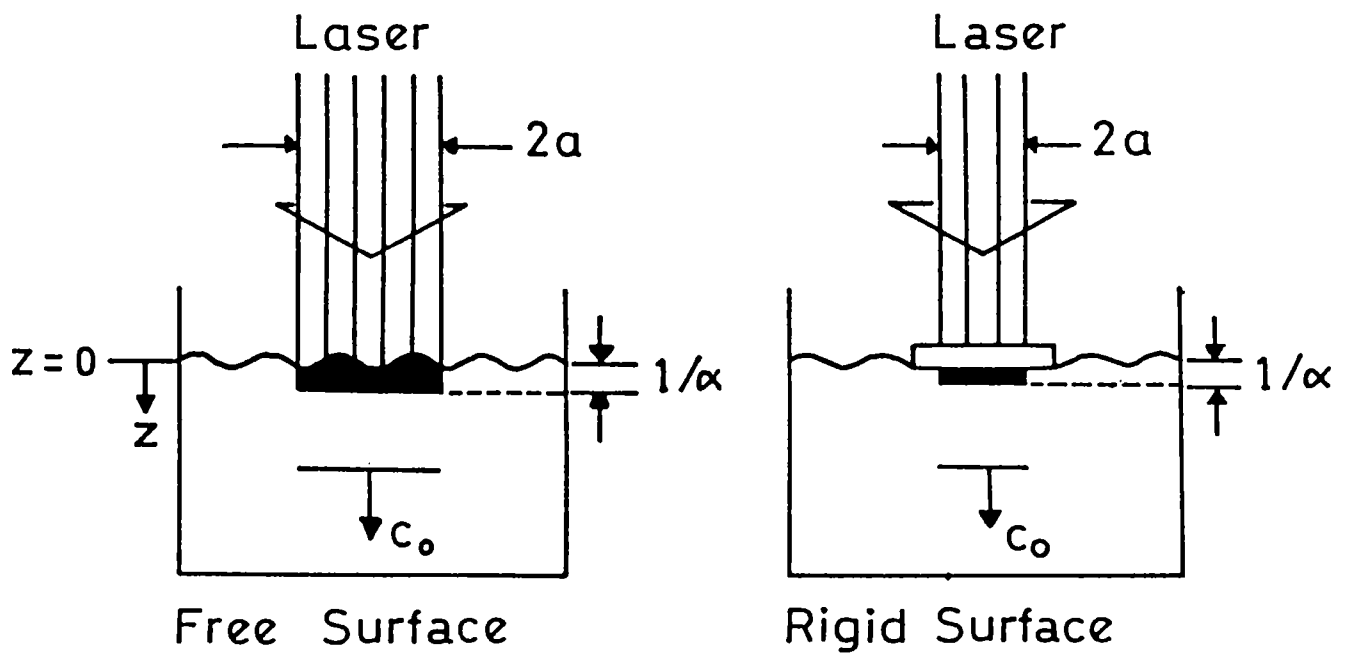


Fig.1.5 : Pulsed PA generation in strongly absorbing liquids. The case of free and rigid boundaries are shown. A free surface can be made a rigid surface by placing a glass plate on the liquid surface as seen in the figure, provided the laser beam diameter is smaller than the glass plate dimensions.

studies on opaque samples if $\mu < 1/\alpha$ where μ is the thermal diffusion length; however the PA signal is proportional to α in that case.

1.1e. Saturation effects in photoacoustics

If the molecule or atom is pumped harder than the upper level can be de-excited, then *optical saturation* (absorption saturation) of the PA signal may occur [50]. Thus at very high intensities q ceases to increase with I_0 , and in fact begins to decrease as $1/I_0$. This effect can be easily observed in gases where the upper state lifetime is $\approx 10^{-6}$ to 10^{-4} seconds [51]. In liquids more power is required, and a report on optical saturation of PA appeared only in 1979, observed in CCl_4 [52].

In strongly absorbing media when the thermal diffusion length becomes larger than the optical pathlength, the gas-microphone PA signal is found to saturate [50]. Hence the increase in the absorption coefficient of a given sample above a certain limit will result in the so-called *photoacoustic saturation*, all other conditions being unaltered. This effect has been demonstrated by McClelland and Kniseley [25], in aqueous solutions of methylene blue dye. They have observed full PA saturation for an α of $\approx 2000 \text{ cm}^{-1}$ at a chopping frequency of 50 Hz. At 1800 Hz, the corresponding α is $\approx 30,000 \text{ cm}^{-1}$. Higher chopping frequencies are hence preferred while working with samples of high optical absorption coefficients.

PART II FLUORESCENCE SPECTROSCOPY

When light absorbing molecules are optically pumped they get excited to one of the higher energy levels. In fluorescent molecules a major part of the absorbed energy is released in the form of radiative emission. In dye solutions fluorescence generally occurs from the lowest excited state of the singlet manifold, since this is the only state with a lifetime longer than the time required for the various collision-dependent relaxation and conversion processes.

In the following sections we briefly discuss the important

aspects of absorption and fluorescence applicable in the case of aromatic molecules.

1.2a Absorption of light

The total energy of a molecule in its electronic ground state (excluding translational energy and internal nuclear energy) is given by

$$E_t = E_e + E_v + E_r \quad (1.38)$$

where E_e is the electronic energy, E_v is the vibrational energy and E_r is the rotational energy of the molecule. Similarly the total energy E'_t of a molecule in an electronic excited state

$$E'_t = E'_e + E'_v + E'_r \quad (1.39)$$

is the sum of its electronic, vibrational and rotational components. If we define an absorption transition as

$$\Delta E_x = E'_x - E_x \quad (1.40)$$

where $x = t, e, v$ or r , then $\Delta E_r \approx 10 \text{ cm}^{-1}$, $\Delta E_v \approx 1000 \text{ cm}^{-1}$ and $\Delta E_e \approx 30,000 \text{ cm}^{-1}$.

A molecule as complex as an aromatic hydrocarbon possesses many alternative vibrational modes, but only a few of them, such as the C-C stretching vibrations, are normally dominant in the room temperature electronic absorption spectrum. More detailed vibronic structure is resolved at low temperatures, but at normal temperatures molecular rotation, thermal broadening, solvent interaction effects etc. will blur the vibronic structure of each electronic band system into a sequence of a few relatively broad maxima.

Let us consider a molecule in which only one vibrational mode is dominant, so that it can be approximated to a harmonic oscillator. Assuming the energy of the fundamental vibrational mode in the ground electronic state to be E_{1v} , we have

$$E_t = E_e + (m + 1/2) E_{1v} \quad (1.41)$$

where $m = 0, 1, 2, \dots$ is the vibrational quantum number. Taking the energy of the fundamental vibrational mode in the excited electronic state to be E'_{uv} , we have

$$E'_t = E'_e + (n + 1/2) E'_{uv} \quad (1.42)$$

where $n = 0, 1, 2, \dots$. If the ground state system is in thermal equilibrium at absolute temperature T , the fraction f_m of ground state molecules in a vibrationally excited state m is determined by the Boltzmann factor,

$$f_m = \exp(-mE_{1v}/kT), \quad (1.43)$$

Since $E_{1v} \approx 1000 \text{ cm}^{-1}$ and $kT \approx 200 \text{ cm}^{-1}$ at room temperature, we see that over 99% of the molecules are in the zero-point vibrational level of energy

$$E_t = E_e + \frac{1}{2} E_{1v}. \quad (1.44)$$

The transitions constituting the main electronic absorption spectrum are given by

$$\begin{aligned} \Delta E_t &= (E'_e - E_e) + \frac{1}{2} (E'_{uv} - E_{1v}) + n E'_{uv} \\ &\approx (E'_e - E_e) + n E'_{uv} \end{aligned} \quad (1.45)$$

since $E'_{uv} \approx E_{1v}$. The lowest energy vibronic transition in a given band system ($n = 0$) is described as the 0-0 transition. The transition to the n^{th} vibrational level of E'_t is the 0- n vibronic transition. Thus the main electronic absorption spectrum yields data about the vibrational levels (nE'_{uv}) of the *excited* electronic states (see Fig.1.6).

Weak absorption transitions may also occur from the vibrationally excited ground state E_t ($m = 1, 2, \dots$) to E'_t ($n = 0$). These are called "hot bands", and their energies lie below the 0-0 transition by mE_{1v} . The intensity of the hot bands decreases with T according to the Boltzmann factor f_m .

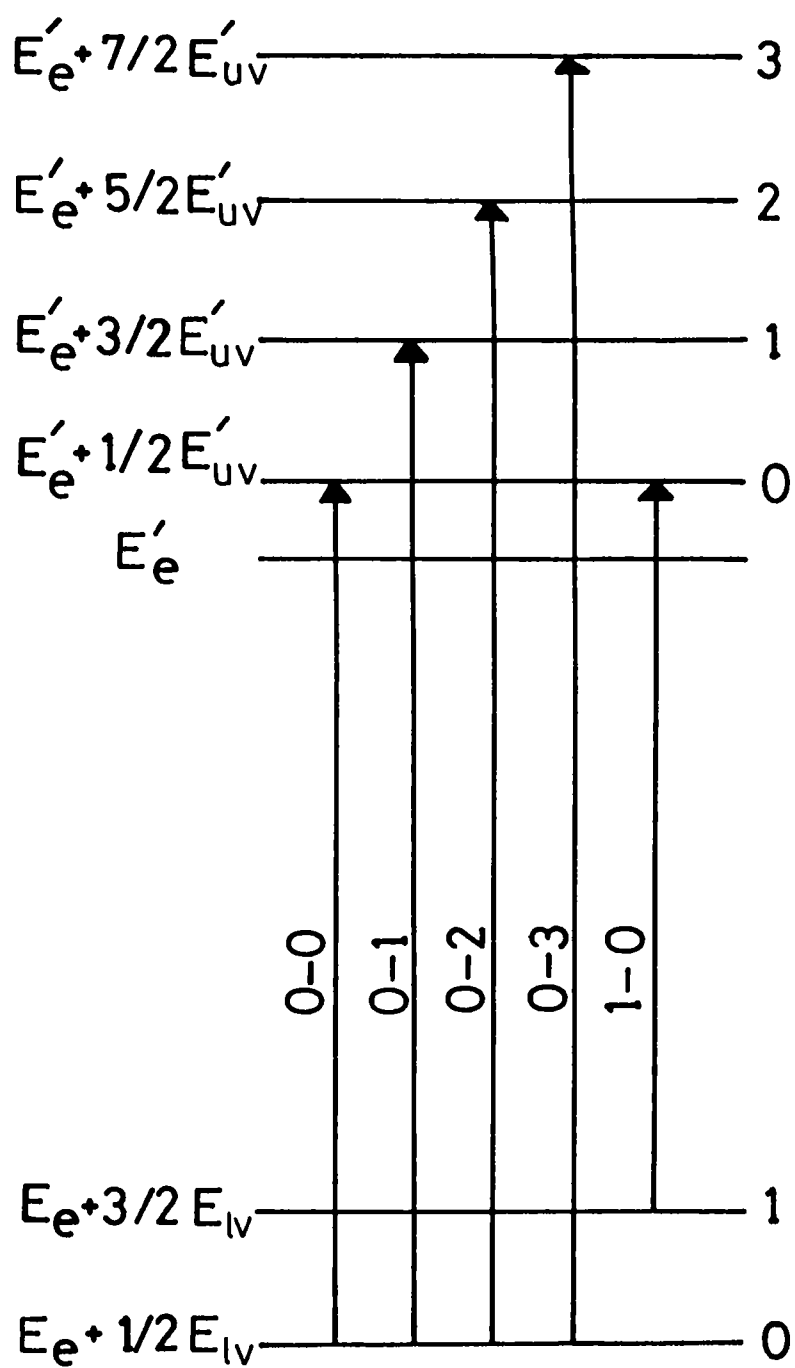


Fig.1.6 : Vibronic absorption transitions. The $1 \rightarrow 0$ transition is a hot band. E_{1v} represent levels in the lower electronic state, and E_{uv} represent those in the upper electronic state.

1.2a1 The Einstein Coefficients

Let a beam of radiation be incident on a large number of molecules, immersed in a transparent medium of refractive index n , in thermal equilibrium within a cavity at temperature T . The energy density of radiation (erg.cm^{-3} per unit frequency range) of frequency ν within the medium is given by Planck's black body radiation law [53]

$$\rho(\nu) = \frac{8\pi h \nu^3 n^3 / c^3}{[\exp(h\nu/kT) - 1]} \quad (1.46)$$

The rate of molecules going from state lm to state un by absorption of radiation is

$$\Delta N_{lm \rightarrow un} = N_{lm} B_{lm \rightarrow un} \rho(\nu_{lm \rightarrow un}) \quad (1.47)$$

where N_{lm} is the number of molecules in state lm , $\nu_{lm \rightarrow un}$ is the frequency of transition and $B_{lm \rightarrow un}$ is the transition probability coefficient, known as the *Einstein B coefficient*. Molecules in state un can go to state lm by spontaneous emission with transition probability $A_{un \rightarrow lm}$ (the *Einstein A coefficient*), or by induced (stimulated) emission with probability $B_{un \rightarrow lm} \rho(\nu_{un \rightarrow lm})$. The rate at which molecules undergo this downward transition is given by

$$\Delta N_{un \rightarrow lm} = N_{un} \left\{ A_{un \rightarrow lm} + B_{un \rightarrow lm} \rho(\nu_{un \rightarrow lm}) \right\} \quad (1.48)$$

where

$$B_{un \rightarrow lm} = B_{lm \rightarrow un} \quad (1.49)$$

$$\nu_{un \rightarrow lm} = \nu_{lm \rightarrow un} \quad (1.50)$$

and N_{un} is the number of molecules in state un . When the system is in equilibrium the rates of absorption and emission transitions are equal, so that by equating 1.47 and 1.48 we obtain

$$\frac{A_{un \rightarrow lm}}{B_{un \rightarrow lm}} = \left\{ \frac{N_{lm}}{N_{un}} - 1 \right\} \rho(\nu_{un \rightarrow lm}) \quad (1.51)$$

The number of molecules in the two states at equilibrium are related by the Boltzmann distribution law,

$$\frac{N_{un}}{N_{lm}} = \exp \left[- h\nu_{un \rightarrow lm} / kT \right] \quad (1.52)$$

Substitution of Eqns. 1.46 and 1.52 in 1.51 gives the 'Einstein relation' between the A and B coefficients for molecules in a medium of refractive index n,

$$A_{un \rightarrow lm} = 8\pi h^3 \nu_{un \rightarrow lm}^3 n^3 c^{-3} B_{un \rightarrow lm} \quad (1.53)$$

The Einstein B coefficient determines the probability of absorption, and is related to the molecular absorption cross section σ . By the definition of σ , the change in energy density $d\rho(\nu)$ of a beam of radiation in passing through a thin layer dx of a specimen containing n' absorbing molecules per cm^3 is

$$d\rho(\nu) = - \sigma n' \rho(\nu) dx = - \sigma N_{10} \rho(\nu) \quad (1.54)$$

where N_{10} is the number of absorbing molecules per cm^2 in the ground state 10.

1.2a2 Transition moments

By the Born-Oppenheimer approximation, the wavefunction ψ of a vibronic state can be expressed as the product of electronic (θ) and vibrational (ϕ) wavefunctions. Thus for the m^{th} vibrational level of a lower electronic state 1, we can write

$$\psi_{1m} = \theta_1 \phi_{1m} \quad (1.55)$$

as the state wavefunction. We note that the wavefunctions for the 10 and un vibronic states can be respectively written as

$$\begin{aligned} \psi_{10}(x, Q) &= \theta_1(x, Q) \phi_{10}(Q) \quad \text{and} \\ \psi_{un}(x, Q) &= \theta_u(x, Q) \phi_{un}(Q) \end{aligned} \quad (1.56)$$

where x and Q are the electronic and nuclear co-ordinates respectively. The *electric dipole transition moment* between any two

states represented by the wavefunctions ψ_1 and ψ_u is defined by the integral

$$M_{1u} = e \langle \psi_1 | \sum z_i \vec{r}_i | \psi_u \rangle \quad (1.57)$$

where \vec{r}_i is the position vector of the i^{th} particle (electron or nucleus) of charge $z_i e$ in the molecule. For the $10 \rightarrow un$ vibronic absorption transition, we obtain

$$M_{10 \rightarrow un} = e \iint \psi_{10}^* \left[\sum_i \vec{r}_i - \sum_{\mu} z_{\mu} \vec{r}_{\mu} \right] \psi_{un} dx dQ \quad (1.58)$$

where suffixes i and μ refer to the electrons and nuclei respectively. If we define the *electronic transition moment* as

$$M_{1u}(Q) = e \int \theta_1^*(x, Q) \left[\sum_i \vec{r}_i \right] \theta_u(x, Q) dx \quad (1.59)$$

then the $10 \rightarrow un$ *vibronic transition moment* will be given by

$$M_{10 \rightarrow un} = \int \phi_{10}^*(Q) M_{1u}(Q) \phi_{un}(Q) dQ. \quad (1.60)$$

If the Born-Oppenheimer approximation is valid, $M_{1u}(Q)$ is not a rapidly varying function of Q , and it may be approximated by a mean value \overline{M}_{1u} which is independent of Q . Hence Eqn.1.60 reduces to

$$M_{10 \rightarrow un} = \overline{M}_{1u} S_{10,un} \quad (1.61)$$

where $S_{10,un}$ is the *vibrational overlap integral* given by

$$S_{10,un} = \int \phi_{10}^*(Q) \phi_{un}(Q) dQ = \langle \phi_{10} | \phi_{un} \rangle \quad (1.62)$$

Eqn.1.61 is the quantum mechanical statement of the Franck-Condon principle, which is discussed below. One can also show that the Einstein B coefficient for the vibronic transition is related to the transition moment by the expression

$$B_{10 \rightarrow un} = \frac{8\pi^3 G}{3h^2} |M_{10 \rightarrow un}|^2 \quad (1.63)$$

where G is a multiplicity weighting factor equal to unity for

$S_0 \longrightarrow S_n$ transitions.

1.2a3 The Franck-Condon principle

The potential energy diagram of a diatomic molecule plots the total (electronic and vibrational) energy of the molecule as a function of the nuclear separation r , and the wavefunctions ϕ of the vibrational modes approximate to those of a harmonic oscillator (Fig.1.7). A similar diagram of E_t and E'_t against a nuclear configuration coordinate Q can be used for the qualitative discussion of more complex molecules such as the aromatic hydrocarbons, although Q no longer corresponds simply to r .

The *Franck-Condon principle* states that, because the time required for an electronic transition is negligible compared with that of nuclear motion, the most probable vibronic transition is one which involves no change in the nuclear coordinates. This transition, which is referred to as the *Franck-Condon maximum*, represents a vertical transition on the potential energy diagram. In quantum mechanical terms, the Franck-Condon maximum corresponds to the maximum overlap between the ground-state vibrational wavefunction and the excited state vibrational wavefunction.

The envelope of the vibronic bands of an absorption band system is referred to as *Franck-Condon envelope*, and its maximum corresponds to the Franck-Condon maximum. This approximates to the position of the most intense vibronic absorption band. If the latter is the 0-0 transition, as in the $S_0 \longrightarrow S_1$ absorption of many aromatic hydrocarbons, this indicates that the mean nuclear configuration of the excited electronic state is similar to that of the ground state. Information about the nuclear configuration of an electronic excited state and its vibrational modes can be obtained from an analysis of the vibronic structure and the Franck-Condon envelope of the absorption band system, since the latter represents the "vertical transform" of the ground state zero-point wavefunction.

At room temperature, absorption takes place from the lowest vibrational level of the ground state, and emission from the lowest vibrational level of the first excited state, making only the 0-0 transition common to both absorption and emission spectra. Frequently

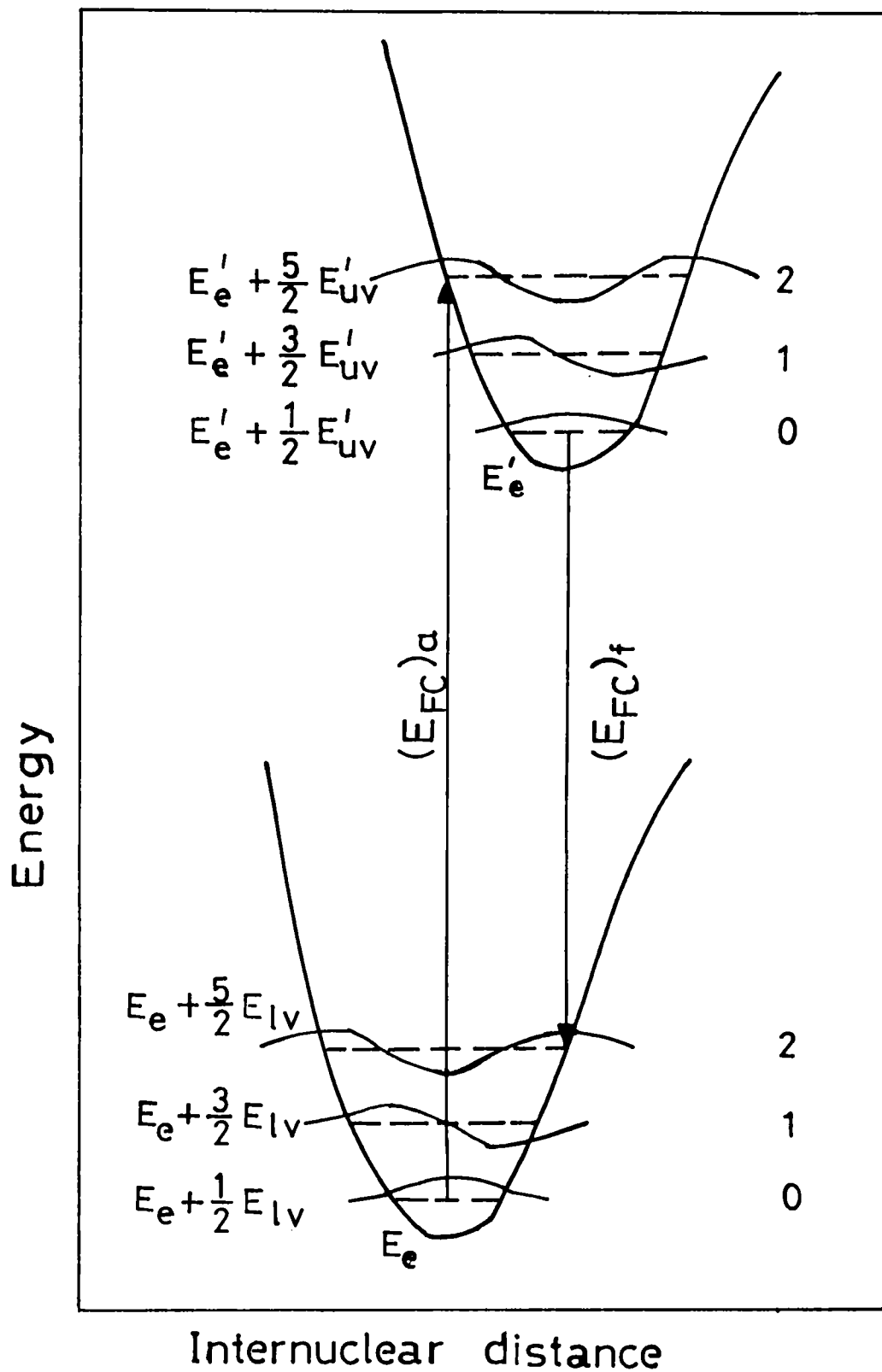


Fig.1.7 : Schematic potential energy diagram of a diatomic molecule, showing vibrational wavefunctions of ground and excited electronic states. $(E_{FC})_a$ is the Franck-Condon absorption maximum, and $(E_{FC})_f$ is the Franck - Condon emission maximum.

the emission spectrum is an approximate mirror-image of the first absorption band because the distribution of vibrational levels in the first excited state, which determines the shape of the first absorption band, is often similar to the distribution of vibrational levels in the ground state, which determines the shape of the fluorescence emission spectrum (Fig.1.8). According to *Stoke's law*, the wavelength of the fluorescence is always longer than that of the exciting light. However at room temperature a very small proportion of the molecules are thermally excited to the lower vibrational levels of the ground state and can therefore undergo an absorption transition which would then be expected to appear in the absorption spectrum as a very weak band. In practice such a band is usually too weak to be observed in the absorption spectrum, but by taking special precautions it is possible to excite molecules at this wavelength and to observe fluorescence emission at a shorter wavelength than that of the exciting light. This is known as Anti-Stokes Fluorescence (ASF). ASF can be induced by multiphoton absorption processes as well.

1.2a4 The extinction coefficient

If a monochromatic beam of intensity I_0 is incident normally on a specimen of thickness l cm containing n molecules per cm^3 , the intensity I of the emerging beam is given by the relation

$$I = I_0 e^{-\alpha l} = I_0 e^{-\sigma n l} \quad (1.64)$$

where α is the absorption coefficient (cm^{-1}) and σ is the molecular absorption cross section (cm^2). This relationship is also expressed in the form

$$\log_{10} \left[\frac{I_0}{I} \right] = \epsilon c_m l \quad (1.65)$$

where c_m is the sample concentration given in moles/lit and ϵ is the decadic molar extinction coefficient ($\text{moles}^{-1} \text{cm}^{-1}$). $\epsilon c_m l$ is known as the *absorbance* or *optical density* of the sample.

1.2b Fluorescence emission

In dyes, transitions usually occur between the various singlet

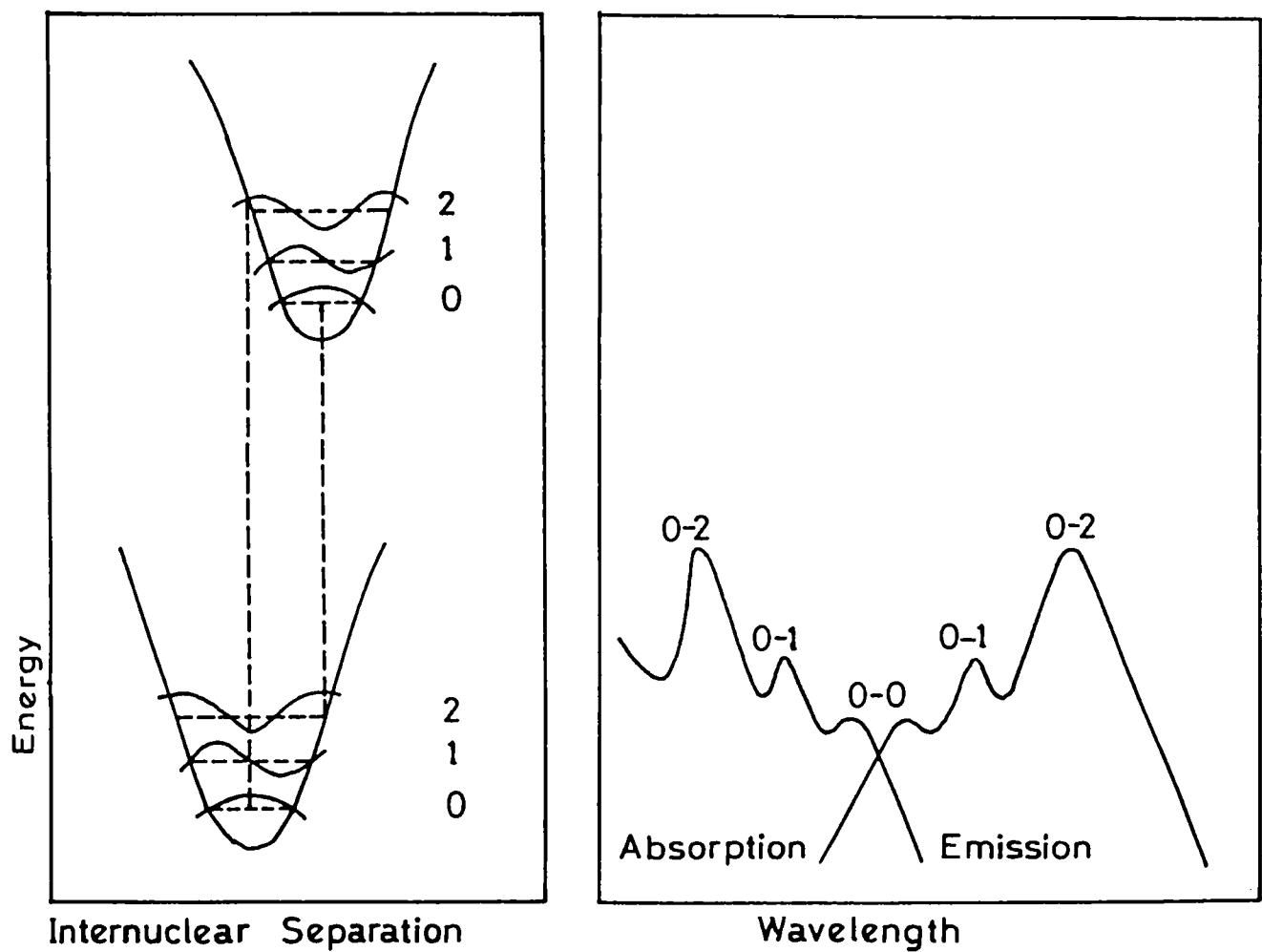


Fig.1.8 : The mirror-image rule. The absorption and emission bands are symmetric about the 0-0 band.

(S) and triplet (T) states. The $S_1 \rightarrow S_0$ fluorescence transition is the inverse of $S_0 \rightarrow S_1$ absorption transition. If the S_1 lifetime is sufficiently long for the excited molecules to attain thermal equilibrium, then fluorescence emission occurs primarily from the zero-point vibrational level of S_1 . This condition is generally valid if the molecules are in a condensed medium, for example in solution, but it may not be true in a rarefied vapour in which the molecules cannot lose their excess vibrational energy in collisions. Since fluorescence occurs due to transitions to various vibrational levels of S_0 , the fluorescence spectrum yields data about the vibrational states of the *ground* electronic state.

1.2b1 Fluorescence parameters

The *molecular fluorescence quantum efficiency* q_{FM} is defined as the ratio of the number of fluorescence photons emitted by a system of molecules in dilute solution to the number of absorbed photons. The molecular fluorescence spectrum $F(\nu)$ is then defined as the relative fluorescence quantum intensity at frequency ν , normalized by the relation

$$q_{FM} = \int_0^{\infty} F(\nu) d\nu \quad (1.66)$$

The probability of the $u0 \rightarrow lm$ vibronic fluorescence transition is given by the appropriate Einstein A coefficient

$$A_{u0 \rightarrow lm} = 8\pi h \nu_{u0 \rightarrow lm}^3 n^3 c^{-3} B_{u0 \rightarrow lm} \quad (1.67)$$

and one can show that

$$A_{u0 \rightarrow lm} \propto \int F(\nu) d\nu \quad (1.68)$$

where the integral is taken over the $u0 \rightarrow lm$ vibronic fluorescence band.

In the absence of nonradiative processes, the *radiative lifetime* τ_{FM} of the fluorophore is defined as the reciprocal of the *radiative transition probability* k_{FM} (in sec^{-1}). k_{FM} is equal to the Einstein A coefficient summed over the complete fluorescence spectrum:

$$1/\tau_{FM} = k_{FM} = A_{u0 \rightarrow l} = \sum_m A_{u0 \rightarrow lm} \quad (1.69)$$

Considering nonradiative transitions also, accounted for by the *non-radiative transition probability* k_{IM} , the *molecular fluorescence lifetime* is given by

$$\tau_M = 1/k_M = 1/(k_{FM} + k_{IM}) \quad (1.70)$$

and the basic fluorescence parameters are related through the equation

$$q_{FM} = \frac{k_{FM}}{k_{FM} + k_{IM}} = \frac{\tau_M}{\tau_{FM}} = \int_0^{\infty} F(\nu) d\nu \quad (1.71)$$

The fluorescence lifetime of a substance usually represents the average amount of time the molecule remains in the excited state prior to its return to the ground state. Lifetime measurements are frequently necessary in fluorescence spectroscopy; for example they can reveal the frequency of collisional encounters with quenching agents, the rate of energy transfer and the rate of excited state reactions.

Another important parameter is the fluorescence anisotropy. The transition moment has a definite orientation in the molecule, and in an isotropic solution the molecules are randomly oriented. When pumped by a polarized beam of light, those molecules with absorption transition dipoles parallel to the electric vector of excitation are selectively excited (photoselection) resulting in partially polarized fluorescence emission. The transition moments for absorption and emission have fixed orientation within each molecule, and the relative angle between these moments determine the maximum measured anisotropy. The *fluorescence anisotropy* (r) and *Polarization* P are defined by

$$r = \frac{I_{\parallel} - I_{\perp}}{I_{\parallel} + 2 I_{\perp}} \quad (1.72)$$

$$P = \frac{I_{\parallel} - I_{\perp}}{I_{\parallel} + I_{\perp}} \quad (1.73)$$

where I_{\parallel} and I_{\perp} are the fluorescence intensities of the vertically (\parallel) and horizontally (\perp) polarized emission when the sample is excited with vertically polarized light. P and r are expressions for the same phenomenon. Several phenomena can decrease the measured anisotropy to values lower than the maximum values, and the most common one is rotational diffusion which occurs during the lifetime of the excited state. Excitation energy transfer also will lead to decreased anisotropies.

1.2b2 Solvent dependence of fluorescence emission spectra

The physical and chemical properties of the solvents are found to affect the emission spectra of many fluorophores, especially those containing polar substituents on the aromatic rings. The absorption process occurs in about 10^{-15} sec, a time too short for significant displacement of nuclei (Franck-Condon principle), but evidently adequate for the redistribution of electrons. Generally the electronically excited states of aromatic compounds possess dipole moments (μ^*) which are larger than those in the ground states (μ). Hence the absorption of a photon by the fluorophore results in the essentially instantaneous creation of a dipole, which perturbs the environment surrounding it. Subsequent to excitation, the solvent responds by a reorganization of the solvent cage surrounding the fluorophore. This process is called solvent relaxation (solvation), the time scale of which is dependent upon the physical and chemical properties of the solvent.

In a broad perspective, the solvent effects can be divided into *general* and *specific* categories. Whereas the general solvent effects are expected to be present always, specific solvent effects will depend on the precise chemical properties of the solvent and fluorophore [54]. However both interactions may result in significant spectral shifts. The general solvent effects are mainly derived from the refractive index (n) and dielectric constant (ϵ). (Note that this ϵ should not be confused with the extinction coefficient discussed in 1.2.a4). These physical constants reflect the freedom of motion of the electrons in solvent molecules, and the dipole moment of these molecules. It is seen that solute-solute interactions occur when the fluorophore is in solution, affecting the energy difference between

the ground and excited states. In fact this energy difference (in cm^{-1}) depends on n and ϵ as given by the Lippert equation:

$$\bar{\nu}_a - \bar{\nu}_f \cong \frac{2}{h c} \left[\frac{\epsilon - 1}{2\epsilon + 1} - \frac{n^2 - 1}{2n^2 + 1} \right] \left(\frac{\mu^* - \mu}{a} \right)^2 + \text{constant} \quad (1.74)$$

where h is the Planck's constant, c the speed of light, a is the radius of the cavity in which the fluorophore resides, and $\bar{\nu}_a$ and $\bar{\nu}_f$ are the wave numbers in cm^{-1} of absorption and emission respectively.

An increase in n or a decrease in ϵ will thus decrease the Stoke's shift, $\bar{\nu}_a - \bar{\nu}_f$. Higher values of n allow both the ground and excited states to be instantaneously stabilized by the redistribution of electrons within the solvent molecule, that result in the decrease of $\bar{\nu}_a - \bar{\nu}_f$. This solvation of the ground and excited states occurs for solvents having large ϵ values too, but only after reorientation of the solvent dipoles. Here the movement of the entire solvent molecule is required, not just its electrons. As a result, the stabilization of the ground and excited states of the fluorophore which depends on the dielectric constant (ϵ) is time dependent and the rate of stabilization depends on the temperature and viscosity of the solvent.

The stokes shift will be very small in nonpolar solvents since they do not possess a dipole moment and hence no dipoles to reorient around the excited state of the fluorophore. In polar solvents, substantially larger Stokes shifts are expected due to the larger orientational polarizability of the molecule, resulting from its dipole moment.

On the other hand, specific solvent effects can be those due to specific chemical interactions between the solvent and fluorophore molecules. Hydrogen bonding, complexation, acid-base chemistry, charge transfer interactions etc. are a few of them.

Thus fluorescence emission is quite a complicated phenomenon in the sense that no single physical property of the solvent, such as polarity, orientation polarizability, viscosity, dielectric constant or refractive index can fully explain the emission characteristics.

PART III

INTRODUCTION TO NONLINEAR OPTICAL PHENOMENA

The interaction of optical radiation with matter is generally understood in analogy with a linear harmonic oscillator model. This becomes possible since the strength of atomic and inter-atomic fields are of the order of $10^7 - 10^{10}$ V/cm, whereas that of conventional non-laser light sources is less than 10^3 V/cm. However the coherence of the laser beam makes it possible to have extremely high spatial concentration of optical power. Here the driving force, ie, the electric field amplitude associated with optical radiation, is very high and the linear harmonic oscillator model fails. For example, the energy density in a 1 MW laser pulse beam of cross section 1 mm^2 is $\cong 10^6 \text{ MW/m}^2$, corresponding to a peak electric field strength $E \cong 3 \times 10^7 \text{ V/m}$. Such optical fields can affect atomic and molecular systems to the extent of changing their optical parameters, and the relationship between the electric polarization P and the field strength E ceases to be linear.

Nonlinearity in electromagnetic interactions had been known before in the case of low frequencies. For example, audio and electrical engineers were familiar with the nonlinear relationship between magnetic induction and field in iron core solenoids in the form of $\vec{B} = \mu(\vec{H}) \vec{H}$. The idea of nonlinearity in optics was first introduced by Nicholas Bloembergen in the early sixties of this century [55].

1.3a The nonlinear optical susceptibility tensor

A dielectric medium when placed in a weak/moderate electric field gets polarized, if the medium does not have a transition at the field frequency. Each constituent molecule acts as a dipole with a dipole moment \vec{P}_i . The dipole moment vector per unit volume, \vec{P} , is given by

$$\vec{P} = \sum_i \vec{P}_i \quad (1.75)$$

where the summation is over the dipoles in unit volume. The orienting effect of the external field on the molecular dipoles depends both on the properties of the medium and the field strength through the *linear*

relationship

$$\bar{P}^{\>} = \epsilon_0 \kappa \bar{E}^{\>} \quad (1.76)$$

where κ is called the *polarizability* or *dielectric susceptibility* of the medium. κ is a constant only in the sense of being independent of E , its magnitude is a function of the frequency. With a sufficiently intense radiation Eqn.1.76 does not hold good since κ becomes a function of E also. Furthermore in most crystalline materials the dielectric susceptibility depends on the direction of propagation, polarization of the electric field and the orientation of the optic axis of the crystal. Since $\bar{P}^{\>}$ and $\bar{E}^{\>}$ are not necessarily parallel in this case the coefficients κ should be treated as tensors. Eqn 1.76 now gets modified to the *nonlinear* form

$$\bar{P}_i^{\>} = \epsilon_0 \left[\kappa_{ij}^{(1)} \bar{E}_j^{\>} + \kappa_{ijk}^{(2)} \bar{E}_j^{\>} \bar{E}_k^{\>} + \kappa_{ijkl}^{(3)} \bar{E}_j^{\>} \bar{E}_k^{\>} \bar{E}_l^{\>} + \dots \right] \quad (1.77)$$

and the coefficients $\kappa^{(2)}$, $\kappa^{(3)}$,etc, which define the degree of nonlinearity, are known as the *nonlinear susceptibility tensors*. Obviously Eqn.1.77 is the general expression for P , and Eqn.1.76 is only an approximation valid at low field intensities. A medium possessing nonvanishing nonlinear susceptibility coefficients is called a *nonlinear medium*. The origin of nonlinear optical susceptibilities has been explained by Bloembergen, by treating the radiation-matter interaction in terms of an electron experiencing the field of an anharmonic potential well [56].

The existence of nonlinear polarization can be visualized in the following way: Suppose the incident field is of the form

$$\bar{E}^{\>} = \bar{E}_0^{\>} \cos \omega t \quad (1.78)$$

Substituting Eqn.1.78 in 1.77 and neglecting the tensor aspect we see that the polarization now becomes [57]

$$P = \frac{1}{2} \epsilon_0 \chi^{(2)} E_0^2 + \epsilon_0 \left[\chi^{(1)} + \frac{3}{4} \chi^{(3)} E_0^2 \right] E_0 \cos \omega t + \frac{1}{2} \epsilon_0 \chi^{(2)} E_0^2 \cos 2 \omega t + \frac{1}{4} \epsilon_0 \chi^{(3)} E_0^3 \cos 3 \omega t + \dots \quad (1.79)$$

The first term is a constant which gives rise to a dc field across the medium, and the second follows the external polarization (first or fundamental harmonic of polarization). The third term oscillating at frequency 2ω is called the second harmonic of polarization, and the fourth term oscillating at 3ω is the third harmonic of polarization, and so on (Figs.1.9 and 1.10). Various nonlinear processes are initiated in the medium by $\chi^{(2)}$ and $\chi^{(3)}$: for example $\chi^{(2)}$ is responsible for second harmonic generation, whereas $\chi^{(3)}$ gives rise to effects like third harmonic generation, two-photon absorption, stimulated Raman scattering etc. [58]. In the following section we briefly discuss second harmonic generation, which originates from the second order optical nonlinearity. The theory of two-photon processes follows.

1.3b Second Harmonic Generation (SHG)

The polarization oscillating at frequency 2ω , as seen from eqn.1.79, radiates an electromagnetic wave of the same frequency that propagates with the same velocity as that of the incident wave. The wave thus produced has the same characteristics of directionality and monochromaticity as the incident wave. This phenomenon is known as second harmonic generation (SHG), which is governed by the second order polarization

$$P_i^{(2)} = \epsilon_0 \sum_{j,k} \chi_{ijk}^{(2)} E_j E_k \quad (1.80)$$

where i, j, k represent the co-ordinates x, y and z (Many of the co-efficients χ_{ijk} are usually equal to zero leaving only one or two nonzero components). Consider an isotropic crystal where $\chi_{ijk}^{(2)}$ is independent of direction, and hence, is a constant. If we now reverse the axis directions ($x \rightarrow -x$, $y \rightarrow -y$, $z \rightarrow -z$) leaving P and E unchanged in direction, we should have

$$- P_i^{(2)} = \epsilon_0 \sum_{j,k} \chi_{ijk}^{(2)} (-E_j) (-E_k) \quad (1.81)$$

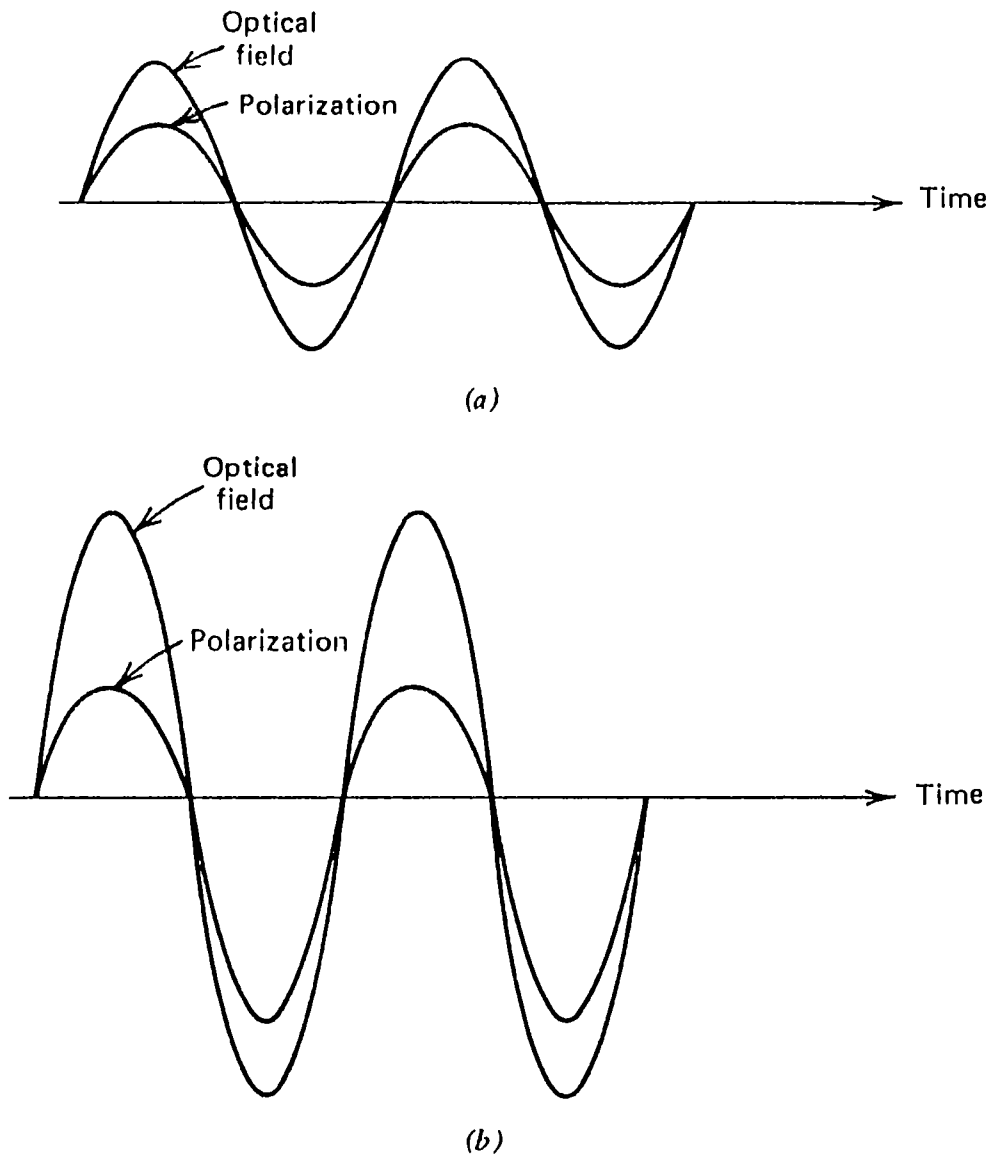


Fig.1.9 : An applied sinusoidal electric field and the resulting polarization, shown for (a) a linear crystal, and (b) a crystal lacking inversion symmetry (nonlinear crystal).

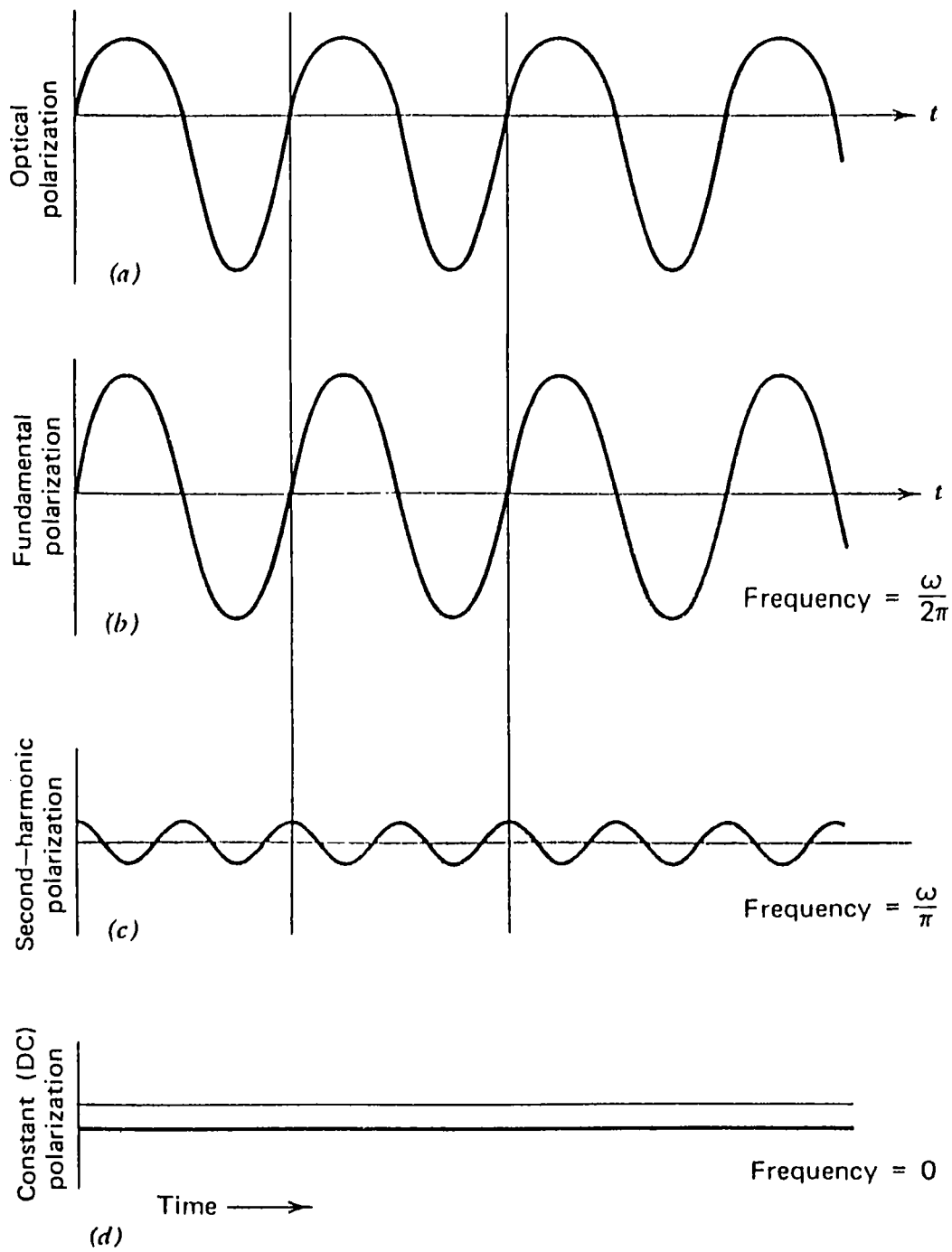


Fig.1.10 :Analysis of the nonlinear polarization wave,(a) of Fig.1.9b shows that it contains components oscillating at (b) the same frequency (ω) as the wave inducing it, (c) twice that frequency (2ω), and (d) an average (dc) negative component.

which means $P_i^{(2)} = 0$, and hence $\chi_{ijk}^{(2)} = 0$. SHG, therefore, cannot occur in an isotropic medium such as liquids or gases, nor in centrosymmetric crystals. Only crystals that lack inversion symmetry exhibit SHG.

For the efficient transfer of energy from the fundamental (ω) to the second harmonic (2ω) mode, the phase matching condition should be fulfilled. Consider a medium of length L . Let $k^{(\omega)} = 2\pi n/\lambda$ be the propagation wave vector of the ω beam; then that of the 2ω beam is $k^{(2\omega)} = 2k^{(\omega)}$. The conversion efficiency is then found to be [56]

$$\frac{P_L^{(2\omega)}}{P_L^{(\omega)}} \propto \frac{\sin^2(\Delta k L/2)}{(\Delta k L/2)^2} \quad (1.82)$$

where $P_L^{(2\omega)}$ is the second harmonic power output, and $\Delta k = k^{(2\omega)} - 2k^{(\omega)}$. We note that if $\Delta k \neq 0$, the 2ω wave generated at some plane (say z_1) having propagated to some other plane (say z_2) is not in phase with the 2ω wave generated at z_2 . This results in the spatial interference pattern described by the RHS term in eqn.1.82. Two adjacent peaks of this pattern are separated by the so called "coherence length",

$$l_c = 2\pi/\Delta k = \frac{2\pi}{k^{(2\omega)} - 2k^{(\omega)}} \quad (1.83)$$

The coherence length l_c is thus a measure of the maximum crystal length that is useful in producing second harmonic power. Under ordinary circumstances it may be no longer than 10^{-2} cm, because the index of refraction $n(\omega)$ normally increases with ω so that Δk is given by

$$\Delta k = \frac{2\omega}{c} \left[n^{2\omega} - n^\omega \right] \quad (1.84)$$

since $k^{(\omega)} = \omega n^\omega/c$. The coherence length is thus

$$l_c = \frac{\pi c}{\omega(n^{2\omega} - n^\omega)} = \frac{\lambda}{2(n^{2\omega} - n^\omega)} \quad (1.85)$$

where λ is the free space wavelength of the fundamental beam. If we take a typical value of $\lambda = 1 \mu\text{m}$ and $n^{2\omega} - n^\omega \cong 10^{-2}$, we get $l_c \cong 100 \mu\text{m}$

The technique that is used widely to satisfy the phase matching condition, $\Delta k = 0$, takes advantage of the natural birefringence of anisotropic crystals. Using the relation $k^{(\omega)} = \omega \sqrt{\mu \epsilon_0} n^\omega$, the phase matching condition becomes

$$n^{2\omega} = n^\omega, \quad (1.86)$$

ie, the refractive indices should be equal at the fundamental and second harmonic frequencies. The refractive index of the extraordinary ray in a uniaxial crystal is given by

$$\frac{1}{n_e^{2\omega}(\theta)} = \frac{\cos^2 \theta}{n_o^2} + \frac{\sin^2 \theta}{n_e^2} \quad (1.87)$$

where θ is the angle between the propagation direction and the optic axis of the crystal. If $n_e^{2\omega} < n_o^\omega$, there exists an angle θ_m at which $n_e^{2\omega}(\theta_m) = n_o^\omega$. So if the fundamental beam at ω is launched along θ_m as an ordinary ray, the second harmonic beam will be generated along the same direction as an extraordinary ray.

The first second harmonic generation experiment was performed by Franken et al [59] in which a focused ruby laser beam at 694.3 nm was used to generate radiation at 347.15 nm in a crystalline quartz plate, with a conversion efficiency $\approx 10^{-8}$. The utilization of more efficient materials, higher intensity lasers and index matching techniques have resulted in conversion efficiencies approaching unity in recent years. The importance of SHG lies in the fact that it is one of the principal methods of effective conversion of infrared radiation into visible, and visible into ultraviolet.

1.3c Two-photon processes

The possibility of multiphoton excitations was theoretically proposed by Goeppert-Mayer as early as in 1931 [60]. A multiphoton process is a nonlinear optical phenomenon, in which the interaction between radiation and matter leads to the absorption or emission, or both, of not less than two photons per elementary act. Two-photon processes hold an important position among multiphoton phenomena. The important categories of two-photon processes are the absorption or emission of two photons, and scattering, in which one photon is absorbed and one emitted. In both, the overall process leading from an

initial state to a final state is described with the help of intermediate states. In two-photon absorption one photon is absorbed to give an intermediate state, and a second absorbed to complete the transition to the final state. There is the analogous process of two-photon emission. The selection rules are different for one- and two-photon processes; a transition which is one-photon forbidden may be two-photon allowed as seen in the case of many polyatomic molecules. Two-photon absorption has become a useful way of studying such forbidden transitions made possible by tunable narrow-band lasers. Two-photon emission is believed to occur in astrophysical systems [61], giving a mechanism of spontaneous decay in addition to one-photon processes allowed only in higher multipole order, such as by quadrupole radiation. Practical applications of two-photon absorption studies include the time-duration measurements of picosecond laser pulses by fluorescence trace analysis [62], investigation of third harmonic generation efficiencies [63] etc.. Prior to the advent of lasers, the only two-photon processes known were Raman and Rayleigh scattering. It is a general feature of multiphoton phenomena, familiar in many applications of second and higher order perturbation treatments including two-photon absorption and emission, that energy conservation does not apply to excitation of the intermediate (virtual) states. The second of the two steps, which destroys the intermediate state, can be thought of as so nearly simultaneous with the first that the uncertainty principle $\Delta E \Delta t \geq h/2\pi$ allows any excited state of the system to be momentarily produced. Hence two-photon and higher order phenomena should be clearly distinguished from multistep processes like excited state absorption where a real intermediate level is involved, and the event can be separated in time into distinct and independent acts.

In the following section we outline the quantum mechanical theory of matter-radiation interaction based on a perturbation approach, by which expressions for molecular transition probabilities are derived.

1.3d Time evolution and time dependent perturbations

The time development of a quantal system is governed by the time dependent Schrödinger equation

$$i\hbar \frac{\partial \psi(t)}{\partial t} = H \psi(t) \quad (1.88)$$

(where $\hbar = h/2\pi$). For a system in which the energy is conserved the Hamiltonian is time-independent and the formal solution of Eqn.1.88 may be written as

$$|\psi(t)\rangle = U(t, t_0) |\psi(t_0)\rangle \quad (1.89)$$

with

$$U(t, t_0) = \exp\left[-iH(t-t_0)/\hbar\right] \quad (1.90)$$

Here $U(t, t_0)$, the time evolution operator, is unitary and it acts on the state at t_0 to give the state at time t , allowing the time evolution to be viewed as the unfolding of a unitary transformation. Where a time-dependent perturbation $V(t)$ is added to the unperturbed hamiltonian H_0 , the total hamiltonian is time-dependent, and it is not possible to write a formal solution of the type given in Eqn.1.90. However, a solution for $U(t, t_0)$ may be found by a perturbation method, separating H into H_0 and a small perturbation $V = V(t)$. This perturbation approach is valid when the following conditions hold: H_0 constitutes the major part of the hamiltonian, is time-independent, and all its eigen states and orthonormalized eigen functions are known. V contains all the time dependence in H , and its role is to cause transitions, real or virtual, between the states of H_0 . Thus

$$H = H_0 + V(t) \quad (1.91)$$

where H_0 is time independent and assumed to have stationary states $|n\rangle$. In the case of interaction of radiation with matter we have

$$V = \vec{M} \cdot \vec{E} \quad (1.92)$$

where $\vec{M} = \sum_j e_j \vec{r}_j$ is the electric dipole moment of the atom and $\vec{E} = \vec{E}_0 \cos \omega t$ is the electric field associated with the electromagnetic radiation. The eigen value equation is

$$H_0 |n\rangle = E_n |n\rangle \quad (1.93)$$

If the system is in state $|\psi(t_0)\rangle$ at t_0 , and the perturbation V is zero, the evolution operator is $\exp\left[-iH_0(t-t_0)/\hbar\right]$. However, only those

changes produced by V are of physical interest. It is thus convenient to separate the term $\exp[-iH_0(t-t_0)/\hbar]$ as a factor and put

$$|\psi(t)\rangle = \exp[-iH_0(t-t_0)/\hbar] U_I(t, t_0) |\psi(t_0)\rangle . \quad (1.94)$$

$U_I(t, t_0)$, the evolution operator in the interaction picture, may then be interpreted as giving the modification in the time evolution due to the interaction V . Now, from Eqn.1.94,

$$\begin{aligned} i\hbar \frac{\partial |\psi(t)\rangle}{\partial t} &= H_0 \exp[-iH_0(t-t_0)/\hbar] U_I(t, t_0) |\psi(t_0)\rangle + \\ & i\hbar \exp[-iH_0(t-t_0)/\hbar] \frac{\partial}{\partial t} U_I(t, t_0) |\psi(t_0)\rangle \end{aligned} \quad (1.95)$$

and since

$$H |\psi(t)\rangle = (H_0 + V) \exp[-iH_0(t-t_0)/\hbar] U_I(t, t_0) |\psi(t_0)\rangle, \quad (1.96)$$

by equating 1.95 and 1.96 and operating on both sides of the resultant equation with $\exp[iH_0(t-t_0)/\hbar]$ we obtain

$$\begin{aligned} i\hbar \frac{\partial}{\partial t} U_I(t, t_0) |\psi(t_0)\rangle &= \exp[iH_0(t-t_0)/\hbar] V \exp[-iH_0(t-t_0)/\hbar] \\ & U_I(t, t_0) |\psi(t_0)\rangle \end{aligned} \quad (1.97)$$

Eqn.1.97 holds for any $|\psi(t_0)\rangle$ and may therefore be written as an operator equation:

$$i\hbar \frac{\partial}{\partial t} U_I(t, t_0) = V_I(t) U_I(t, t_0) \quad (1.98)$$

where

$$V_I(t) = \exp[iH_0(t-t_0)/\hbar] V \exp[-iH_0(t-t_0)/\hbar] \quad (1.99)$$

$V_I(t)$, the perturbation in interaction representation, is the unitary transform of V by the operator $\exp[-iH_0(t-t_0)/\hbar]$ so that the problem of evaluating the time evolution of a system reduces to solving the

equation of motion 1.98 for $U_I(t, t_0)$. The solution of this equation is found to be

$$U_I(t, t_0) = 1 + \sum_{n=1}^{\infty} (i\hbar)^{-n} \int_{t_0}^t dt_1 \int_{t_0}^{t_1} dt_2 \dots \int_{t_0}^{t_{n-1}} dt_n V_I(t_1) \dots V_I(t_n) \quad (1.100)$$

which is a power series in terms of the interaction V_I . This important result forms the starting point for the study of interaction of light with atoms and molecules.

We can use Eqn.1.100 to calculate the probability amplitude of finding the system in state $|f\rangle$ at a time t due to the interaction V switched on at time t_0 , given that at t_0 the system was in state $|i\rangle$. The probability amplitude is

$$\langle f | \exp\left[iH_0(t-t_0)/\hbar \right] |\psi(t)\rangle = \langle f | U_I(t, t_0) |i\rangle \quad (1.101)$$

Let us consider the case of a *constant* perturbation V (Fig.1.11), such that

$$\begin{aligned} H &= H_0 && \text{for } t < t_0 \\ &= H_0 + V && \text{for } t_0 \leq t \leq \tau \\ &= H_0 && \text{for } t > \tau \end{aligned} \quad (1.102)$$

It is to be remembered that V_I is time dependent. Let $|i\rangle$ and $|f\rangle$ be eigen states of H_0 with energies E_i and E_f respectively. In the zeroth order, ie, with the first term only of eqn.1.100,

$$U_I(t, t_0) = 1 \quad (1.103)$$

and

$$\langle f | U_I(t, t_0) |i\rangle = 0 \quad (1.104)$$

because of the orthogonality of $|i\rangle$ and $|f\rangle$. Thus the probability amplitude of finding the system in state $|f\rangle$ vanishes in the zeroth order.

In the first order the amplitude is

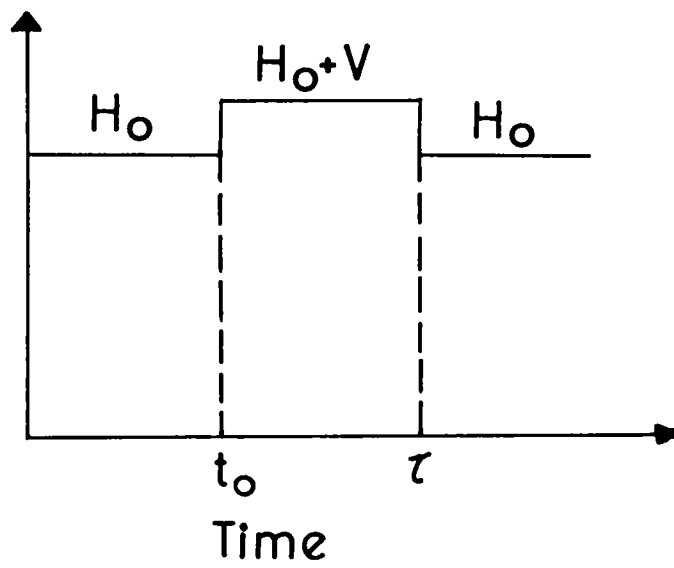


Fig.1.11 :The constant perturbation V , existing in the time interval $t_0 \leq t \leq \tau$.

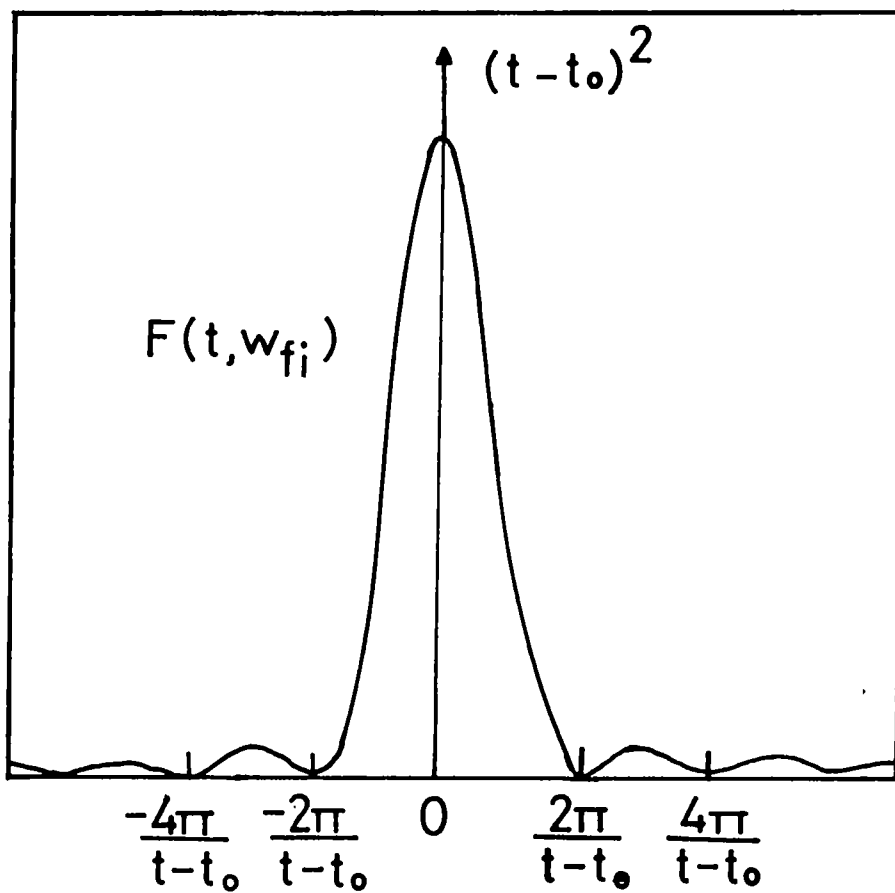


Fig.1.12 :Trigonometric weighting function for the transition probability $P_{fi}(t)$ as a function of the transition frequency.

$$\langle f | U_1(t, t_0) | i \rangle = (i\hbar)^{-1} \langle f | \int_{t_0}^t V_I(t_1) dt_1 | i \rangle \quad (1.105)$$

and using equation 1.99 in 1.105 the probability $P_{fi}(t)$ of finding the system in state $|f\rangle$ at time t is given by

$$P_{fi}(t) = |\langle f | U_I(t, t_0) | i \rangle|^2 = \frac{|\langle f | V | i \rangle|^2}{\hbar^2} \left[\frac{4 \sin^2 \omega_{fi}(t-t_0)/2}{\omega_{fi}^2} \right] \quad (1.106)$$

where

$$\omega_{fi} = (E_f - E_i)/\hbar \quad (1.107)$$

is the transition frequency. The trigonometric function in eqn.1.106 is shown in Fig.1.12 for fixed t . The height of the main peak at $\omega_{fi} = 0$ is $(t-t_0)^2$ and the halfwidth of the band is $2\pi/(t-t_0)$. Assuming that $\langle f | V | i \rangle$ is not zero, we may conclude that the probability for the transition $|f\rangle \rightarrow |i\rangle$ is small unless the energy interval lies within the bandwidth $4\pi\hbar/(t-t_0)$.

For two photon processes the leading contribution to the matrix element is of second order in the interaction term; ie, the second order term of $U_I(t, t_0)$. Let $|i\rangle$ and $|f\rangle$ be the initial and final states of a two photon process. The probability amplitude for finding the system in $|f\rangle$ at a time t , given that at $t=0$ the system was in state $|i\rangle$, is

$$\begin{aligned} & (i\hbar)^{-2} \langle f | \int_0^t dt_1 \int_0^{t_1} dt_2 V_I(t_1) V_I(t_2) | i \rangle \\ &= (i\hbar)^{-2} \langle f | \int_0^t dt_1 \exp[iH_0 t_1/\hbar] V \exp[-iH_0 t_1/\hbar] \times \\ & \quad \int_0^{t_1} dt_2 \exp[iH_0 t_2/\hbar] V \exp[-iH_0 t_2/\hbar] | i \rangle \end{aligned} \quad (1.108)$$

and can be shown to be equal to

$$(i\hbar)^{-1} \sum_I \frac{\langle f|V|I\rangle \langle I|V|i\rangle}{E_{iI}} \int_0^t \exp\left[iE_{fi}t_1/\hbar\right] dt_1 \quad (1.109)$$

such that the two-photon transition probability becomes proportional to $\sum_I |\langle f|V|I\rangle \langle I|V|i\rangle|^2$ where the I summation is over a complete set of intermediate eigen states $|I\rangle$ of H_0 , which are not resonant with the initial or final states, and $E_{fi} = E_{fI} + E_{Ii}$. Thus the rate of two-photon process will be proportional to the square of pump intensity through V. The appearance of the intermediate states in Eqn. 1.109 reflects the possibility of attaining the final state via a series of intermediate states which are connected to the initial and final states by non-zero matrix elements. It must be emphasized here, however, that any multiphoton transition cannot, in general, be divided into a temporal sequence of events. It would be incorrect to assume that first one photon is absorbed and then the next one. In that case the transition is equivalent to two single photon transitions.

The above analysis can be extended to calculate the higher order transition probabilities by choosing the corresponding term from the expansion for $U_1(t, t_0)$ and following the same methodology.

PART IV PROPERTIES OF LASER DYES

1.4a. General properties of organic dyes

Organic compounds, defined as hydrocarbons and their derivatives, can be subdivided into saturated and unsaturated compounds. Unsaturated compounds are characterized by at least one double or triple bond. These multiple bonds have a profound effect on the chemical reactivity and spectroscopic properties of the molecule. Saturated organic compounds usually absorb at wavelengths below 160 nm and the corresponding energies exceed the dissociation energy of most chemical bonds leading to possible photochemical decomposition of the molecule. Hence such compounds are not very suitable as the active medium in lasers. In unsaturated compounds all bonds are formed by σ

electrons; double or triple bonds in addition use π electrons for bonding. A π bond is formed by the lateral overlap of the π electron orbitals which is maximum when the symmetry axes of the orbitals are parallel. Hence in this position bond energy is highest and the energy of the molecule minimal, thus giving a planar molecular skeleton of high rigidity. If two double bonds are separated by a single bond as in the molecule butadiene (Fig.1.13) the two double bonds are called conjugated. Compounds with conjugated double bonds also absorb light at wavelengths above 200 nm. All dyes in the proper sense of the word, mean compounds having a high absorption in the visible part of the spectrum and possessing several conjugated double bonds.

The thermal and photochemical stability of dyes is of utmost importance for laser applications. Thermal stability is closely related to the long wavelength limit of absorption. A dye absorbing in the near infrared has a low lying excited singlet state and even slightly lower than that, a metastable triplet state. Since the triplet state has two unpaired electrons, it is highly reactive and most of the dye molecules that reach this level by thermal excitation will react with solvent molecules, dissolved oxygen, impurities or other dye molecules to yield decomposition products. One can show that preparation of a dye absorbing beyond 1700 nm and stable at room temperature is unlikely. Thus dye laser operation at room temperature in the infrared is restricted to wavelengths not exceeding much beyond 1000 nm. On the other hand the minimum wavelength attainable in any dye laser system cannot be less than 200 nm since below this wavelength photochemical decomposition will effectively compete with radiative de-activation of the molecule.

An important subdivision of dyes is into ionic and uncharged compounds. Most aromatics are uncharged (anthracene, perylene, pyrene, butadiene etc.). They usually have relatively low melting points, relatively high vapour pressures and good solubility in nonpolar solvents. Cationic and anionic dyes have high melting points, very low vapour pressures and good solubility in more polar solvents like alcohols. Many dyes (for example, Fluorescein) can exist as cationic, neutral and anionic molecules depending on the pH of the solution (Fig.1.14).

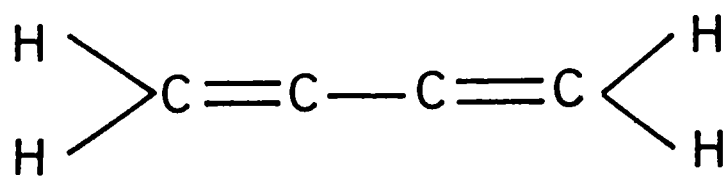
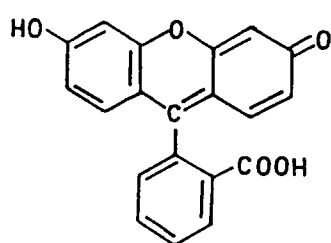
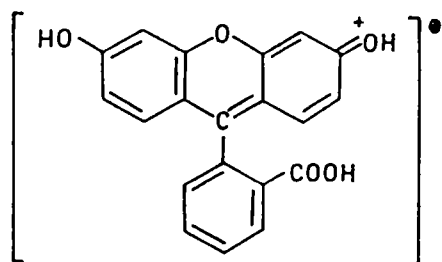


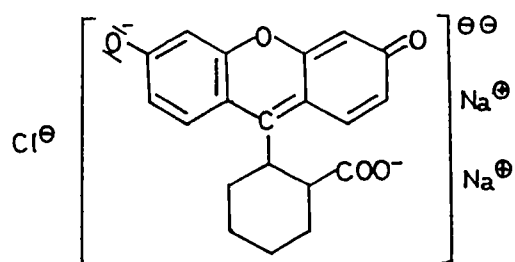
Fig.1.13 :Conjugated double bonds in a butadene molecule.



Neutral form
(alcoholic solution)



Cationic form
(hydrochloric acid solution)



Di-anionic form
sodium hydroxide solution

Fig.1.14 :Cationic, neutral and anionic forms of the Fluorescein molecule.

1.4b. Absorption of light by organic dyes

Absorption of light by dyes can be understood on a semiquantitative basis if we take a highly simplified quantum-mechanical model, such as the free electron gas model [64]. This model takes into account the planarity of the dye molecules, with all atoms of the conjugated chain lying in a common plane and linked by σ bonds. The π electrons will form a charge cloud above and below this plane along the conjugated chain. The centres of the upper and lower lobes of the π electron cloud are about one half bond length away from the molecular plane. Hence the electrostatic potential for any single π electron moving in the field of the rest of the molecule may be considered constant, provided all bond lengths and atoms are the same (Fig.1.15). The energy E_n of the n^{th} eigen state of this electron is given by

$$E_n = h^2 n^2 / 8 m L^2 , \quad (1.110)$$

where h is the Planck's constant, m is the mass of the electron, n is the quantum number giving the number of antinodes of the eigenfunction along the chain and L is the length of the conjugated chain. Thus if we have N electrons, the lower $1/2 N$ states will be filled with two electrons each according to Pauli's exclusion principle, while all higher states are empty. The longest wavelength absorption band then corresponds to a transition from the highest occupied to the lowest empty state with

$$\Delta E_{\min} = \frac{h^2}{8 m L^2} (N+1) = \frac{hc_0}{\lambda_{\max}} \quad (1.111)$$

such that

$$\lambda_{\max} = \frac{8mc_0}{h} \frac{L^2}{N+1} . \quad (1.112)$$

This indicates that to a first approximation the position of the absorption band is determined only by the chain length and by the number of π electrons N . This simple formula predicts the absorption wavelengths of many symmetrical cyanine dyes satisfactorily [65]. A perturbation treatment applied to the above theory makes it useful for analyzing molecules with non-identical atoms and variable bondlengths

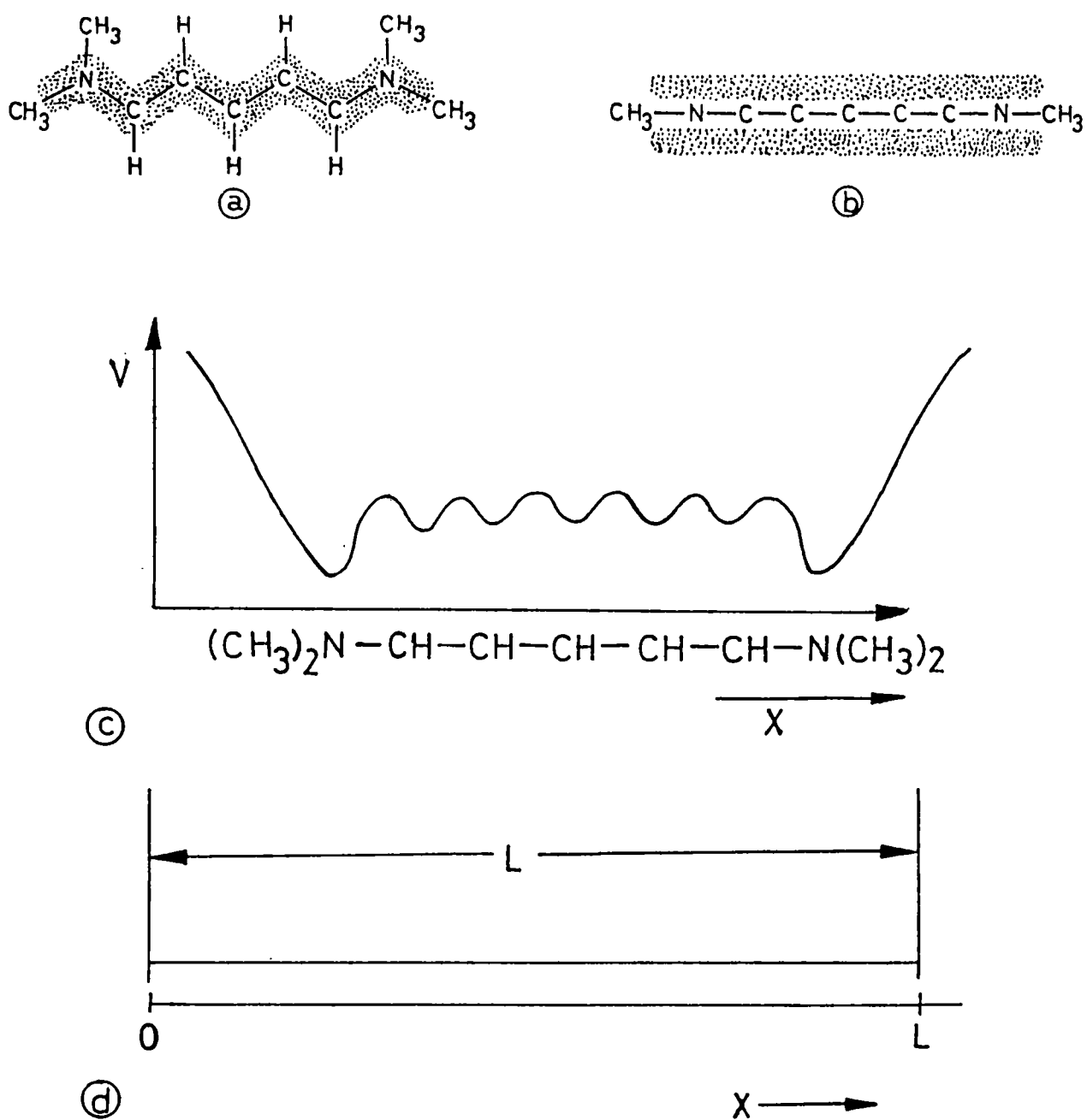


Fig.1.15 : (a) The π -electron cloud of a simple cyanine dye seen from above the molecular plane, (b) the same as seen from the side, (c) the potential energy V of a π -electron moving along the zig-zag chain of carbon atoms in the field of the rump molecule, (d) Simplified potential energy trough; L - Length of the π -electron cloud in (a) as measured along the zig-zag chain.

along the conjugated chain as well. The oscillator strength of the absorption bands can also be calculated using the free-electron model. Nevertheless, a quantitative description of absorption by small molecules of high symmetry like benzene and naphthalene demands a modification of the free electron model taking into account the repulsion between electrons, as suggested by Forsterling et al [88].

A peculiarity of the spectra of organic dyes, as opposed to atomic and ionic spectra, is the width of the absorption bands, which usually covers several tens of nanometers. Recalling that a typical dye molecule may contain fifty or more atoms giving rise to about 150 normal modes of vibration of the molecular skeleton, this is immediately comprehensible. These vibrations, together with their overtones, densely cover the spectrum between a few wavenumbers and 3000 cm^{-1} . The change in electron density associated with an electronic transition will change the bond length, and the molecule will experience a vibration about the new equilibrium position, with an amplitude equal to the change in bond length of the order of 0.002 nm. A molecular skeletal vibration is excited in this way. In the general case of a large dye molecule many normal vibrations of differing frequencies are coupled to the electronic transition. The individual lines of such vibrational series will be broadened by collisional and electrostatic perturbations caused by the surrounding solvent molecules. As a further complication, every vibronic sublevel of every electronic state, including the ground state, has a ladder of rotationally excited sublevels superimposed on it. These are extremely broadened because of the frequent collisions with solvent molecules which hinder the rotational movement. Thus what we find is a quasicontinuum of energy levels superimposed on every electronic state as shown in Fig.1.16. The population of these levels in contact with the thermalised solvent molecules is determined by a Boltzmann distribution. After an electronic transition leading to a non-equilibrium Franck-Condon state, the approach to thermal equilibrium is very fast in liquid solutions at room temperature. The reason is that a large molecule experiences at least 10^{12} collisions/sec with solvent molecules, so that equilibrium is reached in a time of the order of 1 ps. Absorption and emission are practically continuous all over the respective bands : Absorption and fluorescence spectra become mirror images of each other by reflection at the

wavenumber of the purely electronic transition. This condition exists, since the emissive transitions start from the vibrational ground state of the first excited electronic state S_1 and end in vibrationally excited sublevels of the electronic ground state. The resulting typical form of the absorption and fluorescence spectrum of an organic dye is given in Fig.1.17.

1.4c. Deactivation pathways for excited dye molecules

The absorption of optical energy raises the dye molecule typically to one of the excited singlet states, from which they relax within picoseconds to the lowest vibronic level of S_1 , i.e., the upper lasing level. The important processes that can take place from this level are the following:

- (a) Fluorescence
- (b) Internal conversion
- (c) Intersystem crossing, leading to phosphorescence and/or triplet-triplet absorption, and
- (d) Excited state absorption.

1.4c1. Fluorescence

Generally, when a dye molecule is optically excited to any one of the excited singlets, it nonradiatively decays to the S_1 level in a very short time of the order of a few picoseconds. Then fluorescence occurs, which is the emission of optical radiation from S_1 , leaving the molecule in a vibronic level of the ground state S_0 . This is the reason why fluorescence quantum spectra of dyes generally do not depend on the excitation wavelength. The only known exception to these general rules is the aromatic molecule azulene and its derivatives. The fluorescence of this molecule arises from the $S_2 \longrightarrow S_0$ transition [53]. Fluorescence can be spontaneous and/or stimulated. The radiative lifetime τ_{rf} is connected to the Einstein coefficient for spontaneous emission A and the oscillator strength f of the pertinent absorption band by the relation [67]

$$A = 1/\tau_{rf} = (8\pi^2 \mu^2 e_0^2 / m_0 c_0) (\bar{\nu})^2 f \quad (1.113)$$

where

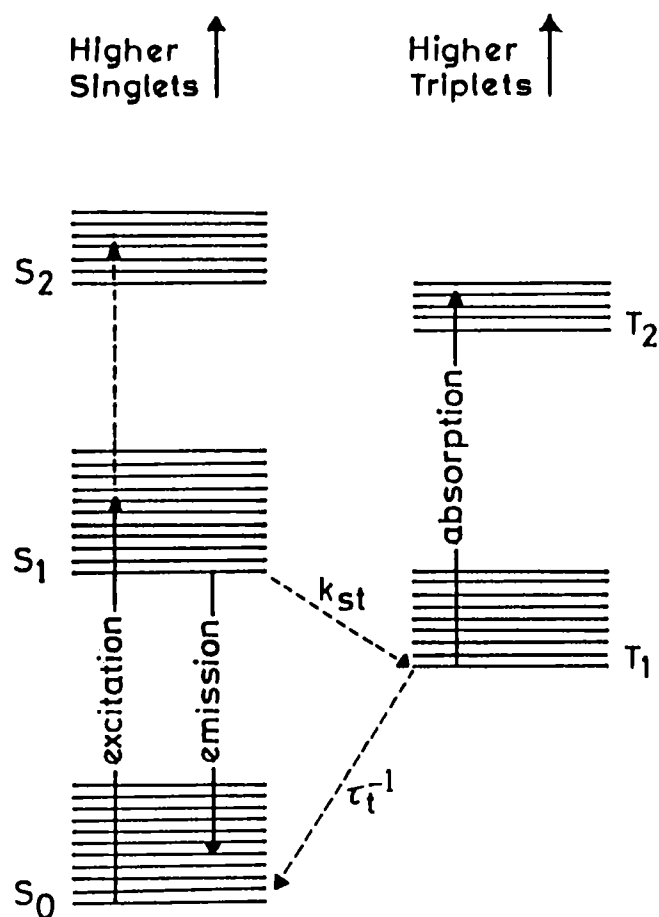


Fig.1.16 : Schematic energy level diagram for a typical dye molecule, showing the singlet and triplet levels. k_{st} is the intersystem crossing rate and τ_t is the lifetime of the T_1 level.

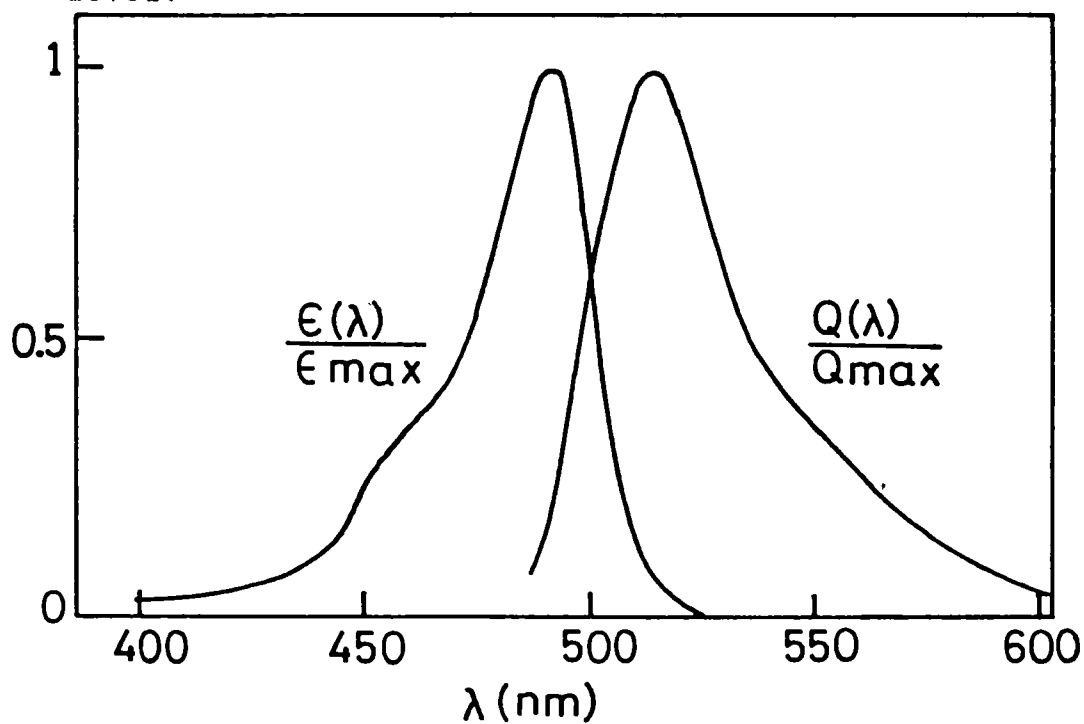


Fig.1.17 : Absorption spectrum $\epsilon(\lambda)/\epsilon_{max}$, and fluorescence spectrum $Q(\lambda)/Q_{max}$ of a typical dye molecule (fluorescien sodium in water).

μ = refractive index of solution,
 e_0 = charge, m_0 = mass of the electron,
 c_0 = velocity of light, and
 $\bar{\nu}$ = wave number of the centre of absorption band.

This equation is valid if the half width of the emission band is small and its position is not shifted significantly from that of the absorption band. However if the fluorescence spectrum is broad with considerable Stokes shift then τ_{rf} can be computed using the relation [68]

$$\frac{1}{\tau_{rf}} = 2.88 \times 10^{-9} \mu^2 \frac{\int F(\bar{\nu}) d\bar{\nu}}{\int \epsilon(\bar{\nu})^{-3} F(\bar{\nu}) d\bar{\nu}} \int_{\bar{\nu}_1}^{\bar{\nu}_2} \frac{\epsilon(\bar{\nu}) d\bar{\nu}}{\bar{\nu}} \quad (1.114)$$

where $F(\bar{\nu}) = dQ/d\bar{\nu}$ is the fluorescence spectrum in quanta Q per wavenumber and $\epsilon(\bar{\nu})$ is the molar decadic extinction coefficient. The limits $\bar{\nu}_1$ and $\bar{\nu}_2$ indicate that the integration is to be carried out over the longest wavelength absorption band.

1.4c2. Internal conversion

Internal conversion is the process of nonradiative decay between the higher excited and lower singlets, $S_n (n > 1) \longrightarrow S_1$. This process is very fast, taking place in less than 10^{-11} sec. $S_1 \longrightarrow S_0$ internal conversion also is possible in dyes [53,69], the degree of which can vary by many orders of magnitude depending on the molecular structure of the dye and properties of the solvent.

1.4c3. Intersystem crossing

A competitive de-excitation process that can take place is the generally forbidden transition from singlet to triplet levels ($S \longrightarrow T$) called intersystem crossing in which there is a change of spin. These transitions can be induced by internal perturbations (spin-orbit coupling, substituents containing nuclei of high atomic number etc.) as well as by external perturbations (paramagnetic collision partners like O_2 molecules in the solution, or solvent molecules containing nuclei of high atomic number). The loss of energy from the lowest triplet to the ground state occurs by a radiative process called

phosphorescence. Phosphorescence lifetimes are large, since triplet levels are metastable.

1.4c4. Excited state absorption (ESA)

As with the ground state S_0 , there is a well defined absorption spectrum associated with molecules that are in the excited states S_1 or T_1 . ESA spectra for $S_1 \longrightarrow S_n$ transitions of cyanine [70], phthalocyanine [71] and xanthene [72] dyes have been reported. $S_1 \longrightarrow S_n$ absorptions give rise to appreciable losses when laser dyes are pumped at high power densities [73]. $T_1 \longrightarrow T_n$ absorption details also have been reported for aoridines [74], rhodamines [75] etc.. Triplet absorption spectra of several compounds have been recorded by various workers [76-78].

1.4d. Environmental effects

The relative contributions of various processes listed above are significantly affected by the environment of the dye molecule such as the solvent and other dye molecules. For example, it is found that fluorescence can be strongly quenched by certain anions [79,80]. Since in many laser dyes the chromophore carries a positive charge, these dyes invariably have an anion, commonly chloride or iodide. The quenching ability which is very strong in the case of iodide (I^-) decreases in the order: Iodide (I^-), thiocyanate (SCN^-), bromide (Br^-), chloride (Cl^-) and perchlorate (ClO_4^-). Hence the use of perchlorate as the anion will be often preferable to the common chloride, as has been shown by Bergman et al [81] in the case of the acidic umbelliferone laser. It is suggested that the excited state of the dye is quenched by a charge-transfer interaction in this case. Whether the fluorescence efficiency is affected by the anion accompanying the chromophore depends on the concentration and polarity of the solvent. For example, anion quenching is not observed for the dyes R6G iodide and R6G perchlorate in 10^{-4} moles/lit solutions in ethanol. However for the same concentration in the polar solvent chloroform, fluorescence of R6G iodide is almost completely quenched while that of R6G perchlorate is not affected [82]. Apparently the dye salts are fully dissociated in the polar solvent ethanol, but practically undissociated in chloroform. Hence in ethanol the

quenching anions do not have sufficient time to reach the excited dye molecules during their lifetime, whereas in chloroform, they are immediately available for a reaction. Anion quenching can be externally induced as well, by adding certain compounds [83]. Another observation has been that heavy-atom solvents like iodomethane or iodobenzene are not suitable for a laser dye, due to an increased intersystem crossing rate, building up the triplet population [53,84,85].

Another mechanism by which the excited states, singlet as well as triplet, are quenched externally can operate if the quenching molecule has a singlet or triplet level of energy equal to or lower than that of the state to be quenched [53,80]. This energy-transfer quenching process is very efficient in liquid solution where the reactants can approach each other very closely. This mechanism is particularly useful since it can be used for quenching the triplet states in dyes, which are undesirable for laser action. Some common quenching agents are, ubiquitous molecular oxygen, cyclooctotetraene, cycloheptatriene etc.. Several other compounds have also been reported to quench triplets of laser dyes [86].

It has long been known that organic dyes in aqueous solution have a tendency to form dimers and higher aggregates especially at high concentrations and low temperatures, which make themselves known through a distinctly different absorption spectrum. In alcoholic solutions also aggregation is found to occur [87,88]. The dimers usually have a strong absorption band at shorter wavelengths than the monomers and often an additional weaker band at the long-wavelength side of the monomer band (Fig.1.18). They are generally weakly fluorescent, or not at all. Not only is part of the pump light absorbed by the nonfluorescent dimers, but they also increase the cavity losses owing to their long-wavelength absorption band, which is in the same region as the fluorescence of the monomers. Various causes have been suggested to account for the aggregation of dye molecules. In aqueous solutions the most probable one seems to be the hydrogen bonding between dye molecules. An interaction of the fluorophore with the accompanying anion is believed to be responsible for dimerization in some cases. In Rhodamine dyes the dimerization tendency has been found to increase with the number and size of alkyl substituents.

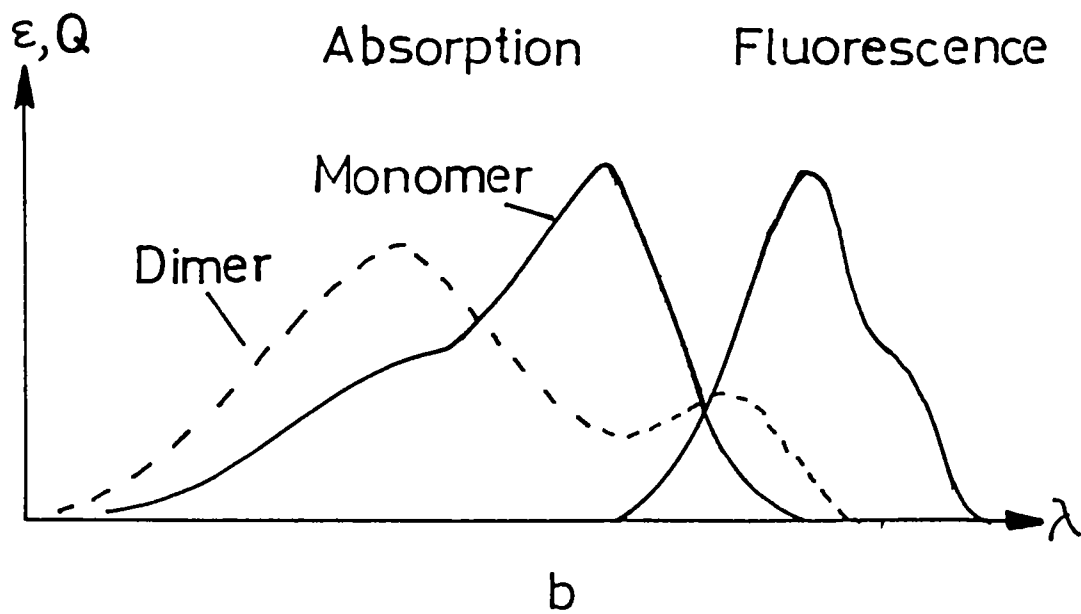
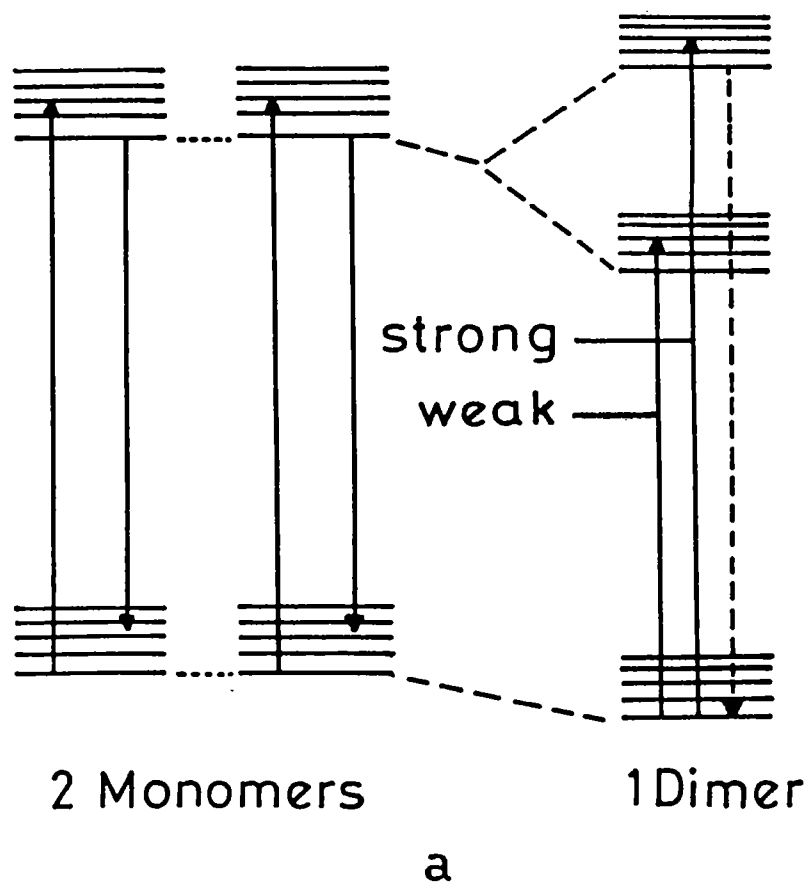


Fig.1.18 : (a) Energy levels of two monomers and the dimer molecule formed by them; (b) the resulting spectra.

It is possible to suppress the aggregation of organic dyes in aqueous solution by the addition of organic compounds like N,N-dimethyldodecylamine-N-oxide, hexafluoroisopropanol, N,N-dipropyl-acetamide etc.[82,89]. Aggregation effects in alcoholic solutions occur only at very high concentrations (typically $> 5 \times 10^{-3}$ moles/lit.), which is above the usual operating concentrations in dye lasers.

Excited state reactions also can be important in some situations. There is usually a strong interaction between excited and ground state molecules which shows up at high concentrations, For example in high concentration solutions of R6G in ethanol (10^{-2} molar) the fluorescence is strongly quenched due to collisions of the excited dye molecules with those in the ground state [80]. However in pyrene and some other compounds a new fluorescence band appears at high concentrations which is attributed to dimers that exist only in the excited state (excimers) [53,69]. Following the emission of a photon, excimers immediately dissociate into ground state monomers. In a somewhat similar fashion, an excited molecule may react with a molecule of a different compound (solvent or other solute) to form an excited complex - exciplex - which, on radiative de-excitation, decomposes immediately into the components. Since the ground state of excimers and exciplexes is unstable these species are ideal lasing compounds, provided the fluorescing efficiency is high and no disturbing triplet effects occur.

PART V

INVESTIGATION OF NONLINEAR ABSORPTIONS BY PHOTOACOUSTICS AND FLUORESCENCE

Nonlinear optical absorptions in several media have been investigated by various research workers [90-95]. Apart from a direct measurement of the light absorbed using an absorption spectrophotometer [96,97], two experimental methods are generally being used for identifying such phenomena. One is the observation of antistokes fluorescence (ASF) resulting from radiative de-excitations of the excited state, and the other is the direct monitoring of the non radiative relaxation processes by the recently introduced

photoacoustic (PA) technique. In ASF, a pump laser beam of longer wavelength is absorbed by the sample, and a weak "antistokes" fluorescence emitted at a shorter wavelength is detected, which is monitored as a function of excitation intensity and wavelength [98-100]. For doing an ASF experiment successfully, the emission should be detectable by a sensitive detector, indicating the necessity of a reasonably good radiative transition probability between the energy levels involved. In the PA technique, the PA spectrum is recorded as a function of the excitation intensity and wavelength [50]. Here also the PA signal generated should be detectable, implying that there should be a strong nonradiative coupling between the energy levels of interest. Obviously, the requirements for PA and ASF are opposite to each other.

1.5a Nonlinear Fluorescence from dye solutions

Earlier investigations on the molecular structure of laser dyes have given reliable models for the transitions occurring between the vibrational manifolds of various electronic energy states. A level diagram for the $S_0 \rightarrow S_1$ transition is given in Fig.1.19. The dyes under consideration have $S_0 \rightarrow S_1$ absorption levels matching with the present 532 nm laser radiation. When pumped by 1064 nm radiation molecules are excited by TPA from the ground state S_0 (level 1) to the Franck Condon level 2 in the first excited singlet manifold S_1 , followed by a fast relaxation to level 3. Three photon absorption from S_0 can occur as well, to the excited state S_2 , if the energy is matched. Generally de-excitation to S_0 occurs through spontaneous emission, stimulated emission and radiationless transition. Relaxation by stimulated emission will be at the pump frequency, ν_L . The pump laser may induce excited state absorption also, from S_1 to higher levels as shown in the figure. The PA signals are generated from non radiative relaxations between different levels. In this model, the non radiative pathways are (a) transitions from $S_n \rightarrow S_1$ ($n > 1$), (b) relaxation within the vibronic manifold of S_1 and (c) relaxation from the Franck Condon state to the lowest vibrational level in S_0 . Another weak channel for non radiative relaxation is the internal conversion from S_1 to S_0 . Intersystem crossing from singlet to triplet levels is neglected since the pump pulses are assumed to be short (≈ 10 ns).

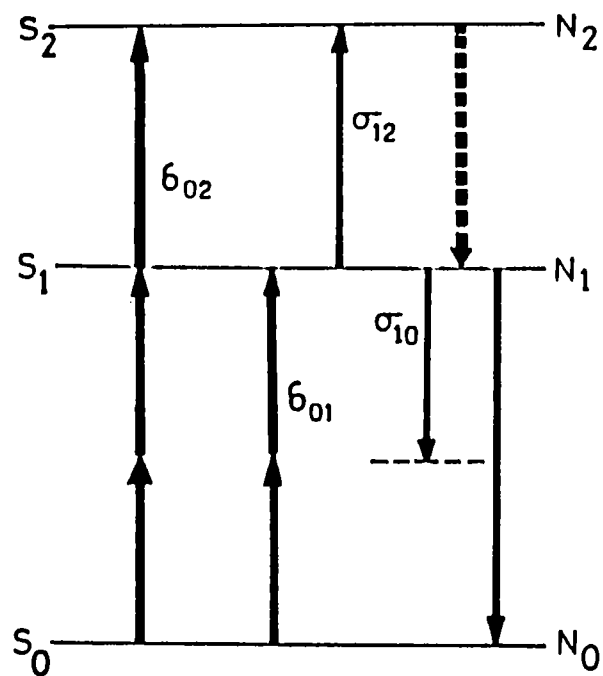


Fig.1.19 : The energy level diagram for the transitions between S_0 , S_1 and S_2 in Rhodamine 6G dye molecule at the pump wavelength of 1064 nm (See text).

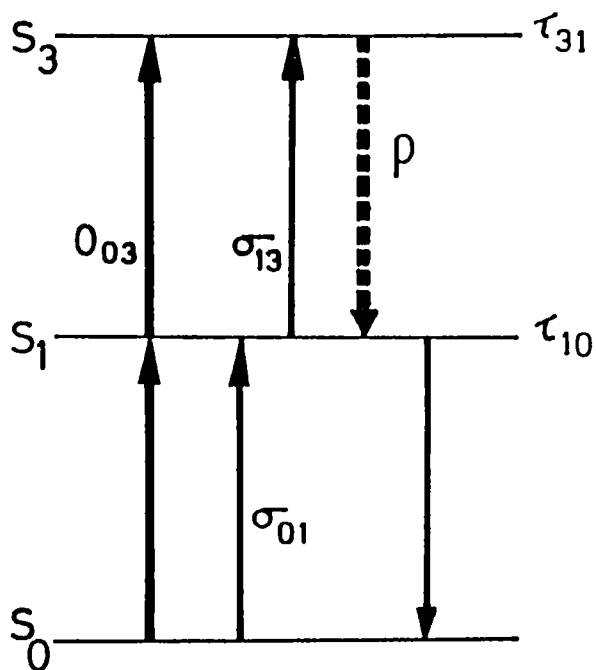


Fig.1.20 : The energy level diagram for the transitions between S_0 , S_1 and S_3 in Rhodamine 6G dye molecule at the pump wavelength of 532 nm (See text).

The cross section δ for an n-photon absorption process is defined

as

$$\delta = I_{FM} / q_{FM} N I_0^n \quad (1.115)$$

where I_{FM} is the fluorescence intensity (photons $\text{cm}^{-2} \text{sec}^{-1}$), I_0 is the excitation intensity (photons $\text{cm}^{-2} \text{sec}^{-1}$), N is the number of molecules per unit volume and q_{FM} is the fluorescence quantum efficiency which is assumed to be the same as that for one-photon absorption. The parameter δ is expressed in units of $\text{cm}^{2n} \text{s}^{n-1} \text{photons}^{-(n-1)} \text{molecule}^{-1}$.

We note that if N_0 is the number of ground state molecules before excitation, then the S_1 state population (N_1) can be expressed (for 1064 nm irradiation) by the rate equation

$$\begin{aligned} \frac{dN_1}{dt} = & N_0 \delta_{01} F^2 + N_0 \rho \delta_{02} F^3 - N_1(1-\rho) \sigma_{12} F \\ & - N_1 \sigma_{10} F - N_1 \tau_{10}^{-1} \end{aligned} \quad (1.116)$$

where F is the laser flux, δ_{01} and δ_{02} are the molecular absorption cross-sections for $S_0 \rightarrow S_1$ (two-photon) and $S_0 \rightarrow S_2$ (three-photon) transitions respectively, σ_{12} and σ_{10} are the one photon cross-sections shown in the figure, τ_{10} is the radiative lifetime of the S_1 state and ρ is the fraction of molecules relaxing to S_1 from S_2 level. The $S_2 \rightarrow S_1$ nonradiative transition is extremely fast, and hence highly probable, so that $\rho \approx 1$. Various terms in the above equation have the following meanings:

$N_0 \delta_{01} F^2$ is the no. of molecules /unit volume/sec, getting excited to the S_1 level from S_0 by TPA,

$N_0 \rho \delta_{02} F^3$ is the no. of molecules /unit volume/sec, getting excited to the S_2 level from S_0 by three photon absorption and relaxing from there to N_1 ,

$N_1(1-\rho) \sigma_{12} F$ is the no. of molecules /unit volume/sec, getting lost by excited state absorption from S_1 to S_2 ,

$N_1 \sigma_{10} F$ is the no. of molecules /unit volume/sec, undergoing stimulated emission from S_1 ,

$N_1 \tau_{10}^{-1}$ is the no. of molecules /unit volume/sec undergoing spontaneous emission from S_1 to S_0 .

Since $N_1 \sigma_{10} F$ can be neglected being very small [101], Eqn.1.116 becomes

$$\frac{dN_1}{dt} = N_0(\delta_{01} F^2 + \rho \delta_{02} F^3) - N_1[(1-\rho) \sigma_{12} F + \tau_{10}^{-1}] \quad (1.117)$$

Assuming the pump pulse to be square shaped, and long in comparison with τ_{10} , we can write the steady state equation

$$\frac{dN_1}{dt} = 0, \quad (1.118)$$

giving

$$N_0(\delta_{01} F^2 + \rho \delta_{02} F^3) = N_1[(1-\rho) \sigma_{12} F + \tau_{10}^{-1}] \quad (1.119)$$

such that the S_1 state population becomes

$$N_1 = \frac{N_0 (\delta_{01} F^2 + \rho \delta_{02} F^3)}{[(1-\rho) \sigma_{12} F + \tau_{10}^{-1}]} \quad (1.120)$$

Since the ASF intensity (I_F) will be proportional to N_1 , as seen from Eqn.1.120 we can expect cubic and quadratic dependences of I_F on the laser flux F , based on the relative strengths of δ_{01} and δ_{02} .

1.5b Generation of photoacoustic signals in dye solutions

The study of TPA and higher order multiphoton excitations in various compounds has been mostly based on the observation of ASF induced by the same from an excited electronic state, usually at a shorter wavelength than the pump wavelength. However, in organic dyes the fluorescence quantum yield of ASF from the S_n ($n > 1$) states is negligible since these higher excited states are immediately

depopulated due to their strong non radiative coupling to the S_1 state. These non radiative relaxations $S_n \rightarrow S_1$ ($n>1$) should give rise to photoacoustic signals of high amplitudes as compared to the weak ASF signal. Let us consider a level diagram for TPA and ESA as shown in Fig.1.20, where an energy equivalent of two 532 nm photons will raise the molecule to the S_3 level. The notations are identical to the previous figure except that the subscripts are different here. We can see that the corresponding rate equations are

$$\frac{dN_1}{dt} = N_0 \sigma_{01} F + N_0 \delta_{03} \rho F^2 - N_1 (1-\rho) \sigma_{13} F - N_1 \tau_{10}^{-1} \quad (1.121)$$

and

$$\frac{dN_3}{dt} = N_0 \delta_{03} F^2 - N_3 \tau_{31}^{-1} + N_1 \sigma_{13} F \quad (1.122)$$

At steady state $dN_1/dt = dN_3/dt = 0$, so that

$$N_1 = \frac{N_0 (\sigma_{01} F + \delta_{03} \rho F^2)}{[(1-\rho) \sigma_{13} F + \tau_{10}^{-1}]} \quad (1.123)$$

and

$$N_3 = \frac{N_0 \delta_{03} F^2 + N_1 \sigma_{13} F}{\tau_{31}^{-1}} \quad (1.124)$$

Recalling that the PA amplitude is proportional to N_3 , we note a linear and quadratic dependence of PA on the pump laser intensity from Eqn.1.124. The slope of a typical $\log N_3$ versus $\log F$ plot for various input parameter values can be conveniently estimated through numerical methods. An interesting observation which is not immediately clear from Eqn.1.124 alone is that, even if δ_{03} is negligibly small, the PA signal can show a quadratic dependence on F provided σ_{13} has a significant value.

CHAPTER 1 - REFERENCES

- [1] Wendlandt W W and H G Hecht, "*Reflectance spectroscopy*", Wiley, New York (1966)
- [2] Wilks P A Jr. and T Hirschfeld, *Appl.spectroscop. Rev.* **1**, 99 (1968)
- [3] Wright G B (ed.), "*Light scattering in solids*", Springer-Verlag, Berlin (1969)
- [4] Bell A G, *Philos.Mag.* **11**, 510 (1881)
- [5] Tyndall J, *Proc.R.Soc.Lond.* **31**, 307 (1881)
- [6] Roentgen W C, *Philos.Mag.* **11**, 308 (1881)
- [7] Mercadier M E, *C R Hebd.Serv.Acad.Sci.* **92**, 409 (1881)
- [8] Preece W H, *Proc.R.Soc.Lond.* **31**, 506 (1881)
- [9] Viengerov M L, *Dokl.Akad.Nauk.SSSR* **19**, 687 (1938)
- [10] Luft K F, *Z.Tech.phys.* **24**, 97, (1943)
- [11] Gorelik G, *Dokl.Akad.Nauk.SSSR* **54**, 779 (1946)
- [12] Slobodskaya P V, *Izv.Akad.Nauk.SSSR, Ser.Fiz.* **12**, 656 (1948)
- [13] Rosencwaig A and A Gersho, *Science* **190**, 556 (1975)
- [14] Rosencwaig A and A Gersho, *J.Appl.phys.* **47**, 64 (1976)
- [15] Bennett H S and R A Forman, *Appl.Opt.* **15**, 2405 (1976)
- [16] Aamodt L C, J C Murphy and J G Parker, *J.Appl.phys.* **48**, 927 (1977)
- [17] Wetsel G C Jr. and F A McDonald, *Bull.Am.Phys.Soc.* **22**, 295 (1977)
- [18] Tam A C and Y H Wong, *Appl.Phys.Lett.* **36**, 471 (1980)
- [19] Korpiun P, B Buchner, A C Tam and Y H Wong, *J.Appl.phys.* **59**, 2944 (1986)
- [20] Tam A C, *Rev.Mod.Phys.* **58**, 381 (1986)
- [21] Onokhov A P, T K Razumova and I O Starobogatov, *Sov.J.Opt.Technol.* **47**, 36 (1980)
- [22] Satheeshkumar M K and C P G Vallabhan, *J.Phys.E*, **18**, 434 (1985)
- [23] Guthrie R W and F D Medina, *J.Appl.Phys.*, **57**, 4485 (1985)
- [24] Adams M J, G F Kirkbright and K R Menon, *Anal.chem.* **51**, 508 (1979)
- [25] McClelland J F and Kniseley R N, *Appl.Phys.Lett.* **28**, 467 (1976)
- [26] Brilmyer G H, A Fujishima, K S V Santhanam and A J Bard, *Anal.chem.* **49**, 2057 (1977)
- [27] Hordvik A and H Schlossberg, *Appl.Opt.* **16**, 101 (1977)
- [28] Farrow M M, R K Burnham, M Auzanneau, S L Oslen, N Purdie and E M Eyring, *Appl.Opt.* **17**, 1093 (1978)
- [29] McQueen D H, *J.Phys. D* **12**, 1673 (1979)

- [30] Bonch-Bruevich A M, T K Razumova and I O Strarobogatov, Opt.Spectrosc.(USSR) **42**, 45 (1977)
- [31] Patel C K N and A C Tam, Rev.Mod.Phys. **53**, 517 (1981)
- [32] Long M E, R L Swofford and A C Albrecht, J.Chem.Phys. **65**, 179 (1976)
- [33] Moses E I and C L Tang, Opt.Lett. **1**, 115 (1977)
- [34] Stone J, Appl.Opt. **17**, 2876 (1978)
- [35] Landau L D and E M Lifshitz, "*Fluid mechanics*", translated by J B Sykes and W H Reid, Pergamon, Oxford (1959)
- [36] Naugol'nykh K A, Sov.Phys.Acoust. **23**, 98 (1977)
- [37] Nelson E T and C K N Patel, Opt.Lett. **6**, 354 (1981)
- [38] White R M, J.Appl.phys. **34**, 3559 (1963)
- [39] Gournay L S, J.Acoust.Soc.Am. **40**, 1322 (1966)
- [40] Hu C L, J.Acoust.Soc.Am. **46**, 728 (1969)
- [41] Liu G, Appl.Opt. **21**, 955 (1982)
- [42] Bebchuk A S, V M Mizin and N Ya Salova, Opt.spectrosc.**44**,91 (1978)
- [43] Brueck S R J, H Kidal and L J Belanger, Opt.Comm. **34**, 199 (1980)
- [44] Lai H M and K Young, J.Acoust.Soc.Am. **72**, 2000 (1982)
- [45] Heritier J M, Opt.Comm. **44**, 267 (1983)
- [46] White R M, J.Appl.Phys., **34**, 3559 (1963)
- [47] Gournay L S, J.Acoust.Soc.Am., **40**, 1322 (1966)
- [48] Terzic M and Sigrist M W, J.Appl.Phys., **56**, 93 (1984)
- [49] Sigrist M W and Z H Chen, Appl.phys.B **43**, 1 (1987)
- [50] Rosencwaig A, "*Photoacoustics and Photoacoustic spectroscopy*", Wiley, New York (1980)
- [51] Pao Y H and P C Clapsy, Case Western Reserve University, final report for subcontract 44343-V, The aerospace corp.
- [52] Sigrist M W and Kneuhbul F K, Appl.Phys.Lett., **34**, 353 (1979)
- [53] Birks J B, "*Photophysics of aromatic molecules*", Wiley-Interscience, London (1970)
- [54] Lakowicz J R, "*Principles of Fluorescence Spectroscopy*", Plenum press, New York and London (1983)
- [55] Bloembergen N, "*Nonlinear optics*", Benjamin, New York (1965)
- [56] Yariv A, "*Quantum Electronics*" (second edition), John Wiley & Sons, New York (1975)
- [57] Laud B B, "*Lasers and Nonlinear optics*", Wiley Eastern Ltd., New Delhi (1985)
- [58] Bloembergen N, Am.J.Phys. **35**, 989 (1967)

- [59] Franken P A, A E Hill, C W Peters and G Weinreich, Phys.Rev.Lett. 7, 118 (1961)
- [60] Goeppert Mayer M, Ann.Phys.9, 273 (1931)
- [61] Craig D P and T Thirunamachandran, "*Molecular Quantum Electrodynamics*", Academic press, London (1984)
- [62] Giordamine J A, P M Rentzepiz, S L Shapiro and K W Wecht, Appl.Phys.Lett. 11, 216 (1967)
- [63] Penzkofer A and Leupacher W, Optical and Quantum Electronics, 19, 327 (1987)
- [64] Kuhn H, in "*Progress in the chemistry of organic natural products*", (ed.) D L Zechmeister, 16, Springer, Wein (1958-59)
- [65] Miyazoe Y and M Maeda, J.Opto-electron. 2, 227 (1970)
- [66] Forsterling H D and H Kuhn, "*Physikalische Chemie in experimenter-Einpraktikum*", Verlag chemie, Weinheim/Bergstr. (1971)
- [67] Schafer F P, Topics in Applied Physics, vol.1, (ed.) "*Dye lasers*" Springer, Berlin (1977)
- [68] Strickler S J and R A Berg, J.Chem.Phys. 37, 814 (1962)
- [69] Parker C A, "*Photoluminescence of solutions*", Elsevier, Amsterdam (1968)
- [70] Muller A, Z.Naturforsch. 23a, 946 (1968)
- [71] Muller A and Pflugler E, Chem.Phys.Lett.2, 155 (1968)
- [72] Hammond P R, IEEE J.Quant.Electron. QE - 15, 624 (1979)
- [73] Weider I, Appl.Phys.Lett. 21, 318 (1972)
- [74] Nouchi G, J.Chem.Phys. 66, 548 (1969)
- [75] Buttner A V, B B Snavely and O G Peterson, in "*Molecular luminescence*", (ed.) E C Lim, Benjamin, New York (1969)
- [76] McClure D S, J.Chem.Phys. 19, 670 (1951)
- [77] Heinzelmann W and H Lanhart, Chem.Phys.Lett., 4, 20 (1969)
- [78] Porter G and M W Windsor, Proc.Roy.Soc.A 245, 238 (1958)
- [79] Pringsheim P, "*Fluorescence and Phosphorescence*", Interscience, New York (1949)
- [80] Forster Th., "*Fluoreszenz organischer Verbindungen*", Vandenhoeck and Ruprecht, Gottingen (1951)
- [81] Bergman A, R David and J Jortner, Opt. Commun. 4, 431 (1972)
- [82] Drexhage K H, "Design of laser dyes", Seventh International Quantum electronics conference, Montreal (1972)

- [83] Leonhardt H and A Weller, in "*Luminescence of organic and inorganic materials*" (ed. H P Kallmann & G M Spruch), Wiley, New York (1962)
- [84] Turro N J, "*Molecular photochemistry*", Benjamin, New York (1965)
- [85] Wehry E L, "Structural and environmental factors in fluorescence", in "*Fluorescence, theory, instrumentation and practice*" (ed. G G Guilbault), Decker, New York (1967)
- [86] Marling J B, L L Wood and D W Gregg, IEEE J.Quant.Electron. **QB-7** 4498 (1971)
- [87] Penzkoffer A and Y Liu, Chem.Phys. **103**, 399 (1986)
- [88] Lopez Arbeloa F, P Ruiz Ojeda and I Lopez Arbeloa, Chem.Phys.Lett. **148**, 253 (1988)
- [89] Tuccio S A and F C Strome Jr., Appl.Opt. **11**, 64 (1972)
- [90] Orner G C and M R Topp, Chem.Phys.Lett. **36**, 295 (1975)
- [91] Catalano I M and A Cingolani, Opt.Commun. **32**, 159 (1980)
- [92] Hermann J P and J Ducuing, Phys.Rev.A **5**, 2557 (1972)
- [93] Rulliere C and P Kottis, Chem.Phys.Lett. **75**, 478 (1980)
- [94] Penzkofer A and W Leupacher, Optical and Quant.Electron. **19**, 327 (1987)
- [95] Vabnits Kh, V A Gaisenok, A I Slobodyanuk and D Shubert, Opt.Spectrosk. **61**, 201 (1986)
- [96] Monson P R and W M McClain, J.Chem.Phys. **53**, 29 (1970)
- [97] Penzkofer A, W Falkenstein and W Kaiser, Appl.Phys.Lett.**28**, 319 (1979)
- [98] Mikami N and M Ito, Chem.Phys.Lett. **31**, 472 (1975)
- [99] Tang HLB, R J Thrash and G E Luoi, Chem.Phys.Lett. **57**, 59 (1978)
- [100] Mueller A and E Pflueger, Chem.Phys.Lett. **2**, 155 (1968)
- [101] Bradley D J, MHR Hutchinson, H Koetser, T Morrow, GHC New and M S Petty, Proc.Roy.Soc.Lond. A **328**, 97 (1972)

CHAPTER - 2

INSTRUMENTATION

The accuracy and reliability of results obtained from scientific experiments primarily depend on the capabilities as well as proper usage of the necessary equipments. The inflow of new ideas in science and technology has called for more sophistication in instrumentation. As a result data acquisition has nowadays become a blend of technology and art. In many situations, proper computer interfacing with software support renders the experiment easier and observations more accurate. As described in the introductory chapter, both pulsed photoacoustics and nonlinear fluorescence have been employed for obtaining the results in our experiments. In this chapter a description of the general features of these techniques from an instrumentation point of view, and details of the equipments used are given.

2.1 Instrumentation for Photoacoustics

A PA spectrometer consists of the following basic modules: (i) a radiation source of sufficient intensity and of the wavelength range of interest (ii) intensity modulator (iii) PA cell, which houses the sample and the acoustic transducer and (iv) data processing unit. The block diagram of a basic PA spectrometer is given in Fig.2.1. Various modifications of this basic set up are used in different PA experiments by various workers.

2.1.a Light sources

A number of light sources suitable for photoacoustic as well as fluorescence experiment are commercially available [1]. Mercury lamps are quite common, which give high intensity and spectral purity. The emission spectral distribution of the mercury lamp can be varied by changing the pressure at which the arc operates. Though it is costly, the Xenon arc lamp is a good choice for many experiments due to its high intensity, typically from 250 W to 2.5 kW. The high power Tungsten filament lamp is an incandescent source good for excitation in the visible region, but its intensity falls off rapidly towards violet and is too low in the ultraviolet. The hydrogen lamp provides a reasonably

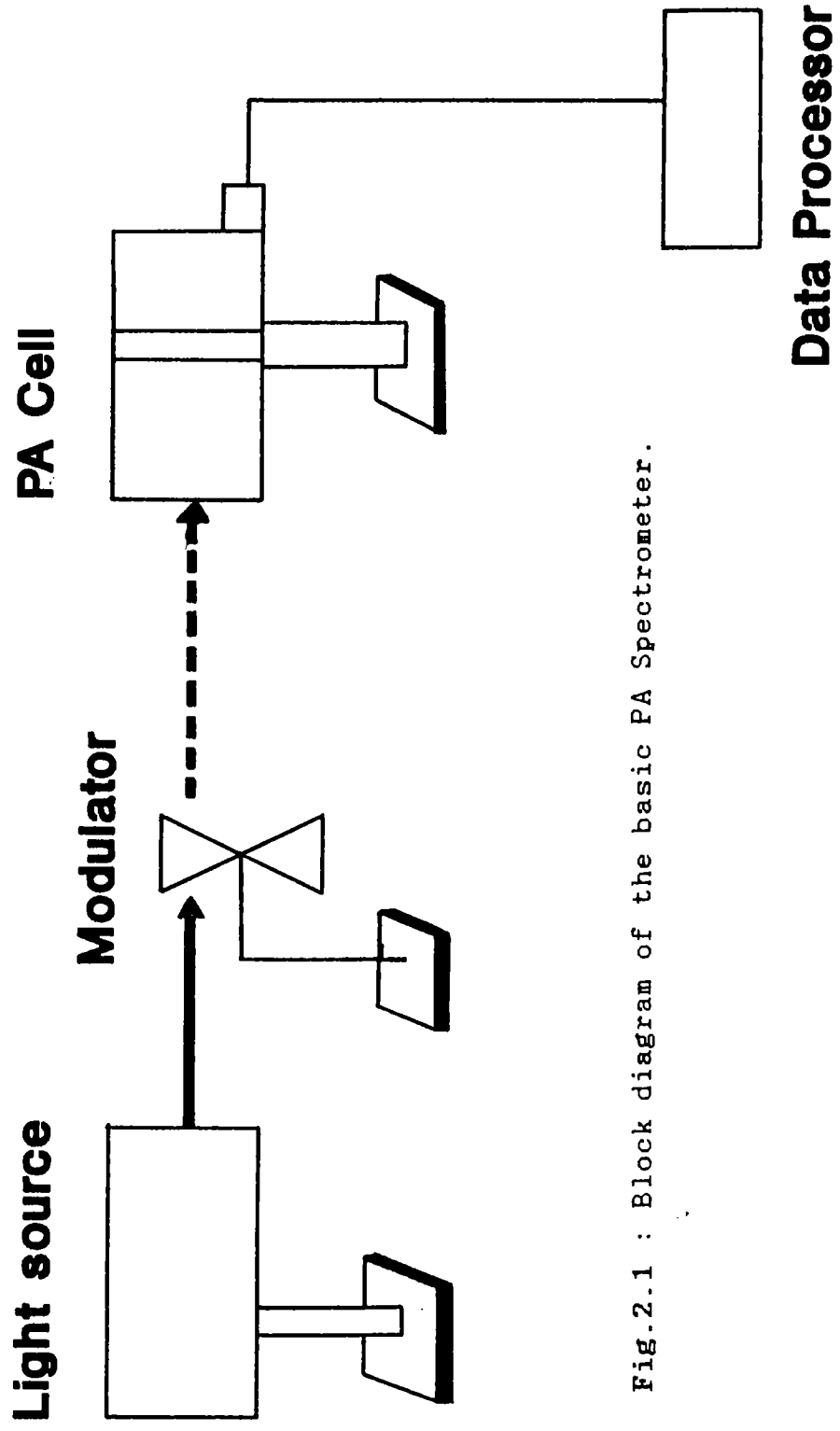


Fig.2.1 : Block diagram of the basic PA Spectrometer.

uniform energy distribution in the ultraviolet region but at a lower intensity. There are other kinds of lamps like Sodium lamp, Cadmium lamp, Zinc lamp etc, and a variety of lamps giving atomic spectra have been described by Elenbaas and Riemens [2].

In spite of this multitude of lamps available, since the advent of laser in 1960 it has been uniquely accepted as the best light source for most of the optical experiments. Frequency tunability of lasers is an obvious advantage in addition to their monochromaticity, coherence and low beam divergence. Excimer, colour centre and high pressure gas lasers, dye lasers, certain diode and solid state lasers, optical parametric oscillators etc. provide primary tunable coherent radiation which can be further extended by Raman shifting and four-wave mixing techniques. Thanks to this variety of materials and techniques, continuously or quasicontinuously tunable laser sources are available for the visible and near infrared and a good part of ultraviolet and far infrared.

2.1.b Modulation

Modulation of the incident light beam is essential for the generation of PA signals. Amplitude modulation methods for the light source include Q-switching, mode locking, flashlamp pumping, mechanical chopping, electro-optic or acousto-optic modulation etc. For cw sources, amplitude modulation using a mechanical chopper is the most used method due to its simplicity, efficiency and low cost. The depth of modulation achieved here is 100 %. Frequency modulation also is employed in some cases; it is well suited for narrow linewidth absorbers such as atomic and diatomic species.

2.1.c The PA cell

The central part of any PA spectrometer is the PA cell in which the sample is placed and the acoustic signal is generated. Since proper design of the cell is very important in PA instrumentation, the following points should be considered:

- (a) The cell should be acoustically isolated from the ambient noise sufficiently,

- (b) Acoustic signals generated from cell windows, walls etc should be minimized and
- (c) The interior of the cell should be free from contaminants.

Many designs of PA cells have been described in literature, aiming at various aspects of signal improvement, noise reduction and ease of use. PA cells may be classified into two general kinds: cells designed for gaseous samples and those designed for condensed matter samples. Besides microphone detection, fiberoptic detection and optical probe-beam-deflection detection can also be used for gaseous samples [3]. For improving the S/N ratio, often Brewster windows, acoustic baffles etc. are added and intracavity or extracavity multipassing is employed. In condensed matter cells both microphones and piezoelectric transducers are in common use for detection. At low enough modulation frequencies or long enough pulse durations of the excitation beam the exact geometry of the PA cell is important, since the acoustic wave can get reflected from the cell walls producing interference and resonances. Resonance enhancement of the PA signal, utilizing the longitudinal, azimuthal or radial acoustic resonance modes of the cell, can be employed for increasing the sensitivity of PA detection, as reviewed by Hess [4]. On the other hand, at very high modulation frequencies or very short pulse durations of the excitation beam, effects of reflections from the cell walls are unimportant, and so is the geometry of the PA cell; indeed, "leaky" or "open" PA cells can be used in such cases. The operational principles of several types of PA cells are given by Rosengren [5] and Dewey [6].

2.1.c1. Detection of PA signals

Acoustic signal detection in PA is accomplished by means of various kinds of transducers, the most common ones being the microphone and the piezoelectric transducer. The choice of the detector is based on considerations of impedance matching, sensitivity, ruggedness, ease of operation etc..

a. Microphone

The sound transducer used in a gas phase PA cell (whether it is used to investigate a gaseous sample or a condensed sample via

indirect PA generation monitored in a coupling gas) is usually a commercial microphone, which is typically a capacitance sensor that senses the deflection of a diaphragm in contact with the gas. In gaseous samples volume changes can be quite large as a result of internal heating. A displacement-sensitive detector like the capacitor microphone proves to be an excellent heat detector here. The amplitude of motion in an elastic medium is given by

$$\Delta x = \Delta p / 2\pi\rho\nu \quad (2.01)$$

where Δp is the pressure fluctuation, ρ is the density of the fluid and ν is the frequency of pressure fluctuation. Since the coefficient of volume expansion of liquids and solids is 10-100 times smaller than that of gases for the same pressure change, measurement of heat production in liquids and solids directly with a displacement sensitive detector such as a microphone would be 10-100 times less sensitive than using a pressure sensitive device such as a piezoelectric detector. Many commercial brands of capacitor and electret microphones suitable for gas phase PA studies are available and the choice generally depends on the best compromise among sensitivity, bandwidth, size and noise. Sensitivity as high as 100 mV/Pa and bandwidth \approx 100 kHz are available in commercial microphones (eg: those from Bruel and Kjaer). However, high sensitivity is usually achieved only as a trade off for lower bandwidths and larger microphone sizes. With present microphones and associated electronics it is possible to detect temperature rises in a gas of the order of 10^{-6} °C, or a thermal input $\approx 10^{-9}$ cal/cm³-sec [7].

b. Piezoelectric transducers

We have mentioned above that displacement sensors like microphones are not best suited for directly detecting PA signals generated in liquids and solids. The conventional solution to this problem is the indirect PA detection, where the periodic optical heating of a condensed medium is sensed from volume fluctuations induced in a coupling gas. But here we encounter the serious problem of acoustic impedance mismatch at the sample-gas interface. The acoustic impedance Z_a is given by

$$Z_a = \rho c_o \quad (2.02)$$

where ρ is the density and c_o is the sound velocity. For most solids $Z_a \approx 10^8 \text{ g/cm}^2 \text{ sec}$, for liquids $\approx 10^5 \text{ g/cm}^2 \text{ sec}$ and for gases $\approx 10^2 \text{ g/cm}^2 \text{ sec}$. The transmission coefficient for an acoustic wave in a gas going through a gas-solid interface is given by

$$(1-R) = \frac{4 Z_a^g Z_a^s}{(Z_a^g + Z_a^s)^2} \approx 10^{-4} \quad (2.03)$$

where the superscripts g and s correspond to gas and solid respectively. On the other hand $(1-R)$ for a liquid-solid interface is $\approx 10^{-1}$ and for a solid-solid interface it is ≈ 1 . Thus a solid piezoelectric ceramic or crystal attached to/immersed in the solid/liquid sample is the most suitable detector of thermally generated pressure or stress variations in condensed media. Further, in a gas-microphone system the signal would be proportional to the light absorbed within a thermal diffusion length of the surface. For bulk samples having low to moderate absorption, this would be only a very small part of the total light absorbed. On the other hand, piezoelectric detection can be made sensitive to the total amount of light absorbed by the entire sample, thereby providing a more efficient measure of the absorbed energy. An added advantage of the piezoelectric transducer is that it can operate at much higher frequencies than the microphone. With these detectors, temperature changes of 10^{-6} to 10^{-7} °C can be detected, which for typical solids or liquids corresponds to thermal inputs of the order of 10^{-6} cal/cm³sec. The pressure sensitivity of a PZT transducer, similar to that employed in our experiments, is typically 3V/atm [3]. It may be noted that this is much smaller than that of a sensitive microphone (eg: B & K model 4166) with a typical sensitivity $\approx 5 \times 10^3$ V/atm. However, PZT transducers are still preferred over microphones in many situations due to the acoustic impedance matching advantage.

Many types of piezoelectric ceramics or crystals like lead zirconate titanate (PZT), lead metaniobate, lithium niobate, crystalline quartz etc are commercially available. These transducers have been extensively reviewed by Mason and Thurston [8]. Further, certain highly insulating thin polymeric films like PVF₂

(polyvinylidene difluoride), teflon, nylon etc. can be made piezoelectric (eg. by poling in a strong electric field at elevated temperatures) and used. There is a strong interest in the use of PVF₂ films as transducers [9] for acoustic imaging (especially for body scanning in medicine) because of the nonringing characteristics of the film (its mechanical Q-factor is much lower than that of PZT), fast risetime, good flexibility and good acoustic impedance matching to liquids like water. PVF₂ foils are inexpensive, can easily be cut to size, and are readily available commercially, whereas for making fast transducers using conventional piezoelectrics a thin slice of the material should be lapped, coated and mounted suitably requiring considerable effort. A disadvantage of PVF₂ is that its sensitivity is typically much lower than that of conventional piezoelectric materials like PZT or lithium niobate.

To achieve ultrafast risetimes of the order of 1 ns or shorter, other thin film piezoelectric materials are needed. Thin ZnO film sputtered onto a polished flat surface of a single-crystal sapphire rod has been used in detecting ultrashort PA pulses of < 1 ns width [10] and in acoustic microscopy [11].

Special capacitance transducers, capable of detecting a displacement of 10⁻² Angstroms, fibre optic sensors with a displacement detectability as good as 2 × 10⁻¹² m Hz^{-1/2} with a bandwidth of 1 MHz etc also have been discussed by various authors [12,13].

c. Piezoelectric relationships

The direct and converse piezoelectric effects are exhibited by piezoelectric crystals in which separation of the "centres of gravity" of their positive and negative charges occurs as a result of mechanical stress. Such a crystal is said to be asymmetrical along the axis normal to the stress (Fig. 2.2). Crystals vary considerably in the number of axes of asymmetry they possess and transducer elements (slices) have to be cut with their faces parallel to such an axis. In a compressed slice the charge centres move relative to one another producing surface charges, and the charge density is proportional to the applied stress within the elastic limit of the crystal. Conversely

with the application of an electric field the slice changes its physical dimensions and the amount of strain is proportional to the electric field intensity.

Let us first consider the direct piezoelectric effect. The surface charge induced on a slice of piezoelectric material is called the *polarization charge* P , related to an applied stress T by

$$P \text{ (coulombs.m}^{-2}\text{)} = T \text{ (newtons.m}^{-2}\text{)}. d \quad (2.04)$$

where d the *piezoelectric strain coefficient*, defined as the charge density per unit applied stress, measured in coulombs/newton under short-circuit conditions (ie., no external electric field applied to the slice). If now an electric field E (volts/m) is applied to the slice, the electric flux density D (coulombs/m²) within it becomes

$$D = E\epsilon + Td \quad (2.05)$$

where ϵ is its permittivity, measured in farads/m.

In the converse piezoelectric effect, if an unstrained slice is subjected to an electric field it undergoes a mechanical strain S which is related to the electric field intensity by

$$S = Ed' \quad (2.06)$$

Consideration of the principle of conservation of energy shows that $d = d'$ and yields an alternate definition for d as the mechanical strain produced per unit applied field, measured in m/v under conditions of no load. The application of a tensile stress T to the slice which possesses an elastic constant ' s ', measured in m²/newton, results in a total strain

$$S = Ts + Ed \quad (2.07)$$

and in a non-piezoelectric material equations 2.05 and 2.07 will reduce to the well-known relations

$$D = \epsilon E \quad (2.08)$$

and

$$S = Ts \tag{2.09}$$

when a compressive stress $-T$ is applied, equation 2.07 becomes

$$S = -Ts + Ed \tag{2.10}$$

and the slice can be effectively clamped if S is made zero by balancing the strain produced by the electric field by the compressive strain. Under these conditions equation 2.10 gives

$$T = eE \tag{2.11}$$

where $e = d/s$ is the *piezoelectric stress coefficient* defined as the stress produced per unit applied field measured in newtons/Vm. Equations 2.04 and 2.11 give

$$P = eS \tag{2.12}$$

and an alternative definition for e , as the charge density obtained per unit strain, expressed in coulombs/m².

These simple relationships, equations 2.04 to 2.12, apply to one direction only, ie, the thickness direction of the slice. However, when a stress is applied in an *arbitrary direction* relative to the slice eighteen piezoelectric stress and eighteen piezoelectric strain constants will be required to specify the complete situation, so that the simple relations of equations 2.06 and 2.09 must be replaced by matrices of stress-field and stress-strain relationships in the manner explained by Mason [14]. However, no piezoelectric output occurs along axes of symmetry; this and considerations of symmetry reduce the number of the relevant constants.

There are two other common piezoelectric coefficients, the coupling factor k and the frequency constant N_0 . Below the resonance frequency k satisfies the relationship

$$k^2 = \frac{\text{stored energy converted}}{\text{stored input energy}} \tag{2.13}$$

Studies of k show that a maximum of 50% electromechanical and mechoelectrical energy conversion can be obtained at low frequencies [7]. The frequency constant N_0 is defined as the product of the resonance frequency and the linear dimension governing the resonance.

2.1.d Signal processor

The simplest data processor for PA experiments is usually a signal amplifier connected to an oscilloscope. However the PA signal can be very weak in general, often several orders of magnitude lower than the ambient noise, and the transducer output has to be carefully processed to improve the S/N ratio. A lock-in amplifier can pick up the required weak signal and separate it from the strong noise background, by electronically "locking" to the modulation frequency in the cw modulation scheme. By lock-in detection the amplitude and phase of the PA signal can be measured and the use of a dual phase lock-in amplifier renders the measurements easier especially when amplitude and phase vary simultaneously. When the excitation source is a pulsed laser, gated integration and boxcar averaging (GIBA) is employed for improving the S/N ratio.

In spectroscopic applications where the excitation source wavelength is tuned in a specified range one should normalize the PA spectrum to the power spectrum of the radiation source, since the PA signal is proportional to the intensity of the incident beam. The general practice is to take the PA signal and the signal output from a power meter/photodiode that monitors variations in source power to channels A and B of a ratiometer respectively. The normalized spectrum is then obtained from the A/B output of the ratiometer.

2.2 The present PA experimental set up

Our experimental set up for PA measurements (Fig.2.3) consists of a pulsed, Q-switched Nd:YAG laser having the second harmonic generation option as the excitation source, a fabricated PA cell that contains the samples, and a fabricated piezoelectric transducer chamber that detects the acoustic signals. A pulse preamplifier also has been designed and fabricated in view of amplifying weak PA signals. The output of the preamplifier is observed on a digital

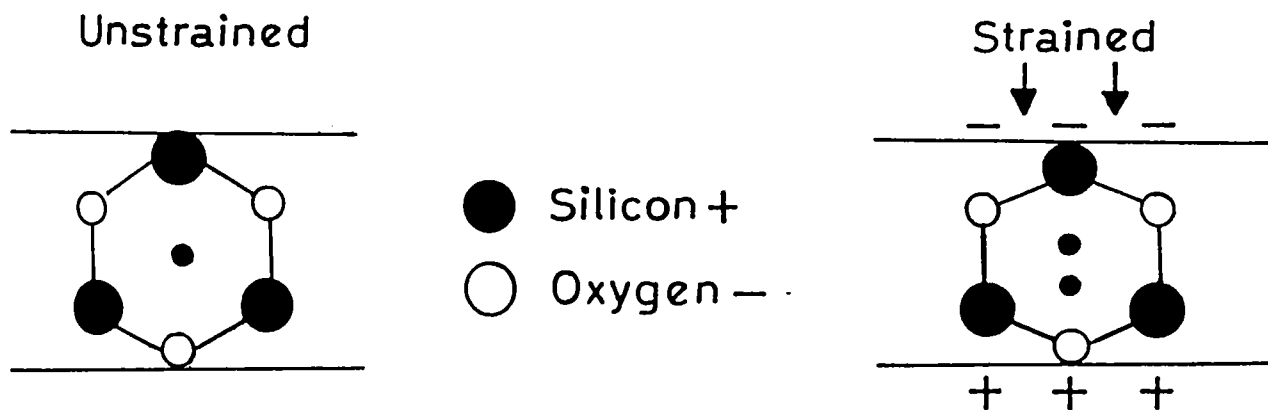


Fig.2.2 : Piezoelectric action in quartz showing separation of charge centres under stress. Centres of positive and negative charges are coincident in the unstrained case whereas Centres of positive and negative charges are separated in the strained case.

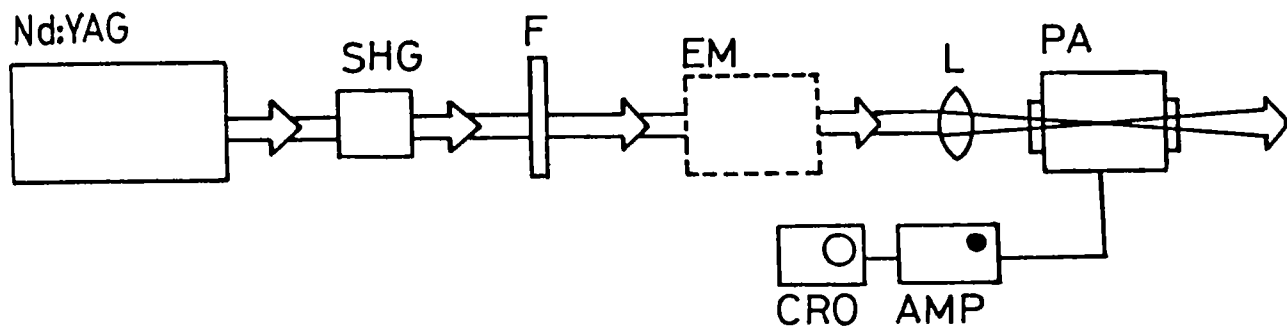


Fig.2.3 : The present experimental set up used for pulsed photoacoustic experiments.

SHG : Second harmonic generator, F : Harmonic separator for blocking the 1064 nm component, EM : Energy/power meter, L : Focusing lens, PA : Photoacoustic cell with transducer, AMP : Pulse preamplifier, CRO : Digital storage Oscilloscope.

storage oscilloscope. Due to the high absorption of most of the dye samples used in these experiments together with the good sensitivity of the transducer, often GIBA has not been necessary for measuring the signal.

In the following paragraphs we discuss the relevant details of the PA cell, transducer chamber and pulse preamplifier used in our work.

2.2.a The PA cell and piezoelectric transducer

The PA cell used in our experiments is shown in Fig.2.4, the design of which is similar to that proposed by Patel and Tam [15] except for a few minor variations. The cell is of stainless steel body with an inner diameter of 2 cm and length 5 cm. Glass windows are fixed with flanges and O-rings to the cell for the entry and exit of the laser beam. One side of the cell has an opening in which the transducer chamber is fixed. A Lead Zirconate-Titanate (PZT) disc of 4 mm thickness and 15 mm diameter is the piezoelectric transducer that is contained in this chamber. The characteristic impedance of this PZT transducer as a function of frequency, measured on an impedance analyzer, is shown in Fig.2.5a. Fig.2.5b shows the equivalent circuit of the transducer. The PZT disc is spring-loaded against the thin front diaphragm as shown, with a thin layer of silicon grease applied between them to ensure good acoustic coupling. The PA signal is taken out through the BNC connector. Besides good sensitivity, this cell has the following advantages over commercial hydrophones:

- (a) The flat polished front face of the transducer reflects most of the stray light scattered onto it; furthermore, the large thermal mass and conductivity of the diaphragm minimize the effect of light absorption.
- (b) There is less likelihood that the liquid sample being studied will get contaminated by the stainless steel transducer chamber as compared to other conventional materials like silver, aluminium or epoxies.
- (c) Nucleation of microbubbles that can reduce the sensitivity is unlikely on the polished stainless steel face of the transducer.

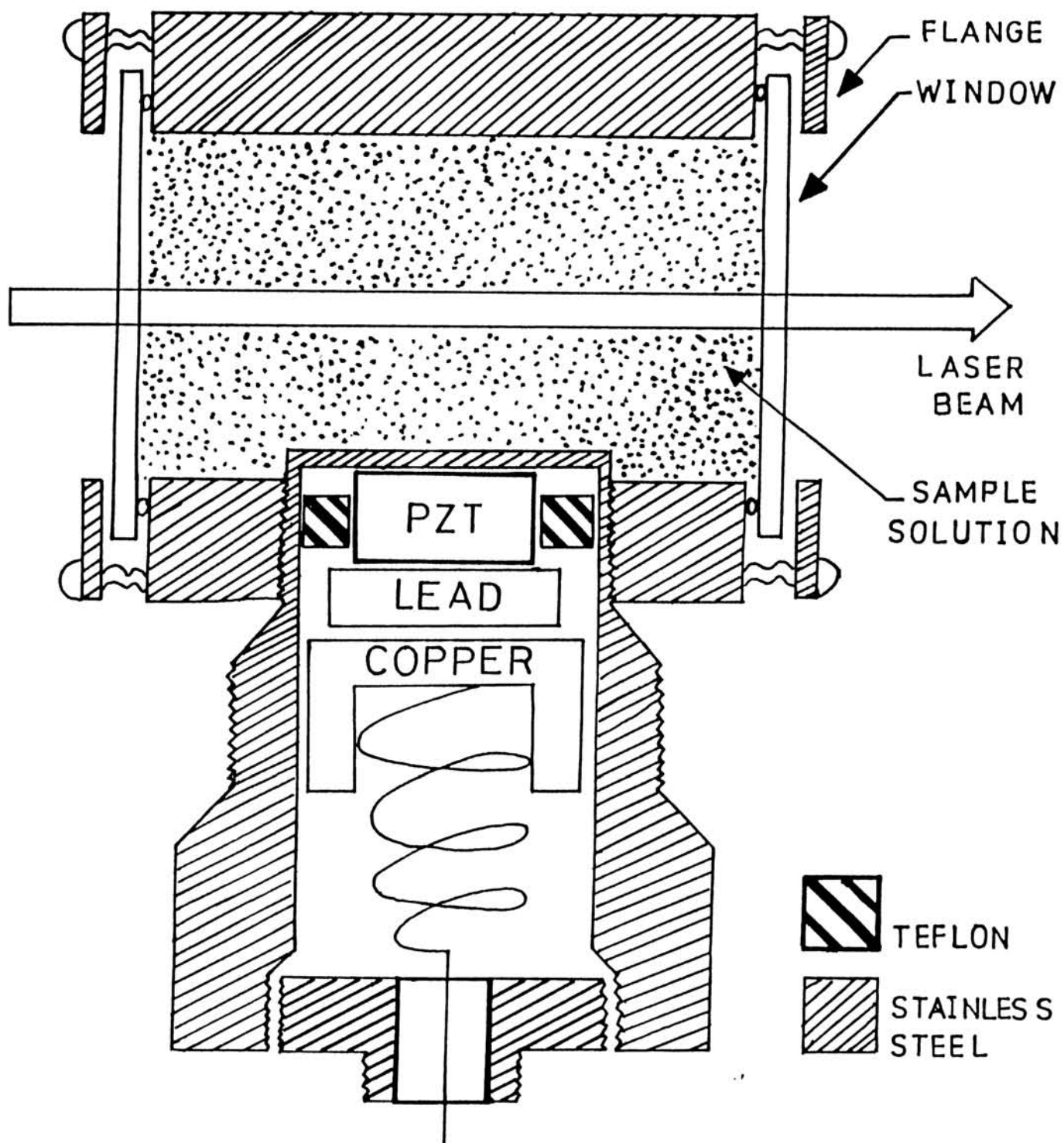


Fig.2.4 : The photoacoustic cell with the transducer chamber screwed in.

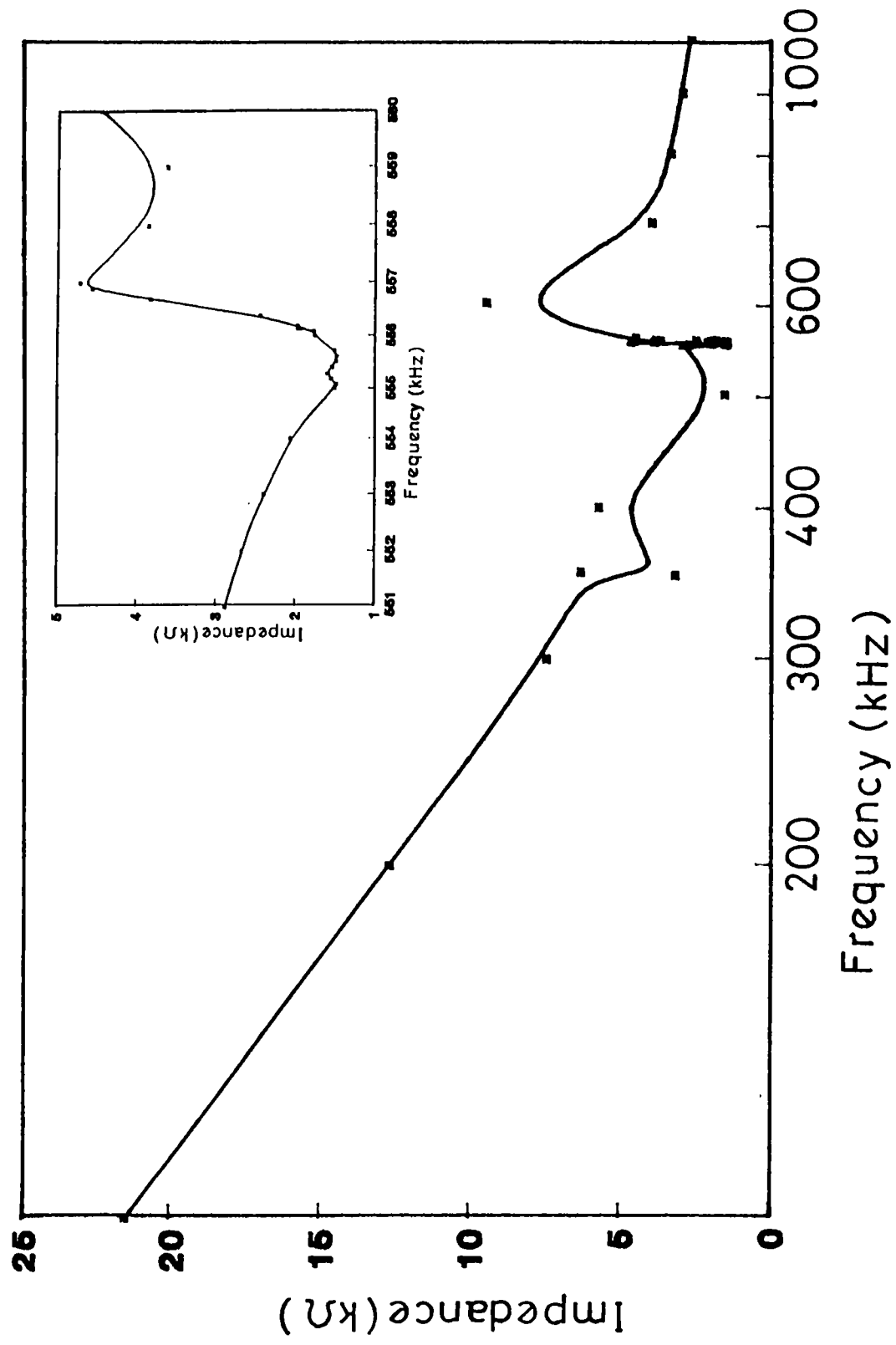


Fig.2.5a :Impedance characteristics of the PZT transducer. Inset shows an expanded view of the minimum impedance region .

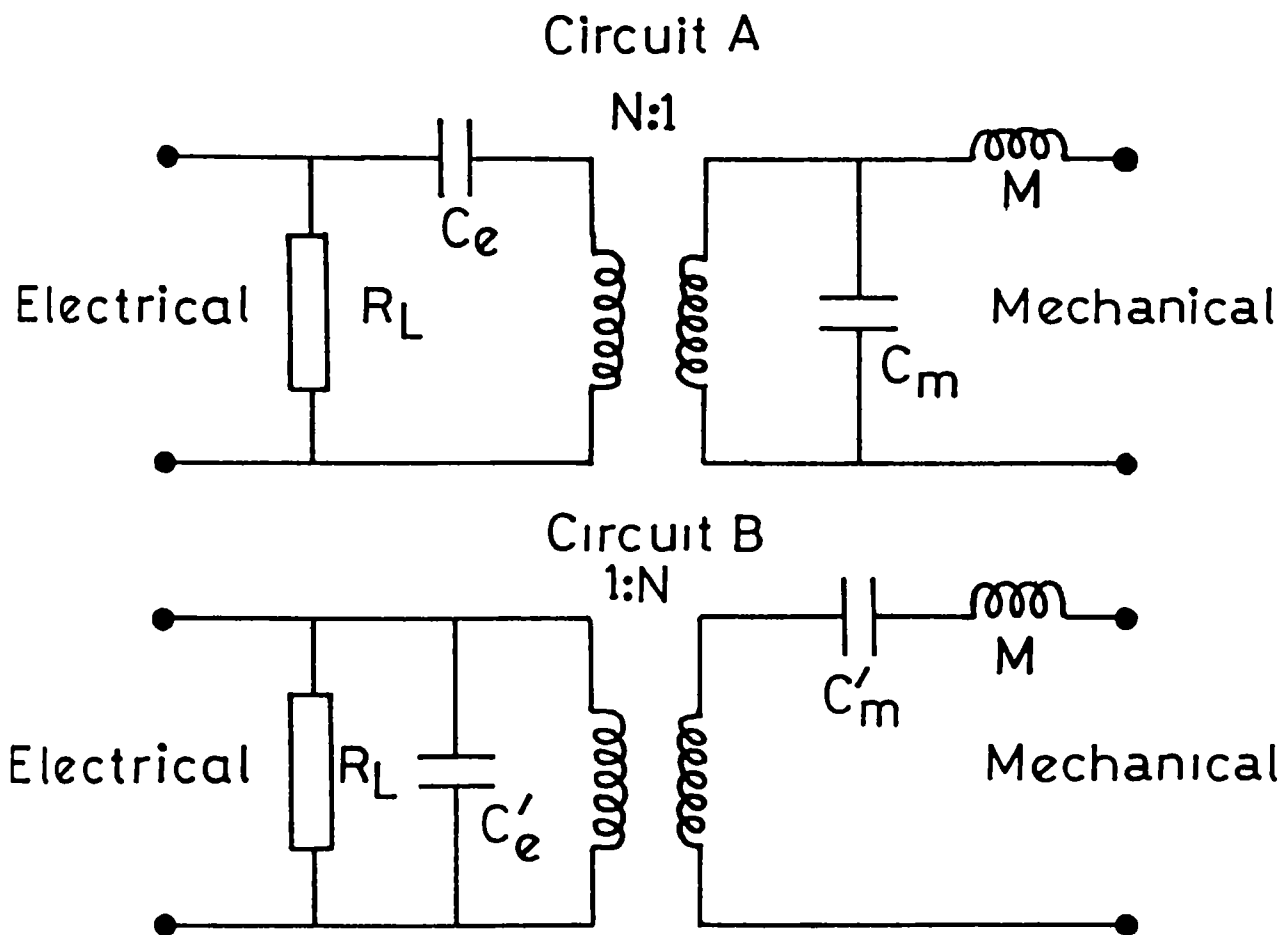


Fig.2.5b : Electrical equivalent circuit of a piezoelectric element. Mechanical terminals represent the face or point of mechanical energy to or from the piezoelectric element. The inductance symbol represents an ideal electromechanical transformer - one that transforms voltage to force and vice versa, without loss of energy storage. Transformation ratios, $N:1$ in circuit A and $1:N$ in circuit B, are ratios of voltage input to force output, and also the ratios of velocity input to current output. The capacitance symbols on the electrical side represent electrical capacitances. The capacitance symbols on the mechanical side represents compliances.

- (d) The use of lead, which has high ultrasonic attenuation, as a backing to the PZT leads to reduced acoustic reflection back into the PZT transducer, thus minimizing "ringing" effects.
- (e) The enclosing of the PZT cylinder in a metal casing minimizes electrical pick-up.
- (f) The acoustic impedances of stainless steel and the PZT material are nearly the same, so that acoustic loss due to the presence of the front diaphragm is small.

Due to its high sensitivity a few mV of electrical signal could directly be obtained from the transducer with a strongly/moderately absorbing sample in the cell. However for very weakly absorbing samples a preamplifier becomes necessary. We have designed and fabricated a pulse preamplifier for this purpose [16] which is described below.

2.2.b Design and fabrication of a PZT Transducer preamplifier

In weakly absorbing media the PA signal may be quite low and a preamplifier becomes necessary for boosting the signal amplitude to millivolt levels. Since piezoelectric detectors usually have a high internal impedance the preamplifier should have a sufficiently large matched input impedance to minimize signal attenuation. There should be enough bandwidth too, to facilitate a faithful reproduction of the high frequency components in the PA transient. It is found that a typical PA pulse detected by our transducer contains frequencies in the 30 kHz - 1 MHz region. On the other hand, a typical laboratory environment has a background acoustic noise spectrum prominent below 1 kHz. Hence a lower cut-off frequency around 1 kHz for filtering out the low frequency ambient acoustic noise as well as line pick-up, if any, is desirable. The pulse preamplifier is designed with these points in mind and the circuit diagram is given in Fig.2.6. Low cost and local availability of components are the two major advantages of this circuit.

An FET (T1) bootstrapped by means of R1 forms the input buffer stage which gives a high input impedance to the amplifier. T2 and T4 form a differential amplifier for which a constant current is supplied by T3. T5 provides one more stage of amplification and T6 is an

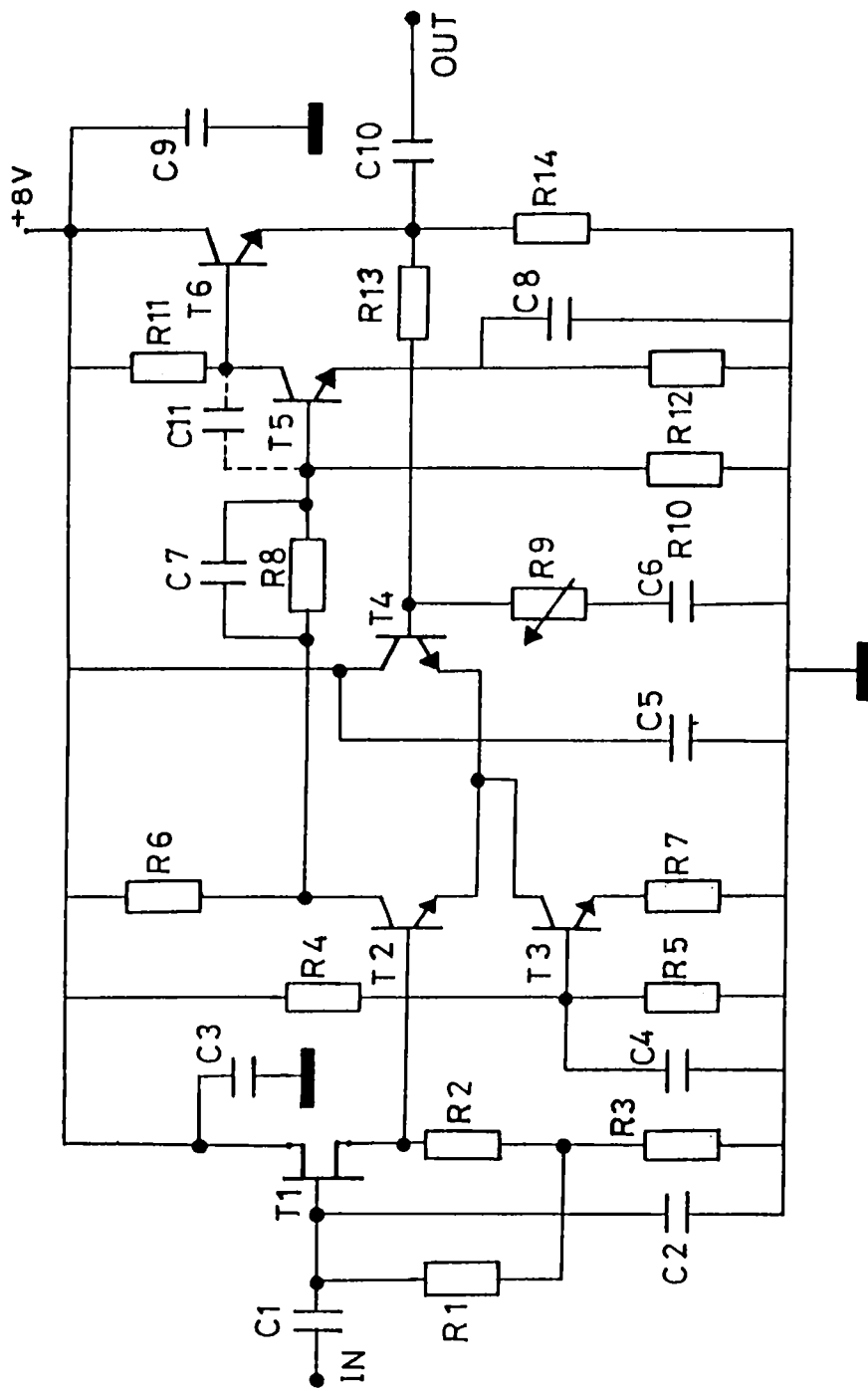


Fig.2.6 : Circuit of the pulse preamplifier designed for amplifying the PZT output.

T1 - BFW 10

T2, T4, T5, T6 - 2N 2222

T3 - BC147

C1, C7, C9, C10 - 0.1 M

C2 - 22 pf, C6 - 2.2 μ f

C3, C4, C5, C8 - 0.01 μ

C11 - 12 pf (see text)

R1 - 1M, R2, R13 - 4.7 K

R3 - 820 Ω , R4 - 15 K

R5 - 8.2 K, R6, R14 - 470 Ω

R7 - 680 Ω , R8 - 10 K

R10 - 1.2 K, R12 - 10 Ω

R11 - 560 Ω

R9 - 500 Ω Lin

emitter follower included to obtain a low output impedance. R13, R9 and C6 constitute the feedback loop, and for low amplifications the gain is given by R13/R9. In the actual circuit R9 is a 500 Ω Lin potentiometer with one 10 Ω resistor connected in series, to facilitate continuous gain control. The bandwidth is limited by the low frequency cut-off given by

$$f_1 = 1 / 2 \pi R9 C6 \quad (2.14)$$

For example, f_1 is \approx 1000 Hz, with R9 = 10 Ω and C6 = 0.15 μ F. The value of f_1 can be varied by changing the value of C6. Capacitor C11 (optional) is connected between the collector and base of T5 for preventing high frequency oscillations. A still higher bandwidth will be obtained if C11 is removed but this should be done with discretion. The sinusoidal response of this amplifier has been measured up to 1 MHz with the maximum gain set at 70, and the frequency response obtained is shown in Fig.2.7a. For a gain of 30, flat frequency response has been obtained up to 10 MHz. When tested in an actual experimental setup the amplifier has performed very well and the maximum gain could be utilized without signal distortion. Fig.2.7b shows a typical PA transient trace amplified by this preamplifier and observed on a storage oscilloscope.

Our experiments have led to the conclusion that this circuit can be efficiently used for amplifying pulsed laser-induced acoustic signals generated from condensed media, with a piezoelectric transducer at the input. Low impedance inputs may be connected as well. Since the frequency response and gain are flexible parameters the circuit can also be modified with necessary alterations for other user-specific requirements.

2.3. Instrumentation for Fluorescence

In general, instrumentation for fluorescence studies is more complicated than that for PA measurements. The simplest spectrofluorometer consists of a source giving a continuum of visible and ultraviolet light, a monochromator to select the required wavelength for excitation, a sample container and a second monochromator fitted with a photomultiplier to analyze the

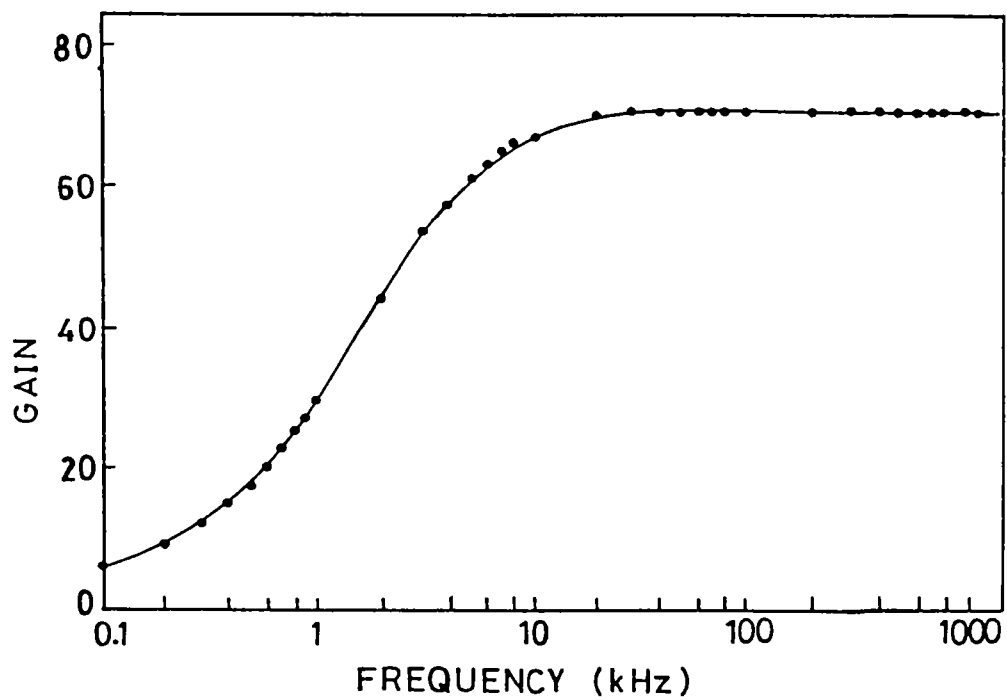
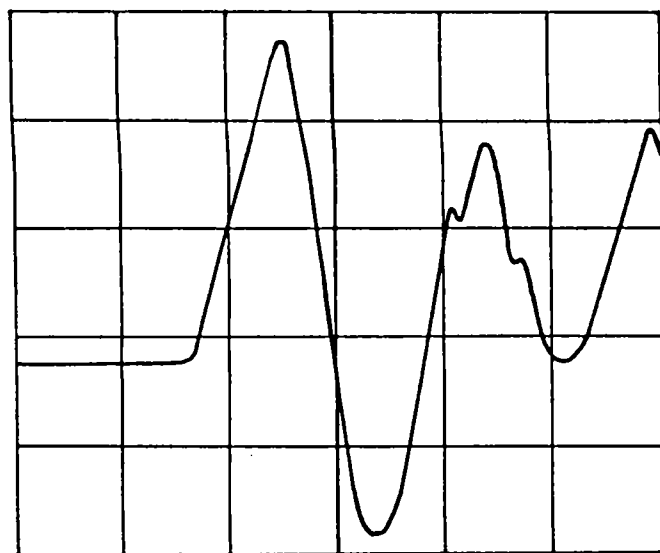


Fig.2.7a :Frequency response of the pulse preamplifier with the gain (V_{out}/V_{in}) set at 70.



Sweep : $5\mu s/div$
 Scale : $10mV/div$

Fig.2.7b :A typical pulsed photoacoustic signal observed on the oscilloscope after amplification using the pulse preamplifier.

fluorescence output. With such an apparatus one can select a narrow band of wavelengths of exciting light and measure the fluorescence spectrum emitted by the sample. But in practice it is difficult to attain high sensitivity with this system because lot of light is wasted at various points in the setup. This inherent difficulty is usually overcome by an optimal choice of the individual components as well as their optical alignment in the system. Fig.2.8 shows the block diagram of a typical fluorescence set-up.

In the following sections we briefly discuss the various components of the basic spectrofluorometer. It may be noted that a description on light sources has already been given earlier, in section 2.1.a.

2.3.a Monochromator

In a conventional spectrofluorometer two monochromators are necessary: one for selecting a narrow band of excitation wavelengths, and the other for the spectral analysis of the output fluorescence radiation. All monochromator systems essentially contain the following components: an entrance slit, a collimator (mirror or lens), a dispersing element (grating or prism), a second mirror or lens to focus the dispersed light and an exit slit. The height and width of the slits are generally variable. The principal parameters which determine the performance of the monochromator are the light gathering power (LGP), resolving power and linear (or angular) dispersion. Grating inefficiencies and scattered light should be minimized in grating monochromators. However, in view of the inherent difficulties involved in the construction of a monochromator with all the necessary good qualities in a practical experimental setup, often a compromise between the various requirements is established based on the specific purpose of the experiment.

2.3.b Sample holder

The geometrical arrangement of the beam of exciting light and the direction of viewing the fluorescence output light in relation to the specimen has been one of the most controversial points in the design of a spectrofluorometer [1]. The choice of a suitable sample holder

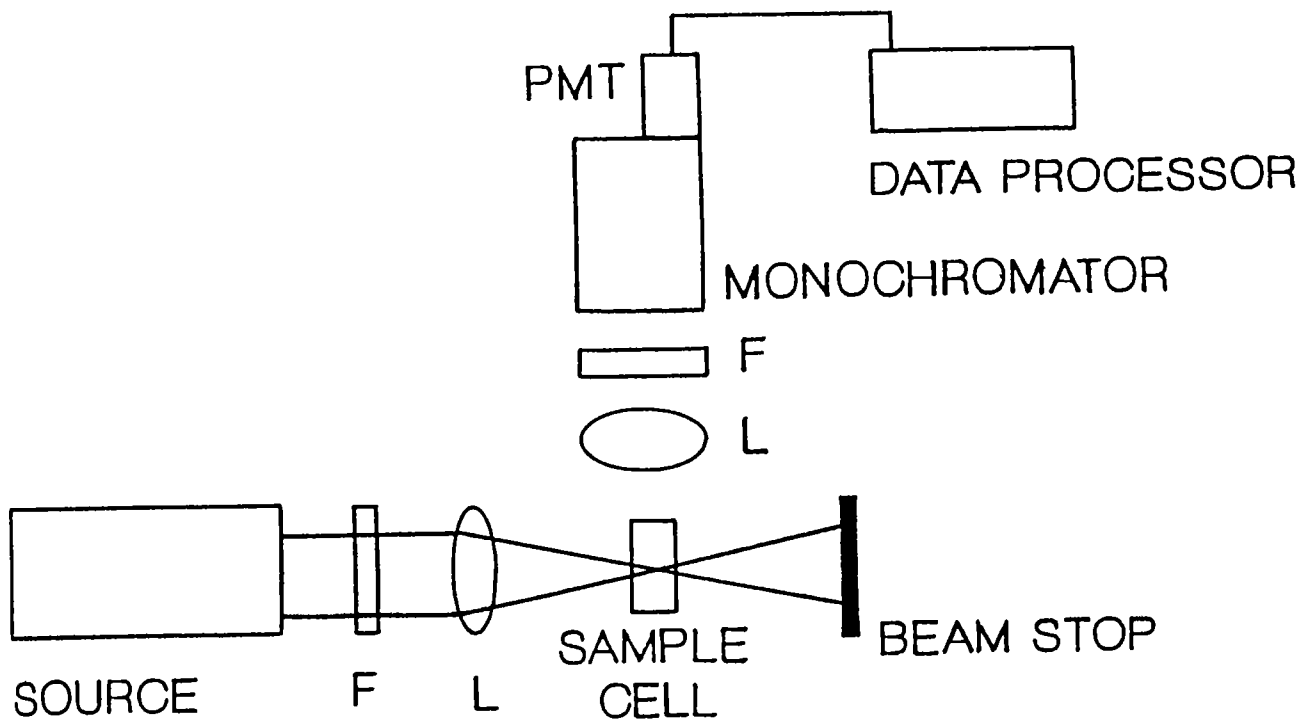


Fig.2.8 : Block diagram of the typical fluorescence spectrometer.

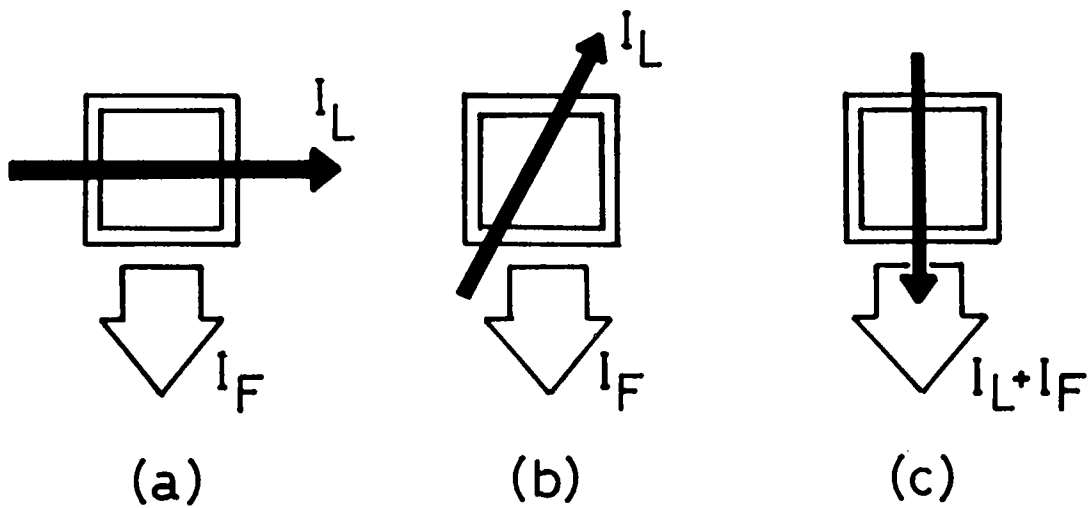


Fig.2.9 : Methods of illumination and viewing of a fluorescent sample. (a) : Right angle method, (b) : Frontal method, (c) : in-line method. I_L and I_F represent the pump and fluorescence radiations respectively.

becomes important in this respect. The reason why one has to be especially careful in this matter is due to the fact that solute quenching and inner filter effect can be easily confused between each other, leading to incorrect inferences. Luminescence quenching is a 'fundamental' effect characteristic of the system under the particular conditions concerned, and independent of the experimental arrangement used to observe it. On the other hand, inner filter effects are instrumental artifacts. They have no influence on the primary processes of emission from the molecules originally excited, but simply reduce the observed intensity of luminescence either by absorption of exciting light or of the luminescence within the material being tested. On general terms there are three types of specimen to be considered: (a) dilute solutions or gases, (b) concentrated solutions and (c) opaque solids. For opaque solids front surface illumination is necessary and for dilute solutions the right-angle geometry is preferred since scattered exciting light, possible fluorescence from sample container and impurity effects are minimally observed here. For concentrated solutions frontal illumination is better. Some workers have used other geometries as well. Different types of specimen arrangement are illustrated in Fig.2.9. Most of our experiments have been carried out in the right-angle geometry, with the samples taken in a 1 cm square quartz spectrophotometer cuvette.

2.3.c Photomultiplier tubes

There are three types of instruments that are generally used to detect or measure light in the visible and ultraviolet regions of the spectrum: the thermopile, various types of photocells and the photoelectron multiplier tube (PMT). Thermopile is the absolute standard for radiation measurement and photocells (photoconductive and photovoltaic) can be used for medium intensities. For the measurement of fluorescence and phosphorescence, particularly at low intensity, the PMT is used almost exclusively because of its extremely high sensitivity. The built-in amplifier system of the PMT containing a series of secondary electrodes (dynodes) may have up to 15 amplification stages, such that one photoelectron can give rise to as many as 10^8 electrons reaching the anode. The sensitivity of a typical PMT can be conveniently varied by changing the voltage applied to the

cathode and dynodes. For a typical tube like EMI 9558Q it can be seen that increasing the applied voltage from 800 to 1800 volts increases the sensitivity by a factor of about 1000. The ultimate sensitivity is limited by the dark current which is caused by the ejection of electrons from the cathode by thermal activation or by traces of radioactivity in the surroundings causing luminescence of the envelope. The dark current problem is more important in tubes sensitive to the near infrared region (eg. type S1 cathodes) since such tubes have cathodes coated with materials of low work function.

Since for low output current levels the PMT may be assumed to act as virtually an ideal constant-current source, the load resistance can be made arbitrarily large, thus converting a low level current output to a high level voltage output. In practice, however, using very large values of load resistance creates the problems of deterioration of frequency response and linearity, as described below [17]. If, as per Fig.2.10a we let the load resistance be R_L and the total of the capacitance of the PMT anode to all other electrodes, including such stray capacitance as wiring capacitance to be C_s , the cut-off frequency f_c is expressed by the relationship

$$f_c = 1/2\pi R_L C_s \quad (2.15)$$

Thus even if the PMT and amplifier have very fast response, the system response will be limited to the cut-off frequency f_c of the output circuit. However, taking into account the input impedance R_{in} of the amplifier, the combined parallel output resistance of the PMT, R_o , is given by $R_L R_{in} / (R_L + R_{in})$ and R_o becomes the effective load resistance to the PMT (Fig.2.10b). When the load resistance is large, at high current levels the voltage drop across R_L becomes large, causing the potential difference between the last dynode stage and the anode to drop. This increases the effect of the space charge, thereby lowering the efficiency of anode in collecting electrons. In effect the output becomes saturated above a certain current, resulting in a loss of linearity. (While this description assumes the load and input impedances to be purely resistive, in practice, stray capacitances, input capacitance, and stray inductances influence phase

relationships. Therefore, as frequency is increased these circuit elements must be considered as compound impedances rather than pure resistances.) Thus the following points should be considered while selecting the load resistance:

- (a) When frequency response is important the load resistance should be made as small as possible.
- (b) When output linearity is important the load resistance should be chosen such that the output voltage is below several volts.

When a high frequency electrical pulse is to be transmitted from one point to another through a transmission line, proper impedance matching should be ensured at the transmitting as well as receiving ends, with respect to the characteristic impedance of the transmission line. Hence a practical high speed output circuit for the PMT should be designed with proper care. If the load resistance is not matched, then part of the pulse energy is reflected back and and dissipated at the PMT itself. However, if there is a mismatch at the PMT output this energy is again reflected back to the load, such that part of the pulse makes a round trip in the transmission line (usually a co-axial cable) resulting in "ringing" of the signal. A practical impedance matched, high speed output circuit for the PMT is shown in Fig.2.10c. For sufficiently strong signals a fast oscilloscope can be connected parallel to R_L for observing the signal. However in most cases the signal will be very weak due to the low value of R_L , and one has to use a high speed amplifier of high gain. To minimize problems due to the inherent noise of the amplifier, the PMT should be brought as close as possible to the amplifier and a load resistance as large as possible should be used (consistent with the preservation of frequency response) to achieve the desired input voltage (Fig.2.10d).

2.3.d Filters

Filters are used for isolating a band of wavelengths of exciting light when measuring a luminescence emission spectrum, or for isolating the required luminescence band when measuring an excitation spectrum. In high sensitivity work filters are often indispensable because one may need to record a very weak emission band against the

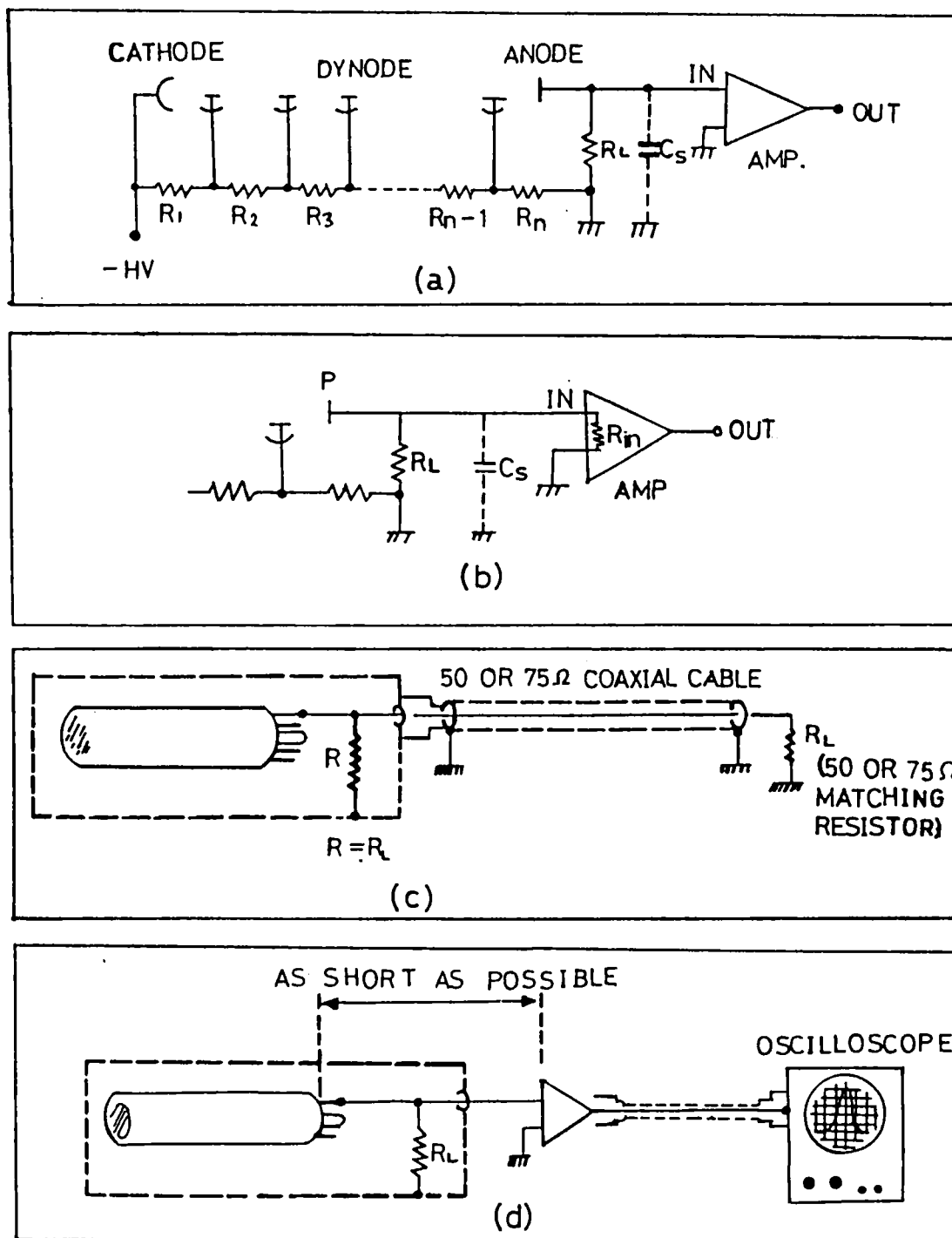


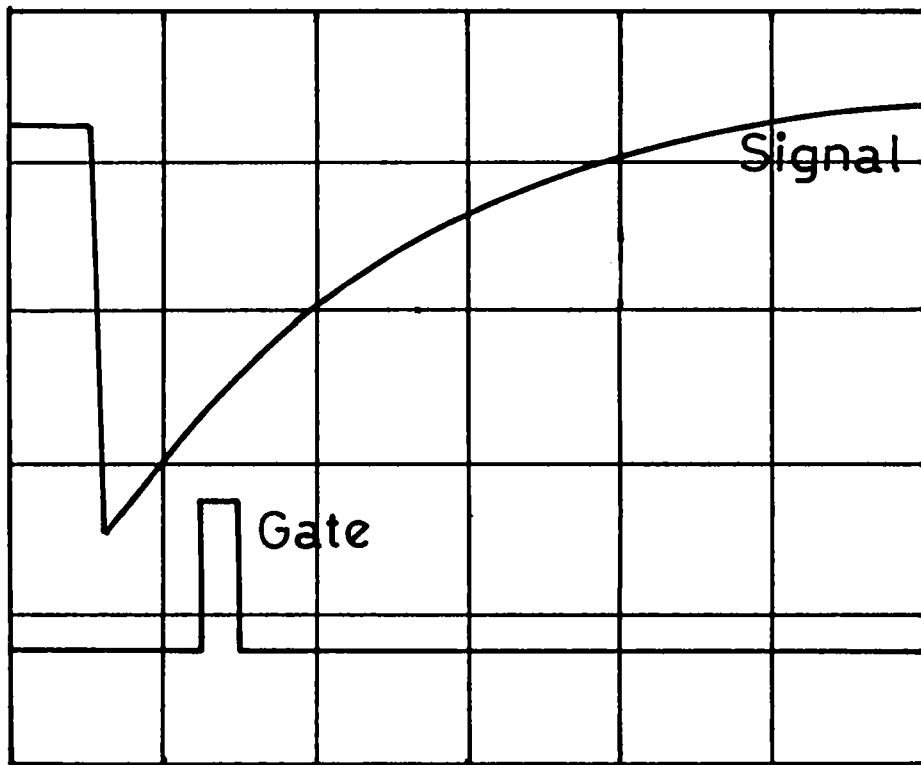
Fig.2.10 : (a) The usual output circuit for PMT, (b) Effect of the amplifier input impedance. R_{in} and R_L are parallel, so that $R_o = R_L R_{in} / R_L + R_{in}$. (c) An impedance-matched, high speed output circuit for the PMT. Note that $R_o \sim 50 \Omega$ only. (d) Waveform observation using an oscilloscope.

background of a strong, unwanted emission. Broad bandpass filters, short wavelength cut-off filters, interference filters etc may be used according to the purpose to be served. In simple fluorometers of low sensitivity and resolution, filters are often used instead of source monochromators for economy. A large variety of glass and gelatine filters are available commercially, and absorbing solution filters can be easily made in the laboratory. Filter combinations may be used for specific applications. Various kinds of filters are extensively discussed in literature [18-20].

2.3.e Data processing

In high sensitivity work like recording two-photon fluorescence spectra the required signal at the PMT output can be completely immersed in noise and the S/N ratio should be improved before recording data. When a pulsed laser is the excitation source, this is accomplished by amplification, gated detection and averaging of the signal. If necessary, this data is then corrected for the spectral response of the Monochromator-PMT combination. Gated detection and averaging is useful for recording weak PA signals as well.

Gating and averaging of a periodic pulse waveform is analogous to the well known lock-in detection in the sense that both techniques aim at an ultimate enhancement of the S/N ratio. The former suits the analysis of a pulse profile whereas the latter is ideal when the excitation beam is chopped at a comparatively lower, but fixed frequency. To understand the underlying principle of gated integration and averaging let us first consider the temporal profile of a typical weak fluorescence signal detected with a PMT (Fig.2.11). The measurements are taken at a particular point in this profile by means of an electronic 'gate', discarding the rest of the signal. Now if we allow 100 signal pulses to be generated, then the gate can be set to measure the amplitudes at the prescribed point for each pulse, add them up and divide by 100 (electronically) giving the average value of the point being measured. A practical GIBA takes the moving average of the signal in time and in this process the random noise will average out to zero, with an efficiency proportional to the square root of the number of samples being averaged. Thus pulse-to-pulse variations in the signal due to the laser jitter as well as random noise is



Sweep : $50\mu\text{s}/\text{div}$

Gate width : $12\mu\text{s}$

Fig.2.11 :Gated detection of a weak fluorescence pulse. The gatewidth is adjustable.

suppressed, resulting in a much better S/N ratio.

2.4 The present fluorescence set up

The parts of our fluorescence spectrometer (Fig.2.12) are the following: an Nd:YAG laser, a 1 cm square quartz spectrophotometer cuvette, a collection lens, an appropriate bandpass filter (CVI/Melles Griot), monochromator (Jarrell-Ash/McPherson), PMT (EMI/Hamamatsu), GIBA system (SRS/EG&G) and X-Y recorder (Rikadenki). Two coated mirrors are used to filter out the 1060 nm fundamental beam from the 532 nm second harmonic beam of the laser. Essential details of the monochromators and PMT s used are given below:

a. Jarrell-Ash, Model 82-000

Jarrell-Ash 82-000 is a 0.5 meter Ebert scanning monochromator having a maximum resolution of 0.02 nm. The monochromator covers a spectral range of 200 nm to 1600 nm with three interchangeable gratings blazed at 180 nm, 500 nm and 750 nm respectively. The reciprocal linear dispersion at exit slit is 1.6 nm/mm. This instrument provides a smooth scanning motion in eight speeds ranging from 0.2 nm/minute to 50 nm/min. The output from the Jarrell-Ash monochromator is detected by an EMI, Model 9683 KQB photomultiplier tube that can be directly mounted at the exit face of the monochromator. Model 9683 is a Head-on type PMT having an S-20 cathode, and performs well in the 300-800 nm region.

b. McPherson, Model 275

McPherson, Model 275 is a 0.2 meter concave holographic grating monochromator that can cover a spectral range of 185 to 4000 nm using appropriate gratings. The wavelength accuracy is ± 0.5 nm and wavelength reproducibility is ± 0.1 nm. The wavelength scanner has nine digitally controlled speeds : 0.5,1,5,10,20,100 and 200 nm/min.. The output of this monochromator is detected by a Hamamatsu R446 PMT, which is a side-on photomultiplier tube having a multialkali photocathode and a 9 stage circular cage dynode structure. Its quantum efficiency is high in the region of 200 nm to 800 nm.

The spectral response curves of the above two systems, calibrated

SHG-Second Harmonic Generator
 HSEP-Harmonic Separator

M-Monochromator

L-Collection Lens

F-Filter

Mirror

Cuvette



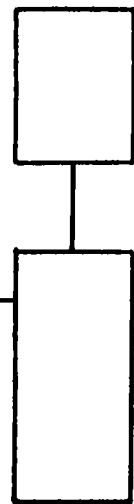
L

F

M

CRO

PMT



GIBA

Chart Recorder

Nd:YAG LASER

1064 nm

532 nm

Fig.2.12 :The present fluorescence set up. HSEP reflects off the 1064 nm part in the 532 nm beam as shown.

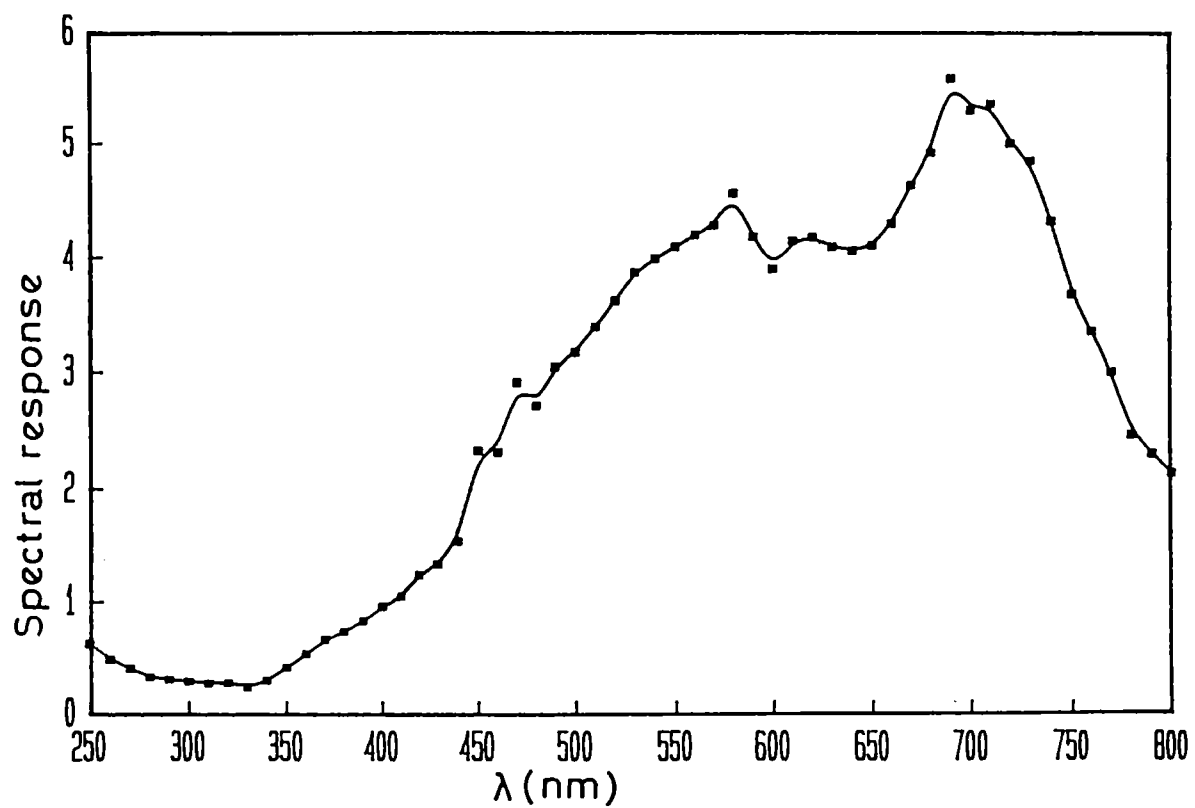


Fig.2.13a : Spectral response curves obtained for the Jarrell-Ash monochromator + EMI 9683 KQB PMT system.

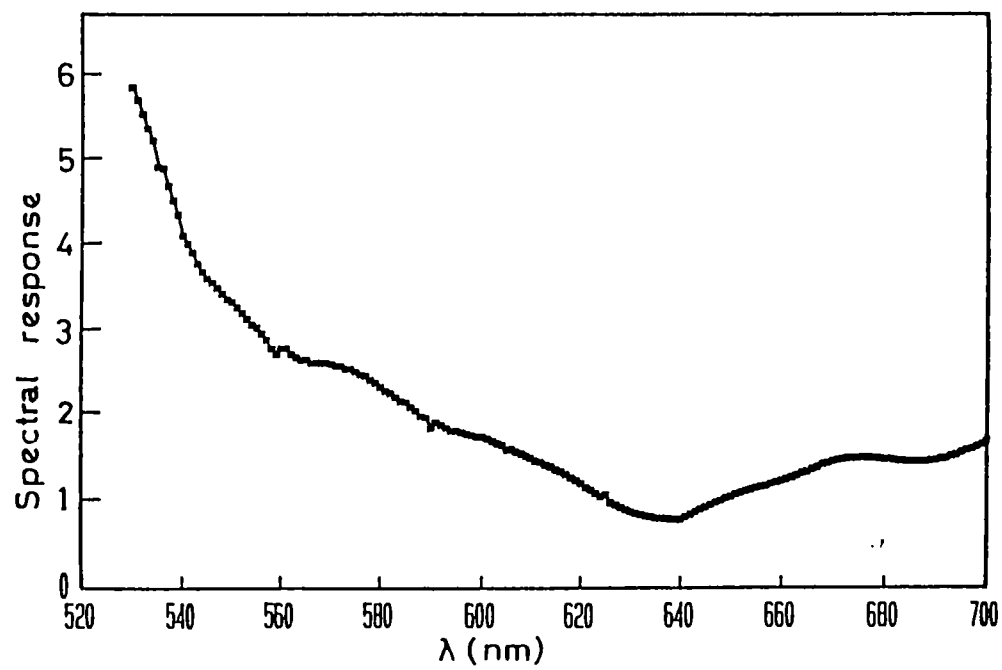
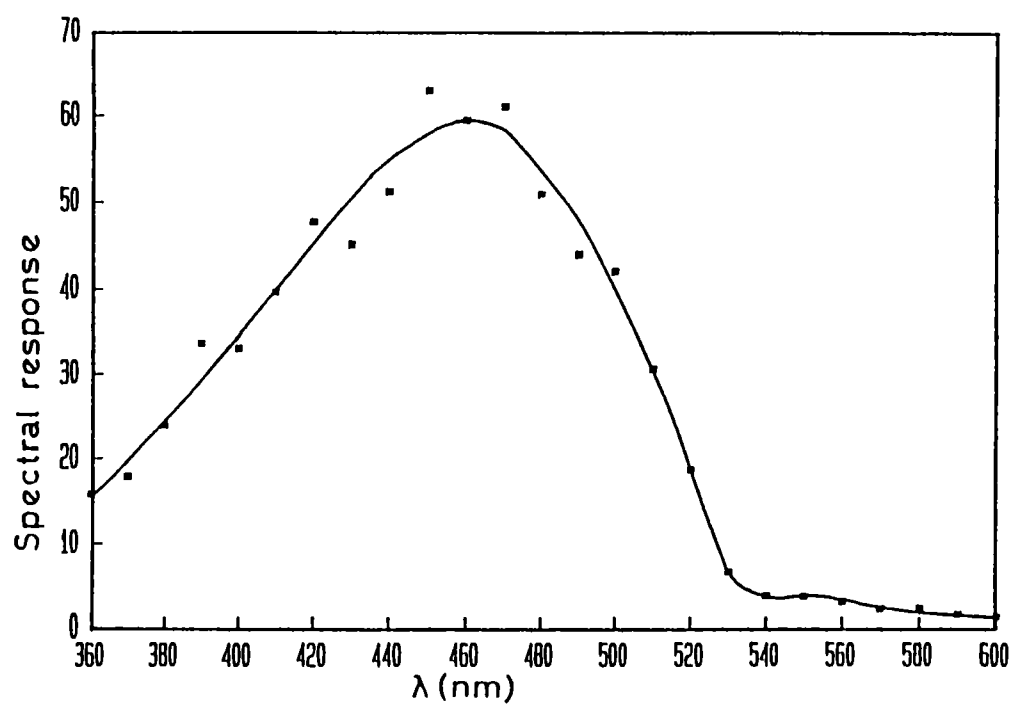


Fig.2.13b : Spectral response curves obtained for the MoPherson monochromator + Hamamatsu R446 PMT system.

against a xenon arc lamp, are shown in Fig.2.13.

2.5 Instrumentation for Stimulated scattering (SS) and Optical phase conjugation (OPC)

The basic setup for SS and OPC is shown in Fig.2.14. The pump laser beam is sent through a polarizer cube and $\lambda/4$ plate and focused by a convex lens into the sample taken in a cylindrical glass cell. The polarizer and $\lambda/4$ plate together forms an optical isolator, which separates the backward scattered phase conjugate beam from the pump beam as shown. The scattered beam is observed by a suitable photodetector. The signal is then processed by means of a fast sampler unit and boxcar averager, and the boxcar output is fed to a chart recorder. When the SRS spectrum is to be recorded a monochromator is used instead of the fast sampler. Further details are given in chapter 5.

2.6 Common instruments used

The same laser source and a few associated equipments have been used in PA, Fluorescence, SS and OPC experiments, details of which are given below.

2.6.a Laser source

The optical source for all the experiments conducted is a Q-switched, pulsed Nd:YAG laser (Spectra Physics, DCR-11) which is a class IV high power laser generating the fundamental infrared beam at 1064 nm. A second harmonic generator crystal-KD*P- doubles this frequency to provide green radiation at 532 nm, which is used in most of our experiments. The laser pulse width is measured to be approximately 10 ns and a maximum of 275 mJ energy is available at 1064 nm. The pulse repetition frequency is variable from 1 Hz to 16 Hz. The laser cavity is a diffraction coupled resonator and the beam is nearly diffraction limited having a diameter of 6.4 mm. Beam divergence is less than 0.5 mrad; cross section is TEM₀₁ mode and the beams at 532 nm and 1064 nm are linearly polarized in mutually perpendicular directions. The linewidth is less than 1.0 cm⁻¹.

Fig.2.15 shows a schematic of this laser system.

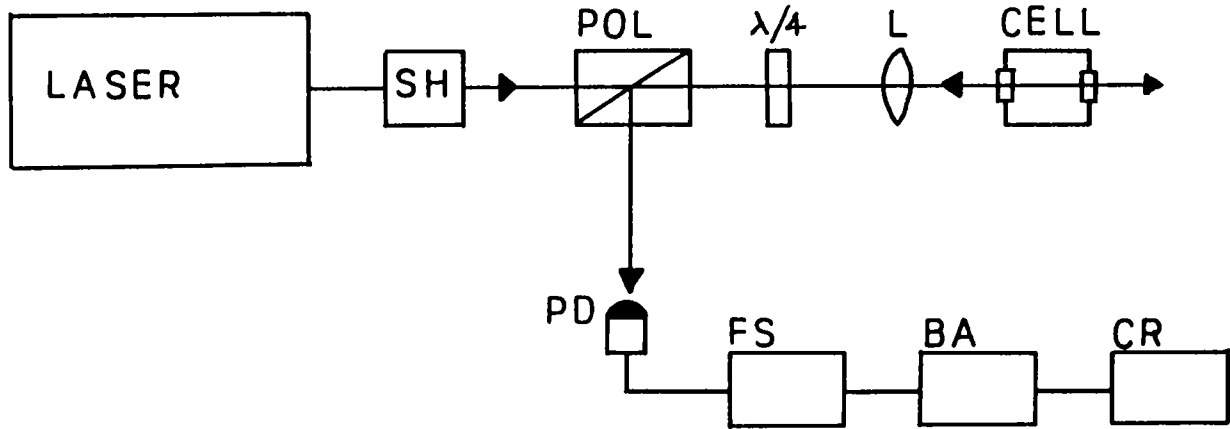


Fig.2.14 : The basic set up for stimulated scattering and phase conjugation studies. The optical isolator separates the backward scattered radiation from the pump radiation by polarization discrimination.

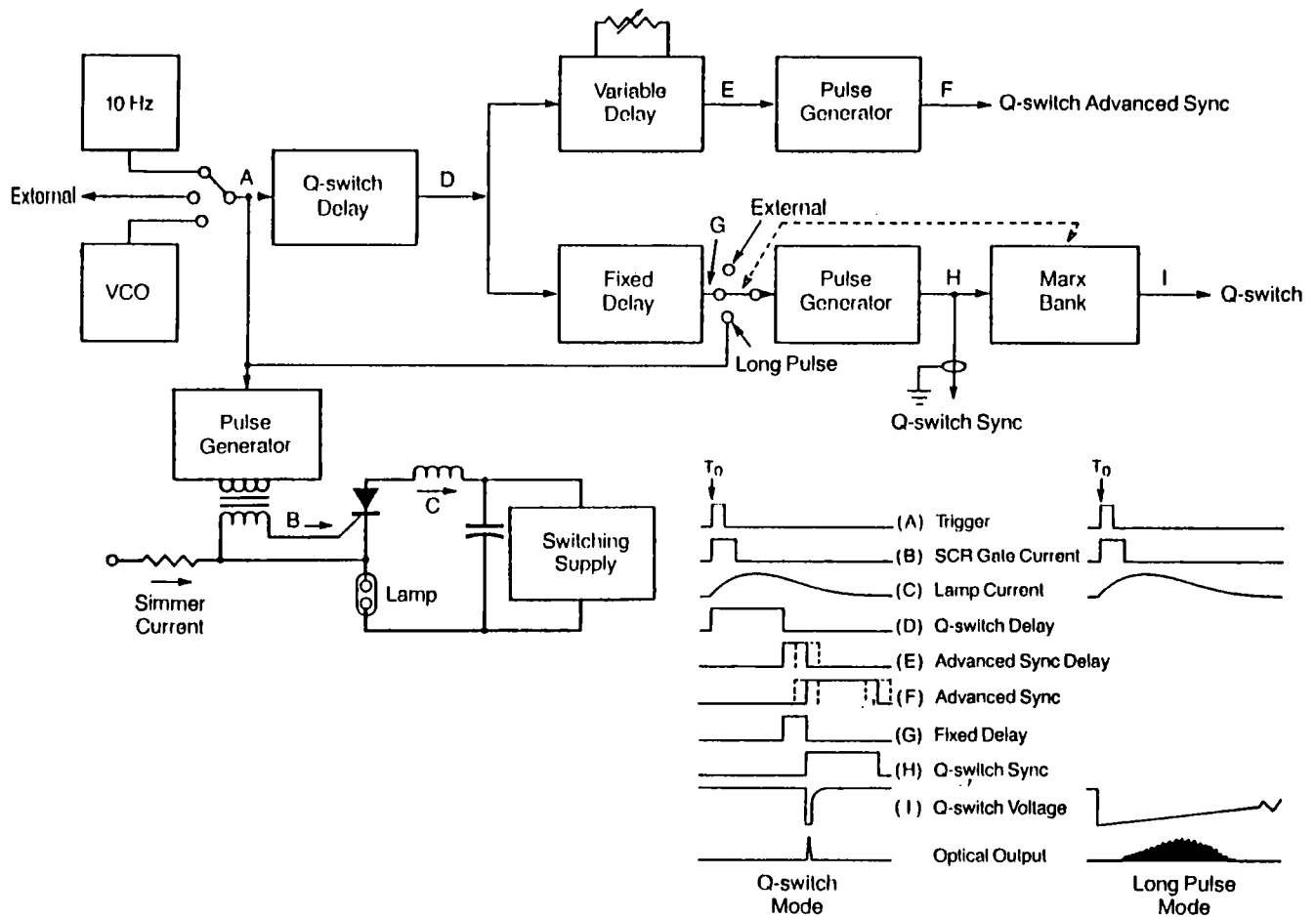


Fig.2.15 : Simplified block diagram of the Nd:YAG laser system (DCR-11, Spectra Physics).

2.6.b Power meters

The phenomena investigated in the present work are strongly dependent on the energy of the optical radiation, which necessitates an accurate measurement of the laser flux being absorbed. We have used the following commercial laser power/energy meters for these measurements:

i. Scientech model 38-0101

Model 38-0101 manufactured by Scientech is a volume absorbing disc calorimeter suitable for measuring energy/power of pulsed and cw lasers. A number of thermoelectric junctions are arranged in series and sandwiched between an absorption surface and a massive heat sink forming a thermopile. When a laser beam falls upon the absorption volume, heat is produced which is converted to an electrical signal by the thermopile. The voltage generated is proportional to the laser power and independent of the spatial characteristics of the beam.

The volume absorbing dielectrics in model 38-0101 are made of schott glass and plastic, and the thermopile can generate 97.2 mV per Watt of heat absorbed. The spectral response is flat from 400 nm to 1200 nm. Maximum limit of average power density is 15.4 Watts/cm² and that of pulse energy density is 1.2 J/cm² (at 400 nm). An attractive feature of model 38-0101 is its large dynamic range covering four decades of power, extending from 0.001 W to 10 W full scale.

ii. Coherent-Labmaster

Labmaster is a microprocessor based laser measurement system manufactured by Coherent, featuring automatic beam alignment indication, digital precision and power versus time data collection capability. The pulse averaging facility gives the average pulse energy of a train of laser pulses, and this is especially useful when there are pulse-to-pulse energy variations. Labmaster, equipped with the pulse detector head LM-P5 has a wide frequency response. It can measure laser pulses in the range of 190 nm to 20 μm. It is an easy-to-use system but has the following limitations:

- (a) The maximum energy density that can be measured without

damage to LM-P5 detector head is only 0.05 J/cm^2 .

(b) Periodic calibration is required for the detector head and processor.

Labmaster is found to be very convenient for measuring moderate laser energies.

iii. Delta developments-Pulsed laser energy meter (PLEM)

It is a photodetector based energy meter manufactured by Delta developments. A polarization compensated beam splitter samples a part of the laser beam that is to be measured. This sampled beam strikes a retro-reflecting diffuser and reaches the photodetector via a "range plate" which attenuates the light appropriately for the range of energies being measured. The geometry is such that all positions on the diffuser give equal signals. Different range plates are used for different energies and wavelengths. The PLEM can safely measure energies up to 300 mJ, but one limitation is that range plates should be changed for different laser wavelengths.

2.8.c Storage oscilloscopes

In the course of this work, digital and analog storage oscilloscopes (Iwatsu, Model DS 8621, 200 MHz and Tektronix, Model 466, 100 MHz) have been used instead of boxcar detectors whenever the signal strength is sufficiently high. For example, a fluctuating PA signal of $100 \mu\text{V}$ amplitude could be amplified to 5 mV by our pulse preamplifier and detected on the Digital storage oscilloscope (DSO) making use of its averaging option. Another advantage is that an RS232 interface port is available on the DSO that can directly drive a plotter.

2.7 Laser beam profile analysis by photoacoustics

To check the performance of the fabricated PA detection system, we have carried out an experiment in which the intensity profile of the above described pulsed Nd:YAG laser has been determined by a PA technique [21]. The proportionality of the PA signal amplitude on incident energy is made use of in this experiment. The experimental

set-up is as shown in Fig.2.16. The second harmonic output (532 nm) of the Nd:YAG laser, with a beam diameter of 6.4 mm, is allowed to pass through a circular aperture of 2 mm diameter. The aperture is fitted to a micrometer so that it can be moved across the beam cross section to scan the intensity point by point. The radiation that passes through the aperture is focused by a lens into the photoacoustic cell that contains acetone. Acoustic signals are generated due to the excitation of higher vibrational overtones in acetone, and these signals are detected by the transducer. The transducer output is directly connected to a storage oscilloscope. The PA signal intensity corresponding to different points on the beam cross section is measured by moving the micrometer across the beam. The plot of the aperture position versus PA signal intensity gives the spatial intensity profile of the laser beam.

The Nd:YAG laser used in our experiment has an unstable resonator configuration. Stable resonators can extract energy only from a small volume near the optical axis of the resonator. However unstable resonators can support large beam diameters, enabling them to extract more energy from active media like typical Nd:YAG laser rods, where cross-sectional area is comparatively larger. The output coupler in an unstable resonator can take a form in which a small reflector mounted on a clear substrate lies on the optical axis of the resonator. Energy escapes the resonator by diffracting around this dot, which gives the diffraction coupled resonator its name. Hence the collimated beam is usually of TEM_{01} mode (doughnut shaped), with a minimum intensity at the centre.

Fig.2.17 shows the beam profile determined using the photoacoustic method, as well as that given by the laser manufacturer [22]. A comparison of the figures shows that the present method reproduces the beam profile with reasonable accuracy. The result indicates that a simple uncalibrated PA cell can replace expensive laser power meters for the comparison of relative optical intensities. The merits of the technique are that the cell fabrication is not complicated, and it has a large dynamic range.

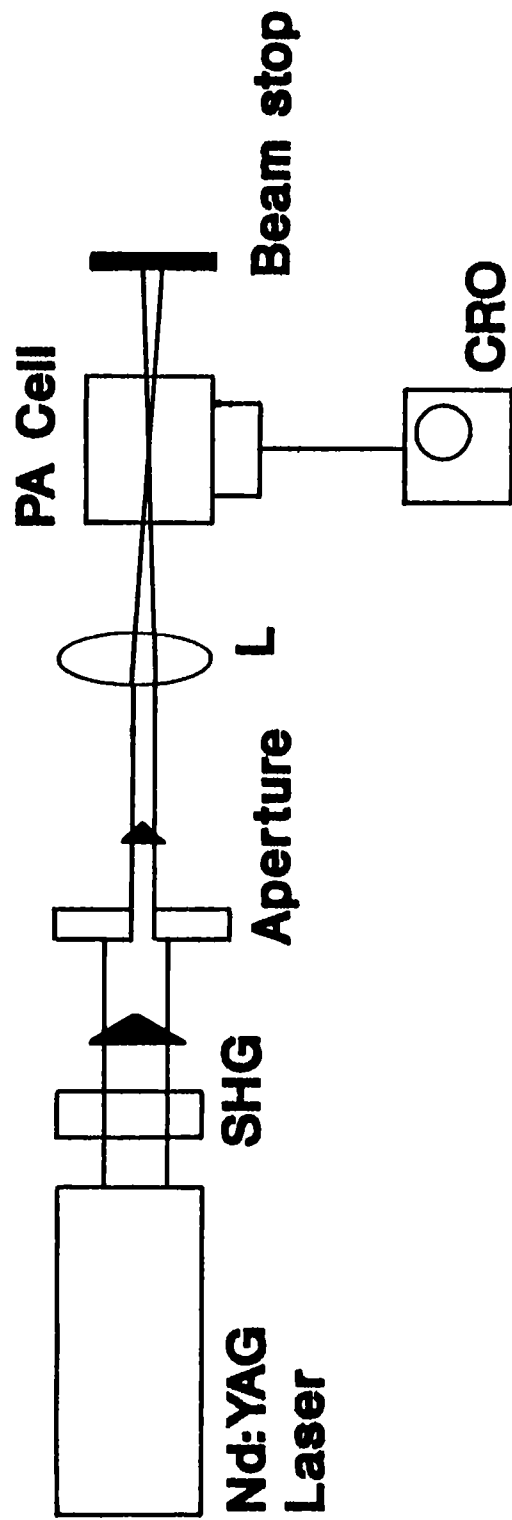


Fig.2.16 :Set up for the photoacoustic measurement of the intensity profile of Pulsed Nd:YAG laser. The aperture is fixed on a micrometer so that it can be moved across the laser beam.

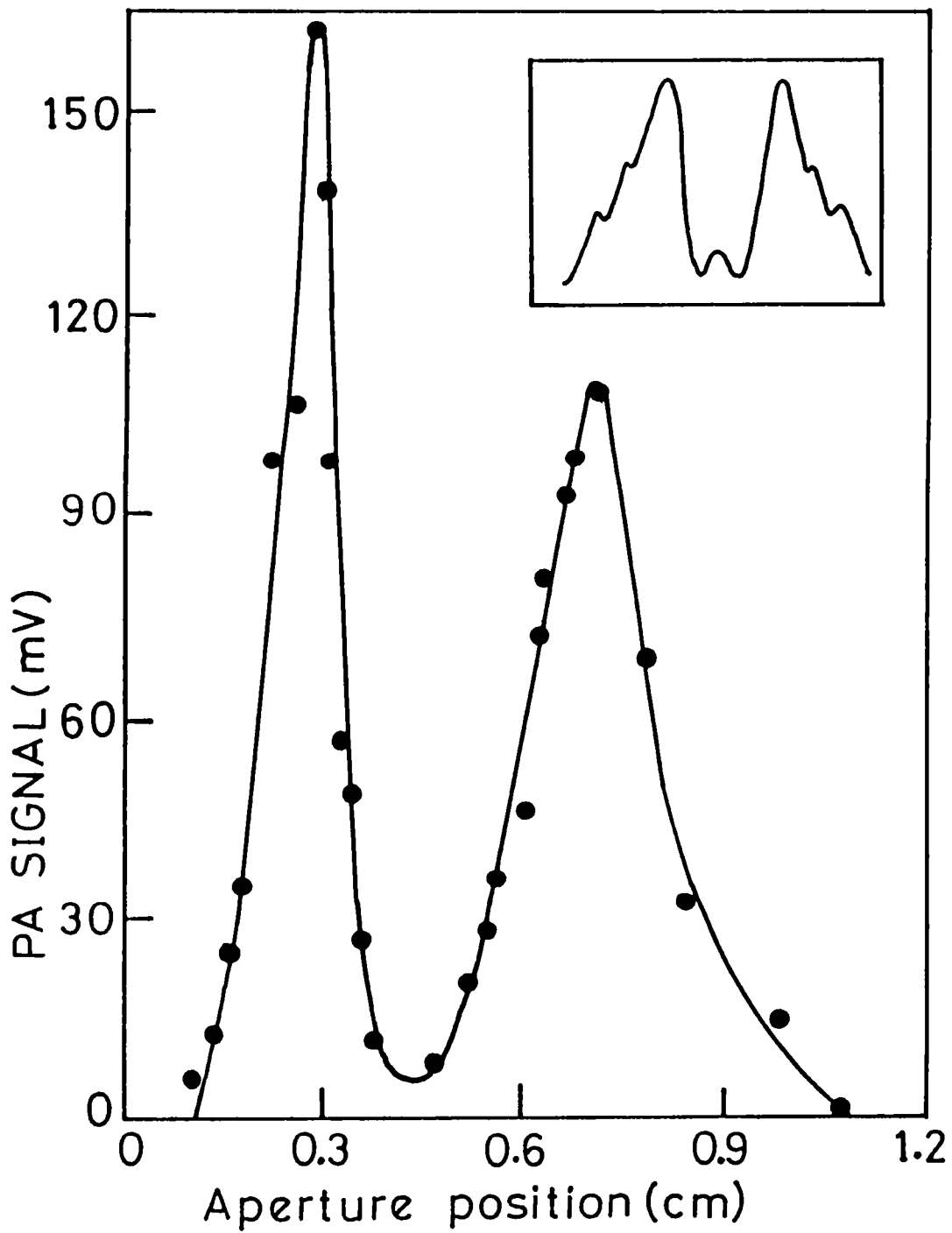


Fig.2.17 :Spatial beam intensity profile of the pulsed Nd:YAG laser, obtained from photoacoustic measurements. Inset shows the beam profile given by the manufacturer (Spectra Physics, USA).

CHAPTER 2 - REFERENCES

- [1] Parker C A, "*Photoluminescence of solutions*", Elsevier, London (1968)
- [2] Elenbaas W & J Riemens, Philips Techn. Rev. **11**, 299 (1950)
- [3] Tam A C, Rev. Mod. Phys. **58**, 381 (1986)
- [4] Hess P, in "*Topics in current Chemistry*", (Ed.) F L Boschke, Springer, Berlin (1983)
- [5] Rosengren L G, Appl. Opt. **14**, 1960 (1975)
- [6] Dewey C F, in "*Optoacoustic spectroscopy and detection*", (Ed.) Y H Pao, Academic Press, New York (1977)
- [7] Rosencwaig A, "*Photoacoustics and Photoacoustic spectroscopy*", Wiley, New York (1980)
- [8] Mason W P and R N Thurston (Eds.), "*Physical Acoustics*", Vol.14, Academic, New York (1979)
- [9] Sussner H, D Michas, A Asstalg, S Hunkfinger and K Dransfield, Phys. Lett. A **45**, 475 (1973)
- [10] Tam A C, Appl. Phys. Lett. **45**, 510 (1984)
- [11] Khuri-Yakub B T & G S Kino, Appl. Phys. Lett. **30**, 78 (1977)
- [12] Cantrell J H and M A Breazeals, J. Acoust. Soc. Am. **61**, 403 (1977)
- [13] Cook R O and C W Hamm, Appl. Opt. **18**, 3230 (1979)
- [14] Mason W P, "*Piezoelectric crystals and their applications to ultrasonics*", Van Nostrand, New York (1950)
- [15] Patel CKN and A C Tam, Rev. Mod. Phys. **53**, 517 (1981)
- [16] in press.
- [17] Catalog on Photomultipliers, Hamamatsu Corporation.
- [18] Calvert J G & J N Pitts Jr., "*Photochemistry*", John Wiley & Sons, New York (1966)
- [19] Bowen E J, "*The chemical aspects of light*", Clarendon press, Oxford (1946)
- [20] Kanha M, J. Opt. Soc. Am. **38**, 929 (1948)
- [21] Reji Philip, P Sathy, VPN Nampoori and CPG Vallabhan, J. Acoust. Soc. Ind. **17**, 332 (1989)
- [22] Catalog on DCR-11 pulsed Nd:YAG laser, Spectra Physics, USA.

CHAPTER - 3

HIGHER ORDER ABSORPTIONS IN DCM

3.1 Introduction

DCM (4-dicyanomethylene -2-methyl-6-p-dimethylamino - styryl- 4H-pyran) , the structure of which is shown in Fig.3.1, is a widely used laser dye belonging to the merocyanine family. It shows a large stokes shift and a consequent small overlap between the absorption and emission bands. Lasing in DCM has been observed with several excitation sources including flashlamp, nitrogen laser, copper vapour laser and argon ion laser. DCM is attractive in the following respects: (a) it exhibits high conversion efficiency over a broad tuning range (≈ 120 nm), (b) produces wavelengths as long as 725 nm when pumped with the blue-green line of an argon ion laser, (c) spans the wavelength region between rhodamine 6G and oxazine 1 dyes with a tunability and efficiency that eclipses the performance of the alternatively used rhodamine 101 and cresyl violet dyes and (d) has a long lifetime under photochemical excitation. According to Marason [1], even after 220 watt-hours of continuous pumping, DCM has not shown any sign of degradation.

The spectral properties of DCM are strongly dependent on the nature of the solvent because of the charge-transfer characteristics of the emitting state. Benzyl alcohol, dimethyl sulphoxide and dimethyl formamide are found to be good solvents for DCM, but it has only limited solubility in the usual solvents like methanol, ethanol and ethylene glycol. A mixture of 40% benzyl alcohol and 60% ethylene glycol has been found to be a good substitute for pure ethylene glycol in the case of DCM in jet-stream operation, where high viscosity and good thermal conductivity are essential. Recently the structure of DCM has been modified by introducing hydrophilic substituents into the molecule [2] to yield higher solubility in various solvents including those mentioned above. For example, DCM in dimethylformamide (DMF) shows a quantum yield of ≈ 0.8 , whereas that for the modified form of DCM is ≈ 0.91 .

This chapter presents the details of investigations carried out

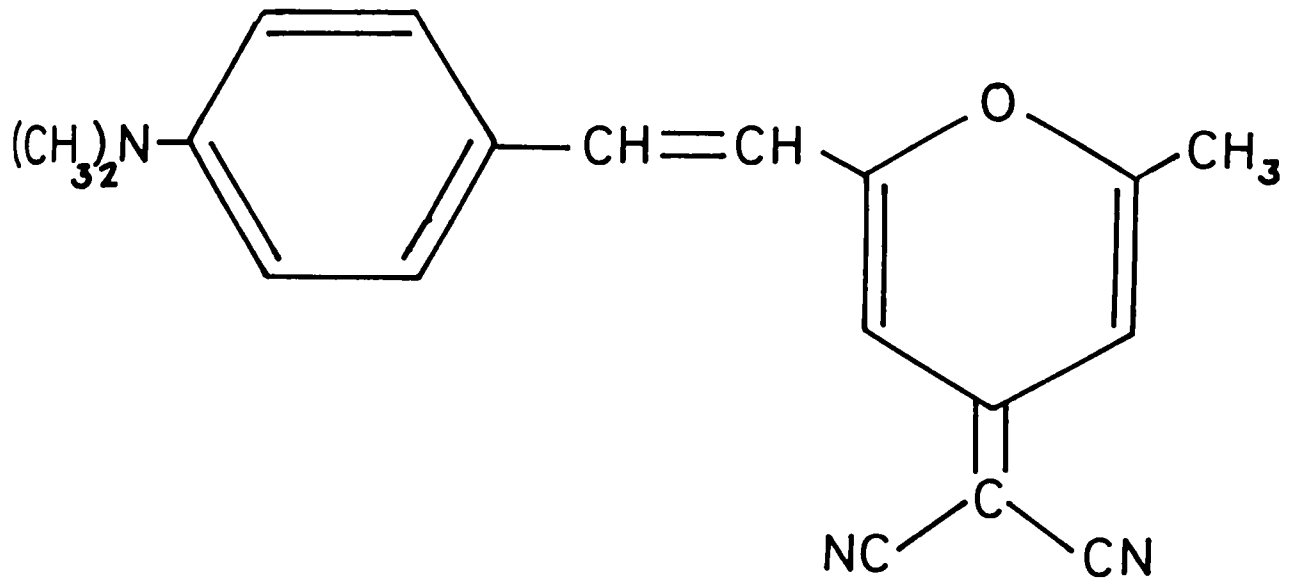


Fig.3.1 : Structure of the DCM molecule.

on higher order absorptions in various concentrations of DCM samples employing photoacoustic and fluorescence techniques. The solutions have been prepared in two recommended solvents, namely DMF and a 6:4 mixture of ethylene glycol and benzyl alcohol (referred to as EGBA henceforth).

3.2 Absorption and Fluorescence properties

The absorption spectra of DCM (exciton) recorded on a UV-VIS-NIR spectrophotometer (Hitachi, model U-3410) in the solvents EGBA and DMF are shown in Figures 3.2a and 3.2b respectively. The samples are taken in a 1 cm square spectrophotometer cuvette. The absorption spectra are identical to those reported earlier, thereby ensuring the purity of the sample. The fluorescence emission from various samples also has been recorded at 90° collection geometry, and the emission spectra corrected for the spectral response of the PMT and grating are shown in Fig. 3.3a and 3.3b respectively. The emission peaks around 640 nm in DMF whereas the peak is approximately at 635 nm in EGBA solution. It is interesting to note that even though a large concentration range is spanned, reabsorption effects are not seen in the spectra, due to the minimal overlap between the absorption and emission bands.

3.3 Investigations by photoacoustics

As seen from the absorption spectra, the long wavelength absorption band of DCM is centred around 490 nm. There is moderate absorption at the present excitation wavelength of 532 nm, whereby some of the molecules can get excited to the S_1 state. Depending on the pump flux and the sample, nonlinear and/or excited state absorption can occur in a typical dye medium. Various nonradiative relaxation channels are active in a highly excited large molecule, which will lead to the generation of photoacoustic signals. Analysis of these PA signals can yield valuable information about the nature of absorption and the distribution of various energy levels of the molecule.

3.3a Experimental

For preparing the samples, an appropriate weight of the dye is

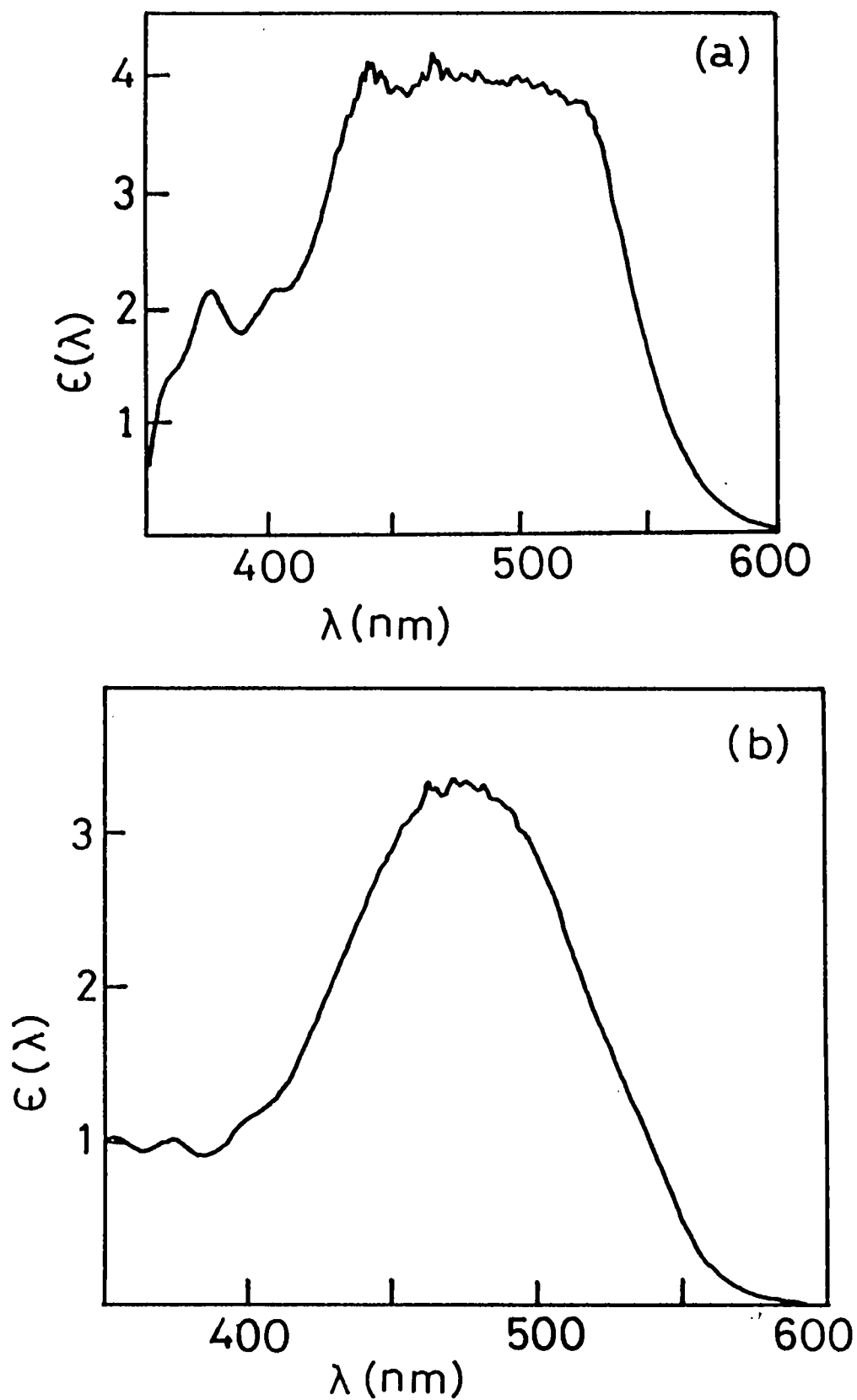


Fig.3.2 : Absorption spectra of DCM. $\epsilon(\lambda)$ is the absorbance. (a) in EGBA solution, concentration : 1.6×10^{-4} moles/lit; (b) in DMF solution, concentration : 7.6×10^{-5} moles/lit. Due to the large absorption in the 1 cm cuvette, detector noise is seen at the peak absorption region.

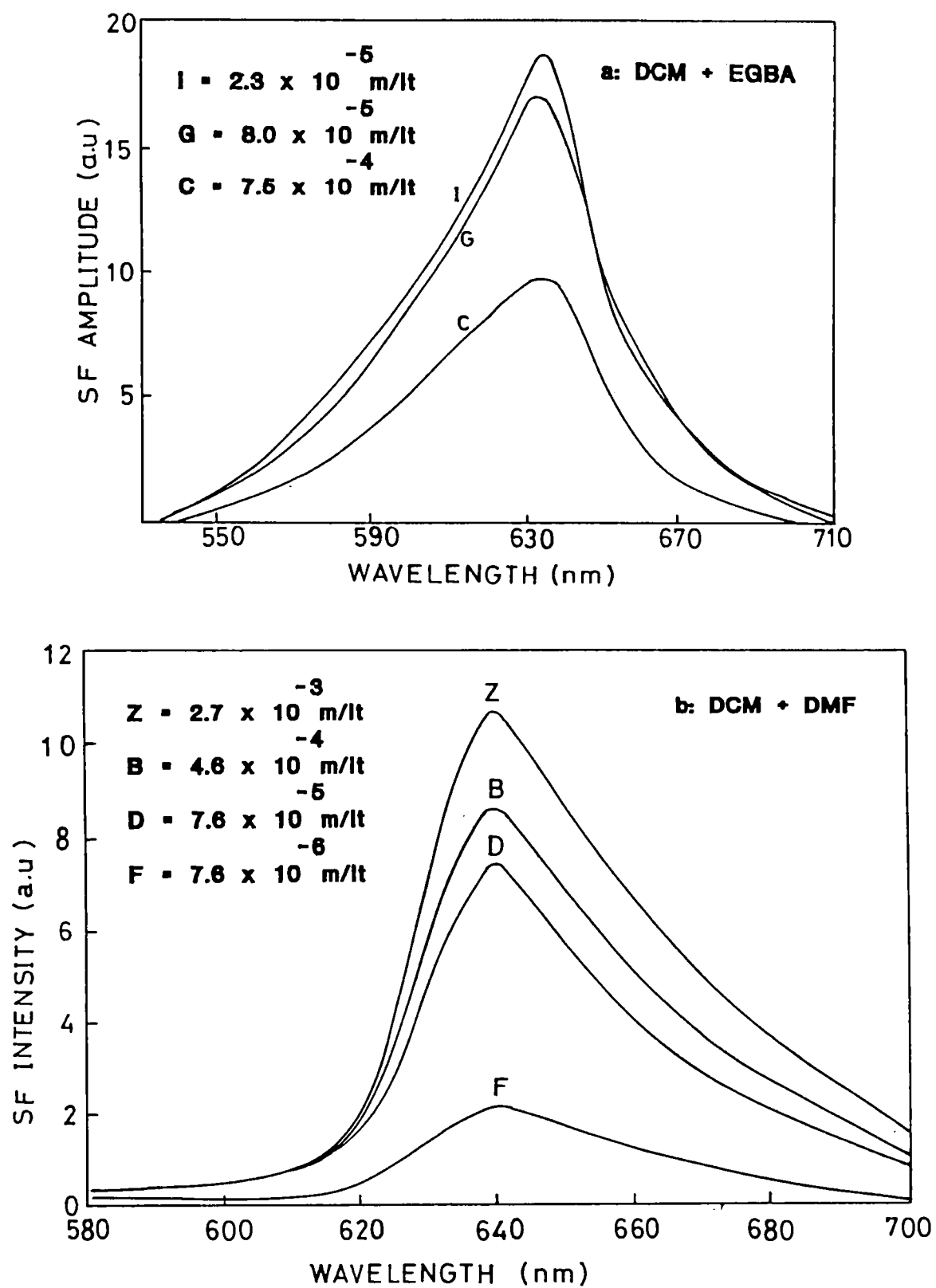


Fig.3.3 : Corrected Fluorescence emission spectra observed in the right-angle geometry from DCM solutions of various concentrations. Reabsorption effects are not seen in the spectra.

initially weighed on an accurate electronic balance and dissolved in the solvent to make a stock solution. Subsequent lower concentration samples are prepared by sequential dilution of this stock solution. The sample is then taken in the PA cell which is firmly held on a holder, and properly aligned with the laser beam axis. The laser is run at a repetition rate of 16 Hz and the focused laser beam passes through the sample in the PA cell. The acoustic signals generated are detected by the PZT, amplified if necessary and observed on the digital storage oscilloscope or boxcar averager. When readings are taken for one sample it is pipetted out and the next sample is filled, without moving the PA cell. The experiment is repeated for various concentrations of the sample, and various pump energies. The experimental setup is shown in Fig.2.3 of chapter 2.

3.3b Results

Figs.3.4a, 3.4b and 3.4c show the log laser pulse energy versus log PA amplitude plots obtained for the DCM + EGBA system, investigated in the concentration range of 2.3×10^{-5} moles/lt to 4.7×10^{-3} moles/lt. In Figs.3.5a and 3.5b the same obtained for DCM + DMF samples are given. The pulse energies are measured in mJ and PA signal in mV. The pulse preamplifier described in the previous chapter has been used in most of the measurements since the PA signals are quite weak at low pump intensities. For example, when 3.6 mJ of laser pulse energy at 532 nm is focused by a 5 cm lens into the PA cell containing a DCM + EGBA sample of concentration 4.7×10^{-3} moles/lt, the PA amplitude obtained without the preamplifier is 166 μ V. On the other hand, when the pump energy is increased to 70 mJ keeping all other parameters the same, 33 mV of PA signal has been achieved. The slopes of the log-log plots have been calculated, and the variation of the slope as a function of sample concentration is shown in Figs.3.6a and 3.6b for the EGBA and DMF solutions respectively. Except for minor variations in the finer details both the curves look essentially similar. However it may be noted that the nonlinearity, as revealed from the slope, is higher in EGBA solutions. At low concentrations the slope seems to be independent of pump energy whereas at higher concentrations it is strongly energy dependent. The mean value of the slope verified from repeated experiments is given in each case, and

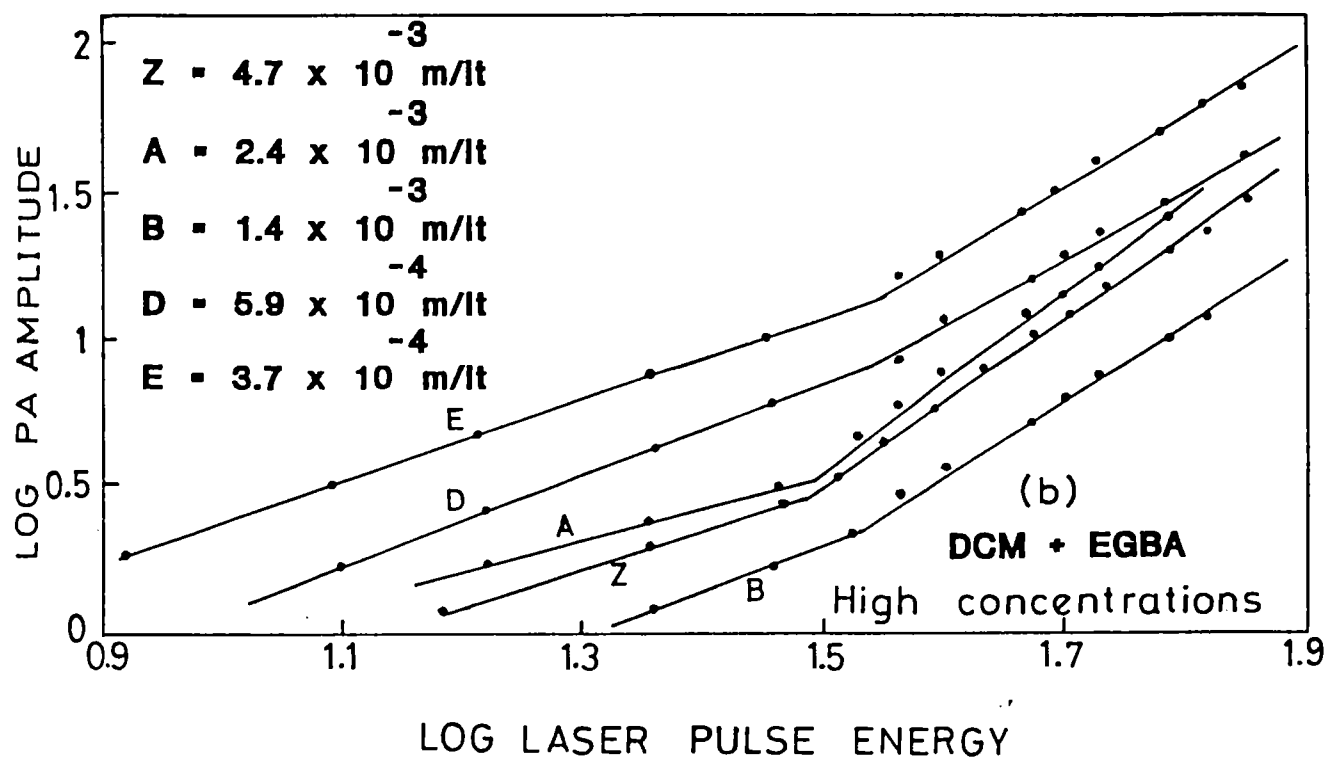
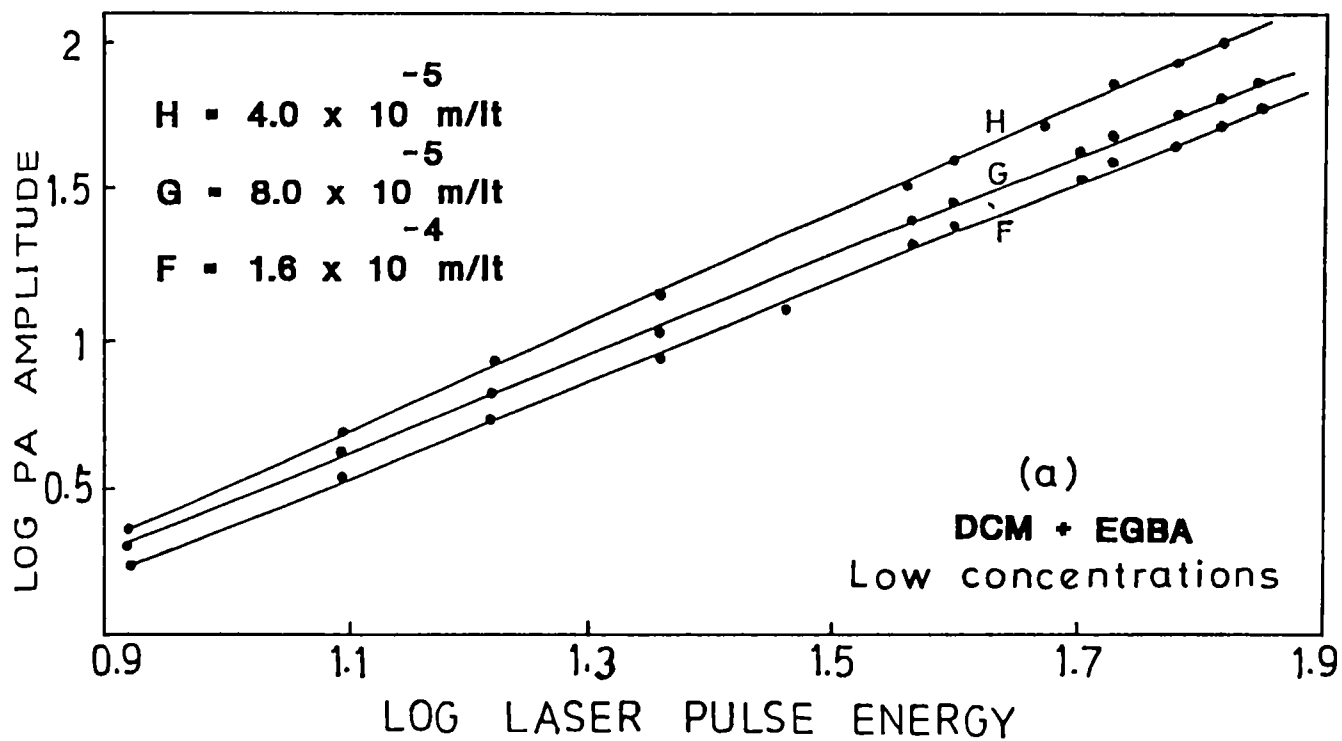


Fig.3.4 : Log laser pulse energy versus log PA amplitude plots, obtained for DCM + EGBA samples at 532 nm pumping.

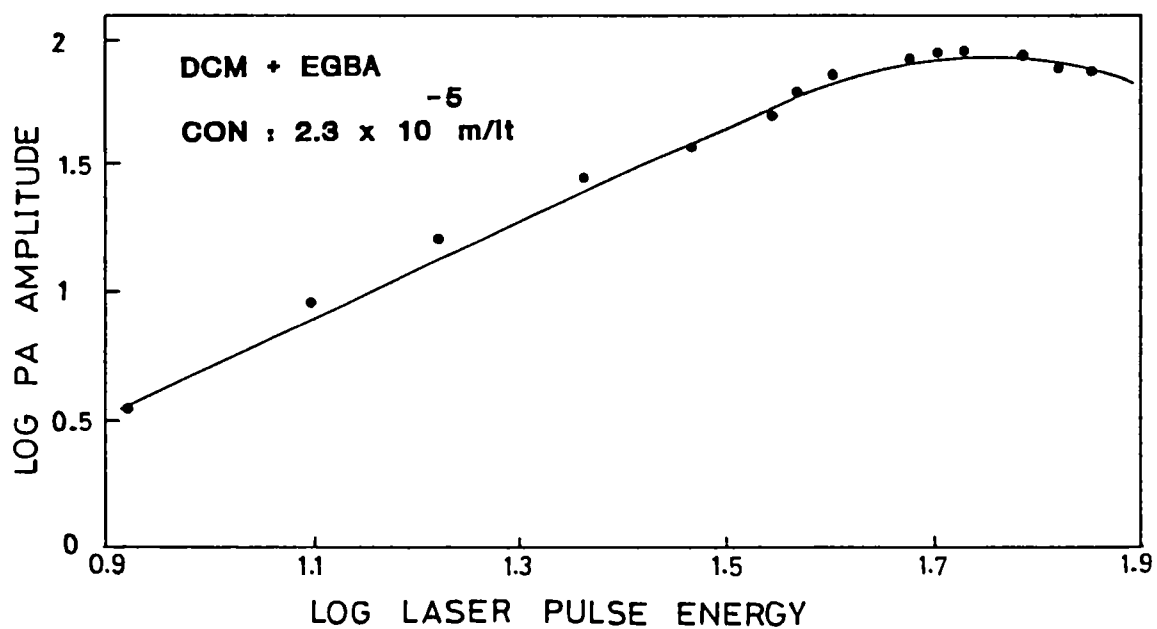


Fig.3.4c : Log laser pulse energy versus log PA amplitude plot, obtained for the lowest concentration of DCM + EGBA sample studied, at 532 nm pumping. PA saturation is seen at high pump energies.

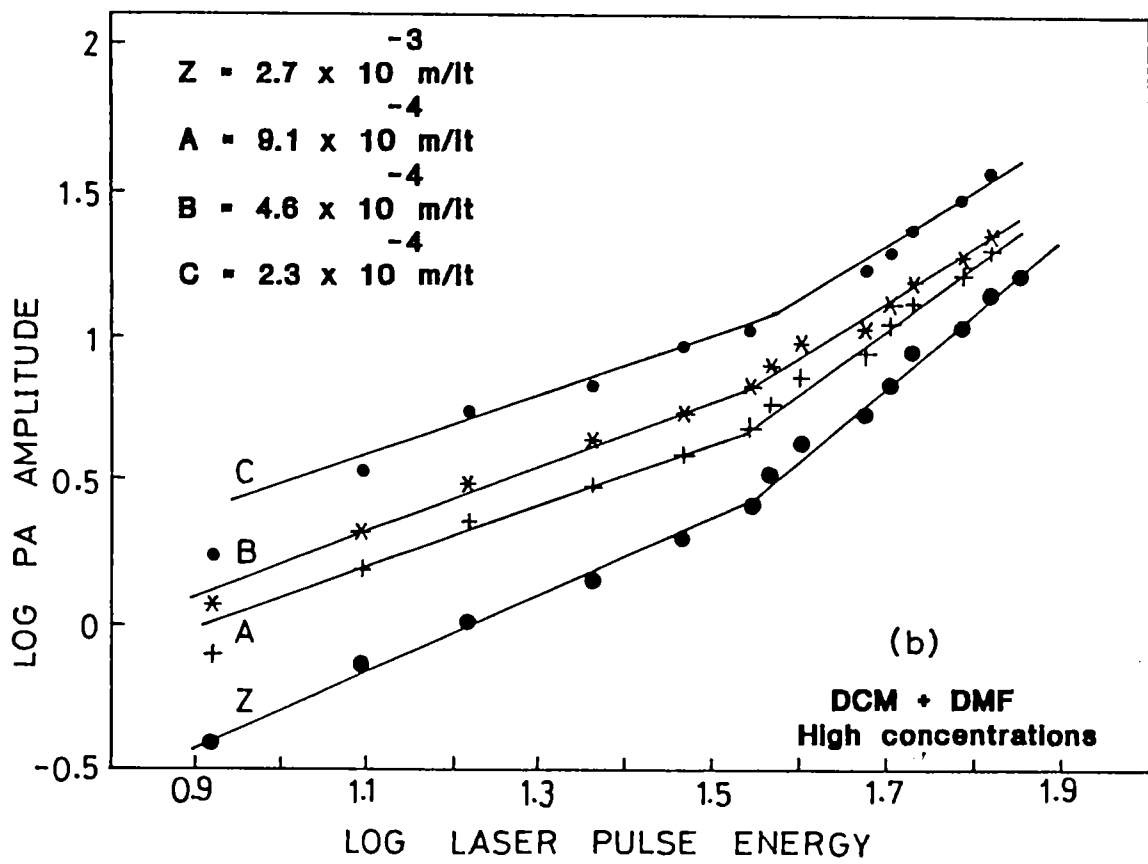
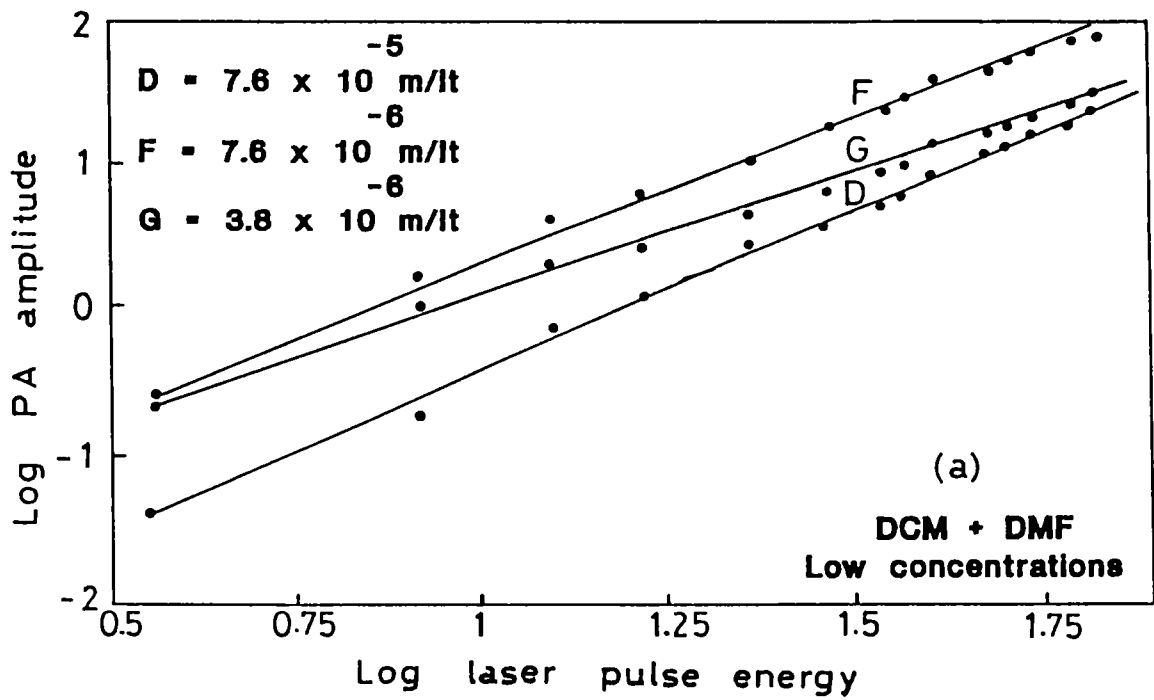


Fig.3.5 : Log laser pulse energy versus log PA amplitude plots, obtained for DCM + DMF samples at 532 nm pumping.

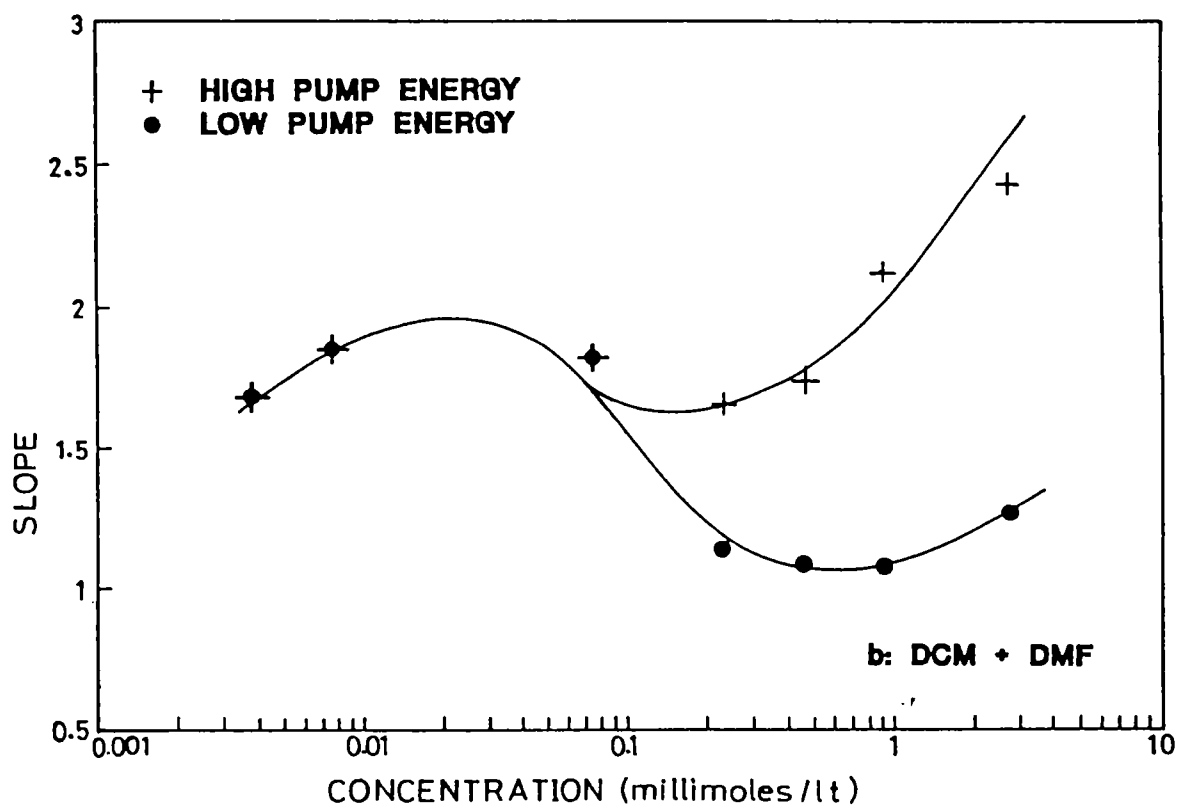
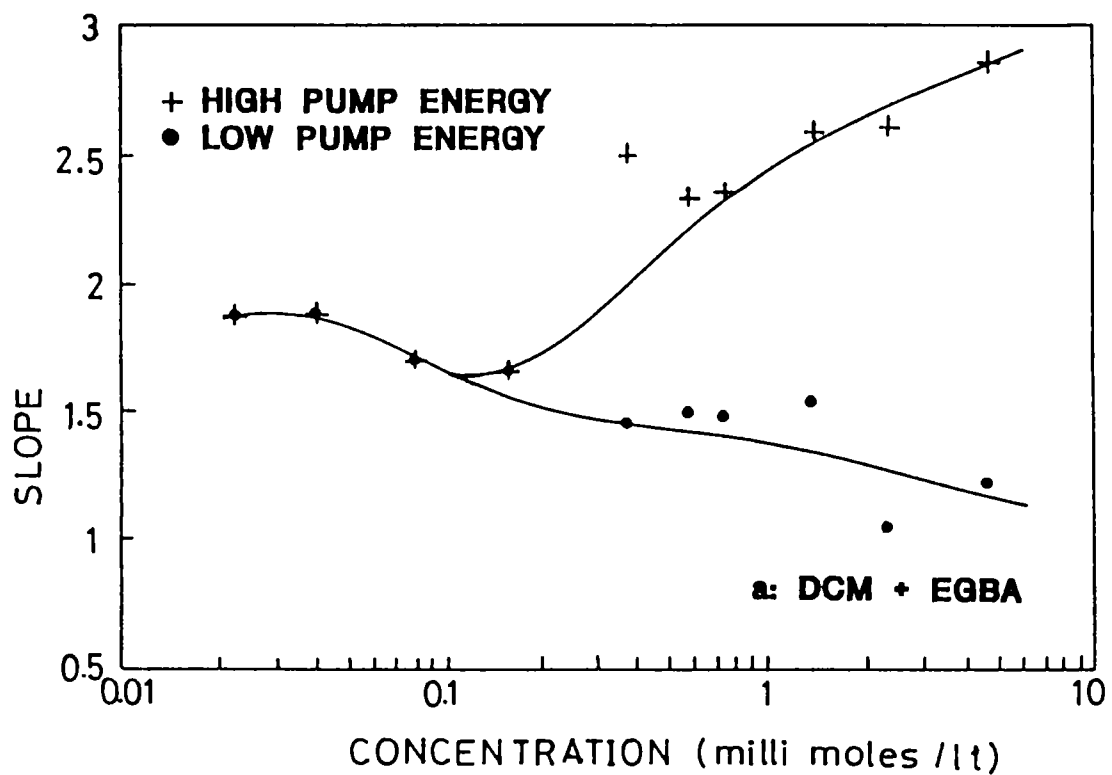


Fig.3.6 : Concentration dependence of the slope of the log-log plots in DCM solutions at 532 nm pumping.

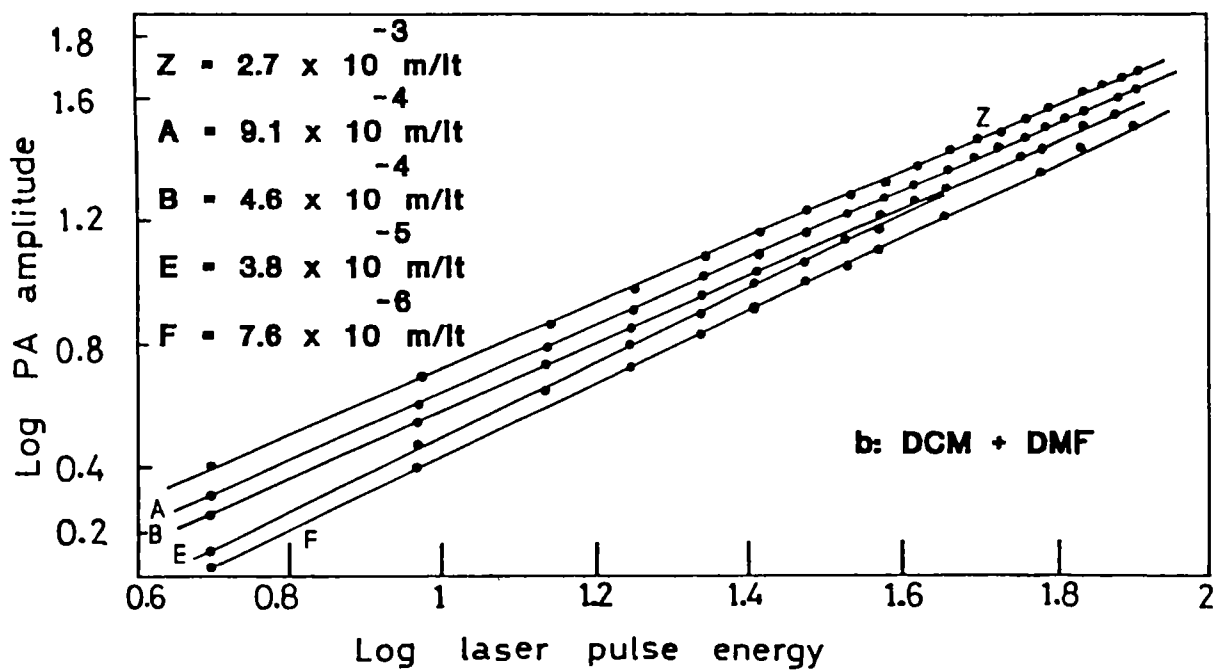
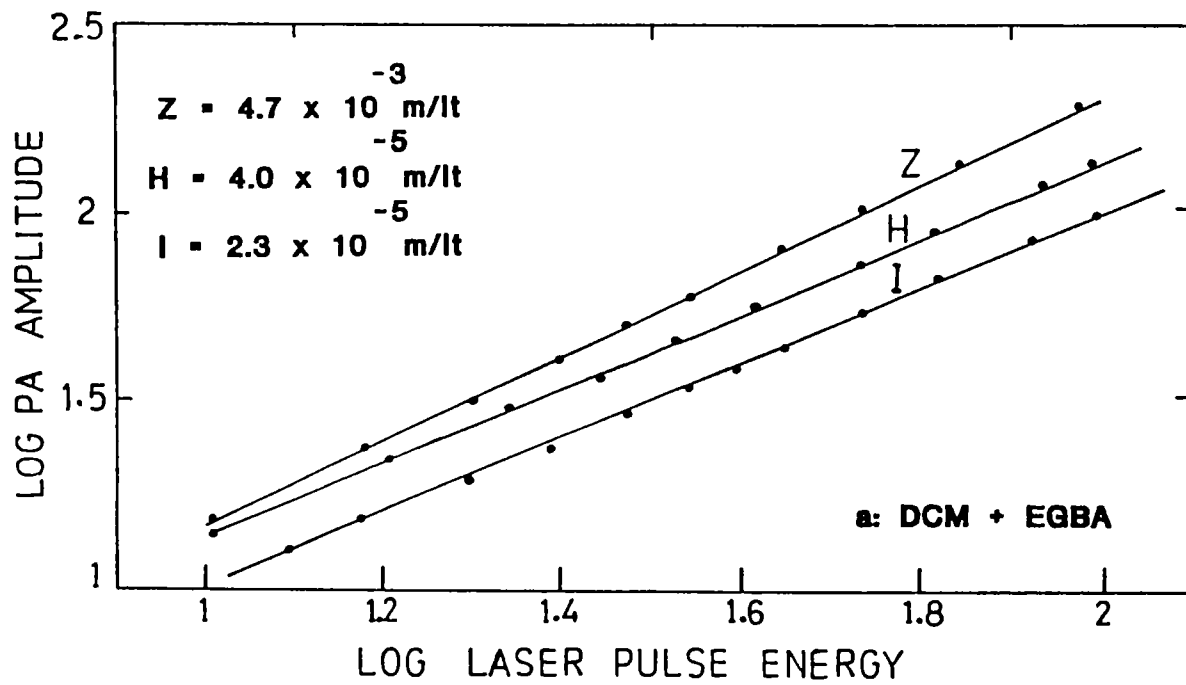


Fig.3.7 : Log laser pulse energy versus log PA amplitude plots, obtained for DCM solutions at 1064 nm pumping.

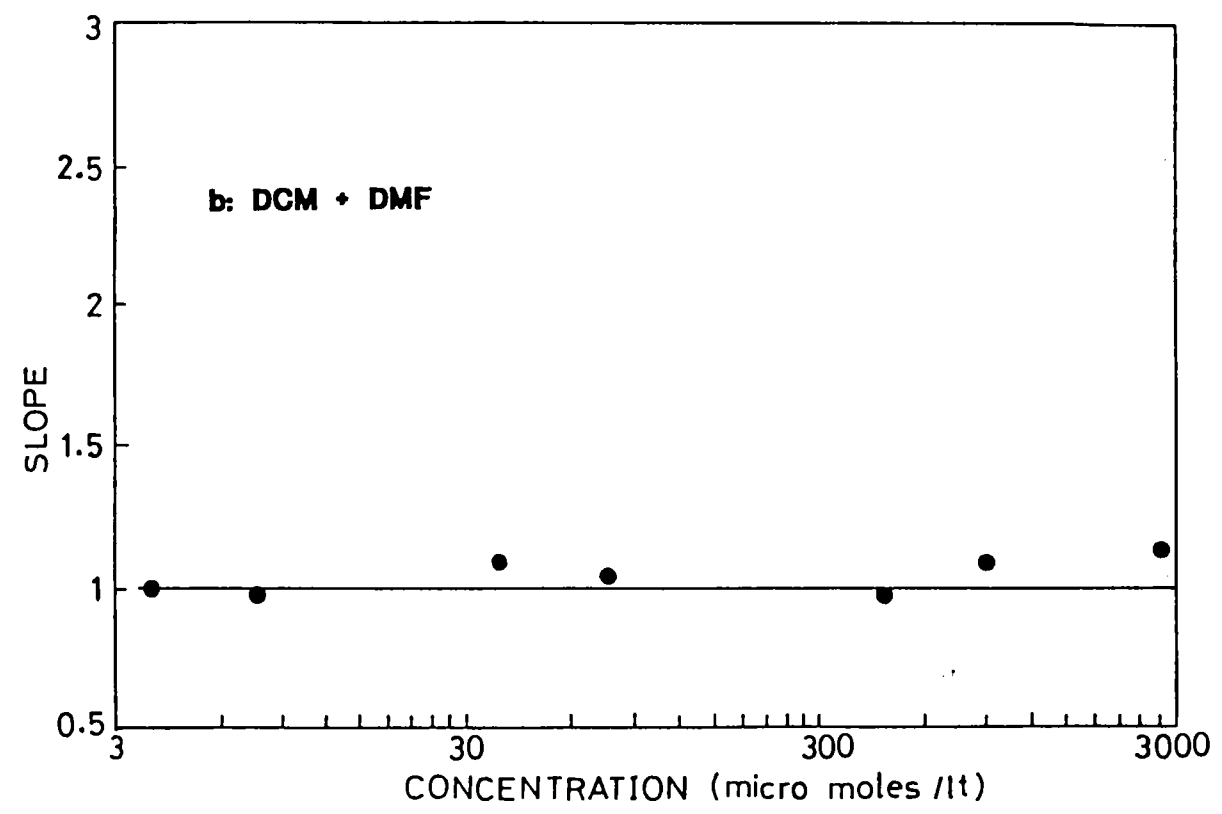
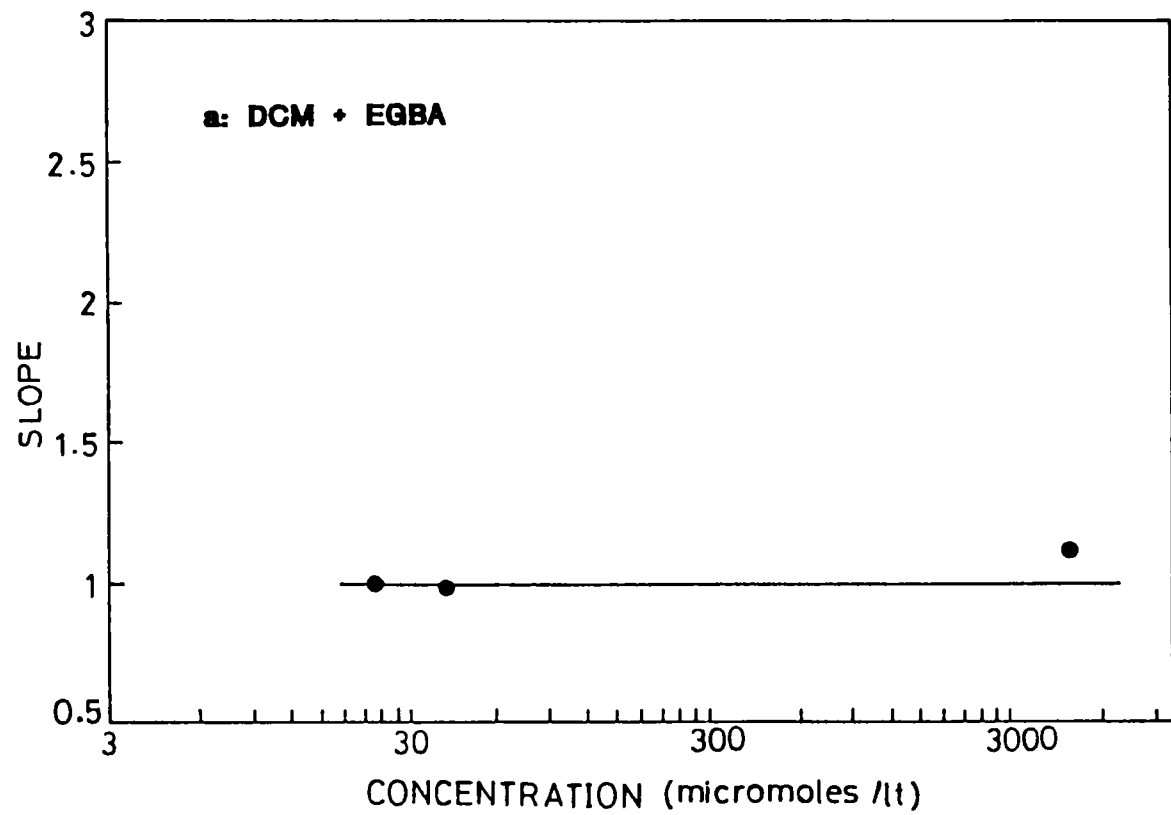


Fig.3.8 : Concentration dependence of the slope of the log-log plots in DCM solutions, at 1064 nm pumping.

the maximum estimated error in the calculated slope is approximately \pm 5%.

The dye samples have been irradiated using 1064 nm radiation also, and PA signals recorded. The results obtained are shown in Figs.3.7a, 3.7b, 3.8a and 3.8b. Irrespective of the sample concentration and pump flux, the slopes are found to take the constant value of approximately 1 in all cases.

3.3c Discussion

Earlier studies have shown that the longitudinal molecular polarizability of a conjugated chain molecule does not obey a bond-additivity rule, but rather exhibits a so-called polarizability exaltation, increasing as the cube of the length of the system [3]. This property is attributed to the broad delocalization of the π electrons over the molecular chain. Strong third order optical nonlinearity has been already observed in several molecules including cyanine dyes, resulting in high values of $\kappa^{(3)}$ which in turn affect the two-photon cross section δ since δ is proportional to the imaginary part of $\kappa^{(3)}$ [4]. Resonance enhancement of two-photon absorption (TPA) as well as its dependence on the state symmetries also can be significant in some cases. The symmetries are determined by the relative orientations of the transition dipole moments ($\bar{\mu}$) of various transitions pertaining to the molecule. For example, Penzkofer and Wiedmann [5] have shown from excited state absorption (ESA) measurements that in Rhodamine 6G (R6G) the orientation of $\bar{\mu}$ ($S_1 \rightarrow S_2$) is parallel to $\bar{\mu}$ ($S_0 \rightarrow S_1$) and perpendicular to $\bar{\mu}$ ($S_0 \rightarrow S_2$). Here $S_1 \approx 18960 \text{ cm}^{-1}$ and $S_2 \approx 28440 \text{ cm}^{-1}$. An obvious consequence in the case of R6G is that, for an anisotropic distribution of S_1 state molecules generated by a polarized laser pulse of the proper frequency, there exists a high probability of $S_1 \rightarrow S_2$ excited state absorption. Besides, since S_0 and S_2 have the same symmetry (A_1), the $S_0 \rightarrow S_2$ TPA cross section also is non-negligible.

The configuration of our present experimental setup is such that the optical path length in the sample solution is about 5 cm. The 532 nm pump beam is not fully absorbed in low concentration samples, whereas in high concentrations the beam is almost completely absorbed

even before the focal point is reached. Obviously this will result in a considerable decrease in the "apparent laser intensity" seen by the high concentration samples. Considering also the fact that the PA signal amplitude is proportional to the volume of the interaction region, one may expect, as we have observed, higher PA signals in low concentration samples. Yet, in the whole power range studied, the slope of the log-log plots does not show a power dependent change in these samples, ($< 10^{-4}$ moles/lt) as seen from Figs.3.6a and 3.6b. If only the low pump power region (< 32 mJ) is considered, then as the concentration increases the general tendency of the slope is to decrease from a value near 2, towards 1. The slope between one and two indicates the simultaneous occurrence of OPA ($S_0 \longrightarrow S_1$), TPA ($S_0 \longrightarrow S_n$) and ESA ($S_0 \longrightarrow S_1 \longrightarrow S_n$) in various degrees (The terminal level reached by ESA and TPA lies approximately at 37920 cm^{-1} . Since DCM shows a continuous absorption in this region without a distinct band structure, we specify this level by S_n , where $n > 2$). These transitions can be visualized in the energy level diagram for DCM (Fig.3.9) drawn from the present absorption and emission spectra and the photoacoustic data. At low concentrations it is particularly easy to saturate the $S_0 \longrightarrow S_1$ absorption leading to strong stimulated emission $S_1 \longrightarrow S_0$ and ESA $S_1 \longrightarrow S_n$ along with the spontaneous emission $S_1 \longrightarrow S_0$. Here, the fraction of molecules which relax nonradiatively in the S_1 manifold subsequent to initial excitation will generate PA signals depending linearly on the pump intensity. The fast nonradiative relaxation $S_n \longrightarrow S_1$ that follows ESA as well as TPA also will contribute to the generation of PA signals, which will show a quadratic pump intensity dependence in our case. The combined effect of these processes is manifest at low concentrations where the slope shows values tending towards 2. Absorption saturation of the PA signal is evident in Fig.3.4c at high pump intensities.

At higher concentrations, due to the enhanced solute-solute and solute-solvent interactions the energy levels of the molecule will be further broadened. We have seen from Eqn.1.109 that the two photon transition probability between the states $|i\rangle$ and $|f\rangle$ is proportional to the quantity

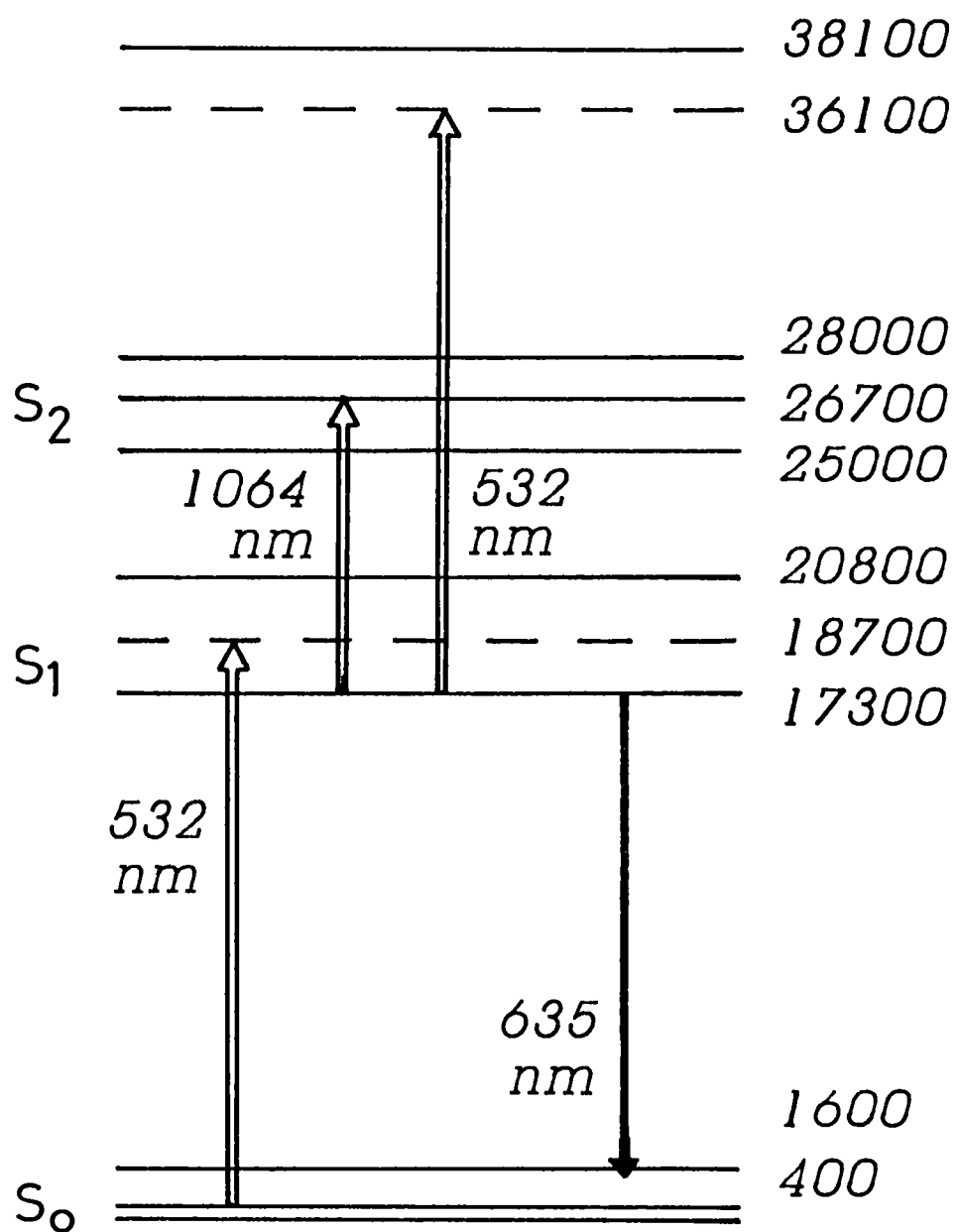


Fig.3.9 : Energy level diagram for the DCM molecule.

$$\sum_{\mathbf{r}} \frac{\langle f|V|\mathbf{r}\rangle \langle \mathbf{r}|V|i\rangle}{E_{i\mathbf{r}}} \quad (3.1)$$

where the \mathbf{r} s represent the intermediate levels. The broadened S_1 band will thus add to the resonant enhancement of the $S_0 \rightarrow S_n$ TPA in DCM. This conjecture is at least qualitatively verified from the observation that $\kappa^{(3)}$ increases with sample concentration [6]. Furthermore, the higher singlets come closer due to band broadening forming a continuum thereby increasing the upward transition probability as well as nonradiative relaxation. Higher concentration always ensures sufficient population of the excited states for stepwise processes to occur, so that ESA also becomes strong. Hence at high pump powers, in high concentration samples even three-step and three-photon processes become possible, which is revealed from the slope curve. However at low pump powers these phenomena have a low profile, due to the high absorptivity at the pump wavelength, resulting in reduced apparent pump intensities.

A reliable estimation of the individual contributions from TPA and ESA to the generation of PA signals can be done only with a previous knowledge of the ESA spectra and the symmetry of the energy levels involved. As to our knowledge, there are no reports published on the ESA spectra of DCM so far. Regarding the symmetry assignment, for a two-photon transition this involves the comparison of the cross sections δ_{π} and δ_{σ} respectively for linearly and circularly polarized excitation radiations [7] which we have not attempted due to technical reasons. However, it can be reasonably assumed, in view of the generally low values of δ as compared to the ESA cross sections, that the role of ESA in generating PA signals is significant in the present case.

The plots corresponding to 1064 nm irradiation, given through Figs.3.7 and 3.8 indicate that the observed PA signal is primarily generated from a strong OPA process, which is undoubtedly the overtone absorption and subsequent vibrational relaxation taking place in the solvent molecules. Considering TPA and ESA occurring at 1064 nm pumping (to be discussed in later sections), $S_2 \rightarrow S_1$ nonradiative relaxation and weak $S_1 \rightarrow S_0$ internal conversion are the additional

pathways for PA generation here, but these channels are found to be masked by the much stronger overtone excitations.

3.4 Investigations by Fluorescence

The energy level diagram for DCM (Fig.3.9) shows that the $S_0 \rightarrow S_1$ absorption matches approximately with the 532 nm laser radiation. Hence it is probable that if the dye samples are strongly irradiated with 1064 nm radiation from the laser, the S_1 level may get populated by two-photon absorption, yielding subsequent $S_1 \rightarrow S_0$ antistokes fluorescence (ASF). To investigate this possibility we have used the same samples employed for the PA measurements. According to Eqn.1.120, the fluorescence should show a nonlinear dependence on the pump intensity that can be extracted from a logarithmic plot.

3.4a Experimental

The sample is taken in a quartz cuvette of 1cm x 1cm x 4 cm dimensions, and pumped by the plane polarized, unfocused 1064 nm radiation from the Nd:YAG laser. The one-photon absorption cross section at 1064 nm is negligible for the samples, eventhough there are losses due to light scattering and vibrational overtone absorption of the solvent. Since the ASF intensity is very weak, the room is completely darkened during the experiment. The laser pulse energy has been fixed at 120 mJ for all samples when the emission spectra are recorded. The fluorescence is collected in 90° geometry and passed through the entrance slit of a 0.2 m concave holographic grating monochromator, to which a sensitive PMT is attached. The PMT output is gated and averaged, and readings taken at fixed intervals of wavelength setting on the monochromator. The readings are then normalized to the spectral response of the grating and the PMT to get the actual fluorescence emission spectrum. During these experiments, the monochromator slits have been kept at a width of 50 microns each, and a height of 5 mm. The experimental set up is shown in Fig.2.12 of chapter 2.

3.4b Results

The corrected fluorescence emission spectra obtained from various

samples are shown in Figs.3.10a, 3.10b (EGBA solution) and Fig.3.11 (DMF solution) respectively. The emission peak is approximately at 633 nm for the former, whereas it is at 630 nm for the latter. No peak shift is observed with concentration. The emission intensity, as a function of concentration, is shown in Figs.3.12a and 3.12b.

The log-log plots for the ASF emission and the slope versus concentration curves are given in Figs.3.13a and 3.14a for EGBA solutions, and in Figs.3.13b and 3.14b for DMF solutions respectively. Measurements are taken at the peak emission wavelength. The calculated slopes are estimated to be accurate within $\pm 5\%$.

3.4c Discussion

The basic phenomena associated with an $S_0 \longrightarrow S_1$ two photon absorption process have been already discussed in detail in section 1.5a of the introductory chapter. In brief, an excited molecule in the S_1 state can either relax to S_0 through spontaneous/stimulated emission and a much weaker radiationless transition, or get excited to higher energy states by excited state absorption (ESA). The ESA probability depends on the respective symmetries of the levels involved. Penzkofer and Leupacher [8] have obtained values for the two-photon and excited state absorption cross sections (δ and σ_{ex}^L respectively) in certain dyes from numerical solutions to a set of coupled differential equations that describe the two photon absorption dynamics. In their study they have estimated a value of $(1 \pm 0.1) \times 10^{-49} \text{ cm}^4 \text{ sec}$ for δ and $(2.5 \pm 1) \times 10^{-17} \text{ cm}^2$ for σ_{ex}^L in the case of R6G for a pump wavelength of 1054 nm. (The $S_0 \longrightarrow S_1$ OPA cross section for R6G at the typical pump wavelength of 530 nm is $3.8 \times 10^{-16} \text{ cm}^2$ [8]). In this connection it is worthwhile to mention here the dispersion of two photon cross section initially observed in rhodamine dyes [10] and later confirmed in cyanine and acridine dyes as well [7] by Hermann and his colleagues. They found that the ratio $\delta_\omega / \sigma_{2\omega}$ (δ_ω : two photon cross section at the frequency ω , $\sigma_{2\omega}$: one photon cross section at 2ω) is a function of the difference between the peak absorption frequency and twice the laser frequency, $\omega_{max} - 2\omega_L$. In R6G, this ratio increased rapidly when $2\hbar\omega_L$ varied from the $S_0 \longrightarrow S_1$ to the $S_0 \longrightarrow S_2$ transition, which has been ascribed to the symmetry

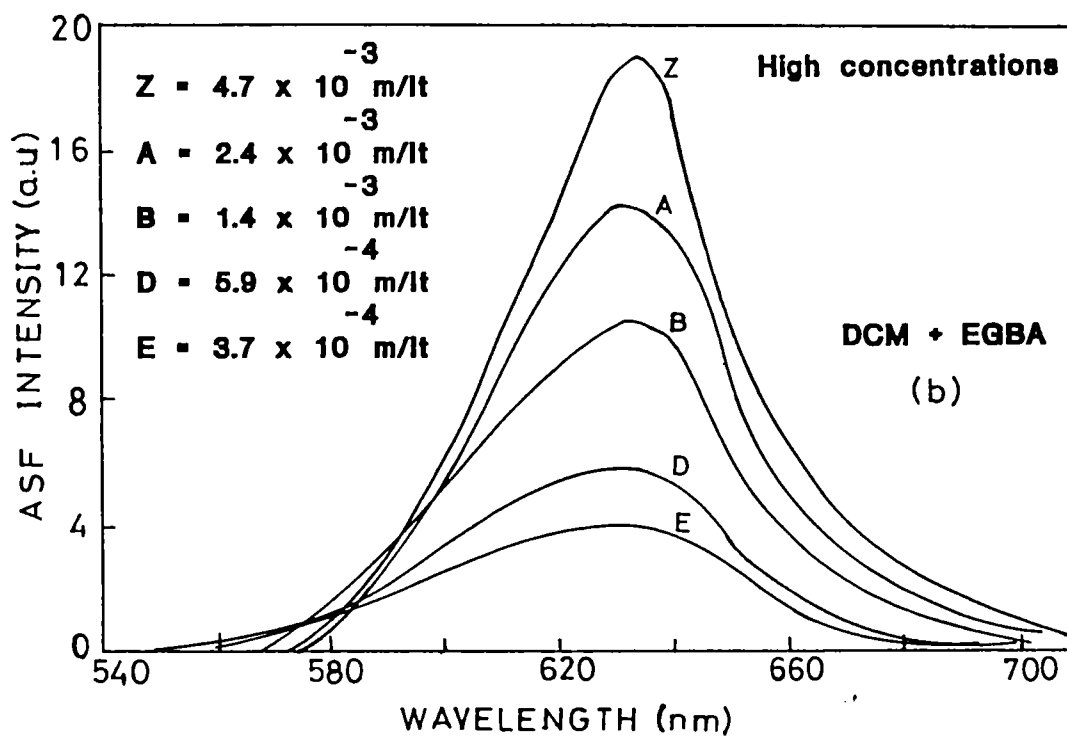
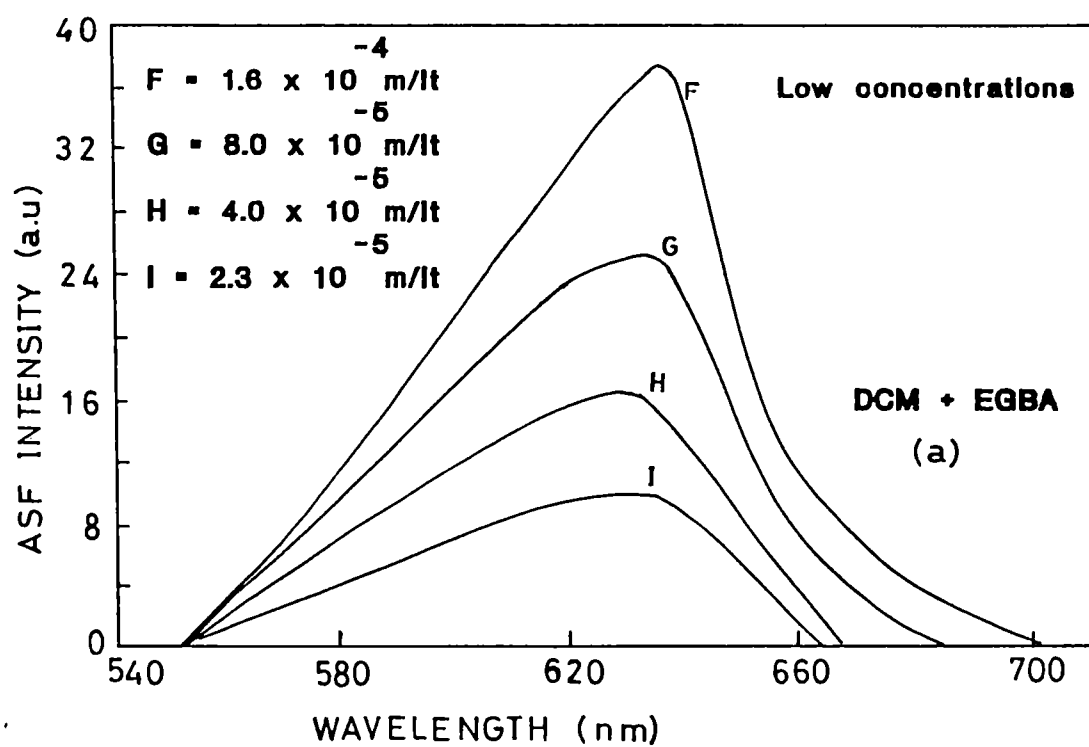


Fig.3.10 : Corrected antistokes fluorescence emission spectra observed in the right-angle geometry from DCM + EGBA solutions of various concentrations, at 1064 nm pumping. Emission peak is ≈ 633 nm.

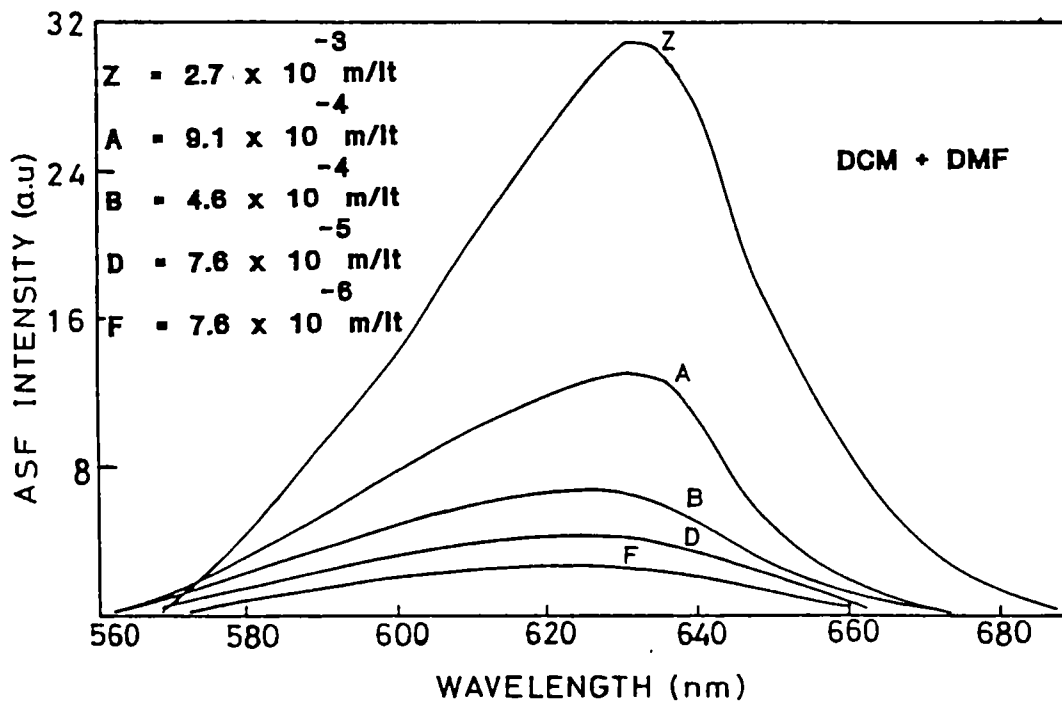


Fig.3.11 : Corrected antistokes fluorescence emission spectra observed in the right-angle geometry from DCM + DMF solutions of various concentrations, at 1064 nm pumping. Emission peak is \approx 630 nm.

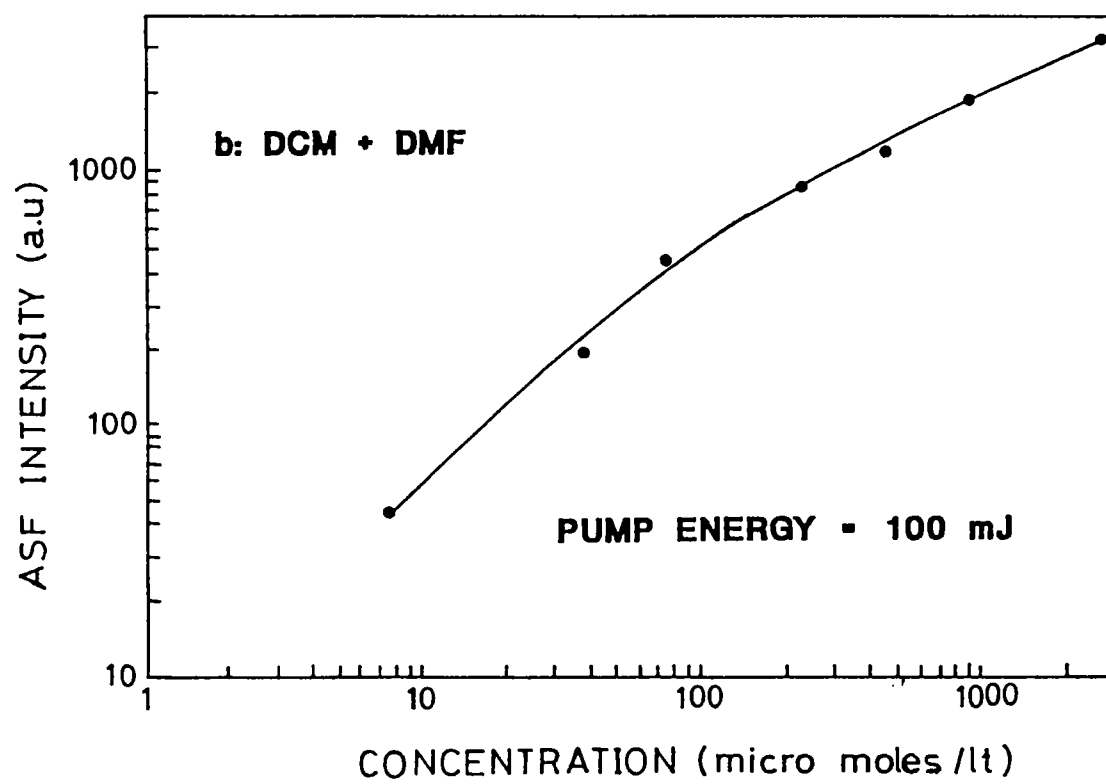
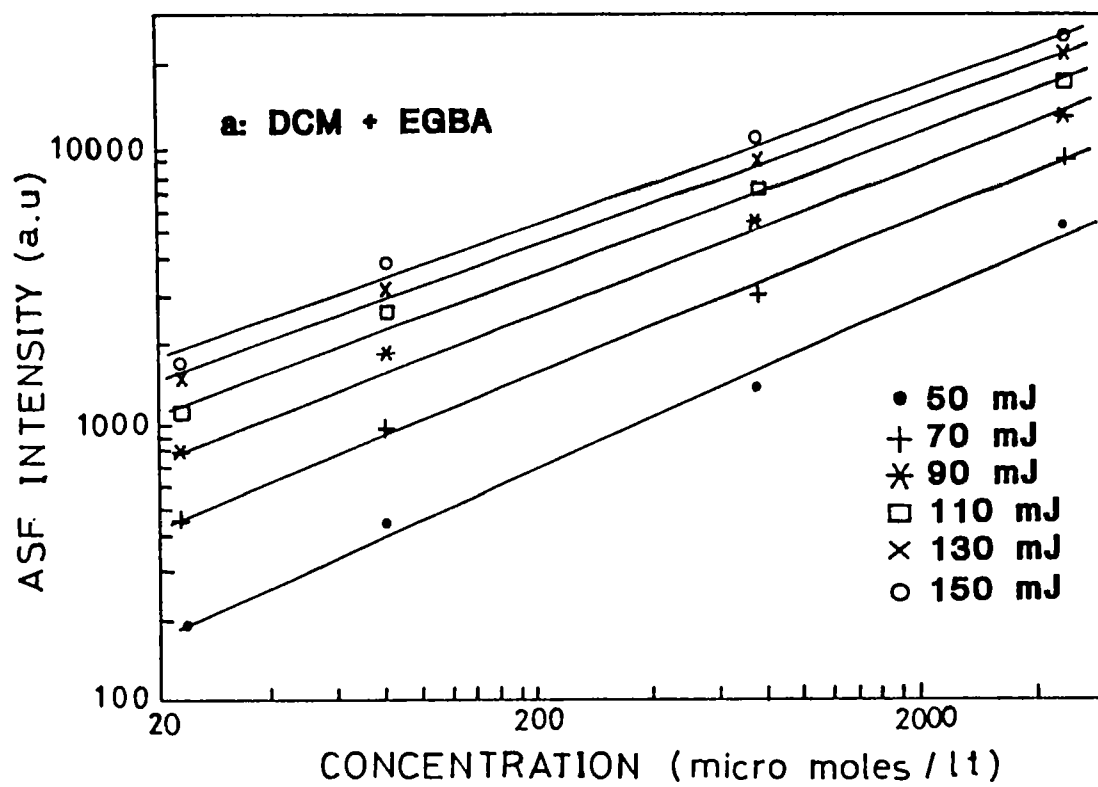


Fig.3.12 : Increase of the antistokes fluorescence intensity with pump energy for various concentrations of DCM solutions, at 1064 nm pumping.

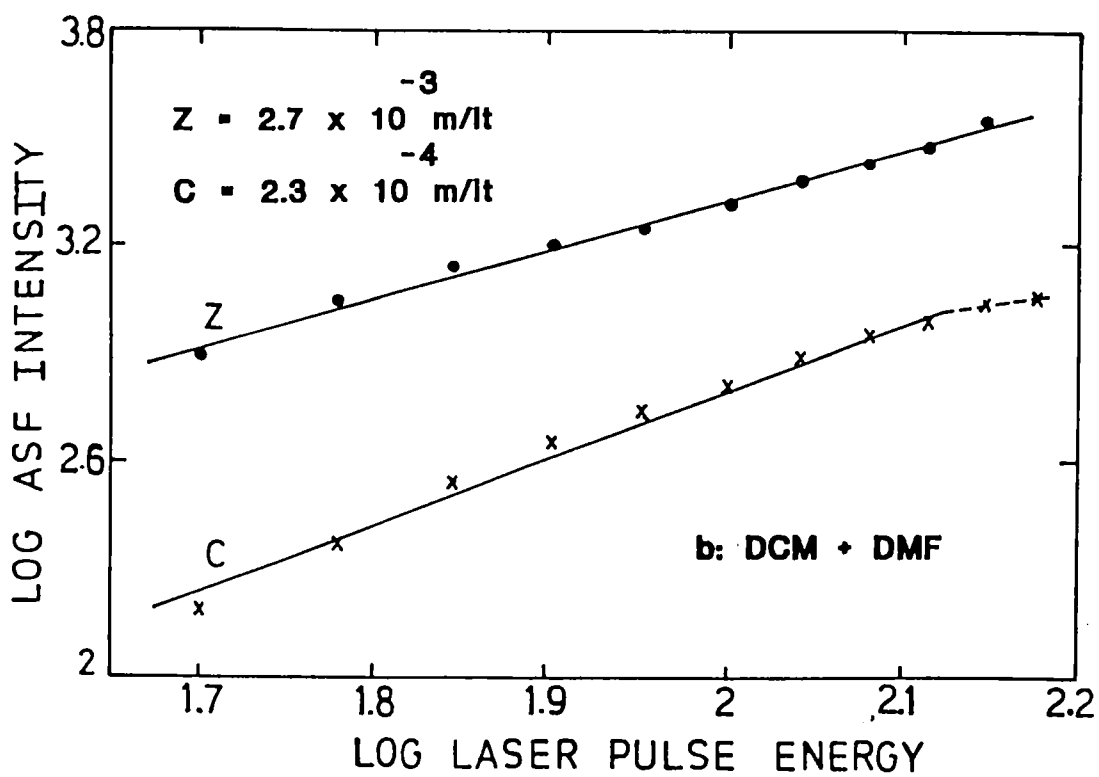
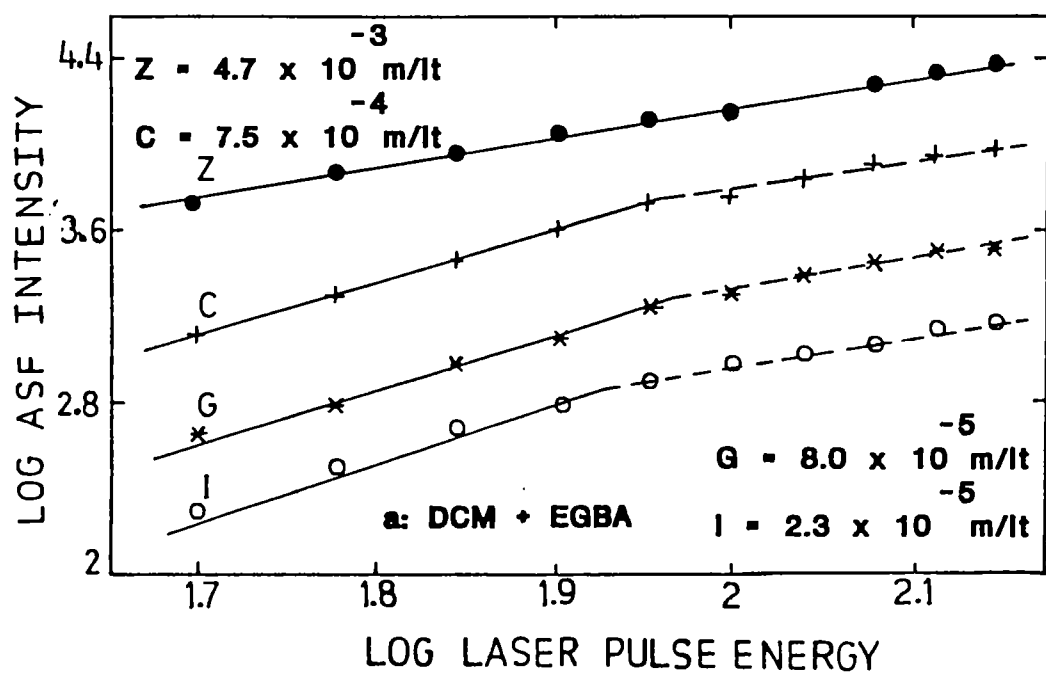


Fig.3.13 : Log laser pulse energy versus log ASF intensity plots obtained for DCM solutions at 1064 nm pumping.

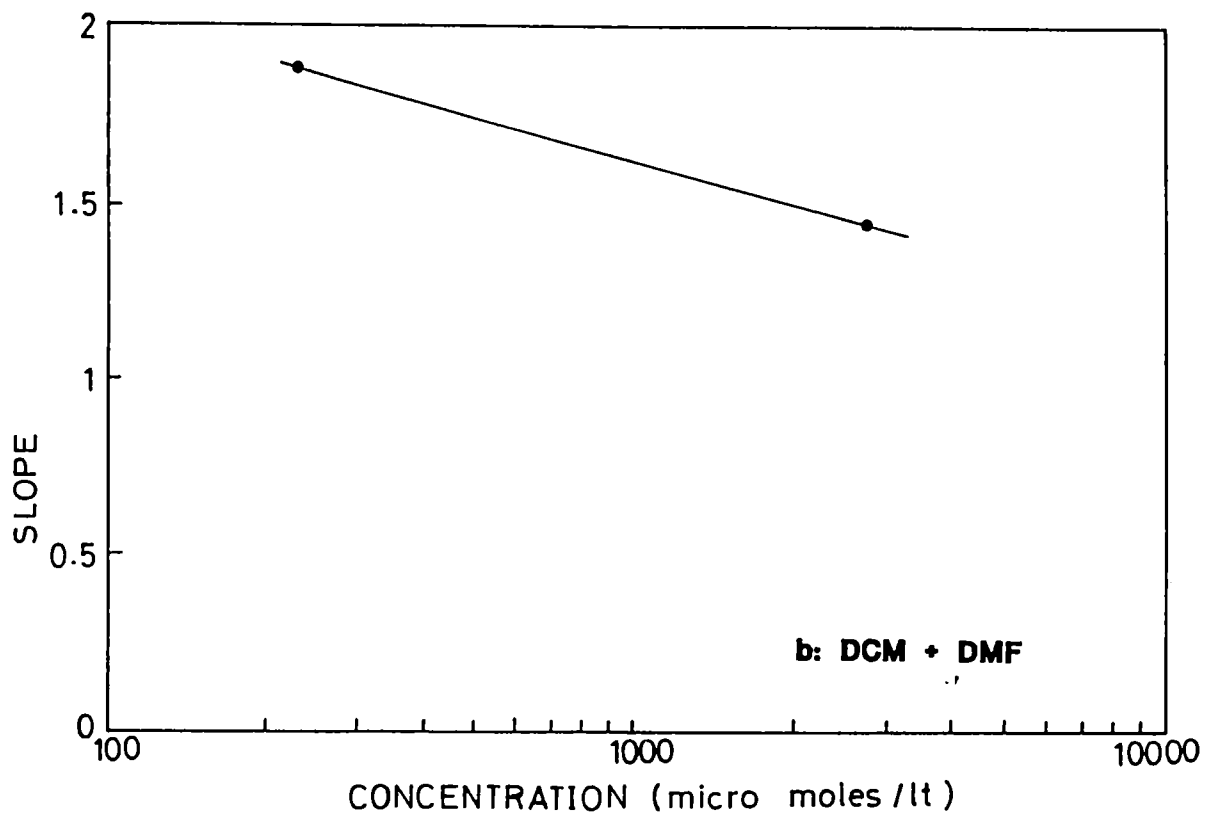
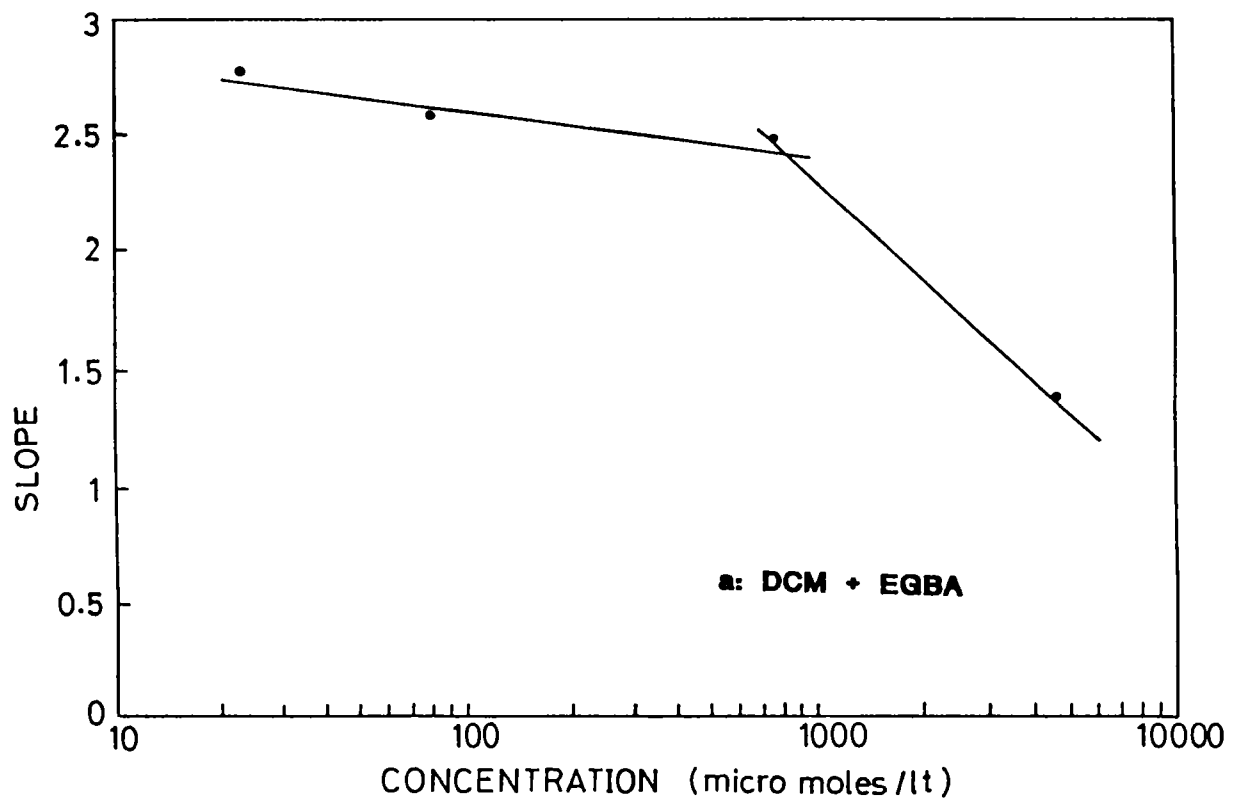


Fig.3.14 : Concentration dependence of the slope of the log-log plots in DCM solutions, for ASF at 1064 nm pumping.

properties of the levels S_0 , S_1 and S_2 . This observation, which is now generally accepted, is in sharp contrast to the Schäfer-Schmidt rule [11] which predicts a proportionality between the one photon cross section and two photon cross section through the relationship

$$\delta_{\omega} = \frac{1}{3} (w/c) (f \cdot \sigma_{\max}) \sigma_{2\omega} \quad (3.2)$$

where σ_{\max} is the value of $\sigma_{2\omega}$ at the absorption peak, c the speed of light in vacuo, w the 'thickness' of the π electron cloud (all molecules assumed to be plane) and f the oscillator strength. The failure of the Schäfer-Schmidt rule, derived from a geometrical model for TPA, results from the fact that state symmetries are not considered in this model.

The increase in the ASF intensity with sample concentration and pump power, given in Figs.3.12a and 3.12b show the expected behaviour. The interesting observation in the present studies is the concentration dependence of the slope, depicted through Figs.3.13 and 3.14. The lower concentration samples show higher slopes in both solvents. The slopes nearing 3 clearly indicate the occurrence of three-photon absorption ($S_0 \rightarrow S_2$), and the suitably placed S_1 level helps in the resonant enhancement of this transition. The S_2 level is placed at $\approx 28000 \text{ cm}^{-1}$, that matches with the energy of three 1064 nm photons (see fig.3.9). Eventhough the ESA cross section can be much larger than the three-photon absorption cross section, ESA will not affect the slope in this case, which we have verified from numerical computation methods. It is to be noted that since TPA losses are low, part of the 1064 nm pump beam is transmitted through the exit face of the cuvette for all concentrations studied, so that there is no lateral image shift at the entrance slit of the monochromator. This possible experimental error is thus out of question, and hence the reason for the decrease of slope at high concentrations should be of a pure molecular origin. We have observed a similar behaviour in solutions of R6G in methanol and water also [12]. Absorption saturation is not to be expected here, and reabsorption of fluorescence, which occurs in R6G at high concentrations [13], will not take place in DCM. According to Penzkofer's calculations [8], the

stimulated emission cross section of a similar cyanine dye, PYC, is $\approx 7 \times 10^{-20} \text{ cm}^2$, under identical pumping conditions. Assuming the same to hold in our case too, the decrease in slope at high concentrations can be attributed mainly to stimulated emission losses [13]. The possible alternatives are (a) absorption from S_1 to higher excited states followed by intersystem crossing or dissociation and (b) possible stimulated Raman scattering [14]. Both of these mechanisms will be predominant at higher pump intensities whereby ASF quenching is observed in most of the samples studied. The substantial reduction in the slope of the highest concentration solutions in EGBA and DMF may be also due to the presence of a one-photon absorption process $S_0 \rightarrow S_1$, occurring from highly excited vibrational levels of the ground state.

3.5 Conclusions

Two-photon absorption, three-photon absorption and excited state absorption phenomena in the laser dye DCM, in the solvents dimethyl formamide and ethylene glycol:benzyl alcohol have been investigated employing photoacoustics and fluorescence techniques. The occurrence of these processes at the pump wavelengths of 1064 nm and 532 nm is clearly identified from the results obtained.

CHAPTER 3 - REFERENCES

- [1] Marason E G, Opt.Comm. 37, 56 (1981)
- [2] Bourson J, D Doizi, D Lambert, T Sacaze and B Valeur, Opt.Comm. 72, 367 (1989)
- [3] Hermann J P, D Ricard and J Ducuing, Appl.Phys.Lett. 23, 178 (1973)
- [4] Hermann J P, Opt.Comm. 9, 74 (1973)
- [5] Penzkofer A and J Wiedmann, Opt.Comm. 35, 81 (1980)
- [6] Leupacher W and A Penzkofer, Appl.Phys.B 36, 25 (1985)
- [7] Foucalt B and J P Hermann, Opt.Comm. 15, 412 (1975)
- [8] Penzkofer A and W Leupacher, Opt.and Quant.Electron. 19, 327 (1987)
- [9] Hillman L W, in "*Dye laser principles-with applications*" (Eds.) F J Duarte and L W Hillman, Academic Press (1990)
- [10] Hermann J P and J Ducuing, Opt.Comm.6, 101 (1972)
- [11] Schaefer F P and W Schmidt, IEEE J.Quant.Electron.,QE-2, 357 (1966)
- [12] Results to be published.
- [13] Bradley D J, MHR Hutchinson, H Koetser, T Morrow, GHC New and M S Petty, Proc.Roy.Soc.Lond. A 328, 97 (1972)
- [14] Eichler H J, D Langhans and U Klein, Appl.Opt. 18, 1383 (1979)

CHAPTER - 4
HIGHER ORDER ABSORPTIONS IN CRESYL VIOLET

4.1 Introduction

Cresyl violet is an oxazine dye belonging to the azine dye family, and absorbs strongly in the yellow-red regions of the spectrum. The structure of cresyl violet is shown in Fig.4.1a. Azine dyes are characterized by a heterocyclic ring with a nitrogen bridge as shown in Fig.4.1b, and they are classified (by the atom X) into Oxazine dyes ($X \equiv O$), Thiazine dyes ($X \equiv S$) and Diazine or Phenazine ($X \equiv N$) dyes [1]. Oxazines are widely used as laser dyes, generally at longer wavelengths than those covered by the Rhodamines. Ethanol, methanol, ethylene glycol etc. are the recommended solvents. When pumped with the conventional N_2 laser or flashlamp, specified amounts of Rhodamine 6G or Rhodamine B may be added to these dyes for increasing the lasing efficiency by an energy transfer mechanism.

Oxazine molecules are planar and rigid like their xanthene relative, and they lase quite efficiently in the red and near infrared regions of the spectrum. They are competent substitutes for cyanines for generating tunable laser radiation in the infrared region. The position of the absorption maximum depends on the end groups of the chromophore in the same fashion as in xanthene dyes, and the fluorescence peak is shifted approximately by 30 nm for oxazine dyes in ethanol [2]. All oxazine dyes are photochemically much more stable than the Rhodamines. Owing to the smaller energy difference between S_1 and S_0 , the influence of hydrogen vibrations at the end groups is more pronounced than in the xanthene dyes and it is comparatively difficult to suppress the processes of internal conversion. Usually triplet problems are not encountered in these dyes.

Laser action in an alcoholic solution of cresyl violet was reported for the first time by Marling et al [3] in 1970. With a tuned cavity, lasing was observed in the region 646 - 703 nm. Runge [4] demonstrated intracavity pumping of a cresyl violet solution with a He-Ne laser, where the dye acted as a mode locker for itself and the

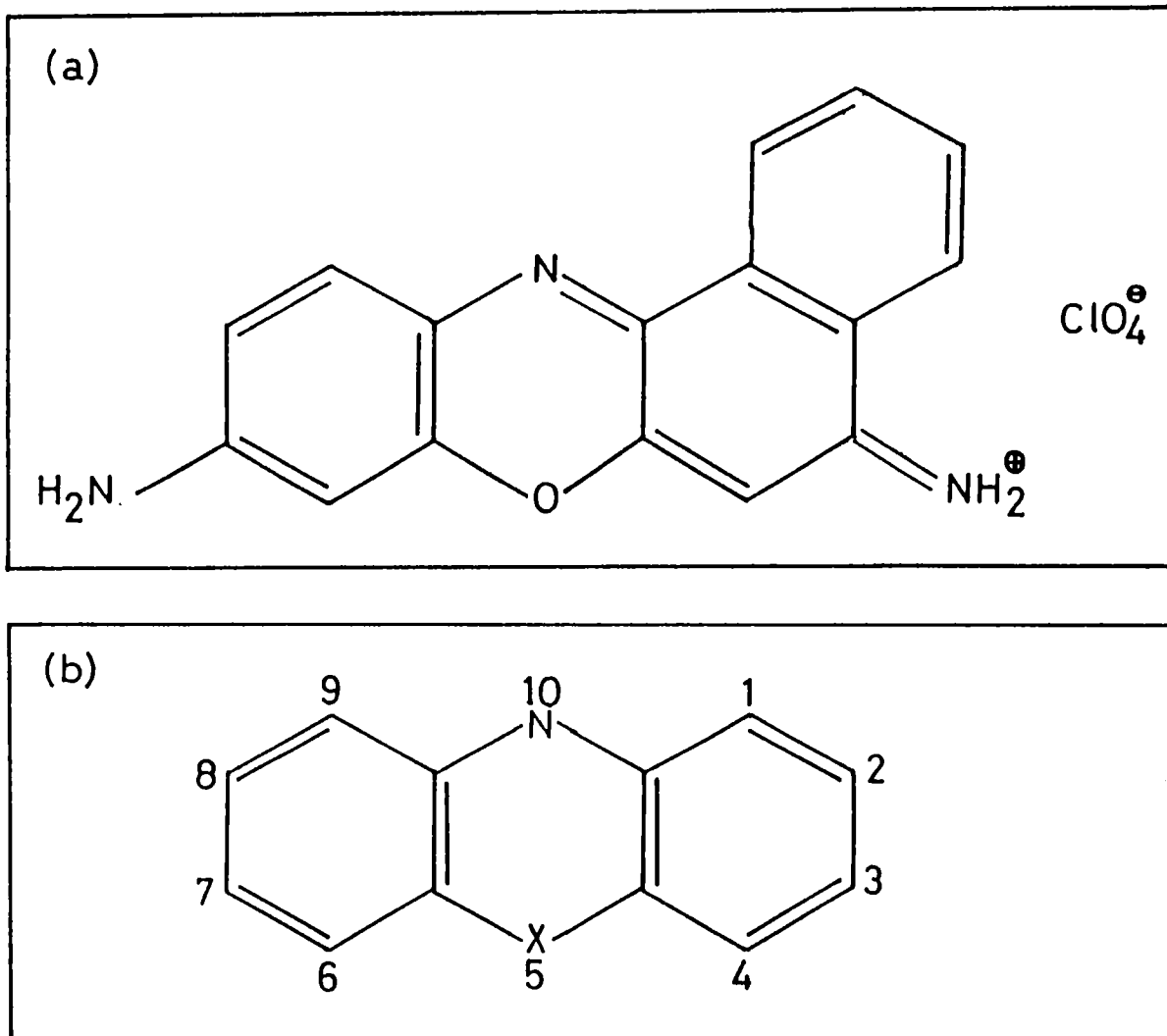


Fig.4.1 : (a) Structure of the Cresyl violet perchlorate molecule, (b) Structure of Azine dyes.

pump laser. The importance of dye purity was pointed out by Gacoin and Flamant [5] who reported a four-fold increase in the laser energy obtained from a specially purified cresyl violet solution. Continuous self mode-locking of the flashlamp pumped cresyl violet dye laser has been employed by Arthurs et al [6] to generate 3-5 ps laser pulses. Cresyl violet has a broad excited singlet state absorption spectrum, which has been investigated by Shah and Leheny [7].

The present chapter discusses the results obtained from the photoacoustic and antistokes fluorescence studies carried out in samples of cresyl violet perchlorate (CVP) dissolved in methanol and methanol:water (referred to as MW henceforth) solutions at various concentrations.

4.2 Absorption and Fluorescence properties

The recorded absorption spectrum of CVP (exciton) dissolved in methanol:water is shown in Fig.4.2. The peak absorption in the visible region is near 600 nm. We have recorded the fluorescence emission from various MW solution samples of CVP and the emission spectra corrected for the detector response are given in Figs.4.3a and 4.3b. The emission peak is found to be around 628 nm. The recorded absorption and emission spectra are in good agreement with those reported by Drexhage [2]. Due to the overlap of the absorption and emission bands in CVP, reabsorption of fluorescence occurs at higher concentrations leading to an apparent shift of the peak wavelength when observed at 90° geometry. The reabsorption effect is minimal for front surface fluorescence collection. (It may be remembered here that reabsorption of fluorescence was not observed in DCM samples). Above a certain threshold pump intensity stimulated emission starts, and the power plot obtained for fluorescence and stimulated emission is shown in Fig.4.3c. Whereas fluorescence increases almost linearly with pump energy (slope ≈ 0.8), stimulated emission is initially superlinear and saturates at higher pump energies.

4.3 Investigations by Photoacoustics: Results and Discussion

For preparing the samples, Cresyl violet perchlorate (purchased

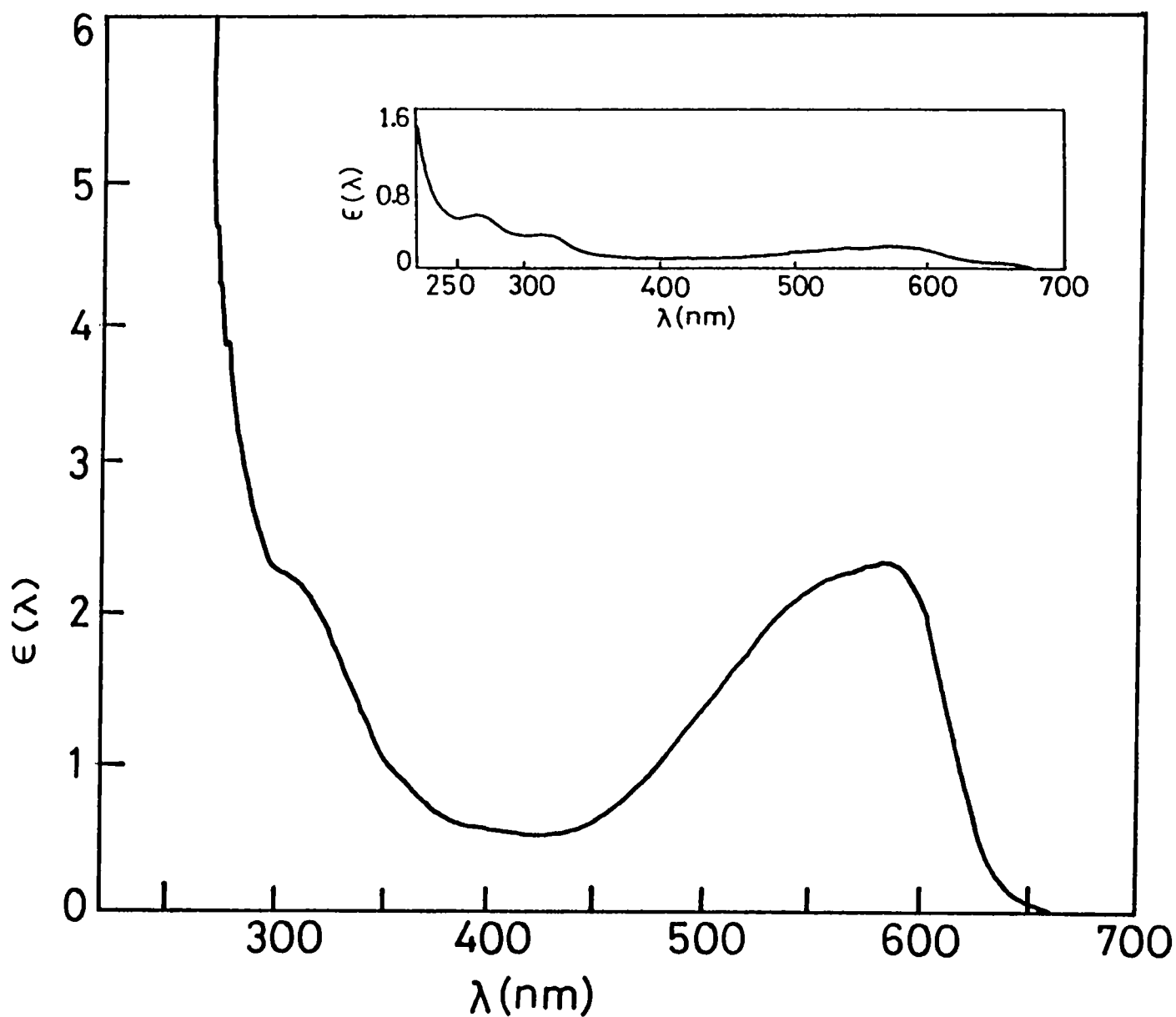


Fig.4.2 : The Absorption spectrum obtained for a CVP + Methanol:water solution of 4.6×10^{-4} moles/lt concentration. $\epsilon(\lambda)$ is the absorbance. Absorption bands in the uv can be seen in the inset spectrum, which corresponds to a sample of 9.6×10^{-6} moles/lt concentration.

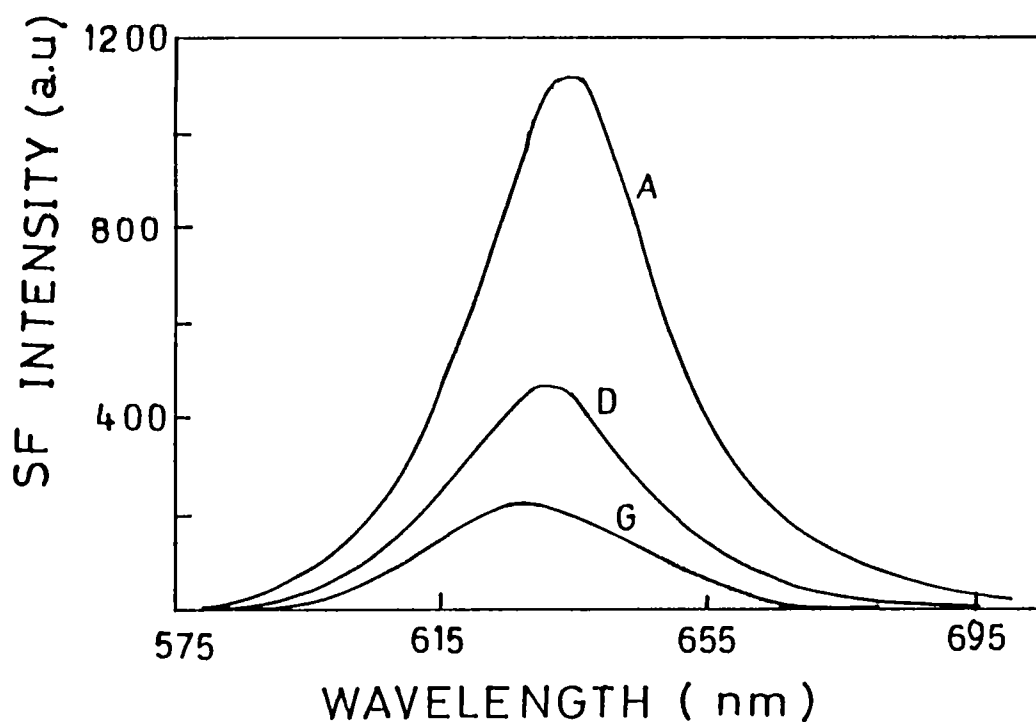


Fig.4.3a : Corrected Fluorescence emission spectra observed at 45° geometry from CVP + Methanol:water solutions. Emission peak is given in brackets. A - 1.4×10^{-3} moles/lt (635 nm), D - 1.5×10^{-4} moles/lt (631 nm), G - 9.6×10^{-6} moles/lt (628 nm)

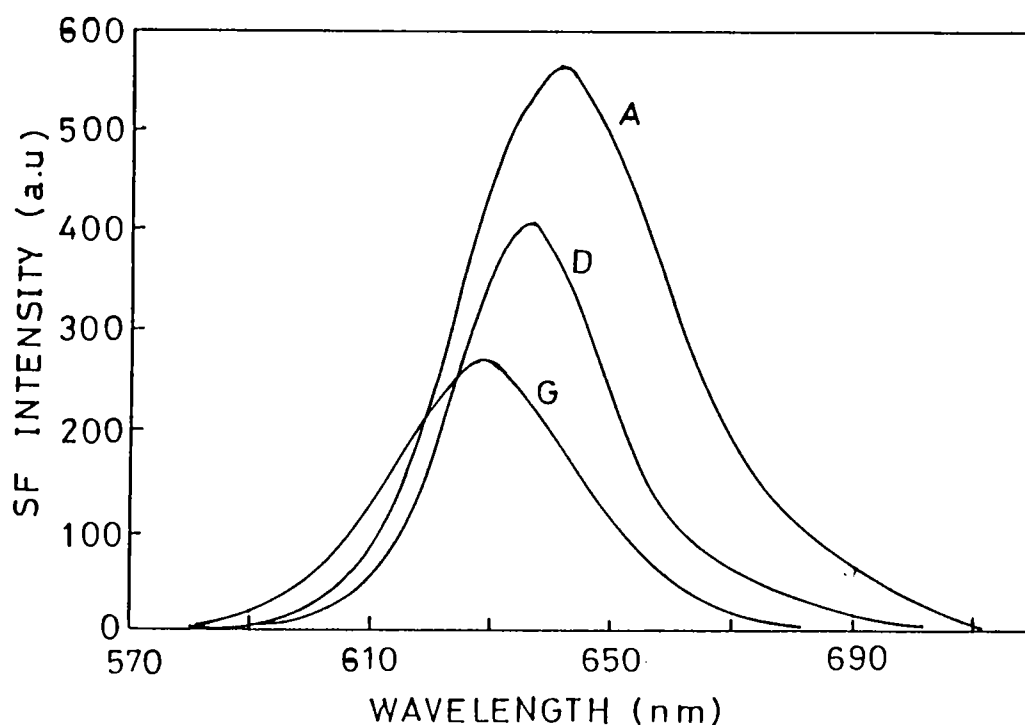


Fig.4.3b : Corrected Fluorescence emission spectra observed at 90° geometry from CVP + Methanol:water solutions. Emission peak is given in brackets. A - 1.4×10^{-3} moles/lt (640 nm), D - 1.5×10^{-4} moles/lt (635 nm), G - 9.6×10^{-6} moles/lt (627 nm)

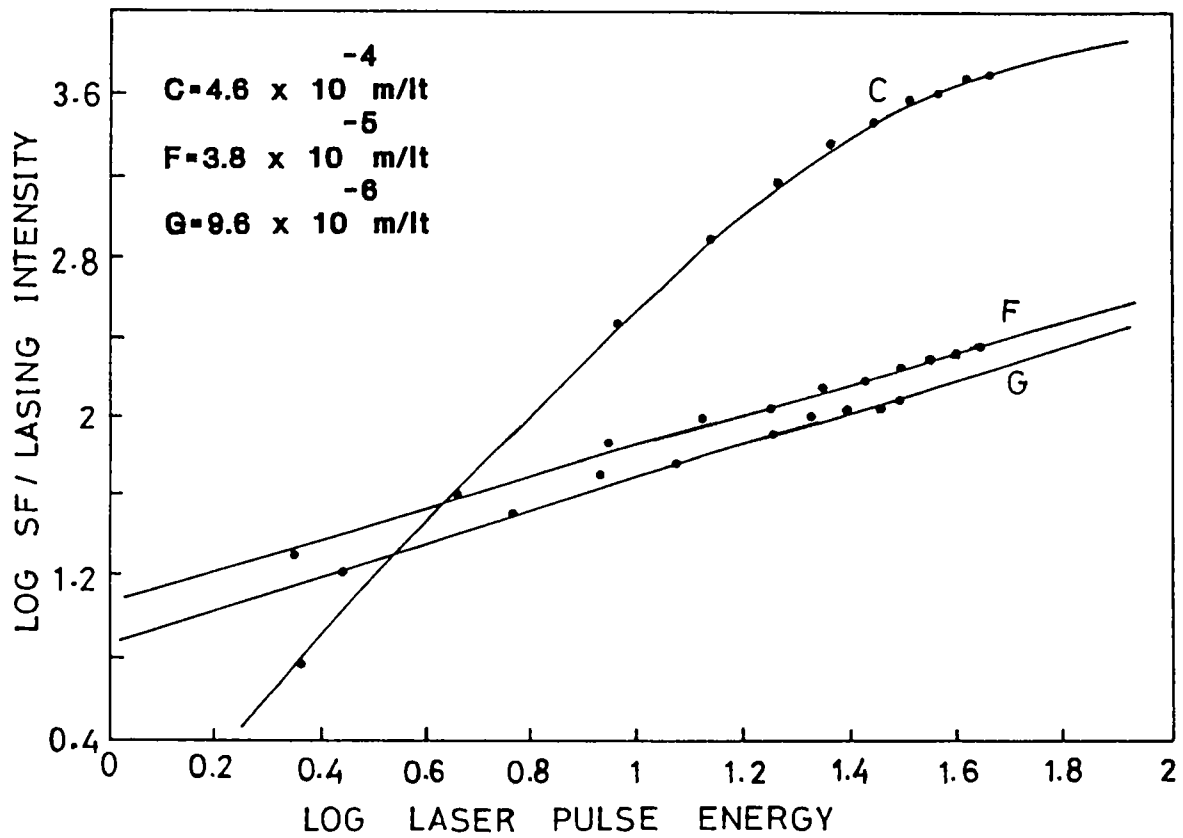


Fig.4.3c : Observed variation of Fluorescence from the samples F and G, and stimulated emission from C in CVP + Methanol:water solutions, with pump laser pulse energy.

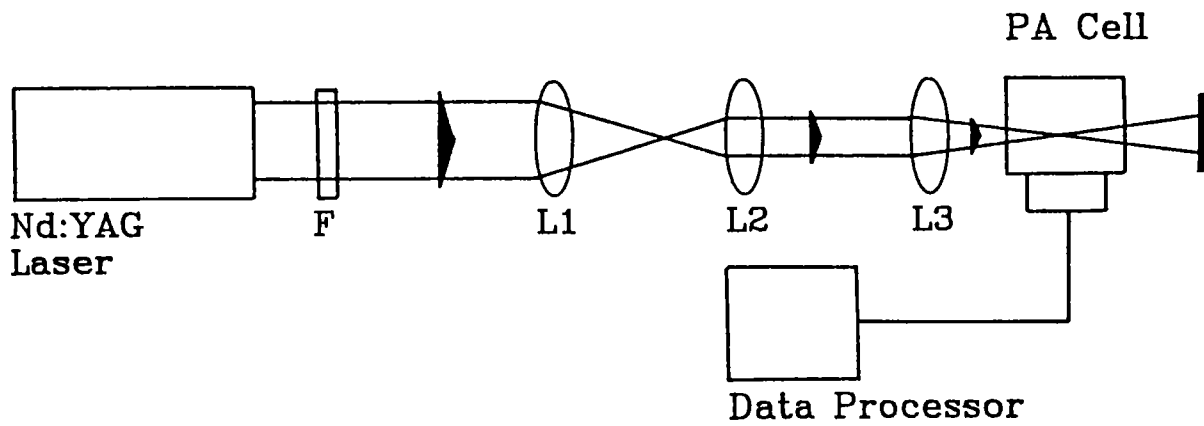


Fig.4.4 : Modified experimental set up for PA measurements, where the laser beam diameter is initially reduced before focusing into the PA cell.

from Exciton) is dissolved in the solvents without further purification. The sample preparation method and the experimental arrangement used in the present studies are very much similar to those employed for the analysis of DCM samples, described in chapter 3. However we have used a modified configuration for the study of methanol solutions of CVP, where the laser beam is initially reduced in diameter approximately to 3.7 mm using two convex lenses. This beam is then focused by a 5 cm lens into the cell (Fig.4.4). This has been done to increase the laser intensity along the entire 5 cm beam path in the PA cell through the sample.

As seen from the absorption spectra the short wavelength tail of the first absorption band permits moderate absorption of the 532 nm pump radiation. Figs. 4.5a, 4.5b and 4.5c show the log laser pulse energy versus log PA amplitude plots obtained for the representative CVP samples dissolved in methanol. The concentration range of 4.8×10^{-6} moles/lt to 4.6×10^{-3} moles/lt is investigated. In Figs.4.6a and 4.6b, the same obtained for CVP + MW samples is given. The slopes of the log-log plots are calculated and plotted as a function of sample concentration in Figs.4.7a and 4.7b. When irradiated by 1064 nm radiation, for all concentrations and pump intensities the slopes are found to be very near to 1, in both solutions. The results for CVP + MW samples are shown in Fig.4.8a and 4.8b. The percentage error in the calculated slope values is estimated to be about $\pm 5\%$.

A general observation is that CVP samples give larger PA signals than the DCM samples for a given concentration and laser pulse energy. For example, when 13.5 mJ of energy at 532 nm is focused by a 5 cm lens into the PA cell containing a CVP + MW sample of 1.4×10^{-3} moles/lt concentration, 1.66 mV of PA signal has been obtained without the preamplifier. On the other hand, a DCM + EGBA sample of the same concentration, under near identical conditions, gave only 500 μ V of PA signal. Yet it is interesting to note that in general, a strong two-photon or ESA process is not indicated from the slopes in CVP samples. As compared to DCM, a relatively stronger nonradiative *one-photon* relaxation mechanism is found to be operative at 532 nm pump wavelength here. Hence the slopes do not increase significantly beyond 2. Moreover, the pump energy dependence of the slopes is not

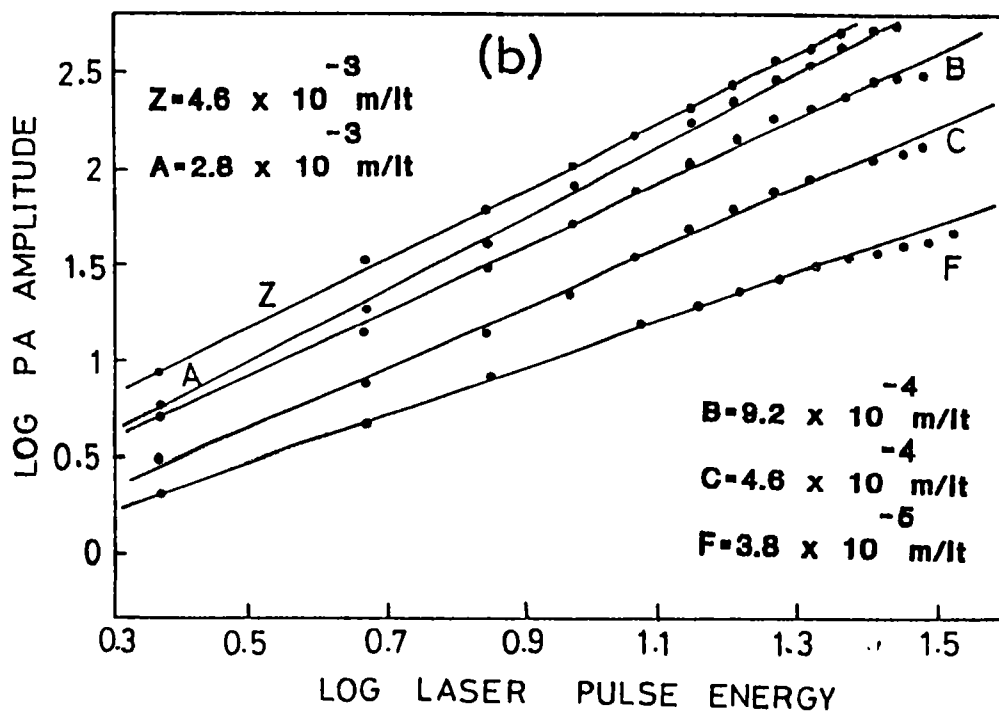
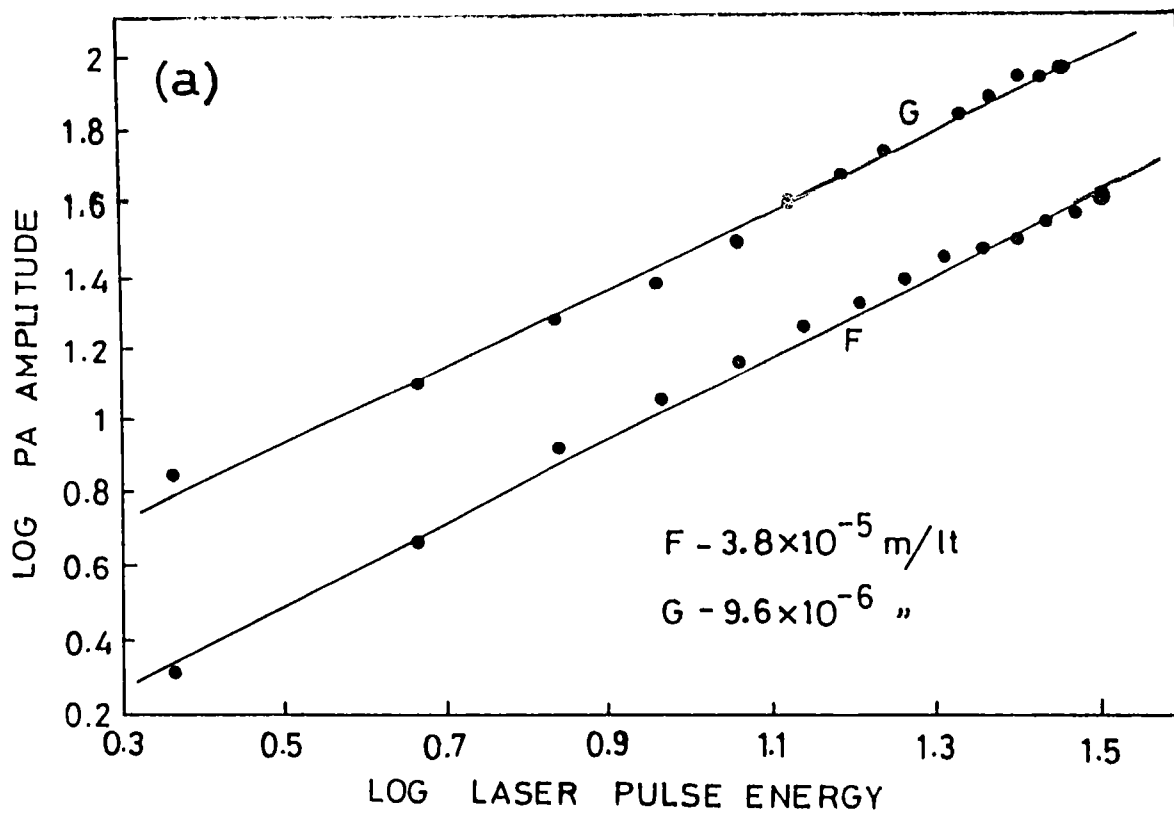


Fig.4.5 : Log laser pulse energy versus log PA amplitude plots, obtained for CVP + Methanol solutions of (a) Low concentrations and (b) High concentrations, at 532 nm pumping.

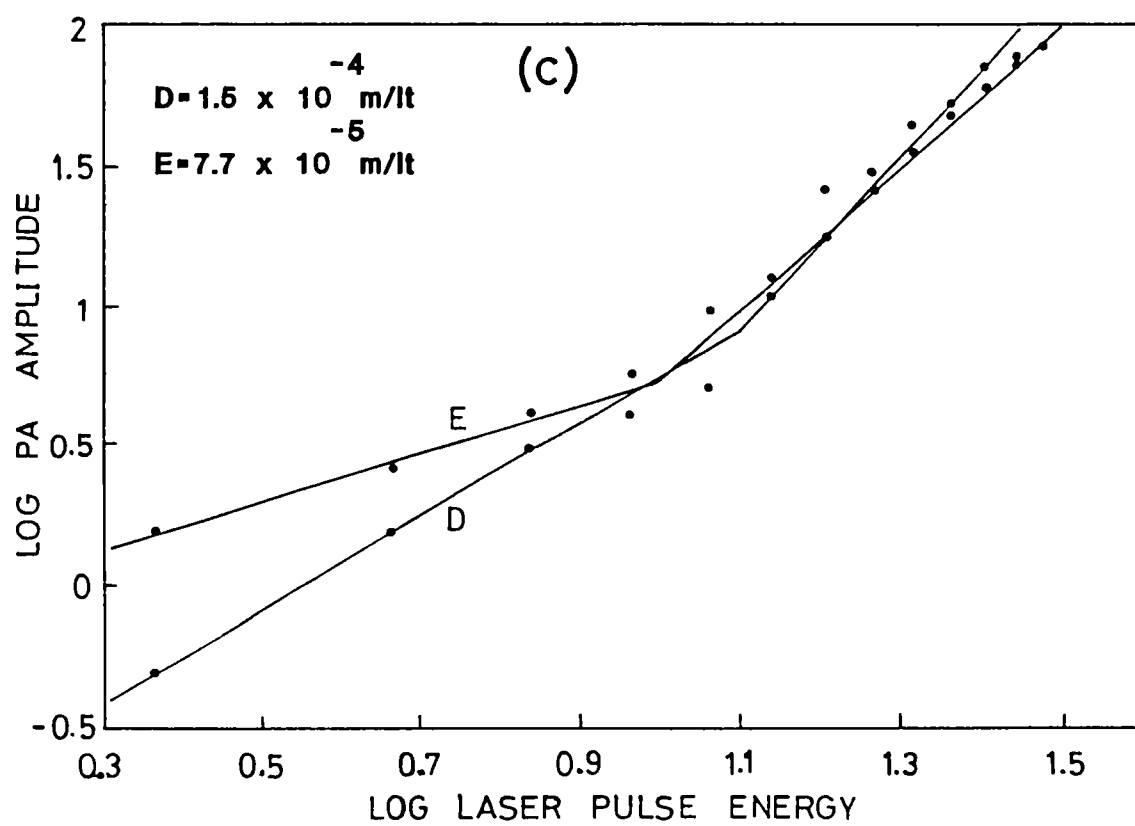


Fig.4.5c : Log laser pulse energy versus log PA amplitude plots, obtained for intermediate concentration solutions of CVP + Methanol, at 532 nm pumping.

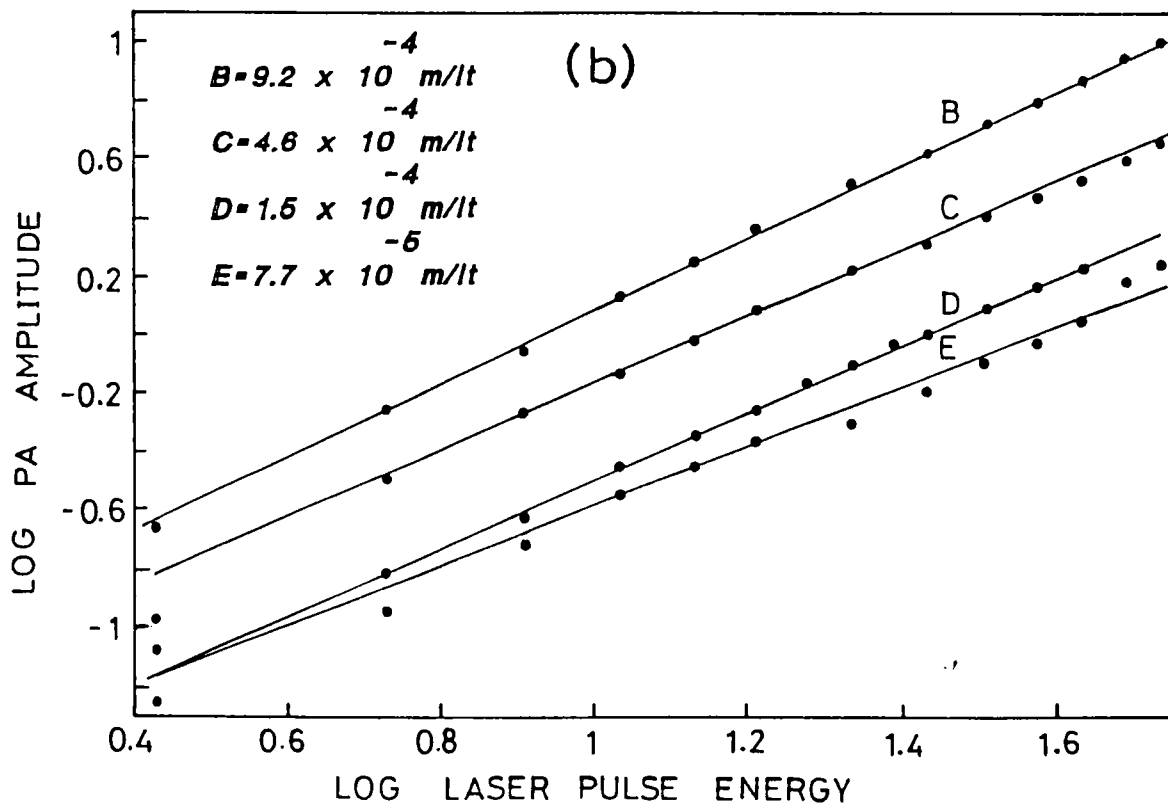
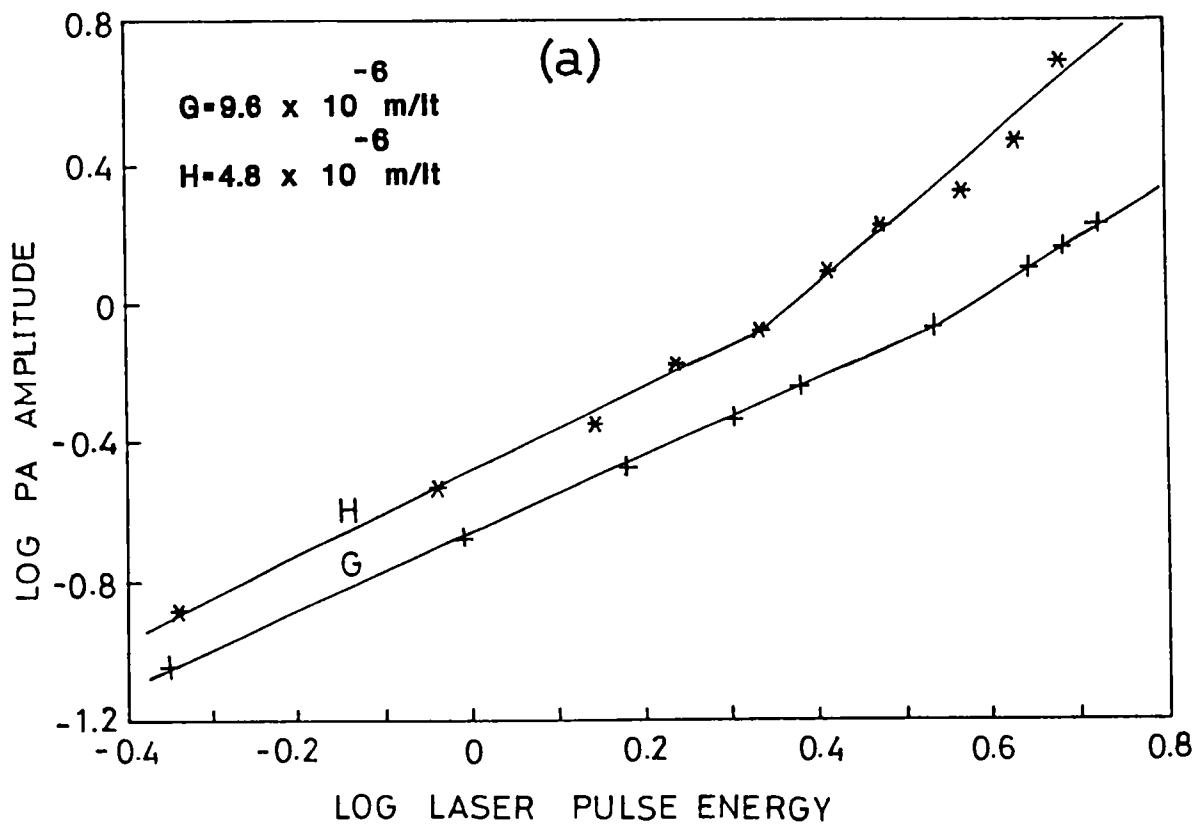


Fig.4.6 : Log laser pulse energy versus log PA amplitude plots, obtained for CVP + Methanol:water solutions of (a) Low concentrations and (b) High concentrations at 532 nm pumping.

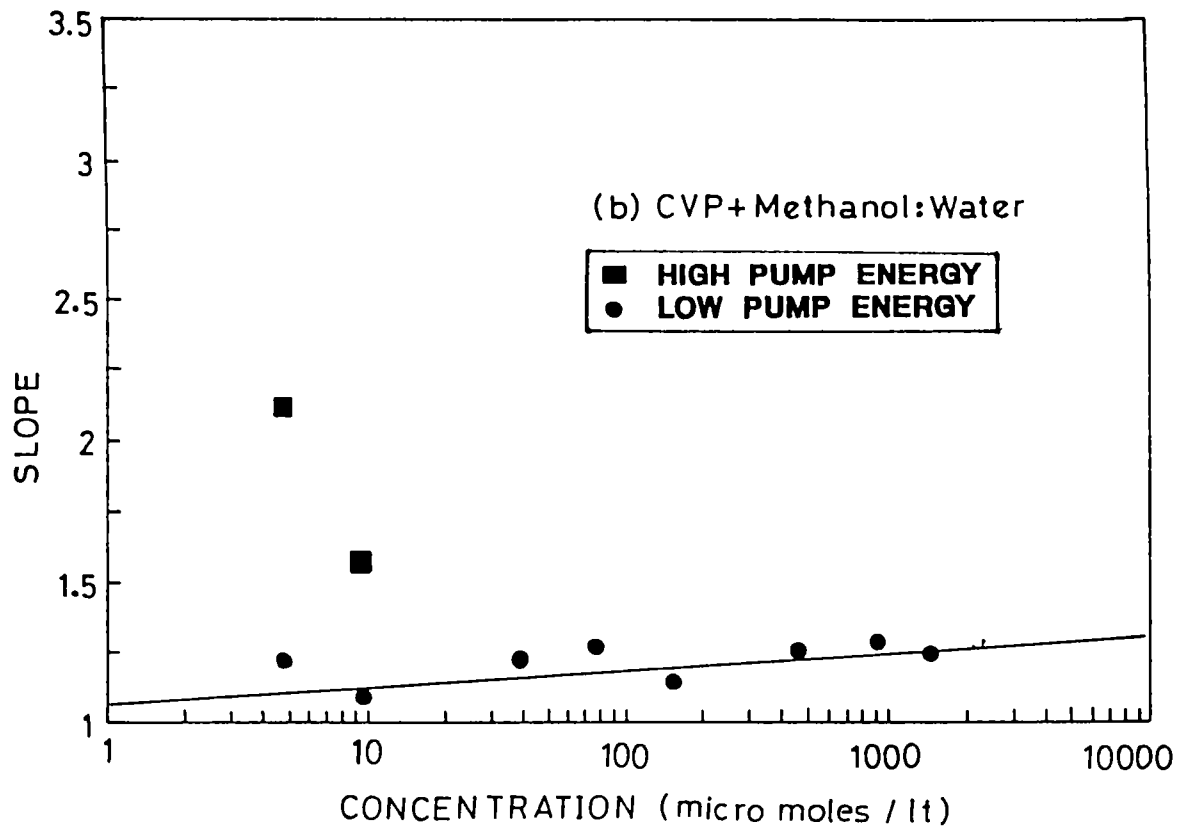
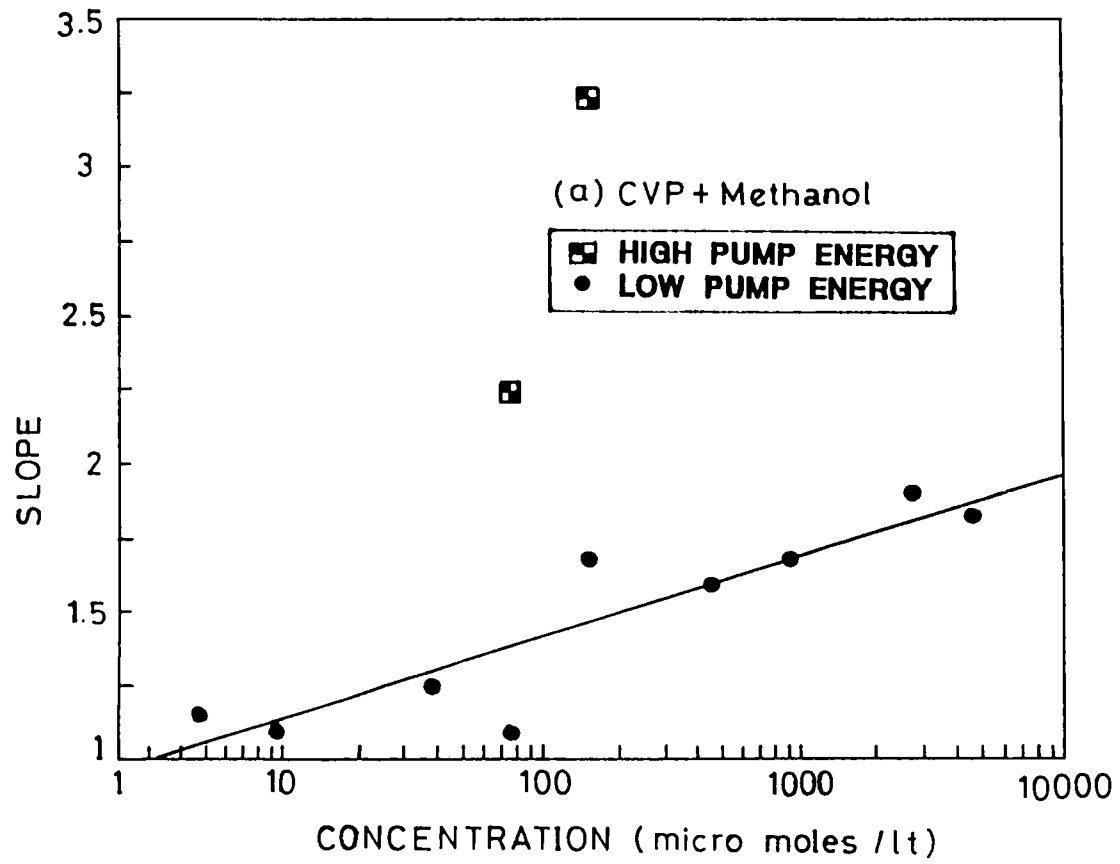


Fig.4.7 : Concentration dependence of the slope of the log-log plots for PA in CVP solutions at 532 nm pumping.

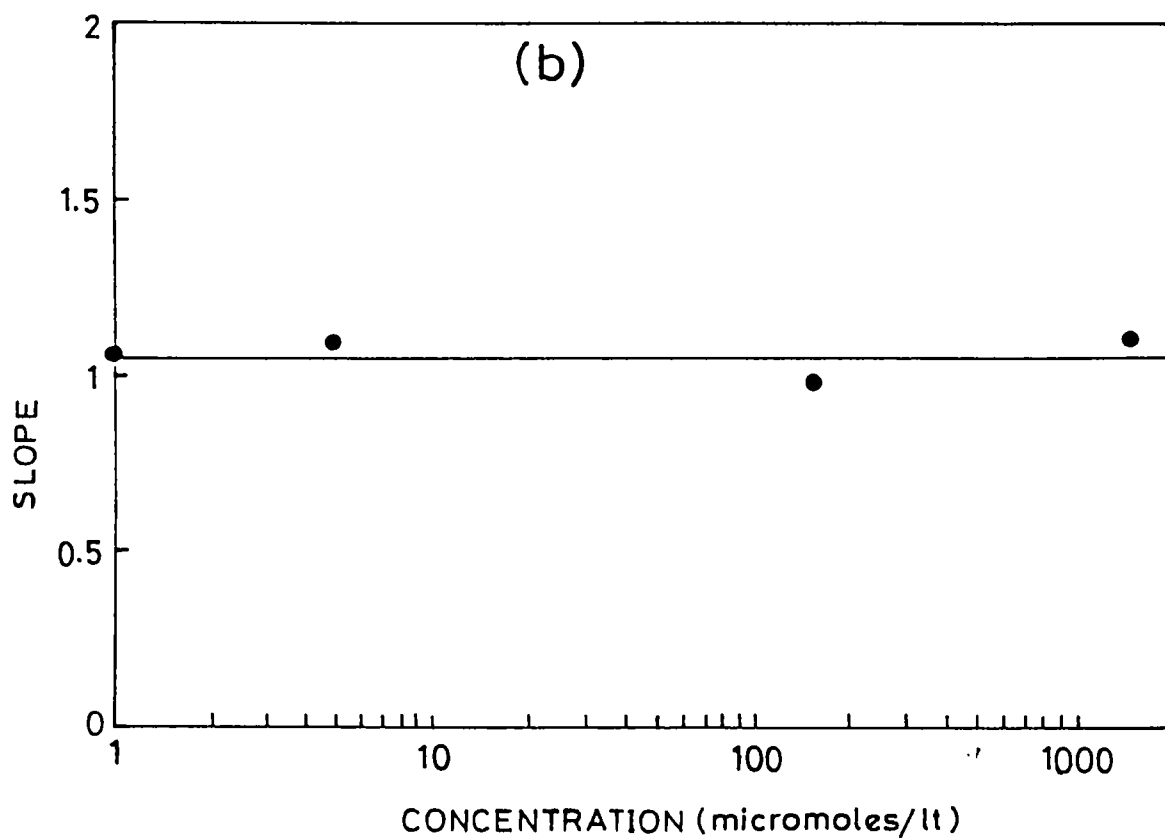
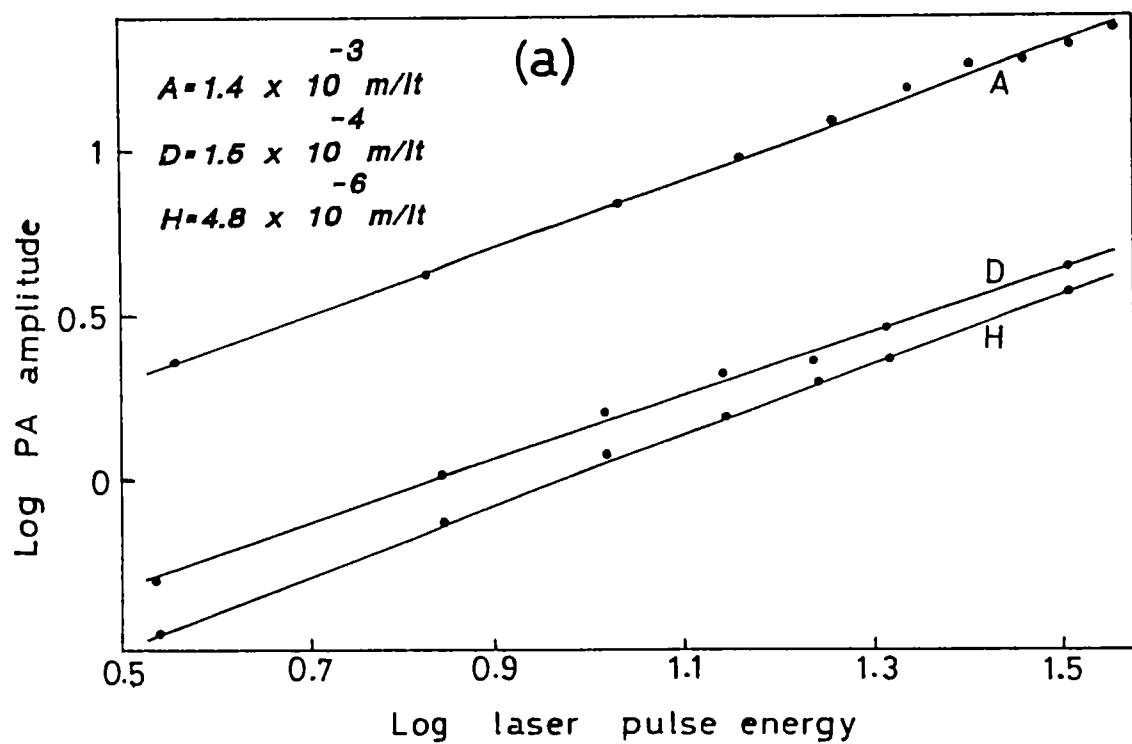


Fig.4.8 : (a) Log laser pulse energy versus log PA amplitude plots, obtained for CVP + Methanol:water solutions at 1064 nm pumping and (b) concentration dependence of the slopes.

very pronounced in this case, as it was for the DCM samples. Let us consider the energy level diagram of CVP shown in Fig.4.9, which is drawn from the previous absorption spectrum. The absorption is almost continuous in the uv and near uv regions, with prominent peaks situated approximately at 600 nm, 318 nm and 274 nm (16666 cm^{-1} , 31447 cm^{-1} and 36496 cm^{-1} respectively). Since the 532 nm excitation is at the shorter wavelength region of the $S_0 \rightarrow S_1$ absorption band of CVP, the molecules get excited to the higher vibrational levels of S_1 ($\approx 18800 \text{ cm}^{-1}$) from which they thermalize to the lowest level of S_1 ($\approx 15900 \text{ cm}^{-1}$) generating PA signals. It seems that this is the prominent mechanism of PA generation in MW solutions, as is evident from Fig.4.7b. Here most of the slopes lie between 1.2 and 1.3, indicating a predominant OPA mechanism. This is not surprising when we remember that the fluorescence quantum yield of CVP is as low as 0.5 in most solvents [8] leading to large $S_1 \rightarrow S_0$ internal conversion rates. However, Excited state absorption (ESA) gains strength in the two lowest concentration samples at high pump energies, revealing higher slopes. It may be noted that the ESA process is stronger in methanol solutions, which is clear from the slopes nearing 2 (Fig.4.7a). This is, however, not because of any solvent effect: it results rather from the higher beam intensities available here due to the reduction of beam diameter before focusing. The slope increases towards higher concentrations in both solutions which is, in general, similar to the behaviour shown by the DCM samples.

Previous studies of ESA from the S_1 level of CVP, carried out by means of saturable absorption and laser photolysis techniques have revealed that the ESA spectrum of the S_1 state is a broad band that extends approximately from 2 eV ($\approx 620 \text{ nm}$) to 2.9 eV ($\approx 428 \text{ nm}$) [7]. These authors have estimated a quite significant ESA cross section of about $1 \times 10^{-16} \text{ cm}^2$ for 532 nm radiation in a methanol solution of CVP at a concentration of 5×10^{-4} moles/lit. The primary effect of ESA on laser performance is a reduction in fluorescence quantum efficiency whenever large pumping flux is required. The decrease in quantum efficiency is explained by the fact that this additional absorption merely recycles the molecules between the first and higher excited states.

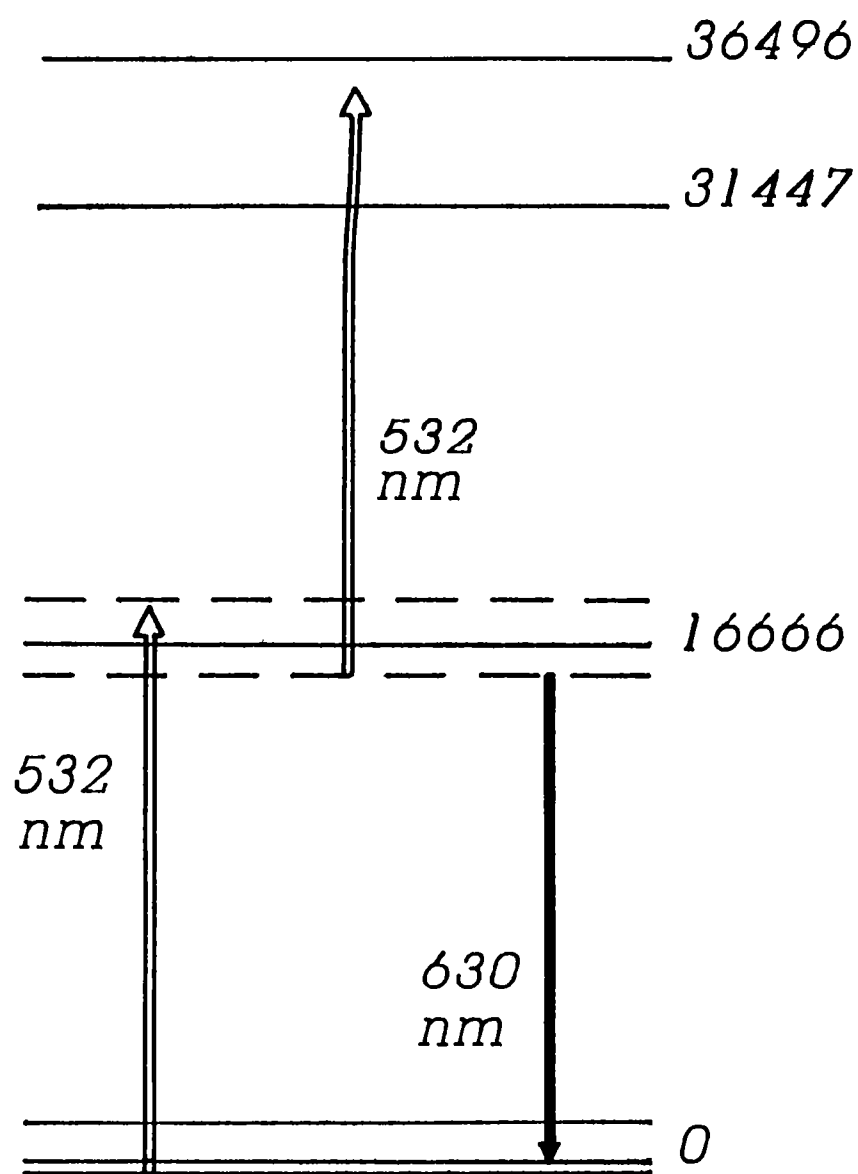


Fig.4.9 : Energy level diagram for the CVP molecule.

At 1064 nm pumping, both solutions show the same behaviour: the slopes are constant around the value of one, indicating the occurrence of large overtone absorptions in the solvent and subsequent nonradiative relaxation.

4.4 Investigations by Fluorescence: Results and discussion

The setup used for recording antistokes fluorescence from solution samples of CVP is the same as that described in chapter 3. Eventhough the OPA cross section at 1064 nm (9398 cm^{-1}) is negligible, energywise, the distribution of various levels is favourable for multiphoton absorption of the 1064 nm radiation. The corrected ASF emission spectra obtained for various methanol and MW solutions of CVP are depicted in figures 4.10a and 4.10b respectively. The emission peak shift due to reabsorption is clearly seen at higher concentrations, and the net shift in the studied range amounts to about 20 nm. The emission intensity, as a function of concentration, is shown in Figs.4.11a and 4.11b. Log laser pulse energy versus log ASF plots and the slope versus concentration curves are given in Figs.4.12 and 4.13. A distinct feature of CVP is the observation that the slope becomes as high as 5, in low concentration MW solutions (Fig.4.13b). Measurements have been taken at the peak emission wavelength and the calculated slopes are estimated to be accurate within $\pm 5\%$.

The range of slopes obtained from the present studies extend from 2.5 to 5, implying large multiphoton absorptions. Similar to that observed in DCM samples, here also ASF intensity increases and slope decreases with concentration. Various reasons for this behaviour (stimulated emission, stimulated Raman scattering, enhanced ESA and $S_0 \rightarrow S_1$ absorption) have already been outlined in the previous chapter. In addition to them reabsorption of emitted fluorescence also can play a role in the case of CVP. However, there are a few differences too: whereas light quenching (radiation quenching) of ASF is observed in low concentrations of DCM, ASF considerably increases with pump energy in low concentrations of CVP. (In CVP+MW solution, light quenching of ASF is seen in one sample, but that is at the highest concentration studied (1.45×10^{-3} moles/lt)). The primary

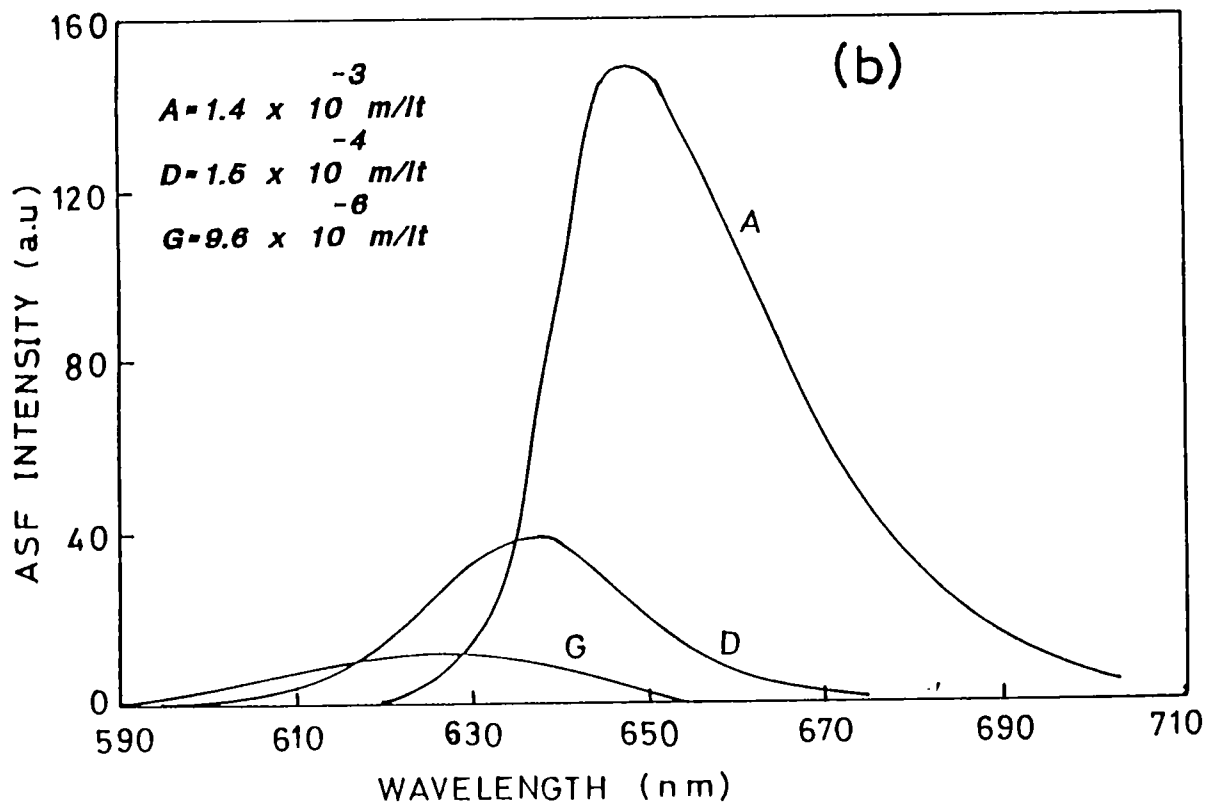
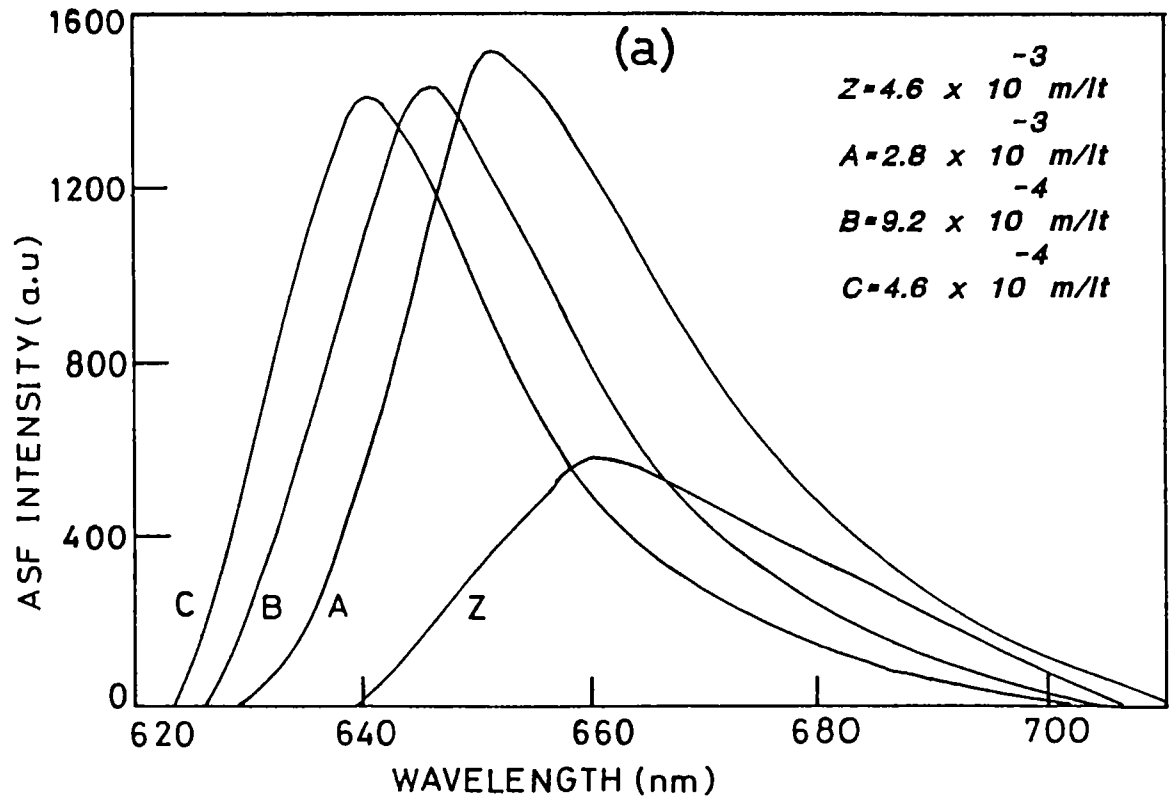


Fig.4.10 : Corrected antistokes fluorescence emission spectra observed in the right angle geometry from (a) CVP + Methanol solutions and (b) CVP + Methanol:water solutions at 1064 nm pumping.

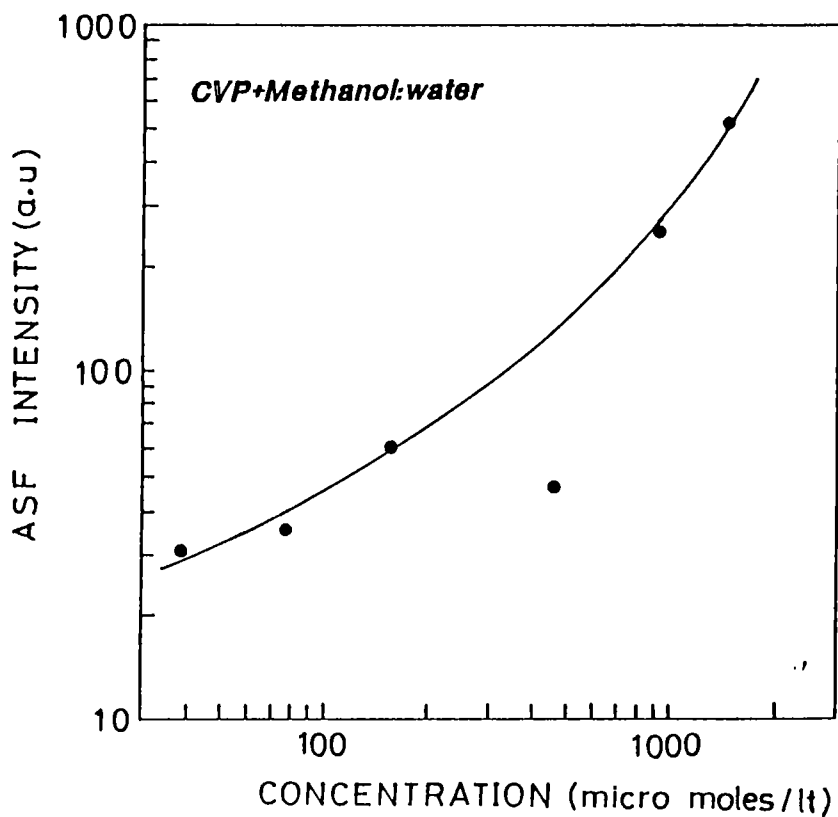
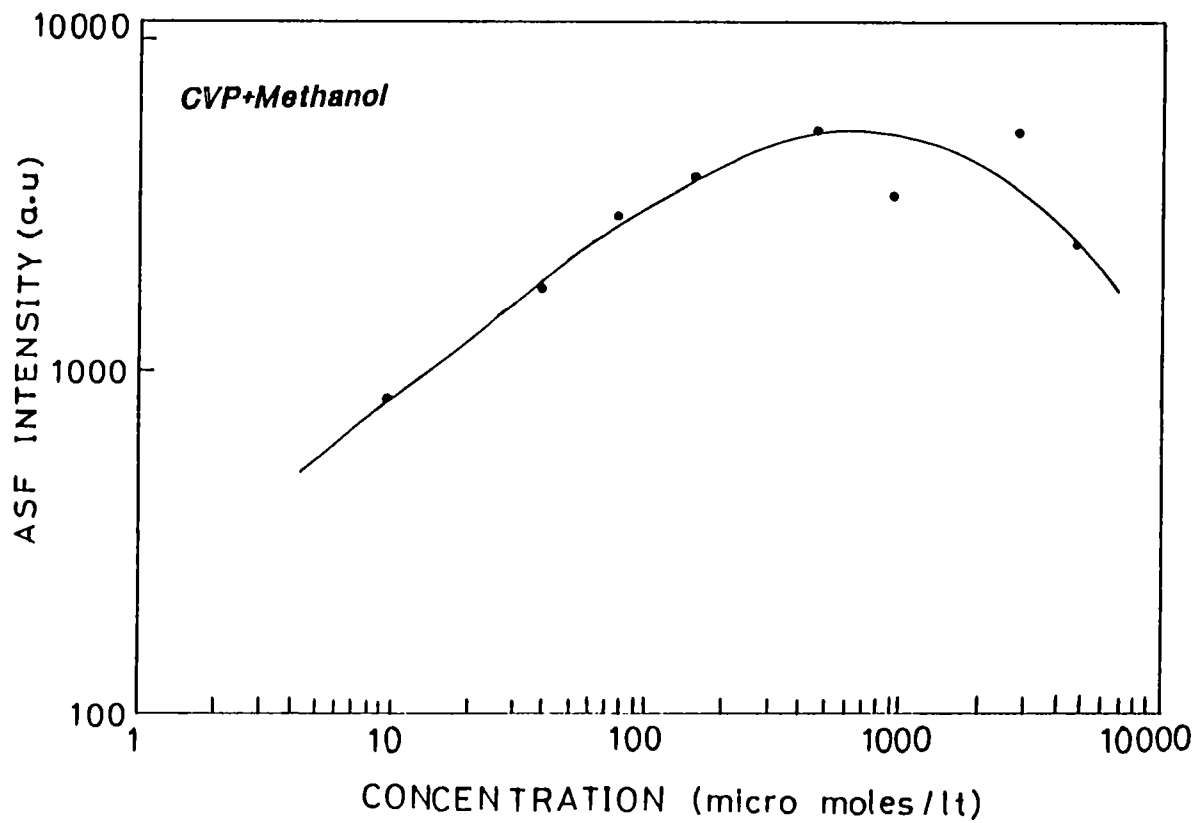


Fig.4.11 : Increase of the antistokes fluorescence intensity with concentration for CVP solutions at 1064 nm pumping. Laser pulse energy is 100 mJ.

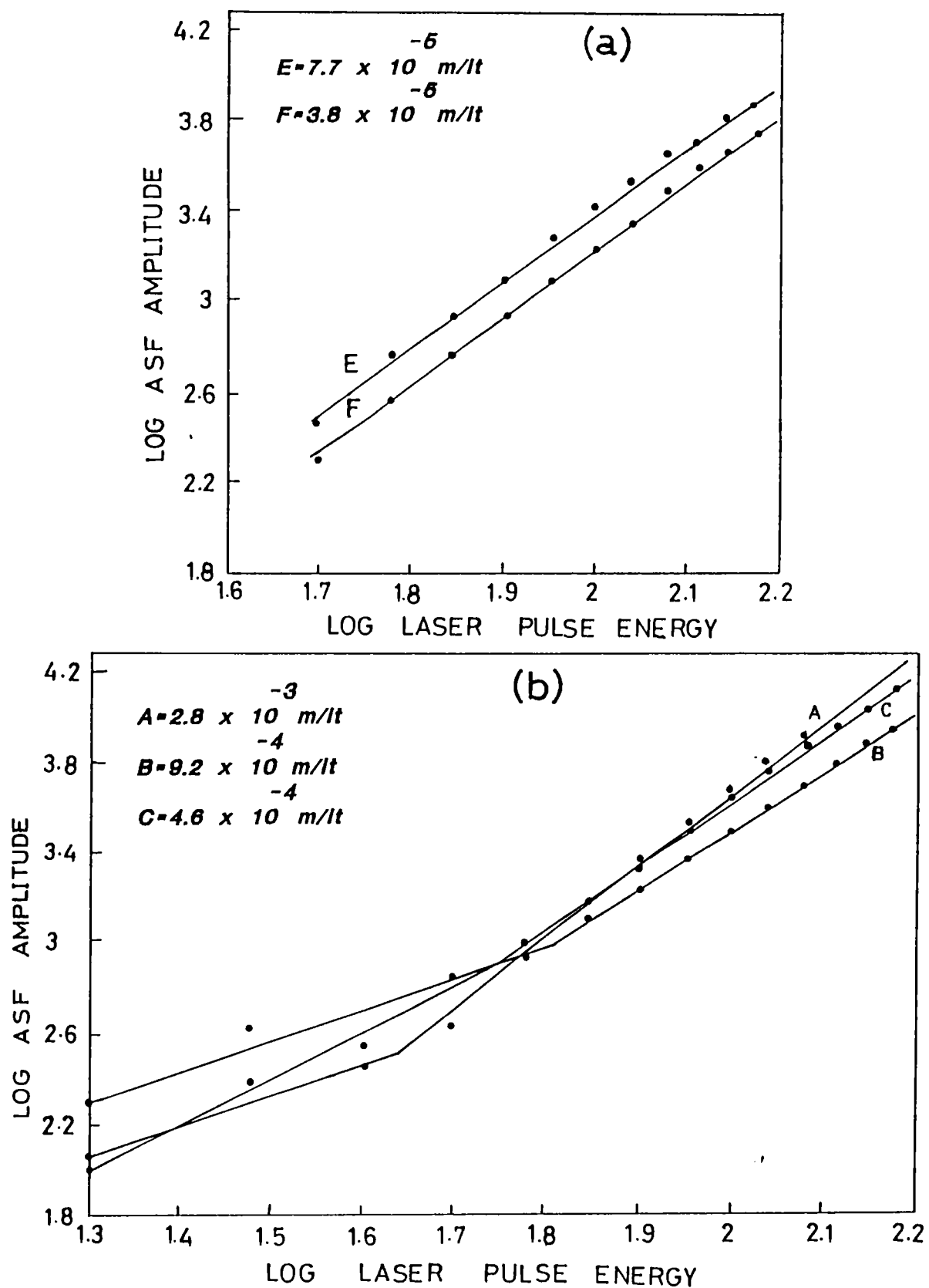


Fig.4.12 : Log laser pulse energy versus log ASF intensity plots obtained for CVP + Methanol solutions of (a) Low concentrations and (b) High concentrations, at 1064 nm pumping.

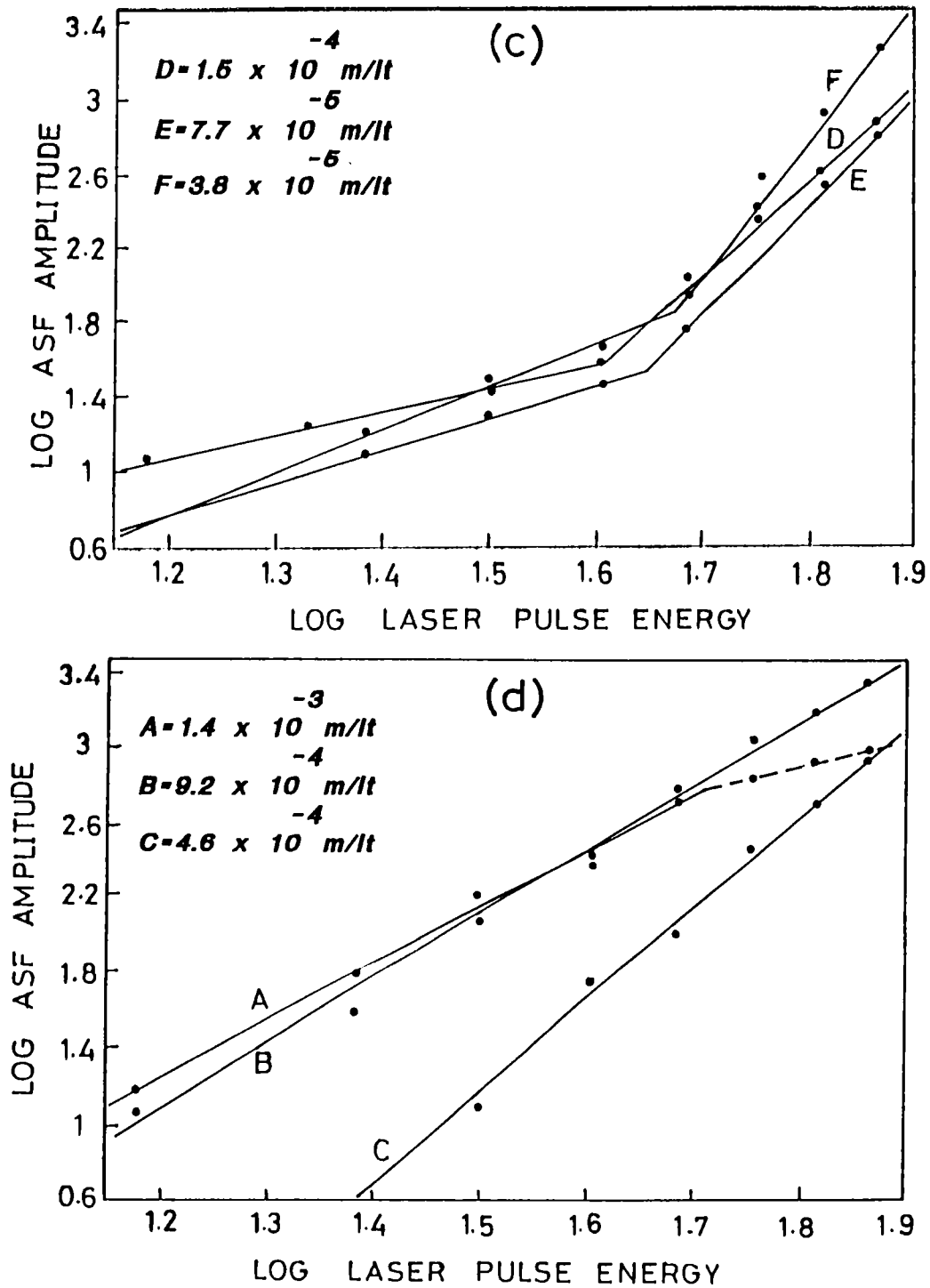


Fig.4.12 : Log laser pulse energy versus log ASF intensity plots obtained for CVP + Methanol:water solutions of (c) Low concentrations and (d) High concentrations, at 1064 nm pumping.

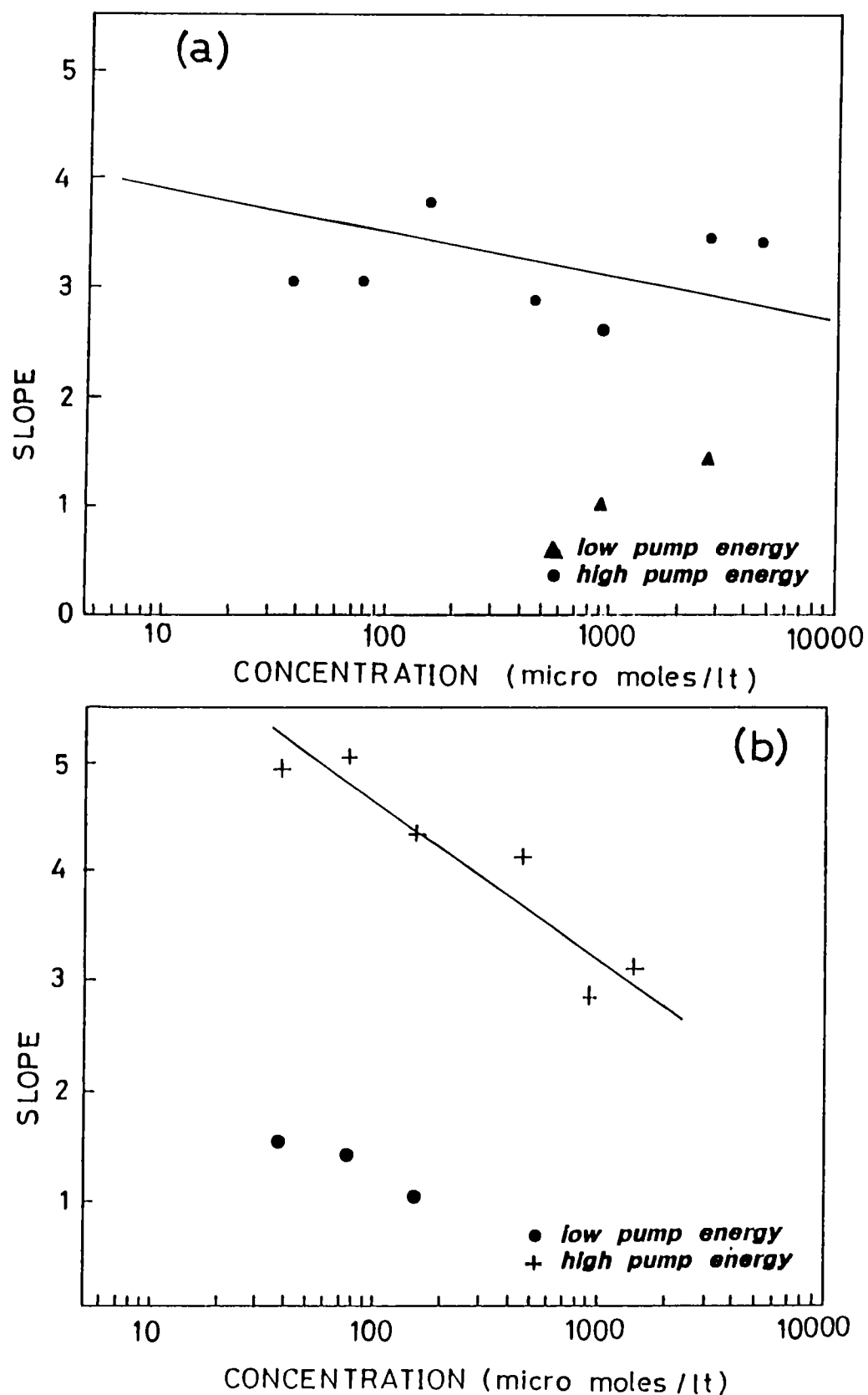


Fig.4.13 : Concentration dependence of the slope of the log-log plots in (a) CVP + Methanol solutions and (b) CVP + Methanol:water solutions for ASF at 1064 nm pumping.

reasons for light quenching are stimulated emission and ESA, and in the case of CVP it seems that the nonlinear multiphoton absorption cross sections are large enough to supersede the quenching process (unlike in DCM). The high slopes seen in MW solutions support this assumption. Concentration quenching of ASF is seen only in methanol solutions (Fig.4.11a). This is due to the enhanced reabsorption, as well as the formation of closely spaced molecular pairs [9] at high concentrations. In *pure water* solutions strong quenching is to be expected at high concentrations, considering the presence of dimers and higher aggregates. However, it is interesting to note that in the present MW solutions quenching is not seen, and the ASF intensity steadily increases with concentration (Fig.4.11b). It appears that in methanol:water solution of CVP aggregates and closely spaced pairs form a negligible fraction. Further work is, however, required to confirm this assumption.

4.5 Conclusions

Multiphoton and excited state absorption phenomena in the laser dye Cresyl violet perchlorate have been investigated in the solvents methanol and methanol:water using photoacoustics and fluorescence techniques. The PA data reveal that large $S_1 \rightarrow S_0$ internal conversion occurs in the dye, which is in agreement with the low quantum yield values reported. Multiphoton absorptions at 1064 nm are found to be quite strong, especially in CVP+methanol:water solutions. Contrary to the normal expectation, aggregation effects appear to be less significant in CVP+methanol:water solutions.

CHAPTER 4 - REFERENCES

- [1] Mitsuo Maeda, in "*Laser dyes*", Academic press (1984)
- [2] Drexhage K H, in "*Dye lasers*", (ed.) F.P.Schaefer, Topics in Applied Physics, Vol.1, Springer-Verlag, Berlin (1977)
- [3] Marling J B, L L Wood and D W Gregg, IEEE J.Quant.Electron., **QE-7**, 498 (1970)
- [4] Runge P K, Opt.Comm., **4**, 195 (1971)
- [5] Gacoin P and P Flamant, Opt.Comm. **5**, 351 (1972)
- [6] Arthurs E G, D J Bradley and A G Roddie, Appl.Phys.Lett., **20**, 125 (1972)
- [7] Jagdeep Shah and R F Leheny, Appl.Phys.Lett., **24**, 562 (1974)
- [8] Magde D, J H Brannon, T L Cremers and Olmsted J, J.Phys.Chem., **83**, 696 (1979)
- [9] Penzkofer A and Y Lu, Chem.Phys.Lett., **103**, 399 (1986)

CHAPTER - 5

STIMULATED RAMAN AND BRILLOUIN SCATTERING FROM DYE SOLUTIONS

5.1 Introduction

The basic Raman process is an inelastic light-scattering process in which an incident quantum $h\nu_L$ is scattered into a quantum $h\nu_s$, while the difference in energy $h(\nu_L - \nu_s) = h\nu_{ba}$ is absorbed by the material scattering centre. In principle the excitation $h\nu_{ba}$ of the material system may be a pure electronic excitation, but it is often a vibrational or rotational excitation of a molecule. The frequency ν_s is called a Stokes frequency which is smaller than the incident light frequency. If the system is in an excited state to begin with, it may make a transition downward while the light is scattered. In that case the scattered light contains anti-stokes frequencies which are higher than the incident frequency; $\nu_{as} = \nu_L + \nu_{ba}$ (Fig.5.1). In the stimulated Raman process (SRS) a light wave at frequency ν_s is incident on the material system simultaneously with a light wave at ν_L . A quantum $h\nu_s$ is added to the wave at ν_s , which consequently becomes amplified, while the incident light beam loses a quantum $h\nu_L$ and the material system is excited by a quantum $h(\nu_L - \nu_s)$ (Fig.5.2). On the other hand, Brillouin scattering refers to the scattering of light from thermally excited acoustic waves, and in stimulated Brillouin scattering (SBS) the acoustic waves are formed from a time-varying electrostrictive strain induced in the medium by the electric field of the incident electromagnetic radiation itself. The presence of an acoustic wave modulates the optical dielectric constant causing an exchange of energy between electromagnetic waves whose frequencies differ by an amount equal to the acoustic frequency. SBS is thus analogous to SRS with acoustic waves playing the role of molecular vibrations.

SRS, SBS and a few other nonlinear optical phenomena result from the existence of a nonlinear polarization which is a cubic function of the electric field amplitudes present in the optical radiation. This is the lowest-order nonvanishing nonlinearity in media with inversion symmetry, in the absence of which homogeneous plane travelling waves propagate independently of each other. The nonlinearity of the

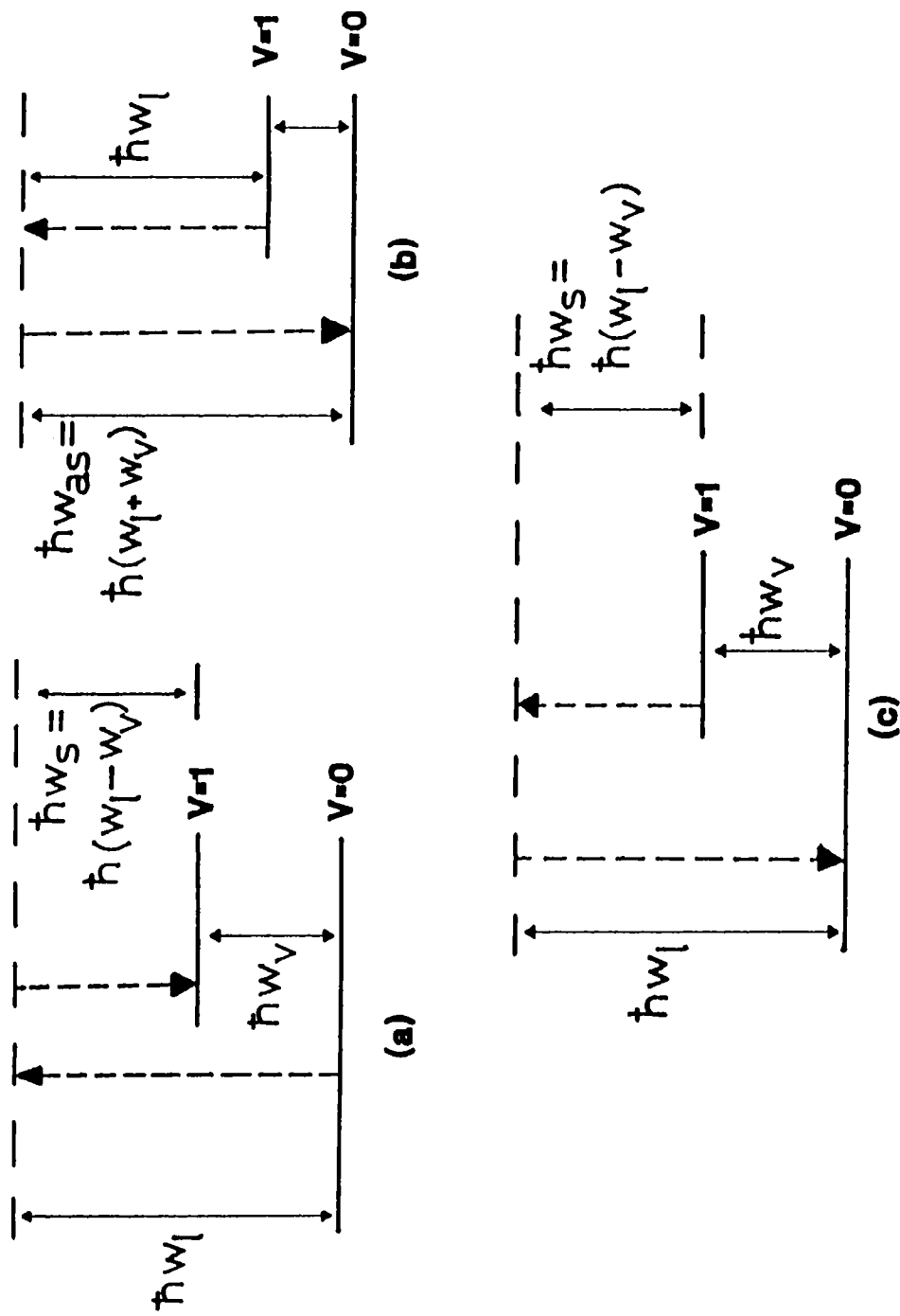


Fig.5.1 : (a) A Stokes scattering in which a laser photon at ω_l is absorbed, while a Stokes ($\omega_l - \omega_v$) photon is created along with a vibrational ($v = 1$) quantum. (b) An anti-Stokes scattering in which a laser photon at ω_l and a vibrational (ω_v) quantum are absorbed, while a photon at $\omega_l + \omega_v$ is created. (c) A process in which the presence of laser radiation at ω_l stimulates the absorption of Stokes photons at $\omega_l - \omega_v$, that is, the reverse of (a).

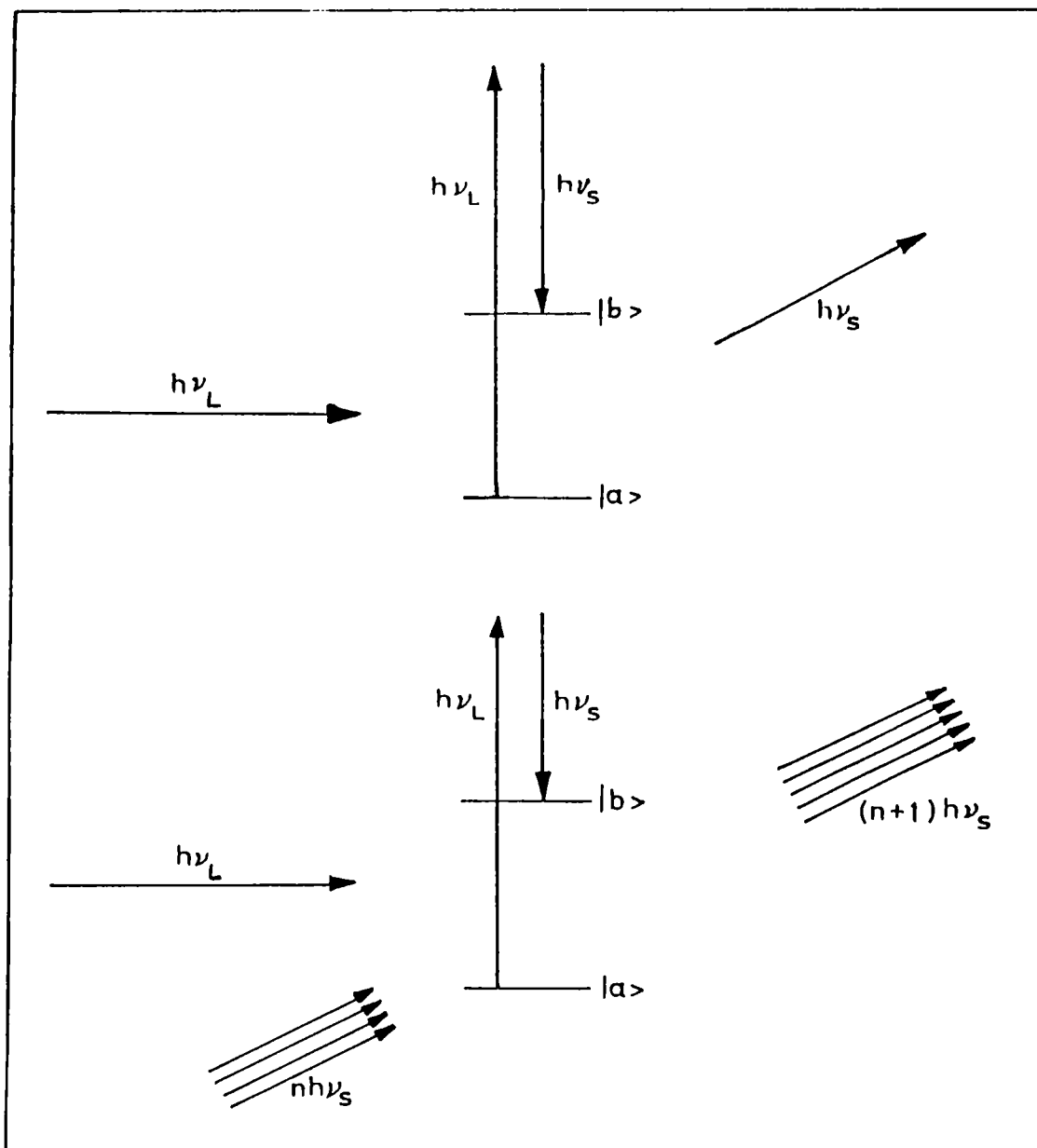


Fig.5.2 : Diagram of spontaneous (top) and stimulated (bottom) Raman scattering as a quantum process.

dielectric medium provides a coupling between different homogeneous plane waves. Consider, for example, the existence of a polarization at the sum frequency, created by the simultaneous presence of three electromagnetic waves with frequencies ω_1 , ω_2 and ω_3 and wave vectors \vec{k}_1 , \vec{k}_2 and \vec{k}_3 respectively. This nonlinear polarization at the frequency $\omega_p = \omega_1 + \omega_2 + \omega_3$ has a spatial distribution characterized by a wave vector $\vec{k}_p = \vec{k}_1 + \vec{k}_2 + \vec{k}_3$. If i , j , k and l define cartesian components of the nonlinear polarization and the three waves, respectively, an element of a cubic nonlinear susceptibility tensor may be defined by [1]

$$\hat{P}_i^{NL}(\omega_p, \vec{k}_p) = \chi_{ijkl}^{(3)}(-\omega_p, \omega_1, \omega_2, \omega_3) \vec{E}_j(\omega_1, \vec{k}_1) \vec{E}_k(\omega_2, \vec{k}_2) \vec{E}_l(\omega_3, \vec{k}_3) \quad (5.1)$$

The notation adopted for χ is sufficiently general such that all possible sum and difference frequency combinations can be treated: for example $\chi(-\omega_1, \omega_2, \omega_3, -\omega_4)$ relates a nonlinear polarization at the frequency $\omega_1 = \omega_2 + \omega_3 - \omega_4$ to the electric field amplitudes of the waves at the last three frequencies. In general the nonlinear polarization given by the above equation will couple to a fourth electromagnetic traveling wave at $\omega_4 = \omega_p$. The electromagnetic wave E_4 thus generated will, of course, couple in turn with the first three waves through the nonlinearity. The coupling will be appreciable if the momentum mismatch $\Delta\vec{k} = \vec{k}_4 - \vec{k}_1 - \vec{k}_2 - \vec{k}_3$ is not too large. One thus arrives at the picture of four electromagnetic plane waves whose amplitudes and phases may vary in space due to the nonlinear coupling, described by a set of four coupled complex amplitude differential equations for E_1 , E_2 , E_3 and E_4 . The solutions lead to distinct physical processes according to the special relationships between the four frequencies, or whether the nonlinear susceptibility is real or imaginary. Table 5.1 lists a few nonlinear optical phenomena resulting from the third order nonlinear susceptibility.

5.2 Electromagnetic treatment of Stimulated Raman scattering

The quantum treatment of Stimulated Raman scattering (SRS) is based on the concept of transition rates, where the electromagnetic field quantities appear only as photon densities so that all phase information is absent. Even though it is possible to have a quantum mechanical description of the phases in terms of coherent states, the

Table 5.1

Process	Nonlinear Susceptibility
1. Third harmonic generation	$\chi^{(3)}(-3\omega, \omega, \omega, \omega)$
2. Two photon absorption	$\chi^{(3)}(-\omega, \omega, \omega, -\omega)$
3. DC Kerr effect	$\text{Re } \chi^{(3)}(-\omega, \omega, 0, 0)$
4. Raman scattering	$\chi^{(3)}(-\omega \pm \Omega, \omega, -\omega, \omega \pm \Omega)$
5. Brillouin scattering	$\chi^{(3)}(-\omega \pm \Omega, \omega, -\omega, \omega \pm \Omega)$

electromagnetic treatment is more illustrative.

The induced electronic dipole moment of a molecule can be written as $\mu_i = \epsilon_0 \alpha E$ where α is the molecular polarizability and E is the applied electric field. For a vibrating molecule α is a function of the normal co-ordinate of vibration, X . The first two terms in the series expansion of $\alpha(X)$ can be taken as [2]

$$\alpha(X) = \alpha_0 + \left(\frac{\partial\alpha}{\partial X}\right)_0 X \quad (5.2)$$

where α_0 is the equilibrium polarizability, and $\left(\frac{\partial\alpha}{\partial X}\right)_0$ is referred to as the differential polarizability. In addition, an asymmetric molecule may possess a permanent dipole moment μ_p also, given by $\mu_p(X) = \mu_p^0 + \left(\frac{\partial\mu_p}{\partial X}\right)_0 X$. For transitions between vibrational levels that are induced by a radiation field we consider the perturbation Hamiltonian

$$H' = -\vec{\mu} \cdot \vec{E} = -[\mu_p^0 + \left(\frac{\partial\mu_p}{\partial X}\right)_0 X + \epsilon_0 \alpha_0 E + \epsilon_0 \left(\frac{\partial\alpha}{\partial X}\right)_0 XE] E \quad (5.3)$$

where E is the electric field component parallel to $\vec{\mu}$. The first and third terms in the square bracket are independent of X and hence cannot cause transitions between adjacent vibrational levels since the eigen functions $\psi_v(X)$ are orthogonal to each other. The second term gives rise to direct infrared absorption at ω_v . The term that gives rise to Raman scattering is the last one:

$$H'_{\text{RAM}} = - \left(\frac{\partial\alpha}{\partial X}\right)_0 \epsilon_0 XE^2 \quad (5.4)$$

In our model the Raman medium is taken as consisting of N harmonic oscillators per unit volume, each oscillator representing one molecule. The oscillators are independent of each other, and each is characterized by its position z (the analysis is one-dimensional so that $\partial/\partial x = \partial/\partial y = 0$) and normal vibrational co-ordinate $X(z,t)$. The equation of motion for a single oscillator is then

$$\frac{d^2X(z,t)}{dt^2} + \gamma \frac{dX}{dt} + \omega_v^2 X = \frac{F(z,t)}{m} \quad (5.5)$$

where γ is the damping constant chosen so that the observed

spontaneous Raman linewidth is $\Delta\nu = \gamma/2\pi$, ω_v is the (undamped) resonance frequency, m is the mass and $F(z,t)$ is the driving force. The driving term can be derived by considering the electromagnetic energy in the presence of the molecules. The electrostatic stored energy density is

$$E = \frac{1}{2} \epsilon \bar{E} \cdot \bar{E} \quad (5.6)$$

where ϵ is the dielectric constant. Now, since

$$\epsilon = \epsilon_0 [1 + N\alpha] = \epsilon_0 \left\{ 1 + N \left[\alpha_0 + \left(\frac{\partial\alpha}{\partial X} \right)_0 X \right] \right\}, \quad (5.7)$$

E can be written as

$$E = \frac{1}{2} \epsilon_0 \left\{ 1 + N \left[\alpha_0 + \left(\frac{\partial\alpha}{\partial X} \right)_0 X \right] \right\} \overline{E \cdot E} \quad (5.8)$$

The force per unit volume of polarizable material is $\partial E / \partial X$, that, after dividing by N , gives the force per oscillator as

$$F(z,t) = \frac{1}{2} \epsilon_0 \left(\frac{\partial\alpha}{\partial X} \right)_0 \overline{E \cdot E} \quad (5.9)$$

where the overbar indicates averaging over a few optical periods since the molecules cannot respond to optical frequencies. This shows that because of the nonvanishing differential polarizability, $(\partial\alpha/\partial X)_0$, the molecular vibration can be driven by the optical electric field.

Next we shall see how the field-induced excitation of molecular vibration $X(z,t)$ reacts back on the electromagnetic fields. According to Eqn. 5.7, the molecular vibration at ω_v causes a modulation of ϵ (and hence the refractive index) at ω_v leading to phase (frequency) modulation of any radiation field present, creating sidebands separated by ω_v . Stated differently, the modulation of ϵ at ω_v caused by molecular vibrations can lead to energy exchange between electromagnetic fields separated in frequency by multiples of ω_v , such as, for example, the laser and stokes ($\omega_s = \omega_1 - \omega_v$) fields. Supposing a single stokes field ω_1 to be generated in this way by the pump laser field ω_2 , we have now the total field as

$$\vec{E}(z, t) = \frac{1}{2} \hat{e}_1 E_1(z) e^{i\omega_1 t} + \frac{1}{2} \hat{e}_2 E_2(z) e^{i\omega_2 t} + \text{c.c.} \quad (5.10)$$

so that

$$\overline{E \cdot E} = \hat{e}_1 \cdot \hat{e}_2 \frac{1}{4} E_2(z) E_1^*(z) e^{i(\omega_2 - \omega_1)t} + \text{c.c.} \quad (5.11)$$

Substituting Eqn.5.11 in Eqn.5.9 and then in Eqn.5.5 we obtain

$$\frac{1}{2}(\omega_v^2 - \omega^2 + i\omega\gamma) X(z) e^{i\omega t} = \frac{\hat{e}_1 \cdot \hat{e}_2 \epsilon_0}{8m} \left(\frac{\partial \alpha}{\partial X} \right)_0 E_2 E_1^* e^{i(\omega_2 - \omega_1)t} \quad (5.12)$$

where $\omega = \omega_2 - \omega_1$, and

$$X(z, t) = \frac{1}{2} X(z) e^{i\omega t} + \text{c.c.} \quad (5.13)$$

From Eqn.5.12 it follows that the molecular vibration is driven at a frequency $\omega = \omega_2 - \omega_1$ with a complex amplitude

$$X(z) = \frac{\epsilon_0 \left(\frac{\partial \alpha}{\partial X} \right)_0 E_2(z) E_1^*(z) \hat{e}_1 \cdot \hat{e}_2}{4m[\omega_v^2 - (\omega_2 - \omega_1)^2 + i(\omega_2 - \omega_1)\gamma]} \quad (5.14)$$

The stokes field at ω_1 will induce a polarization in the molecules, given by

$$\begin{aligned} P &= \epsilon_0 N \alpha(z, t) E(z, t) \\ &= \epsilon_0 N \left[\alpha_0 + \left(\frac{\partial \alpha}{\partial X} \right)_0 X(z, t) \right] E(z, t) \end{aligned} \quad (5.15)$$

and we see that P has a linear and nonlinear part given by $P = P_L + P_{NL}$, where

$$P_L(z, t) = \epsilon_0 N \alpha_0 E \quad (5.16a)$$

and

$$P_{NL}(z, t) = \epsilon_0 N E \left(\frac{\partial \alpha}{\partial X} \right)_0 X(z, t) \quad (5.16b)$$

Our concern here is with the nonlinear polarization $P_{NL}(z, t)$. Using Eqns.5.10 and 5.14 in Eqn.5.16b we will get an expression for $P_{NL}(z, t)$ that contains polarizations oscillating at ω_1 , ω_2 , $2\omega_1 - \omega_2$

and $2\omega_2 - \omega_1$. Let us concentrate on the ω_1 term; the corresponding P_{NL} is given by

$$P_{NL}^{(\omega_1)}(z, t) = \frac{1}{2} P_{NL}^{(\omega_1)}(z) e^{i\omega_1 t} + c.c \quad (5.17)$$

where

$$P_{NL}^{(\omega_1)}(z) = \frac{\epsilon_0^2 N \left(\frac{\partial \alpha}{\partial X}\right)_0^2 |E_2|^2 \hat{e}_1 \cdot \hat{e}_2}{8m [\omega_v^2 - (\omega_2 - \omega_1)^2 - i(\omega_2 - \omega_1)\gamma]} E_1(z). \quad (5.18)$$

Since the coefficient relating an induced polarization to the inducing field is the susceptibility, we can define a *complex Raman nonlinear susceptibility* through the relation

$$P_{NL}^{(\omega_1)}(z) = \epsilon_0 \chi_{RAM}(\omega_1) |E_2(z)|^2 E_1(z) \quad (5.19)$$

so that for $\hat{e}_1 \parallel \hat{e}_2$,

$$\chi_{RAM}(\omega_1) = \frac{\epsilon_0 N \left(\frac{\partial \alpha}{\partial X}\right)_0^2}{8m [\omega_v^2 - (\omega_2 - \omega_1)^2 - i(\omega_2 - \omega_1)\gamma]} \quad (5.20)$$

We can split $\chi_{RAM}(\omega_1)$ into the in-phase (real) and quadrature (imaginary) components such that

$$\chi_{RAM}(\omega_1) = \chi'_{RAM}(\omega_1) - i\chi''_{RAM}(\omega_1) \quad (5.21)$$

where

$$\chi'_{RAM}(\omega_1) \approx \frac{\epsilon_0 N \left(\frac{\partial \alpha}{\partial X}\right)_0^2 [\omega_v - (\omega_2 - \omega_1)]}{16m\omega_v \{[\omega_v - (\omega_2 - \omega_1)]^2 + \gamma^2/4\}} \quad (5.22)$$

and

$$\chi''_{RAM}(\omega_1) \approx \frac{-\epsilon_0 N \left(\frac{\partial \alpha}{\partial X}\right)_0^2 (\gamma/2)}{16m\omega_v \{[\omega_v - (\omega_2 - \omega_1)]^2 + \gamma^2/4\}} \quad (5.23)$$

where the approximation applies to the high Q regime ($\gamma \ll \omega_v$), which is usually the case (typically $\gamma \leq 10^{-2} \omega_v$). The nonlinear Raman susceptibility is thus Lorentzian, and is plotted in Fig.5.3. The

Raman gain has an exponential dependence on the length of the medium, given by

$$E^{(\omega_1)}(z) = E^{(\omega_1)}(0) \exp \left\{ -ik_1 z \left(1 + \frac{|E_2|^2 \chi'_{RAM}(\omega_1)}{2n_1^2} \right) - k_1 z \frac{|E_2|^2 \chi''_{RAM}(\omega_1)}{2n_1^2} \right\} \quad (5.24)$$

where

$$k'_1 = k_1 \left[1 + \frac{\chi_{RAM}(\omega_1)}{2n_1^2} |E_2|^2 \right] \quad (5.25)$$

is the propagation constant modified from k_1 to account for the presence of a Raman polarization at ω_1 . The exponential gain coefficient in Eqn. 5.24 is

$$g(\omega_1) = \frac{-k_1}{2n_1^2} |E_2|^2 \chi''_{RAM}(\omega_1) \quad (5.26)$$

where $n_1 = (\epsilon/\epsilon_0)^{1/2}$ is the refractive index of the medium, far from resonance. $g(\omega_1)$ is positive since $\chi''_{RAM}(\omega_1) < 0$. Using Eqn. 5.23, Eqn. 5.26 can be rewritten as

$$g(\omega_1) = \frac{k_1 \epsilon_0 \left(\frac{\partial \alpha}{\partial X} \right)_0^2 N \gamma |E_2|^2}{32n_1^2 m \omega_v \{ [\omega_v - (\omega_2 - \omega_1)]^2 + \gamma^2/4 \}} \quad (5.27)$$

One may note that $(\partial \alpha / \partial X)_0$ is related to the spontaneous differential Raman scattering cross section $(d\sigma/d\Omega)$ through the relation

$$\left(\frac{d\sigma}{d\Omega} \right) = \frac{\omega_1^4 \bar{h} \left(\frac{\partial \alpha}{\partial X} \right)_0^2}{2m\omega_v c^4} \quad (5.28)$$

which is applicable in the resonant case, i.e., when $\omega_2 - \omega_1 = \omega_v$.

Quantum mechanical consideration of the Raman scattering problem shows that antistokes radiation at $\omega_3 \approx \omega_2 + \omega_v$ can be generated by

Raman transitions originating in the excited vibrational states. To treat the problem electromagnetically let us consider the ω_3 polarization induced in the Raman medium due to an electric field

$$E(z,t) = \frac{1}{2} [E_1(z) e^{i\omega_1 t} + E_2(z) e^{i\omega_2 t} + E_3(z) e^{i\omega_3 t} + c.c] \quad (5.29)$$

where $\omega_3 - \omega_2 = \omega_2 - \omega_1$. The induced polarization can be derived as before here also, and the result shows that the nonlinear polarization

$$P_{NL}^{(\omega_3)}(z) \propto E_2 E_2 E_1^* e^{-i(2\vec{k}_2 - \vec{k}_1) \cdot \vec{r}} \quad (5.30)$$

will generate a field at ω_3 with a spatial dependence $E_2 e^{-i\vec{k}_3 \cdot \vec{r}}$ such that

$$\vec{k}_3 = 2\vec{k}_2 - \vec{k}_1 . \quad (5.31)$$

Antistokes radiation will thus be emitted in any direction \vec{k}_3 that satisfies Eqn.5.31. This phase matching condition is illustrated in Fig.5.4, and we see that antistokes Raman radiation is emitted in the form of a conical shell about the laser propagation direction.

5.3 Stimulated Brillouin scattering (SBS)

The theoretical treatment of SBS can be developed similar to that for SRS. If E_2 , E_1 and u_s represent the pump field, Brillouin scattered optical field and the acoustic displacement respectively, then the growth or decay of u_s and E_1 as a function of distance q along the propagation direction is given by

$$\frac{du_s}{dq} = \frac{-\eta}{2\rho V_s} u_s - \frac{\gamma}{16\rho V_s^2} E_2 E_1^* \quad (5.32)$$

and

$$\frac{dE_1^*}{dq} = \frac{-\alpha E_1^*}{2} - \frac{\gamma k_1 k_s}{4\epsilon_1} E_2^* u_s \quad (5.33)$$

Assuming an exponential growth rate we take

$$u_s(q) = u_s^0 e^{gq} \quad (5.34a)$$

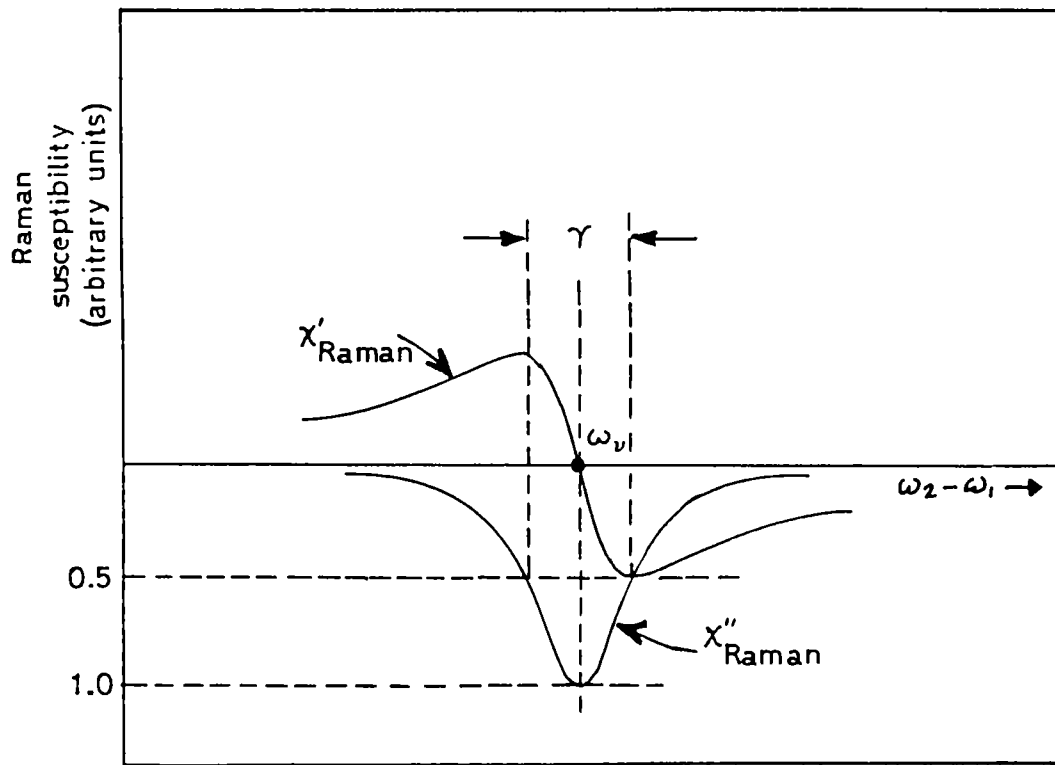


Fig.5.3 : The in-phase (χ'_{Raman}) and quadrature (χ''_{Raman}) components of the Raman nonlinear susceptibility as a function of the Stokes frequency ω_1 (ω_1 increases from right to left).

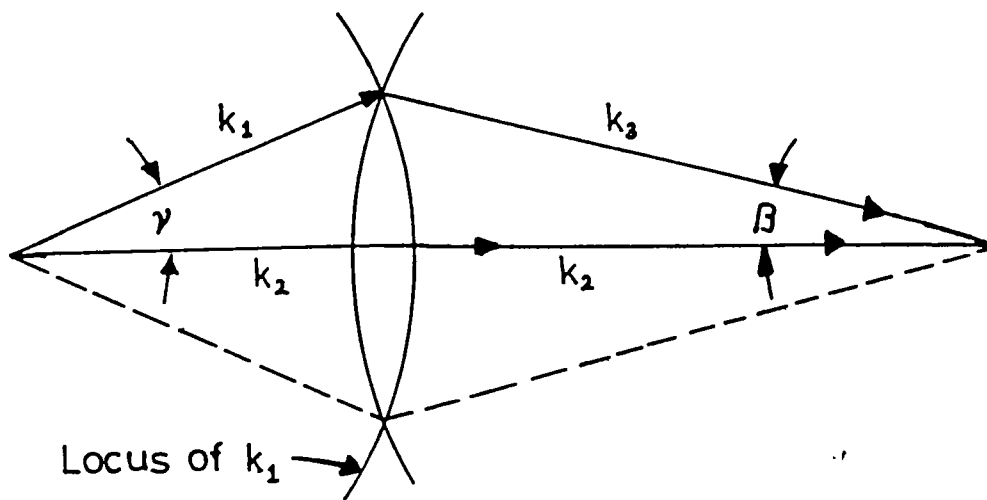


Fig.5.4 : A construction for finding the direction of propagation \vec{k}_3 of the anti-Stokes radiation.

and

$$E_1^*(q) = (E_1^0)^* e^{gq} \quad (5.34b)$$

and the exponential gain constant is given by

$$g = -\frac{1}{4}(\alpha_s + \alpha) + \frac{1}{4} \left[(\alpha_s + \alpha)^2 - 4 \left(\alpha_s \alpha - \frac{k_1 k_s \gamma^2 |E_2|^2}{16\rho \epsilon_1 v_s^2} \right) \right]^{1/2} \quad (5.35)$$

where

- $\alpha_s = \eta/\rho v_s$ is the acoustic attenuation coefficient
- α : optical absorption coefficient for the ω_1 beam
- γ : a constant that relates the change in optical dielectric constant to the electrostrictive strain
- ρ : mass density and
- v_s : free propagation velocity of acoustic waves in the medium.

We see that g increases with the acoustic frequency $\omega_s = k_s v_s$. The propagation vector \vec{k}_s is determined by

$$\vec{k}_s = \vec{k}_2 - \vec{k}_1. \quad (5.36)$$

Since $\omega_s \ll \omega_2$ ($\omega_s \sim 10^9$ Hz) we have $\omega_2 \approx \omega_1$ and in isotropic media $k_2 \approx k_1$. The above vector relationship thus becomes identical to that for Bragg scattering (Fig.5.5). It follows that

$$k_s = 2k_2 \sin\theta \quad (5.37)$$

so that maximum gain is obtained for the case of backward scattering, $\theta = \pi/2$ where $k_s = 2k_2$ and the resulting forward acoustic wave has a frequency

$$(\omega_s)_{\max} = 2\omega_2 \frac{v_s n_2}{c}. \quad (5.38)$$

When g is positive the ω_s and ω_1 fields are simultaneously amplified along their respective directions. The condition $g \geq 0$ for stimulated scattering occurs when

$$|E_z|^2 \geq \frac{16T\varepsilon_1\alpha_s\alpha}{\gamma^2 k_1 k_s} \quad (5.39)$$

(where $T = \rho V_s^2$ is the bulk modulus of the material) which sets the threshold condition for SBS.

An estimate for quartz shows that the SBS threshold power is given by approximately 10^7 Watts/cm², which is easily available from a Q-switched laser. In most liquids the experimental thresholds are found to be even lower, due to self-focusing effects.

5.4 Optical phase conjugation by stimulated scattering (OPC-SS)

In the very first experiments on stimulated scattering itself it was observed that the scattered beams were highly directional. The problem of relating the complicated structure of the incident wavefront to that of the scattered wavefront was raised for the first time by Zeldovich et.al. [3], who realized that under certain circumstances the scattered wave can be nearly phase-conjugate to the incident wave. (In Russian literature optical phase conjugation is referred to as wavefront reversal). It is a surprising fact that even though the Stokes wave develops from spontaneous noise photons, the amplified SS wave assumes the transverse structure which is, to a high accuracy, phase conjugated with respect to the structure of the pump wave, ie,

$$E_s(\vec{r}) \propto E_L^*(\vec{r}) \quad (5.40)$$

Two properties of SS underlie the physical mechanism of OPC-SS; the very high total gain of the Stokes wave, $\exp(gz) \approx \exp(30)$, and the high spatial nonuniformity of the local Stokes gain $g(R) = G |E_L(R)|^2$ caused by spatial inhomogeneities of the pump intensity $|E_L(R)|^2$ in the scattering volume [4]. Exciting radiation having an irregular divergence θ_0 has a speckle structure, with a characteristic transverse dimension of the inhomogeneities of the order of $\Delta r \approx k\theta_0^{-1}$ and a characteristic length $\Delta z \approx (k\theta_0^2)^{-1}$, where the radiation diffracts from one inhomogeneity to the other (Fig.5.6). Under the conditions necessary for OPC, these dimensions must be much smaller

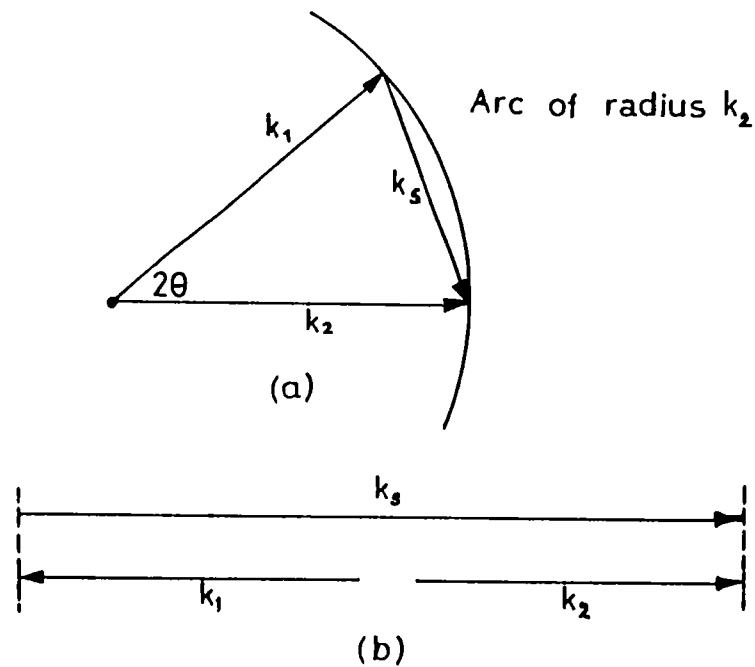


Fig.5.5 : The vector relationship $\vec{k}_2 - \vec{k}_1 = \vec{k}_s$ for stimulated Brillouin scattering in an isotropic medium ($k_2 \cong k_1$), (a) for an arbitrary angle θ , (b) for backward scattering ($\theta = \pi/2$).

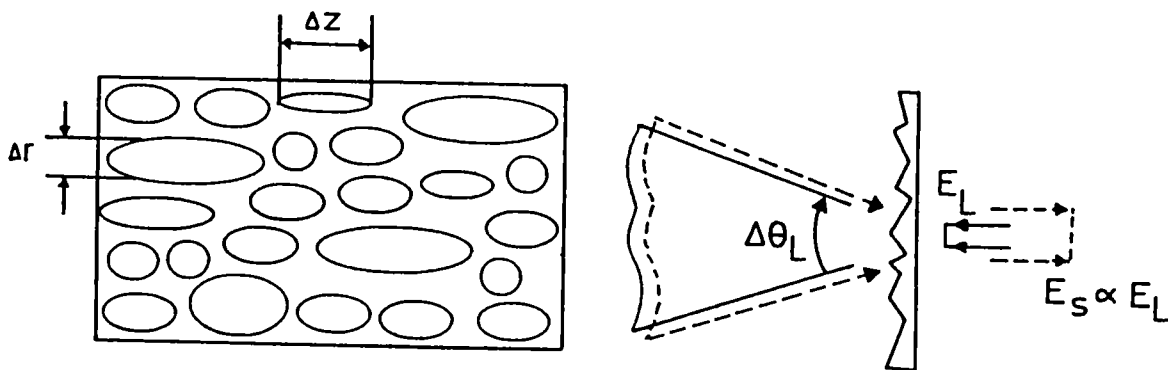


Fig.5.6 : A scheme for OPC by stimulated scattering (OPC-SS). The dimensions of small-structure inhomogeneities in the pump intensity $|E_L(R, z)|^2$ are determined by the angular divergence $\Delta\theta_L$, where $\Delta r \sim \lambda/(\Delta\theta_L)$ and $\Delta z \sim \lambda/(\Delta\theta_L)^2$. A large number of inhomogeneities are present within the interaction volume. The scattered wave E_S is excited at the far (left) end of the cell by spontaneous noise and acquires, in the process of an exponential gain, the structure which is phase conjugate to the pump $E_L(R)$.

than those of the interaction region. The effective gain for a given configuration of the scattered field $E_S(\vec{r}, z)$ is determined in every section $z = \text{constant}$ in the pump field $E_L(\vec{r}, z)$ by the intensity overlap integral

$$g_{\text{eff}} = \frac{G \int |E_L(r, z)|^2 |E_S(r, z)|^2 d^2r}{\int |E_S(r, z)|^2 d^2r} \quad (5.41)$$

so that a maximum of gain is observed for a wave $E_S(\vec{r})$ whose local maxima coincide with the maxima of the wave $E_L(\vec{r})$ everywhere in space. While propagating, each of the fields $E_L(\vec{r}, z)$ and $E_S(\vec{r}, z)$ varies its transverse structure due to diffraction and interference. If such variations are large enough, then the only possibility of keeping the intensity inhomogeneities co-ordinated throughout the whole interaction volume in case of counterpropagation consists in requiring the scattered field $E_S(\vec{r}, z) \exp(ikz)$ to be phase-conjugated with respect to the exciting field $E_L(\vec{r}, z) \exp(-ikz)$, ie, $E_S(\vec{r}, z) \propto E_L^*(\vec{r}, z)$. As a result it is the Stokes wave conjugated with respect to the pump wave that, under conditions of very high total gain, is primarily amplified and represented in the scattered radiation with an overwhelming weight. The remaining unconjugated waves are discriminated against owing to a lower gain. Thus, the physical mechanism of OPC-SS is based on amplification discrimination against the non-conjugated configurations of the backward scattered wave in the field of an inhomogeneous pump wave. It is observed that the quality of OPC-SS is high when the pump field has a developed speckle structure in the interaction volume, and to obtain good quality OPC of a weakly distorted beam (with a divergence close to the diffraction limit) at a power near the SS threshold, the focusing of the beam should be such that the waist is located completely inside the medium.

From the foregoing discussion it is obvious that backward SBS is the most suitable process for OPC-SS, considering the fairly high constant $G \sim 10^{-1} - 10^{-2}$ cm/MW, and the small frequency shift $\Omega_0 \leq 1 - 10^{-2}$ cm⁻¹. However, OPC has been studied to various extents by stimulated Raman scattering [5-8], stimulated Rayleigh wing scattering [5], stimulated temperature scattering [9] and superluminescence [10]. Even though SRS and superluminescence are characterized by a

relatively large frequency shift of the amplified radiation, several workers have shown that OPC-SS is still possible by these techniques.

5.5 Anomalous experimental results in SRS

Theoretical considerations of the preceding sections predict one set of equally spaced Raman lines $\nu_L - n\nu_{ba}$ in a typical SRS experiment, corresponding to the Raman transition with the lowest threshold and its possible higher order lines. These lines would be narrower than the spontaneous linewidth due to the much higher Raman gain and feedback. The stokes gain per unit length should be the same in all directions provided the stokes field is polarized parallel to the laser field. However, actual experimental results show significant deviations from these theoretical predictions [1,11]. In addition to various Stokes lines, bright cones of anti-stokes light also have been observed at frequencies $\nu_L + n\nu_{ba}$. The stokes and anti-stokes components often show a remarkable frequency broadening many times larger than the width of spontaneously emitted lines. The experimentally observed gain of stokes radiation in forward and backward directions is often much larger than the theoretical values, and the forward-backward ratio is not unity. Further, off-axis Raman oscillations are extremely difficult to obtain. These anomalies observed in various SRS experiments emphasize the role of other nonlinear optical processes which are, in most cases, intertwined inextricably with stimulated Raman scattering. Most of the anomalous properties of SRS have been found to be intimately connected to self-focusing of the pump laser beam in the nonlinear medium [1,2,12,13].

For ordinary Q-switched intensity in a non-absorbing medium we may write for the index of refraction [12]

$$n = n_0 + n_2 |E_L|^2 \quad (5.42)$$

where the second term on the RHS is the intensity-dependent part of the refractive index, related to the nonlinear susceptibility through

$$n_2 = (n_{2\alpha} + n_{2\rho} + n_{2e}) = 2\pi n_0^{-1} \chi'_{1111} \quad (5.43)$$

and the terms $n_{2\alpha}$, $n_{2\rho}$ and n_{2e} signify the contributions from Kerr effect, electrostriction and nonlinear electronic polarizability respectively. For most liquids these are given by the values

$$\begin{aligned} n_{2\alpha} &\approx 10^{-13} - 10^{-11} \text{ esu} \\ n_{2\rho} &\approx 10^{-11} \text{ esu} \\ n_{2e} &\approx 10^{-15} - 10^{-14} \text{ esu} \end{aligned}$$

and obviously, n_{2e} is negligible as compared to $n_{2\alpha}$ and $n_{2\rho}$. However Kerr effect, rather than electrostriction, is believed to give the dominant contribution to n_2 in liquids. This is because the Kerr effect, arising from molecular reorientation and redistribution, responds instantaneously to the Q-switched pulse but the electrostrictive effect which involves mass transfer to a region of high beam intensity, cannot follow the rapid intensity variation of the pulse.

Now if we consider a laser beam of finite radius a with the intensity profile resembling a gaussian distribution

$$I = I_{\max} \exp(-r^2/2a^2) \quad (5.44)$$

then this profile also describes the variation of the index of refraction in the medium according to Eqn.5.42. The index of refraction is highest on the beam axis. Consider a light ray initially parallel to the axis which moves in a medium with a transverse gradient of the index,

$$\frac{\partial n}{\partial r} = n_2 \frac{\partial |E_L|^2}{\partial r} \quad (5.45)$$

This ray will be refracted toward the axis, since the laser beam has produced its own lens like medium. As the beam focuses more the transverse gradient becomes larger, and hence the onset of the light concentration (self focusing) here is more sudden than the focusing of a lens. A limiting case of self focusing action occurs for a critical total power flux in the beam given by [1]

$$P_{cr} = 5.763 \lambda_c^2 / 16\pi^2 n_2 \quad (5.46)$$

where the focusing is just compensated by the natural defocusing due to diffraction. In this case the light is trapped (self trapping) in a filament, creating its own waveguide. The filamentary structure is often quite complicated and usually light is trapped in several different filaments with diameters ranging from a few microns to about 80 microns, and lengths of several cms. The light intensity in the filaments can be orders of magnitude higher than the nominal intensity of the incident laser beam, providing anomalously high gain and leading to the onset of all kinds of nonlinear processes simultaneously with SRS. A small change in the geometry and structure of the pump beam can sensitively affect the self trapping pattern, thereby influencing the SRS characteristics considerably.

The anisotropic polarizability of the molecules of several media is found to be a major cause for the frequency broadening of laser light as well as various orders of Stokes and Antistokes radiation. It can be shown that if a second light wave of frequency ω'_L , close to the laser frequency ω_L is present in the medium, the modulation of the index of refraction may cause a whole series of side bands or combination frequencies to appear, thereby broadening the Stokes line [1,13]. The ω'_L beam may be generated by stimulated Rayleigh scattering, or stimulated Brillouin scattering itself. In fluids like CS_2 , benzene and many of its derivatives, where the molecules have a large anisotropic polarizability and nonlinear index n_2 , one can expect forward-backward asymmetry in SRS, broadening of the SRS lines, anomalous high gain etc.

5.6 Experimental

As we have seen, backward stimulated scattering in certain organic solvents (eg. CS_2) has been closely associated with phase conjugation. Since phase conjugation can be utilized to correct wavefront distortions in an optical beam propagating through aberrating media this technique has attracted considerable attention from an application point of view. The OPC property of SS can generate BSBS and BSRS of considerably larger intensities as compared to FSBS and FSRS respectively [14,15]. This forward-backward asymmetry can be

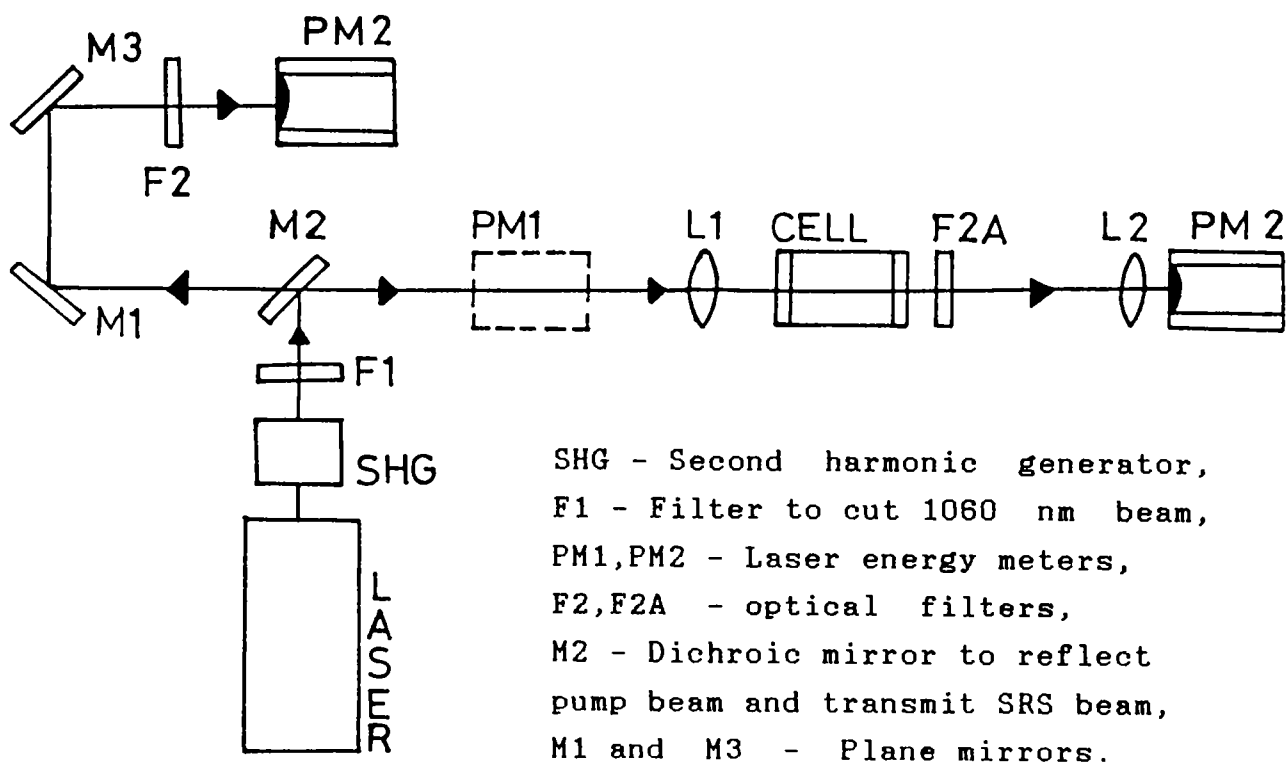


Fig.5.7 : The present experimental set up used for SRS studies.

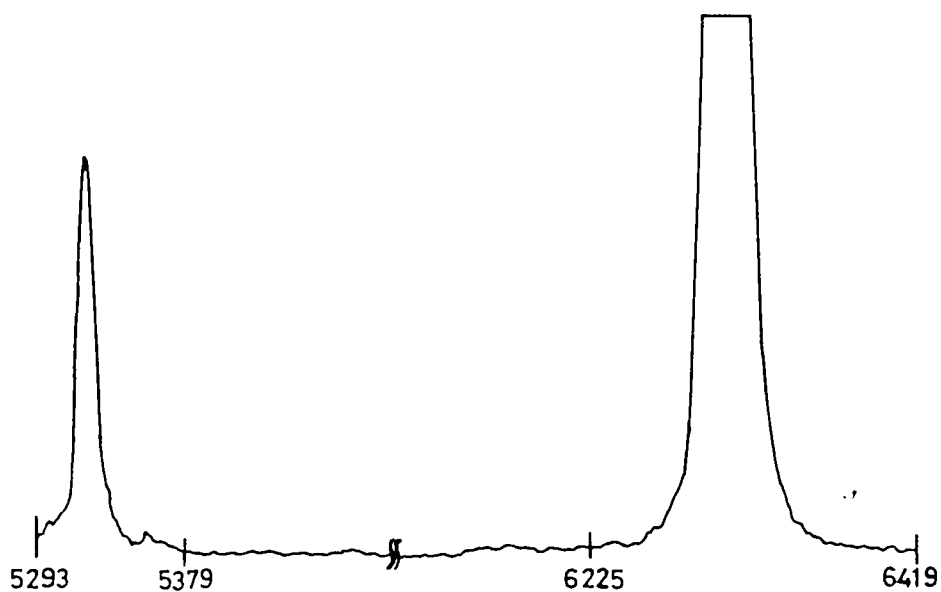


Fig.5.8 : Stimulated Raman spectrum obtained in acetone and dilute solutions of Rhodamine 6G. The smaller peak corresponds to the scattered laser radiation.

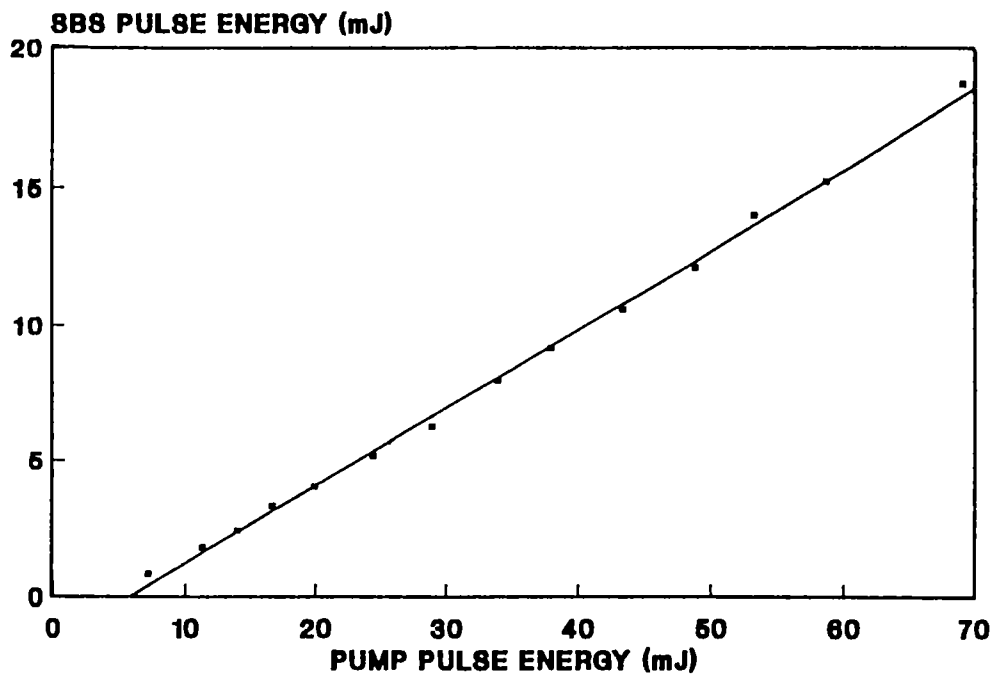


Fig.5.9 : Variation of the backward SBS energy with pump energy observed in acetone.

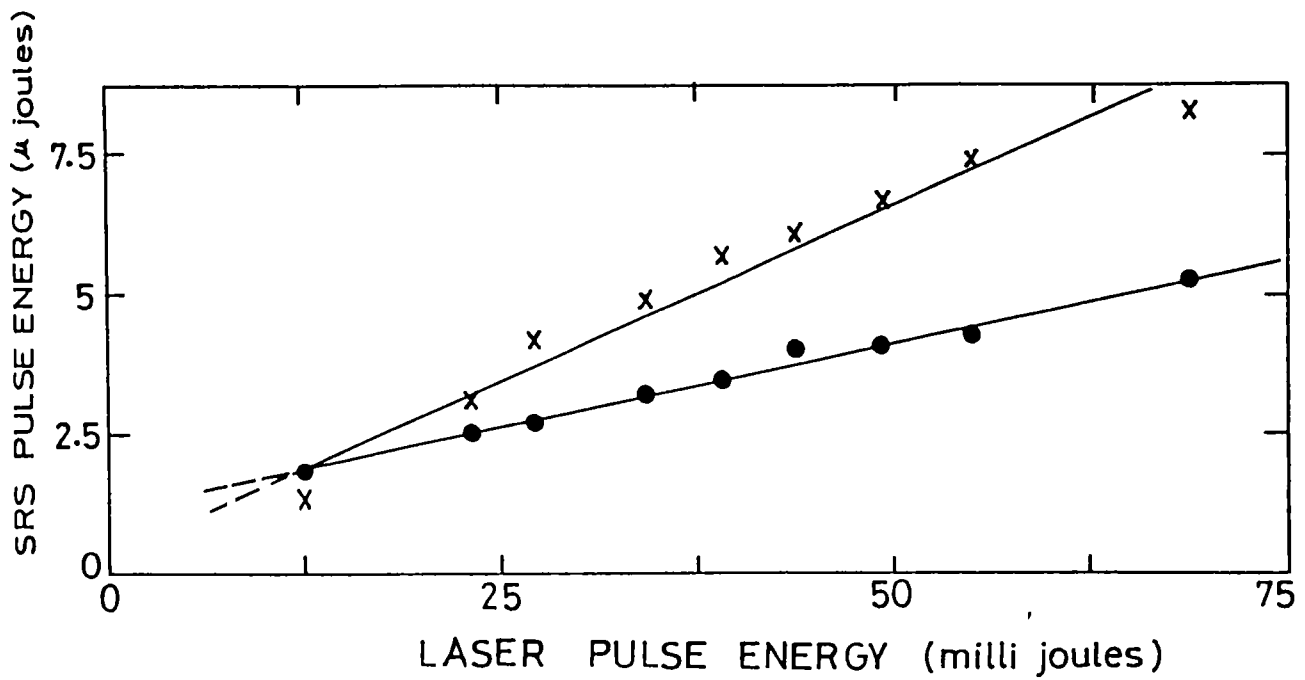


Fig.5.10 : Energy of SRS beam in forward and backward directions, as a function of the pump energy

X - BSRS, O - FSRS

Denariez [16] a linear variation of SRS is found in our case also in the range of power levels used (< 7 MW). However, almost from the threshold level itself BSRS begins to grow in intensity in comparison with FSRS. According to Shen and Bloembergen [17] the gains in the forward and backward directions are expected to be the same at low pump intensities, whereas actually with stronger pump beams a considerable enhancement in BSRS has been observed before, in different media [18,19]. Obviously, in addition to pump depletion, several nonlinear processes like self focusing, stimulated Brillouin scattering (SBS), phase conjugation etc. are contributing in various degrees to the observed forward-backward asymmetry. Even though the low Kerr coefficient of acetone indicates that self focusing may not occur, Shen and Shaham [12] have shown from their temperature dependence studies that SBS in the near-forward direction can lead to self focusing phenomenon in liquids like acetone. The contribution of SBS to self focusing is thus indeed non-negligible in liquids with relatively small Kerr constants. It is worth noting that in acetone phase conjugation by SBS has been already reported [20]. Apart from a qualitative description, an estimation of the relative importance of these and other processes taking place in the medium is quite complicated even though their collective effect is manifested as a significant enhancement in BSRS intensity in the whole range of power levels used here. However, the fact still remains that since in acetone the stimulated Raman cross section is quite high the primary mechanism leading to an enhancement of BSRS is phase conjugation by SRS itself.

SRS from dilute solutions of R6G in acetone shows interesting characteristics. Following Kaiser and Maier [21], we can write the spatial dependence of pump (I_1), FSRS (I_s^f) and BSRS (I_s^b) as

$$\frac{dI_1}{dz} = -g_1 [I_1(I_s^f + I_s^b) + \alpha] \quad (5.47)$$

$$\frac{dI_s^f}{dz} = g_s I_s^f I_1 \quad (5.48)$$

and

$$\frac{dI_s^b}{dz} = g_s I_s^b I_1 \quad (5.49)$$

where g = gain factor, α = linear optical absorption coefficient for the pump wavelength λ_1 and $z' = -z$. For acetone α is negligibly small when excited with 532 nm ($\approx 10^{-4} \text{ cm}^{-1}$) as compared to the dilute dye solution, where $\alpha \approx 10 \text{ cm}^{-1}$, resulting in nondirectional fluorescence emission centred around 570 nm. (Absorption losses of I_s^f and I_s^b are neglected since the Raman emission lies far away from the absorption band of R6G). Hence, in the presence of R6G the depletion in pump energy along the beam axis in the medium should result in a reduced SRS emission in comparison with that of pure acetone, thereby shifting the threshold at which the BSRS/FSRS ratio equals unity towards a corresponding higher value of the pump pulse energy. Our experimental observation of an obvious increase in this threshold value with dye concentration (Fig.5.11) confirms this assumption. The threshold energy shifts from 25 mJ/pulse at 2.9×10^{-8} moles/lt to 87.6 mJ/pulse at 3.9×10^{-6} moles/lt. There is a net reduction in SRS intensity with concentration which is expected from dye fluorescence losses. The comparative reduction in BSRS intensity occurs due to the fact that phase conjugation of the pump beam becomes less prominent in an absorbing medium, thereby reducing its energy coupling to the BSRS beam. However the intensity of FSRS radiation increases with concentration (Fig.5.12a and 5.12b). If we take the sum of forward and backward intensities and compare it with that in acetone, we find that at low pump energies the total intensity (FSRS + BSRS) decreases with concentration while at higher laser energies it is almost the same as that in pure acetone (Fig.5.13). We note that R6G solution has a nonlinear absorption coefficient which depends on the pump intensity as

$$\alpha = \alpha_0 / (1+I') \quad (5.50)$$

where

$$I' = I_1/I_{\text{sat}} \quad (5.51)$$

and I_{sat} is the absorption saturation intensity with α_0 as the linear absorption coefficient. When $I_1 > I_{\text{sat}}$ we have $\alpha < \alpha_0$ and the transmission characteristics will become more similar to that of the solvent (acetone). Hence Eqn.5.47 can be modified to give

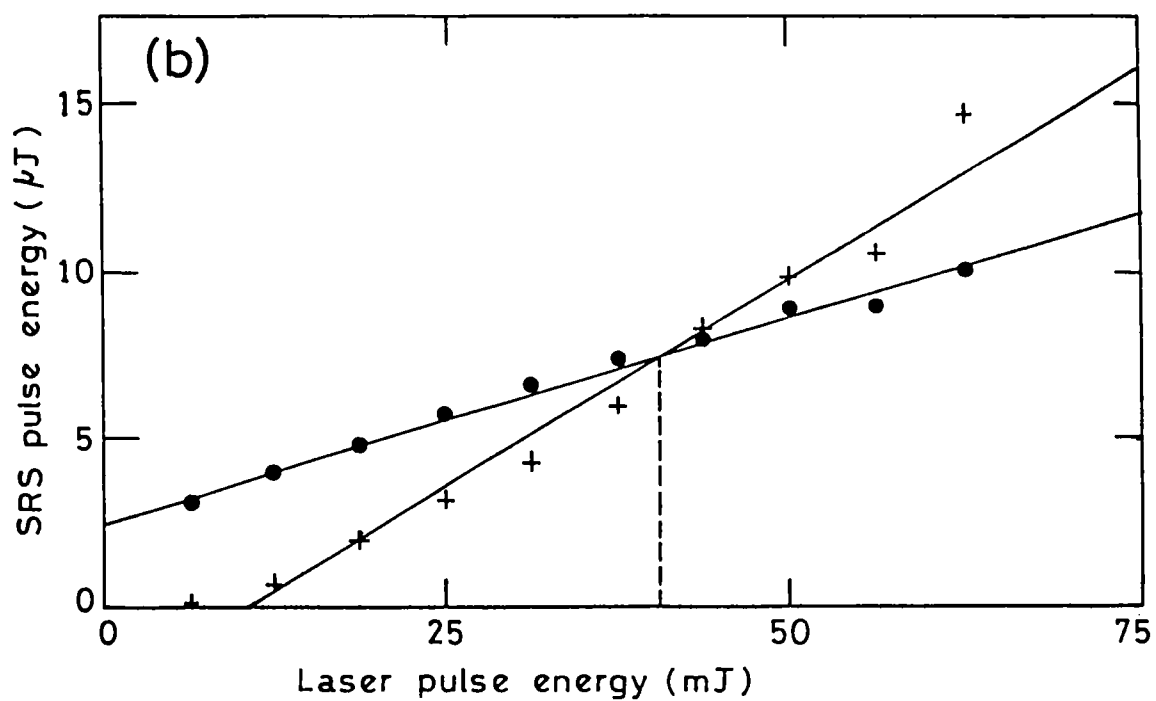
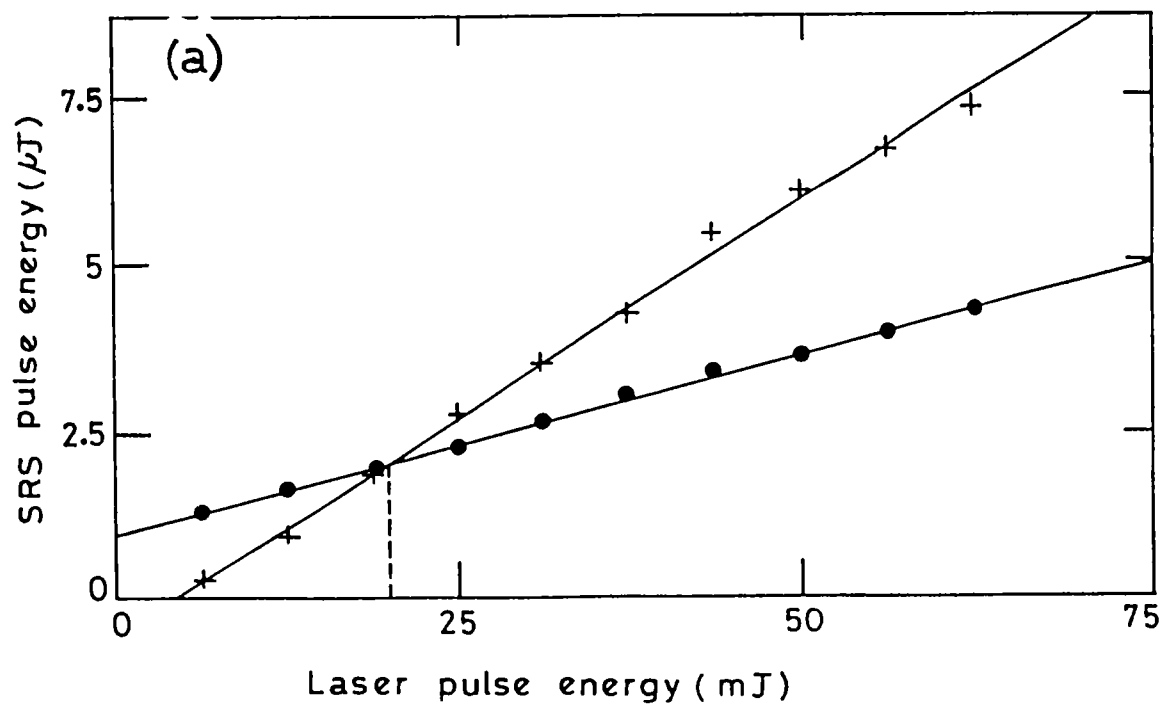


Fig.5.11 : Variation of the SRS pulse energy with pump laser pulse energy for a R6G solutions. (a) 2.9×10^{-8} moles/lt, (b) 4.3×10^{-7} moles/lt.

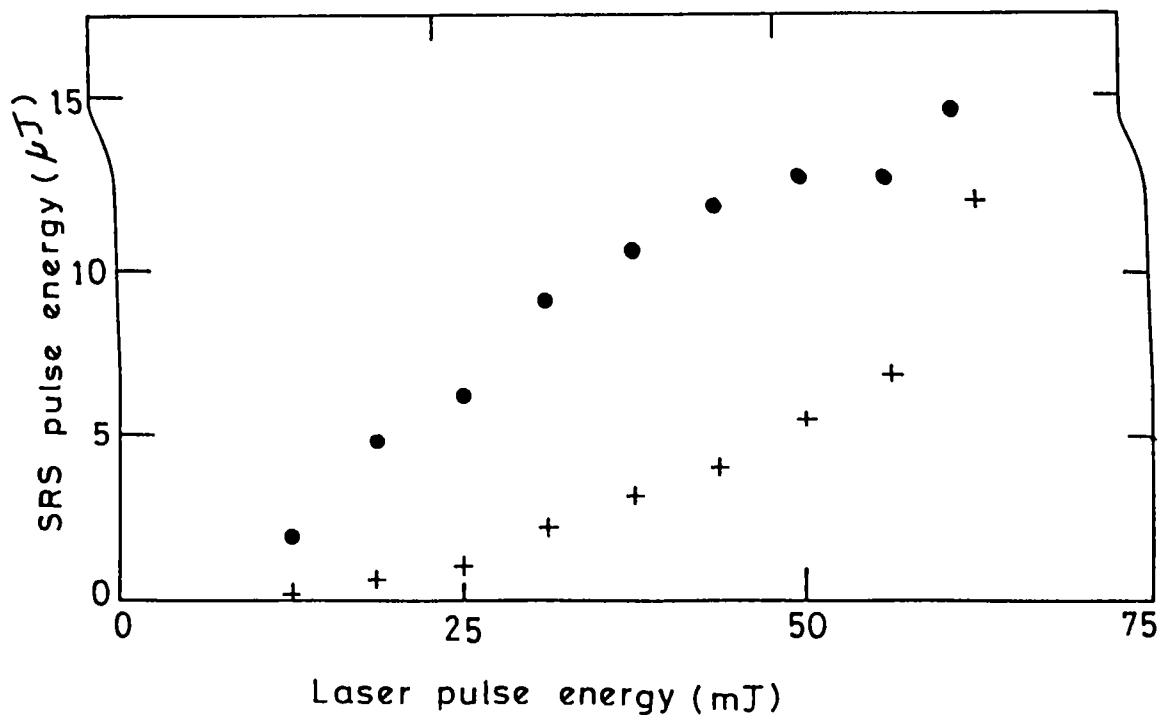


Fig.5.11c : Variation of the SRS pulse energy with pump laser pulse energy for a R6G solution of 3.9×10^{-6} moles/lt concentration.

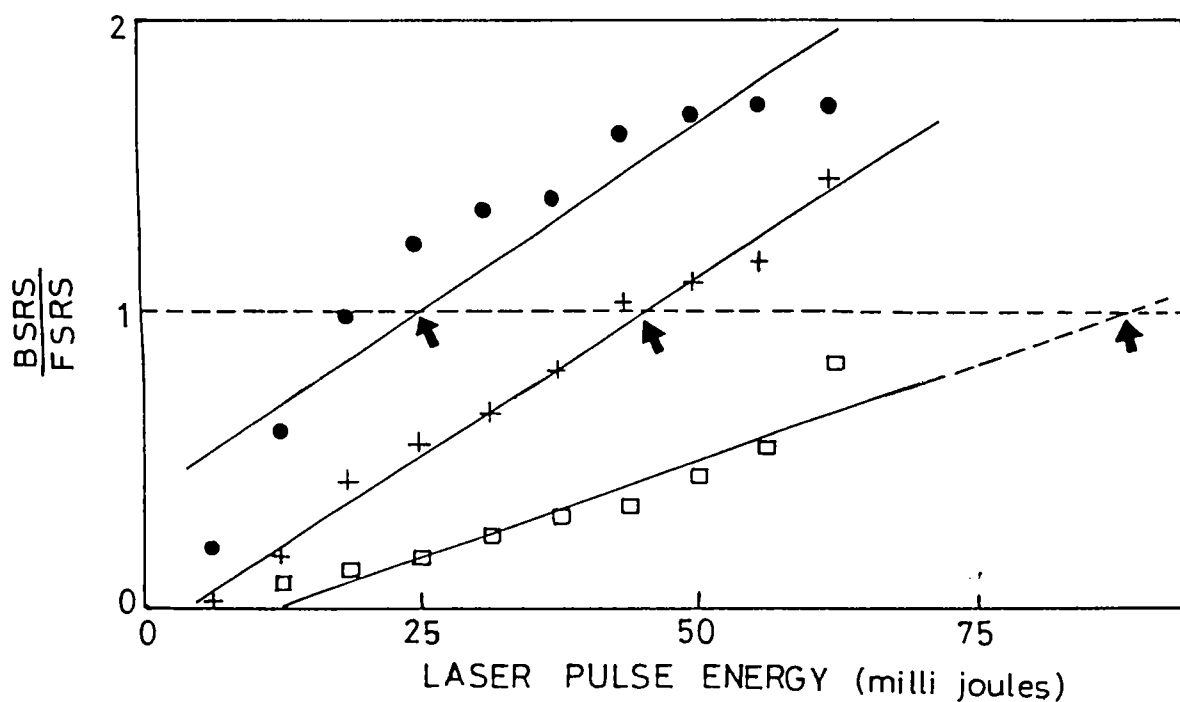


Fig.5.11d : Ratio of BSRS to FSRS in various concentrations, as a function of the pump energy. ● - 2.9×10^{-8} moles/lt, + - 4.3×10^{-7} moles/lt, □ - 3.9×10^{-6} moles/lt.

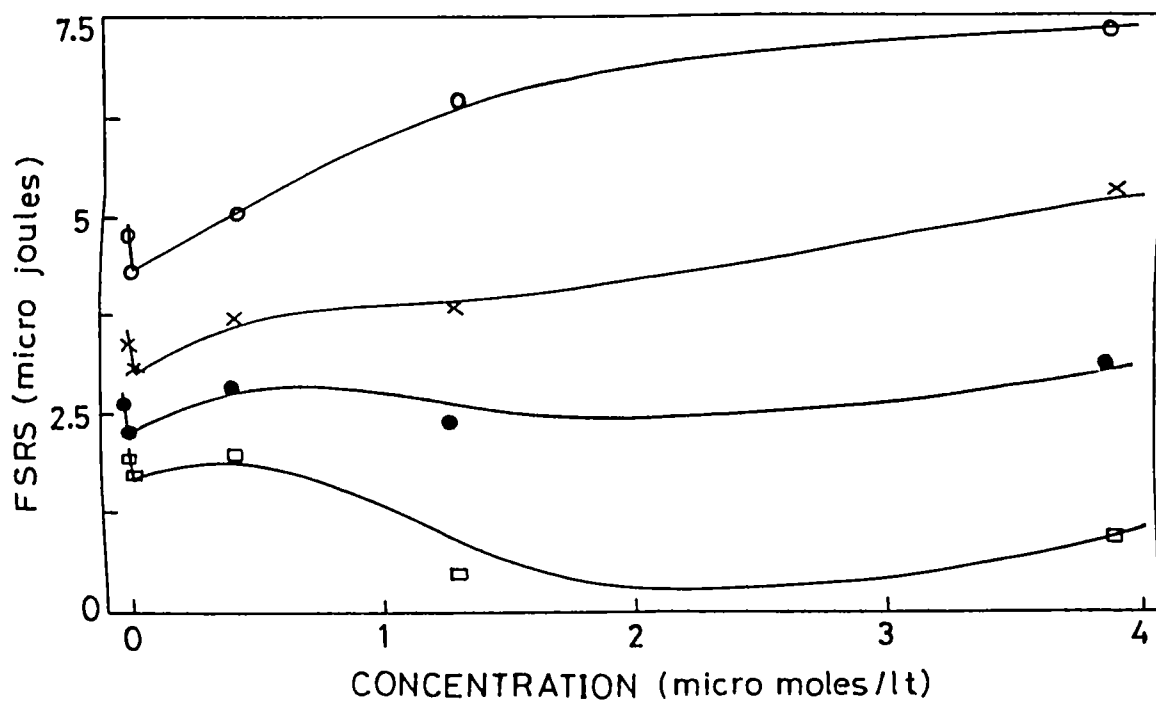


Fig.5.12a : FSRs intensity variation with Rhodamine 6G concentration, for various pump energies.

□ - 12.5 mJ, ● - 25 mJ, X - 37.5 mJ, ○ - 62.5 mJ

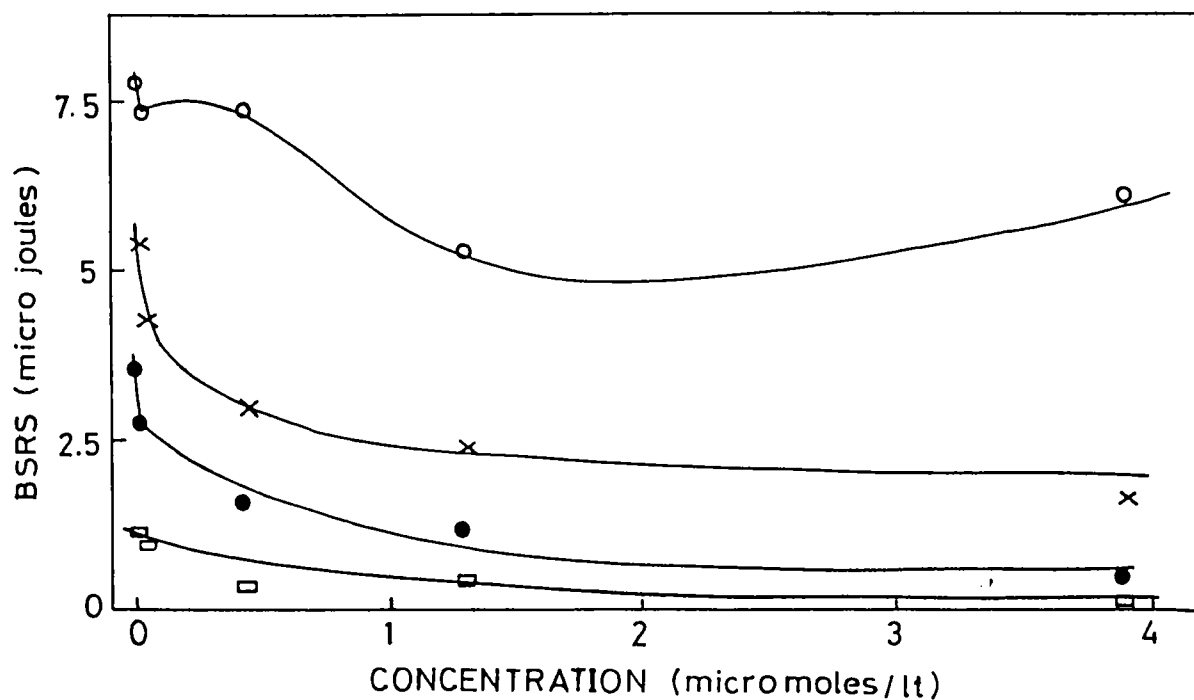


Fig.5.12b : BSRS intensity variation with Rhodamine 6G concentration, for various pump energies.

□ - 12.5 mJ, ● - 25 mJ, X - 37.5 mJ, ○ - 62.5 mJ.

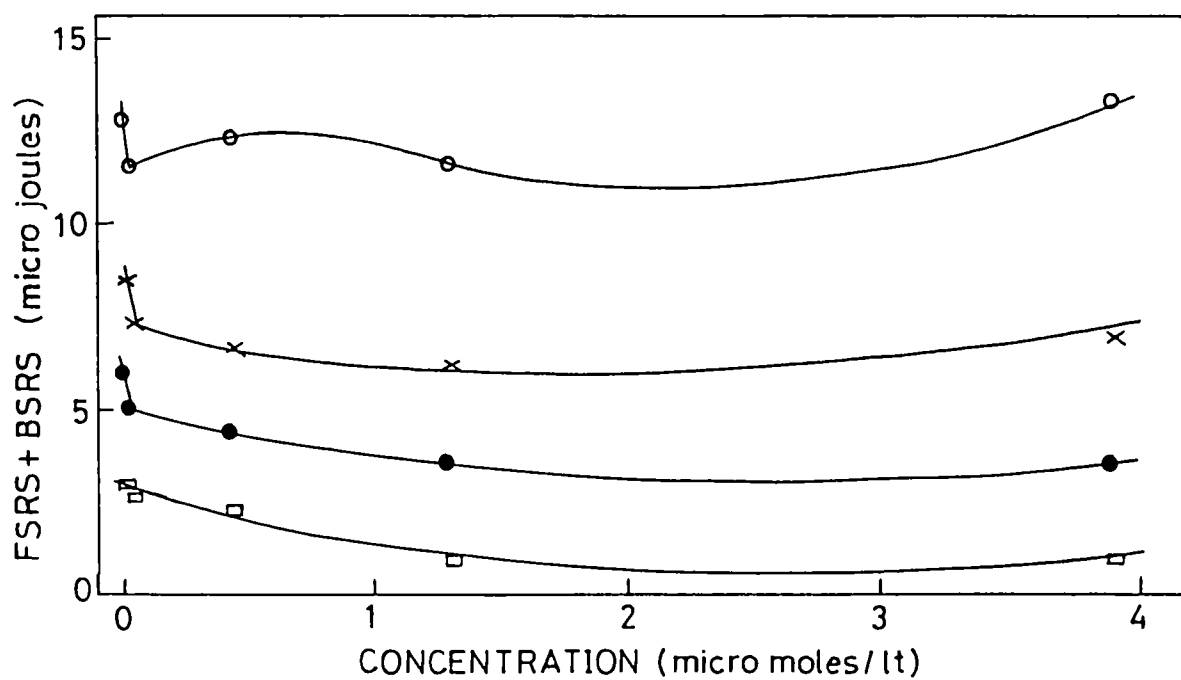


Fig.5.13 : Total SRS intensity variation with Rhodamine 6G concentration, for various pump energies.

□ - 12.5 mJ, ● - 25 mJ, X - 37.5 mJ, ○ - 62.5 mJ

$$\frac{dI_1}{dz} = -g_1 [I_1(I_S^f + I_S^b) + \frac{\alpha_0}{1+I'}] \quad (5.52)$$

At large I_1 , $I' \gg 1$ and $\alpha \ll \alpha_0$, resulting in a significantly reduced net absorption. This implies that at higher laser energy, the presence of the dye apparently does not affect the total scattered intensity from acetone, thereby maintaining the scattering efficiency to be almost the same as that of pure acetone. However, the anisotropy of scattered intensities in backward and forward directions is modified, which is obvious from the given figures.

It has been reported that optical pulse compression is possible in stimulated scattering [11,22,23]. Narrower pulses are attractive for two major reasons : (a) they have higher peak powers and (b) they are preferred for probing fast molecular dynamics in general. The results of our studies to observe pulse narrowing are shown in Figs.5.14a to 5.14c. By adjusting the laser pulsewidth (FWHM) to be approximately 30 ns, SRS and SBS have been generated in pure acetone. The pulse profiles have been scanned in time and recorded, by employing a scanning gate generator having a fast gate of 100 ps width, run at 3.33 ns/second resolution (Models SR 200 and SR 255, Stanford Research systems). Pulsewidths (FWHM) of 19 ns and 11 ns have been obtained for the SBS and SRS pulses respectively.

Recently there has been some interest in the application of optical feedback for the enhancement of stimulated radiation from scattering media [24]. If the feedback path is short then multiple passes are possible within the Raman cell during the laser pulse duration, thus increasing the SRS output. We have used an experimental set up given in Fig.5.15 for feedback enhancement studies in acetone. The curves shown in Fig.5.16a and 5.16b, for BSRS and FSRS respectively, show that there is a noticeable increase in the scattered radiation intensity. By reducing the feedback cavity length and using AR coated optical elements a much better performance can normally be expected.

5.8 Conclusions

The theory of stimulated Raman and Brillouin scattering is

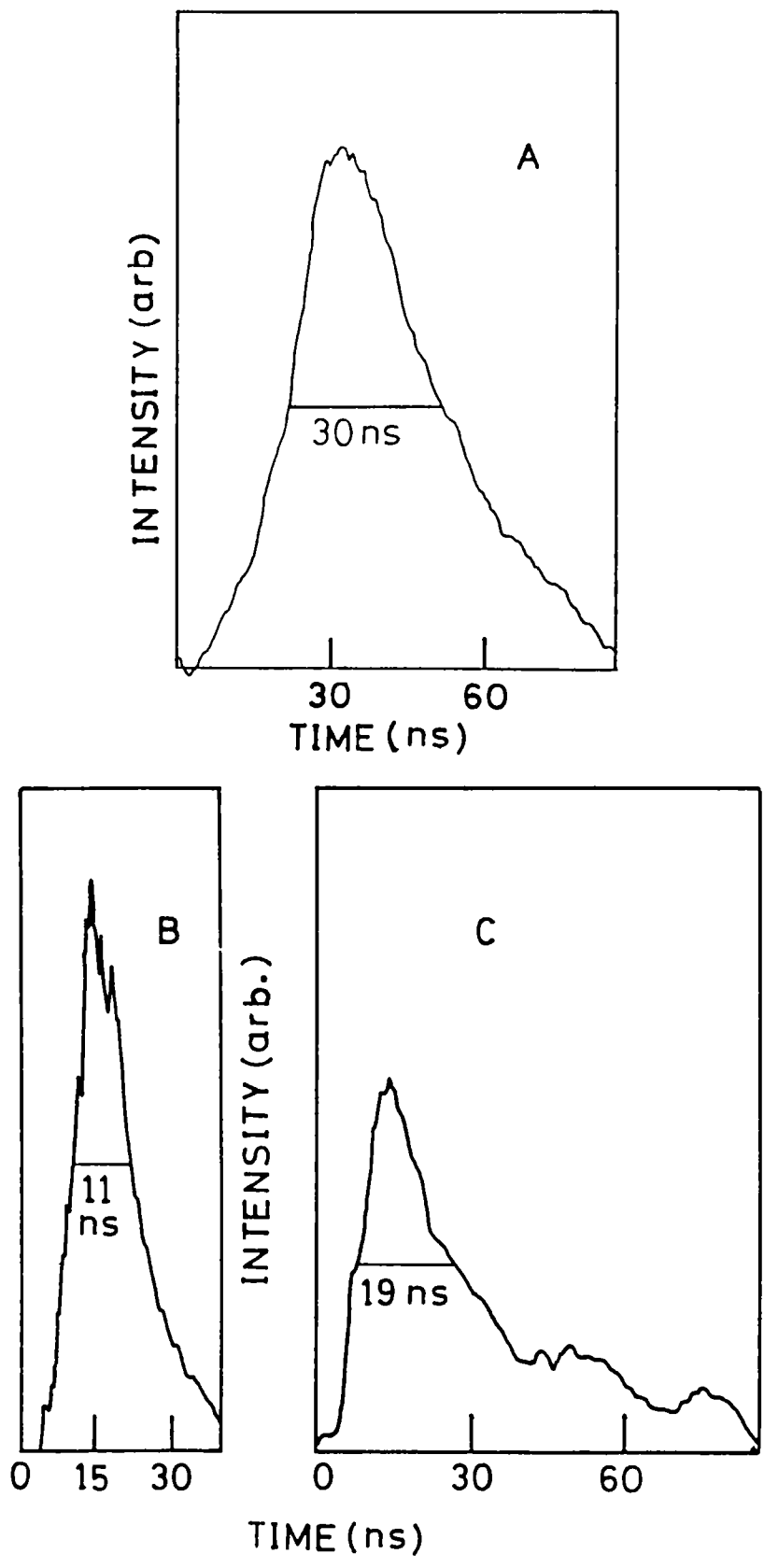


Fig.5.14 : (A) Temporal profile of the Nd:YAG laser pulse; FWHM \approx 30 ns. (B) Temporal profile of the SRS pulse; FWHM \approx 11 ns (C) Temporal profile of the SRS pulse; FWHM \approx 19 ns.

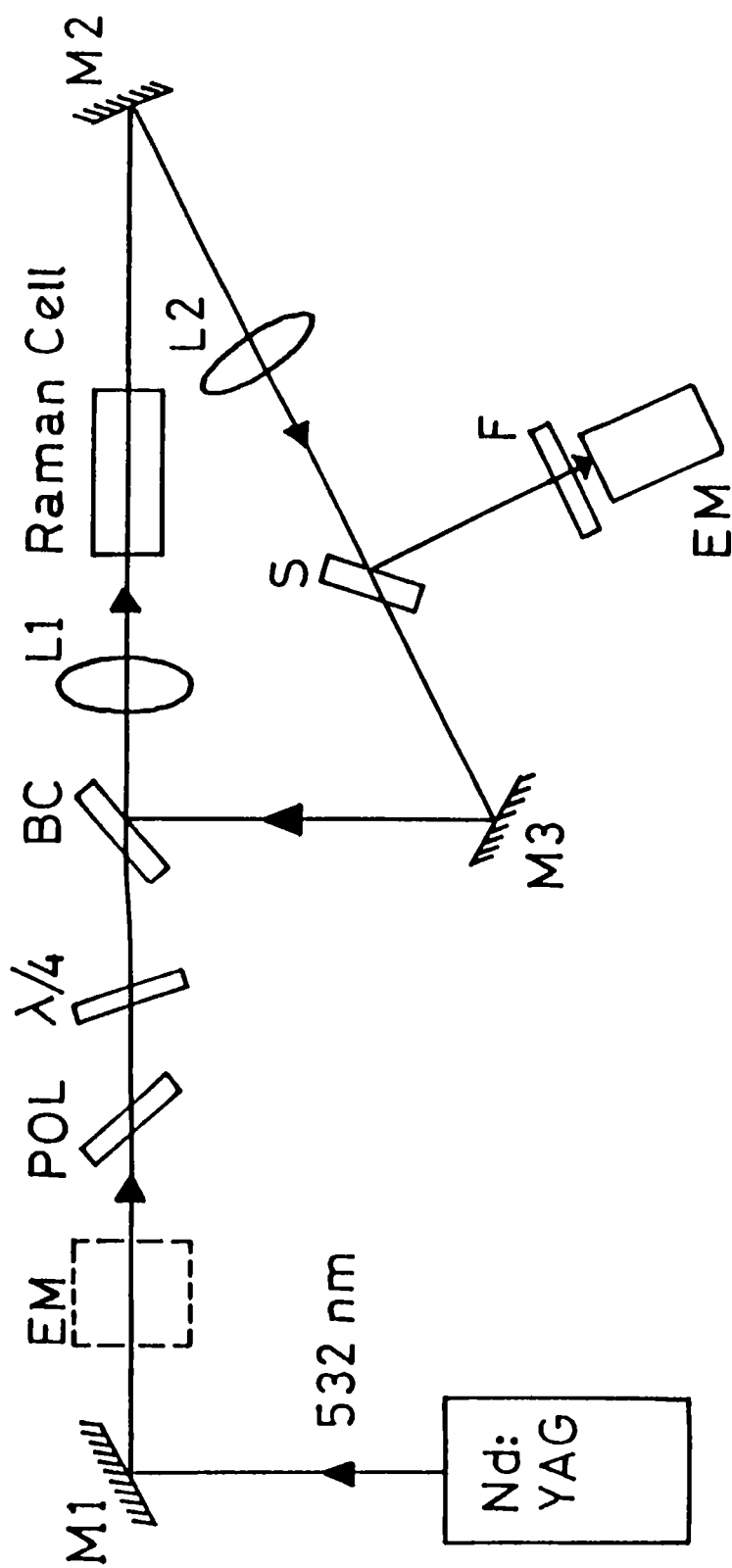


Fig.5.15 : Experimental set up for feedback enhancement of SRS from acetone.

EM : Energy meter, POL : Polarizer, $\lambda/4$: $\lambda/4$ plate, BC : Dichroic mirror, S : Glass slide, F : Band pass filter to cut the 532 nm radiation.

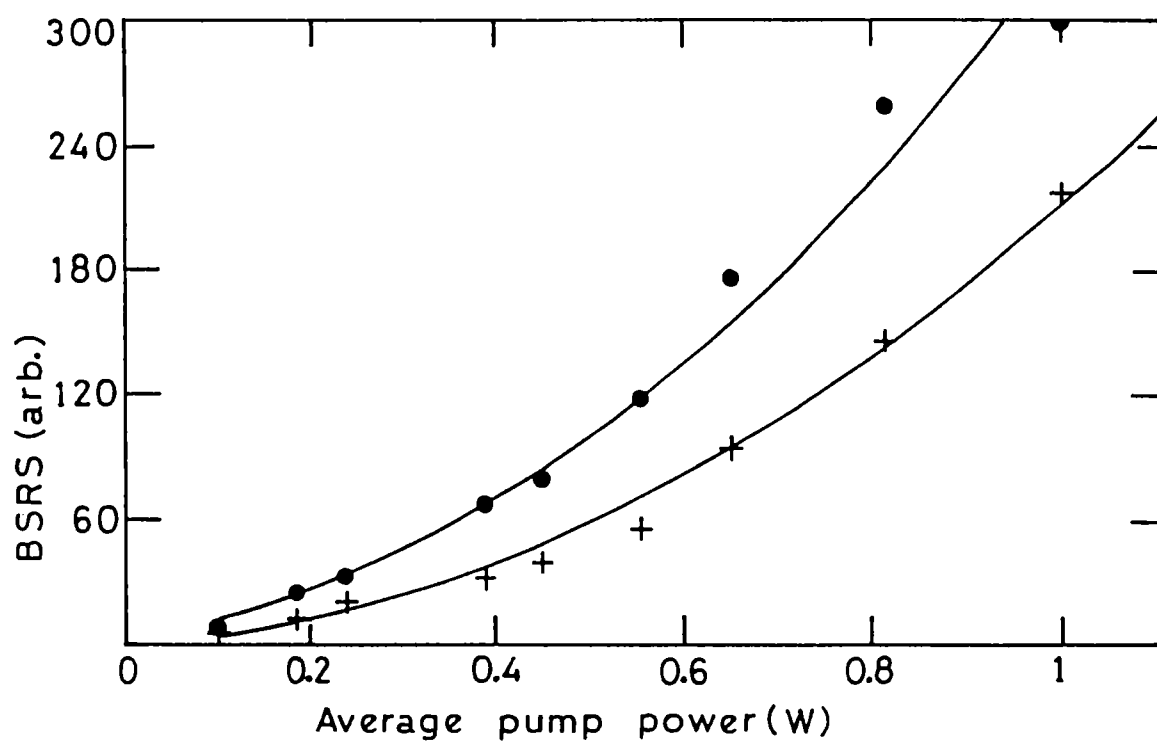


Fig.5.16a : Feedback enhancement observed in BSRs.

● - with feedback, + - without feedback.

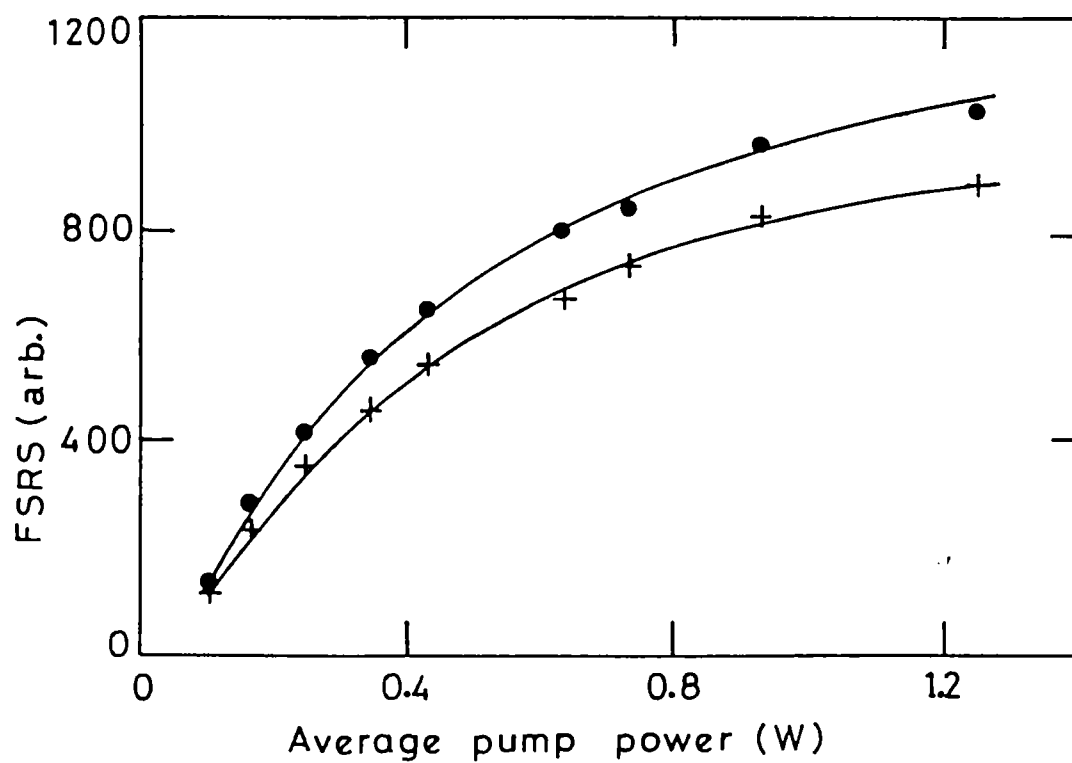


Fig.5.16b : Feedback enhancement observed in FSRS.

● - with feedback, + - without feedback.

briefly discussed. The addition of an absorbing impurity in small quantities to the Raman active medium is found to affect the forward-backward asymmetry of SRS. It is shown that because of absorption saturation at high pump pulse energies the scattering efficiency can be maintained the same, while modifying the asymmetry. Optical pulse narrowing and feedback enhancement in stimulated scattering have also been investigated.

CHAPTER 5 - REFERENCES

- [1] Bloembergen N, Am.J.Phys., 35, 989 (1967)
- [2] Yariv A, "Quantum Electronics", John Wiley & Sons (1989)
- [3] Zel'dovich B Ya, V I Popovichev, V V Ragulsky and F S Faizullov, JETP Lett. 15, 109 (1972)
- [4] Zel'dovich B Ya, N F Pilipetsky and V V Shkunov, "Principles of phase conjugation", Springer-Verlag (1985)
- [5] Kudriavtseva A D, A I Sokolovskaya, J Gazengel, N P Xuan and G Rivoire, Opt.Comm. 26, 446 (1978)
- [6] Sokolovskaya A I, G L Brekhovskikh and A D Kudriavtseva, Sov.Phys.Dokl. 22, 156 (1977)
- [7] Sokolovskaya A I and G L Brekhovskikh, Dokl.Akad.Nauk. SSR 243, 630 (1978)
- [8] Zel'dovich B Ya and V V Shkunov, Sov.J.Quantum Electron, 7, 610 (1978)
- [9] Krivoschchekov G V, S G Struts and M F Stupak, Sov.Tech.phys.Lett., 6, 184 (1980)
- [10] Koptev V G, A M Lazaruk, I P Petrovich and A S Rubanov, JETP Lett., 28, 434 (1979)
- [11] Fisher R A (ed), "Optical phase conjugation", Academic press (1983)
- [12] Shen Y R and Y J Shaham, Phys.Rev., 163, 224 (1967)
- [13] Bloembergen N and P P Lallemand, Phys.Rev.Lett., 16, 81 (1966)
- [14] Brekhovskikh G L, A D Kudriavtseva and A I Sokolovskaya, Sov.J.Quantum.Electron., 8, 1028 (1978)
- [15] Hellwarth R W, in "phase conjugation by stimulated backscattering", in "Optical Phase Conjugation", (ed) Robert A Fisher, Academic press, New York (1983)
- [16] Bret G and M Denariez, Appl.phys.Lett., 8, 151 (1966)
- [17] Shen Y R and N Bloembergen, Phys.Rev., 137, A1786 (1965)
- [18] Maier M, W Kaiser and J A Giordamine, Phys.Rev.Lett., 17, 1275 (1966)
- [19] Maier M, W Kaiser and J A Giordamine, Phys.Rev., 177, 580 (1969)
- [20] Balkevicius P I, A Dement'ev, J P Lukosius, E K Maldutis and V P Tarulis, Bitovskii Fizicheskii Sbornik, 24, 81 (1984)
- [21] Kaiser W and M Maier in "Stimulated Rayleigh, Brillouin and Raman spectroscopy", in "Laser Handbook", vol.2 (ed.) F T Arecchi, North Holland, Amsterdam (1972)

- [22] Bourne O L, A J Alcock and Y S Huo, Rev.Sci.Instrum. **56**, 1736 (1985)
- [23] Ghosh Roy D N and D V G L N Rao, J.Appl.phys., **59**, 332 (1985)
- [24] Wong G K N and M J Damzen, IEEE J.Quantum Electronics, **26**, 139 (1990)

CHAPTER - 6

GENERATION OF BROADBAND LASER PULSES FROM DYES

6.1 Evolution of the dye laser

Even though dye lasers entered the scene at a time when several hundreds of laser active materials were known, they were not just another addition to the already existing long list of lasers. First of all they provided wavelength tunability of monochromatic radiation over wide ranges of wavelengths. Dye lasers are attractive in several other respects: dyes can be used in solid, liquid or gas phases and their concentration (and hence their absorption and gain) can be readily controlled. Liquid solutions of dyes are especially convenient: the active medium can be obtained in high optical quality and cooling is simply achieved by a flow system, as in gas lasers. Optically induced damages in a liquid are self-repairing, and output powers of magnitudes comparable to solid state lasers are available from dye lasers. Finally, the cost of the active medium, the organic dye, is negligibly small as compared to that of solid state lasers.

There had been early speculations about the possible use of organic compounds as laser materials [1,2]. It was proposed to make use of the vibronic levels of electronically excited organic molecules as the active medium [3]. The first experimental study that might have led to the realization of an organic laser was by Stockman et al [4] and Stockman [5]. Using a high power flashlamp to excite a solution of Perylene in benzene between two resonator mirrors, Stockman found an indication of a small net optical gain in his system. Unfortunately the aromatic molecule perylene has high losses due to triplet-triplet absorption and excited singlet state absorption, resulting in very small gains. In 1966 Sorokin and Lankard at IBM's Thomas J Watson research centre obtained stimulated emission from an organic compound, chloro-aluminum-phthalocyanine for the first time [6]. In fact they had set out to observe the resonance Raman effect in this dye excited by a giant pulse ruby laser. Instead of sharp Raman lines, they found a weak diffuse band at 755.5 nm, the peak of one of the fluorescence bands. They immediately suspected this might be a sign of incipient

laser action and indeed, when the dye cell was incorporated into a resonator, a powerful laser beam at 755.5 nm emerged. The tunability of dye laser emission was first observed by Schäfer et al [7] by a change in dye concentration or resonator mirror reflectivity. They fabricated a simple dye laser system employing the dye 3,3'-diethyltricarbocyanine, the output wavelength of which could be tuned over more than 60 nm by varying one or both of the above parameters. Subsequently various laboratories became active in dye laser research, and laser action in various dyes, spanning a broad spectral range were reported [8-14].

The next important step was the substitution of one of the resonator mirrors by a diffraction grating for introducing wavelength dependent feedback [15]. These authors obtained effective spectral narrowing from 6 to 0.06 nm and a continuous tuning range of 45 nm. Since then many different schemes have been developed for tuning the dye laser wavelength [16-20]. Flashlamp pumped dye lasers also appeared around this time [11].

Initially it was believed that cw operation of the dye laser was not feasible due to the losses associated with the accumulation of dye molecules in the metastable triplet state. However, Snavely and Schäfer [21] showed that triplet quenching by oxygen decreased the steady state population of the triplet state, far enough to permit cw operation for Rhodamine 6G in methanol. Later, unsaturated hydrocarbons also were used as triplet quenchers [22-24]. Peterson et al [25] at Eastman Kodak research laboratory used a cw argon ion laser to pump a solution of Rhodamine 6G in water with some detergent added. Water as solvent has the advantage of high heat capacity, thus reducing temperature gradients which are further reduced by the high velocity of the flow of dye solution through the focal region. The detergent acts both as a triplet quencher and prevents the formation of non-fluorescing dimers of dye molecules, which produce a high absorption loss in pure water solutions.

Efforts to produce ultrashort laser pulses from dyes also were initiated around 1968. It is the very large gain bandwidth of dye lasers that makes them attractive candidates for ultrashort pulse

generation. First attempts to produce ultrashort pulses with dye lasers involved pumping a dye solution with a mode-locked pulse train from a solid state laser, with the dye cuvette placed in a resonator with a round trip time exactly equal to, or a simple submultiple of, the spacing of the pump pulses [26-28]. The superradiant travelling wave emission from a wedged dye cuvette also was employed eliminating the resonator [29]. The pulsewidths obtained were generally in the range of 10-30 ps. By self mode-locking of a flashlamp pumped dye laser, a pulsewidth of 2 ps was obtained [30]. Ruddock and Bradley [31] introduced the colliding pulse mode-locked laser with a pulse width of 300 fs, which was subsequently upgraded to 65 fs through a modified design [32]. Pulse durations less than 30 fs have been achieved now [33] and the lowest pulsewidth reported to date is 6 fs [34]. Table 6.1 gives an account of the historical evolution of pulsewidth reduction [35].

Many more developments have been sparked off by the demands of various applications of lasers. An example is the distributed feedback dye laser, first described by Koegelnik and Shank [36] which have great scope as active elements for integrated optics. In their design the distributed-feedback structure was produced by inducing a periodic spatial variation of the refractive index of the medium. Shank et al [37] have shown that a distributed-feedback amplifier can also be operated with the feedback produced by a periodic spatial variation of the gain of the dye solution. More recently, laser emission arising from morphology-dependent resonances (MDRs) in spherical or cylindrical cavities has been discovered in micrometer sized droplets of dye solutions [38-40]. Such resonances occur when an integral number of wavelengths equals the circumference of the droplet, and these 'micro' lasers are now called whispering-gallery-mode lasers in analogy to the whispering-gallery acoustic waves which have been known for a long time. These lasers elucidate the very high gain of the dye medium, permitting the use of extremely small active lengths.

6.2 Practical dye laser configurations

Dye lasers can be broadly divided into the laser-pumped and flashlamp pumped types. So far only the fluorescence band is used for

Table 6.1

Year	Technique	pulsewidth
1960	Laser (Mainman)	≈ 1 ms
1961	Q-switching (Hellwarth)	≈ 10 ns
1965	Mode-locking (Mocker, Collins)	≈ 10 ps
1966	Dye lasers (Sorokin)	≈ 10 ns
1968	Mode-locked dye lasers (Schäfer)	≈ 10 ps
1981	colliding-pulse mode-locked (CPM) dye lasers (Fork)	≈ 100 fs
1985	Dispersion balanced CPM dye lasers (Valdmanis)	$\approx 20-60$ fs
1987	compression of fs pulses (Fork)	≈ 6 fs
1992	Kerr-lens mode-locked Ti:sapphire laser (Schmidt et al)	≈ 15 fs

lasing, and a preliminary report of a dye laser utilizing the phosphorescence band [41] has been suggested to be in error [42]. The allowed $S_1 \rightarrow S_0$ transition in fluorescent dyes is capable of giving a high amplification factor even at low dye concentrations, but a complication in such systems is the low-lying triplet states. $S_1 \rightarrow T_1$ intersystem crossing has a two-fold consequence : firstly it reduces the population of the excited singlet state and hence the amplification factor; and secondly, it enhances triplet-triplet absorption losses. It can be shown that a slowly rising pump light pulse (usually > 100 ns in duration) would transfer most of the molecules to the triplet state and deplete the ground state correspondingly, and experimental evidence for the premature stopping of laser action due to triplet losses can be found in almost any flashlamp pumped dye laser. Fig.6.1 gives the dye laser efficiency as a function of the excitation pulse width [43]. It is obvious that in the case of long pump pulses and for cw operation, a steady state should be maintained - for example, using triplet quenchers - where the triplet production rate equals the deactivation rate.

6.2.a Dye laser oscillator

Once the amplification factor of the dye medium is sufficient enough to maintain a net gain in the system, the next problem is that of a wavelength selective resonator. Even though a coarse tunability is possible by judicious choice of the dye, the solvent and the resonator Q ; fine tuning and simultaneous attainment of small linewidths can be achieved only by using a wavelength selective resonator. The first of its kind was constructed by Soffer and McFarland [15] by replacing one of the broadband dielectric mirrors of the dye laser cavity by a plane optical grating in Littrow mounting. One disadvantage of grating tuning is the substantial insertion loss, due to the fact that most gratings have only about 65 % reflection efficiency. However, high quality gratings can have 95 % efficiency at blaze wavelengths. Further, beam expanding optics like an intracavity telescope is often necessary for preventing grating damage as well as ensuring the spectral resolution. Burning of the grating can also be avoided by placing an additional semitransparent mirror in front of the grating [44]. In gas lasers where the laser lines are sharp and

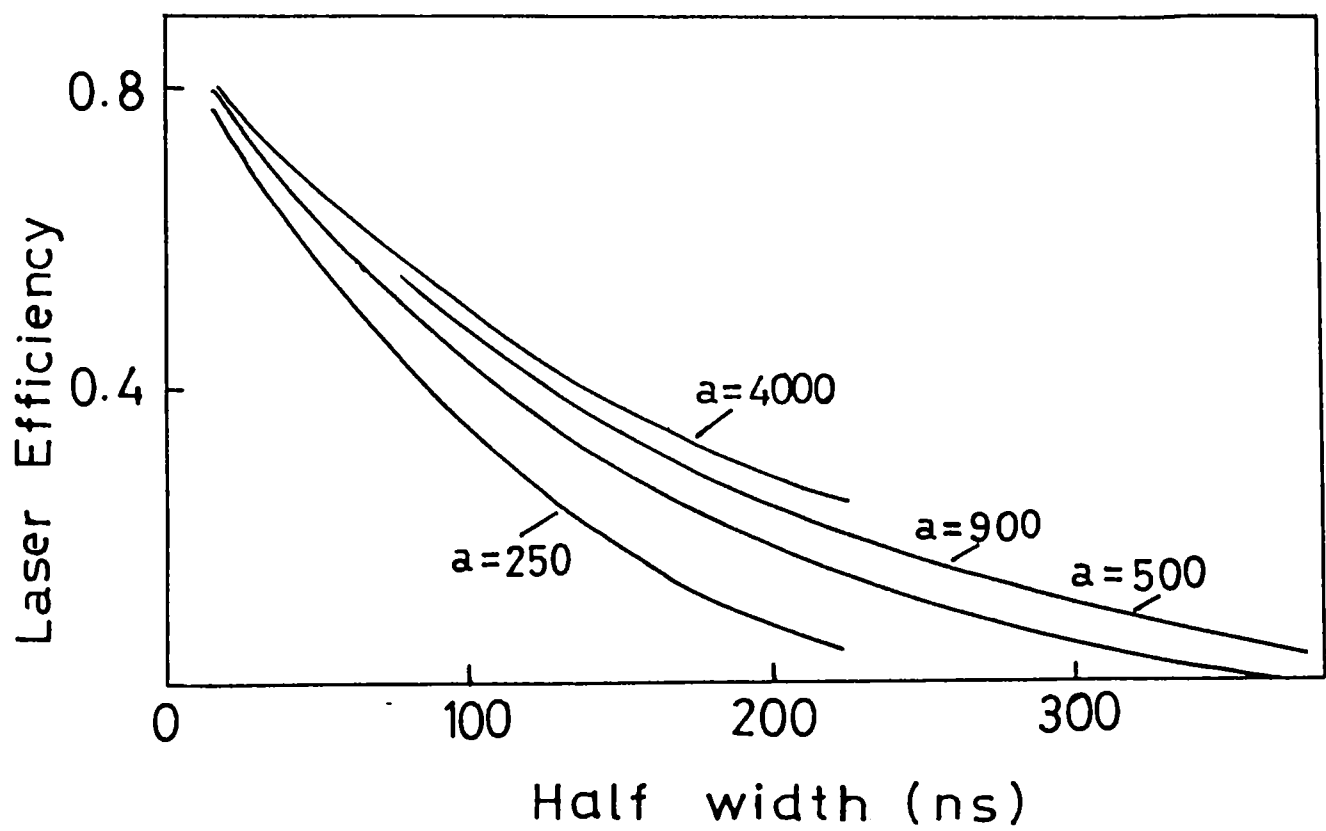


Fig.6.1 : A typical curve showing the decrease of dye laser efficiency with the half-width of pumping pulse at constant pulse energy (parameter a). The parameter ' a ' is the ratio of the total number of photons in the excitation pulse to the number of photons at threshold.

mutually isolated, tuning and spectral narrowing with prisms instead of gratings have long been employed [45]. However due to the relatively small angular dispersion of prisms, for flashlamp pumped dye lasers multiple prism arrangements are required to obtain sufficient spectral resolution. A five prisms arrangement reported by Strome and Webb [46], and a six prisms arrangement suggested by Schäfer and Miller [47] are generally used in ring lasers. It is interesting to note that the cumulative insertion loss of even six prisms near the Brewster angle is much smaller than that of one grating [42]. Grazing incidence resonators and multiple prism-grating configurations also have been described by various authors [48-51].

Fabry-perot etalons or interference filters are generally used for reducing the spectral bandwidth further. For example, the insertion of a Fabry-perot etalon into a dye laser cavity having telescopic beam expansion reduced the bandwidth from 3 pm to 0.4 pm [52]. As Fabry-perot etalons one usually uses either plane-parallel quartz plates coated with dielectric multilayer broadband reflective coatings, or optically contacted air Fabry-perots. Some other designs make use of the rotation of polarization for wavelength selection. Birefringence [53], rotatory dispersion of z-cut quartz crystals [54], Faraday rotation [55] etc. have been utilized in these designs. Details of the performance of various narrow-linewidth dye laser oscillators are given in Table 6.2.

6.2.b Dye Amplifiers

The dye laser oscillators described above can be considered as broadband amplifiers with selective or nonselective regenerative feedback. Because of its high inherent gain, a dye laser needs very little feedback to reach the threshold of oscillation. Thus it is usually somewhat difficult to build a dye laser amplifier, carefully avoiding all possibilities of regenerative feedback. The first report of a dye acting as an amplifier medium came in 1967 [56]. Here a ruby laser, a Raman cell containing toluene and a dye cuvette containing DTTC dissolved in dimethyl sulphoxide are aligned in a straight line, so that the ruby beam and the first stimulated Raman line pumps the dye solution longitudinally. Broadband laser emission is obtained with

Table 6.2: Performance of Narrow-Linewidth Dye Laser oscillators

Cavity type	Linewidth	% Efficiency	Pump source
Telescopic	2.5 GHz	20	N ₂ laser
	300 MHz ¹	2-4	N ₂ laser
Grazing-incidence	2.5 GHz	~ 4	Nd:YAG laser ⁵
	420 MHz ²	~ 6	N ₂ laser
	300 MHz ³	2	Nd:YAG laser ⁵
	150 MHz	3	Nd:YAG laser ⁵
MPL	1.61 GHz	14	N ₂ laser
HMPGI	1.15 GHz	7-10	N ₂ laser
MPL	60 MHz ¹	5	Cu laser
HMPGI	400-650 MHz	4-5	Cu laser
HMPGI and MPL	250-375 MHz ⁴		Flashlamp

1 : Incorporates intracavity etalon

2 : Open-cavity configuration

3 : Single-pulse linewidth, tuning mirror replaced by a second grating

4 : Single-pulse linewidth

5 : Frequency doubled

MPL : Multiple-prism Littrow configuration

HMPGI : Hybrid multiple-prism grazing-incidence

the four percent Fresnel reflection from the windows. However, when the concentration of the dye is set to a value such that the dye would lase near or at the wavelength of the second Stokes line at 806.75 nm, the broadband oscillation of the dye is quenched and the sharp Stokes line strongly amplifies instead. The Raman signal, being present from the beginning of the pump process, uses up all available inversion in the dye so that no free laser oscillation can start. Similar results have been obtained in cryptocyanine also, with CS₂ as the Raman liquid. Most of the dye lasers nowadays utilize one or more amplification stages for amplifying a weak laser beam generated in an oscillator cell. Different authors have given various designs for high gain dye amplifiers [57-59].

6.3 Theory of a simple dye laser

Consider a dye solution of concentration $n \text{ cm}^{-3}$ taken in a cuvette of length $L \text{ cm}$, having parallel end windows coated for a broadband reflectivity R . In this simplest form the cuvette walls are the cavity mirrors and the cuvette itself is the resonator of the dye laser. Assuming the pump pulse to be short ($< 100 \text{ ns}$) all triplet effects can be neglected to a first approximation. If $n_1 \text{ molecules/cm}^3$ are excited to the first singlet state the dye laser will start oscillating at a wavenumber $\bar{\nu}$ if the overall gain is equal to or greater than one as given by the equation [42]

$$\exp \left[- \sigma_a(\bar{\nu}) n_0 L \right] R \exp \left[+ \sigma_f(\bar{\nu}) n_1 L \right] \geq 1 . \quad (6.1)$$

Here $\sigma_a(\bar{\nu})$ and $\sigma_f(\bar{\nu})$ are the cross sections for absorption and stimulated fluorescence at $\bar{\nu}$ respectively, and n_0 is the population of the ground state. The first exponential term gives the attenuation due to reabsorption of fluorescence by the long wavelength tail of the absorption band. The attenuation becomes more important when the overlap between the absorption and fluorescence bands is significant. The cross section for stimulated fluorescence is related to the Einstein coefficient B through the relation

$$\sigma_f(\bar{\nu}) = g(\bar{\nu}) B h \bar{\nu} / c_0 \quad (6.2)$$

where $g(\bar{\nu})$ is the lineshape function such that

$$\int g(\bar{\nu}) d\bar{\nu} = 1 \quad (6.3)$$

where the integration is over the fluorescence band. Substituting the Einstein coefficient A for spontaneous emission according to

$$B = \frac{1}{h\bar{\nu}} \frac{1}{8\pi\bar{\nu}^2} A \quad (6.4)$$

and recalling that $g(\bar{\nu})A\phi_f = Q(\bar{\nu})$ is the number of fluorescence quanta per wavenumber interval, one obtains

$$\sigma_f(\bar{\nu}) = \frac{1}{8\pi c_0 \bar{\nu}^2} \frac{Q(\bar{\nu})}{\phi_f} \quad (6.5)$$

Since the fluorescence band is usually a mirror image of the absorption band the maximum values of the cross sections in absorption and emission are found to be equal, ie,

$$\sigma_{f,\max} = \sigma_{a,\max} \quad (6.6)$$

Taking the log of equation 6.1 and rearranging, we get the oscillation condition in a form which makes it easier to discuss the influence of the various parameters:

$$\frac{S/n + \sigma_a(\bar{\nu})}{\sigma_f(\bar{\nu}) + \sigma_a(\bar{\nu})} \leq \gamma(\bar{\nu}) \quad (6.7)$$

Here $S = (1/L) \ln(1/R)$ and $\gamma(\bar{\nu}) = n_1/n$. The constant S contains only the parameters of the resonator, L and R. Scattering and diffraction losses may be accounted for by an effective reflectivity term R_{eff} . The value $\gamma(\bar{\nu})$ is the minimum fraction of molecules that must be raised to the first singlet state to reach the threshold of oscillation. One may then calculate the function $\gamma(\bar{\nu})$ from the absorption and fluorescence spectra for any concentration n of the dye and value S of the cavity. In this way one finds the frequency for the minimum of this function, which will be the start oscillation

frequency. This frequency can also be obtained by differentiating equation 6.7 and setting $d\gamma(\bar{\nu})/d\bar{\nu} = 0$. This yields

$$\frac{\sigma_a'(\bar{\nu})}{\sigma_f'(\bar{\nu}) + \sigma_a'(\bar{\nu})} \left[\sigma_f(\bar{\nu}) + \sigma_a(\bar{\nu}) \right] = S/n \quad (6.8)$$

(prime means differentiation with respect to $\bar{\nu}$) from which the start oscillation frequency can be obtained. Figures 6.2a and 6.2b show the relationship between the length of the cuvette L , reflectivity R , concentration n and the laser wavelength λ (ie, the wavelength at which the minimum of $\gamma(\bar{\nu})$ occurs).

6.4 Design of the broadband resonator

We have observed that a good quality, square, all-side-polished uncoated spectrophotometer cuvette containing the absorbing dye solution can be used as a broadband laser oscillator, when pumped with the 532 nm radiation from the frequency-doubled Nd:YAG laser (Fig.6.3a). The pump beam is focused as a line on the front face of the cuvette, along which the amplification takes place. The Fresnel reflection from the glass-air interface at the cuvette walls (approximately 4%) provides optical feedback into the cavity, and laser oscillations are sustained due to the high gain of the dye medium. In this case the dye laser beam is propagated in two directions, perpendicular to the propagation direction of the pump beam. However in most of the following experiments an external cavity has been employed, using a 100% broadband reflector at one end and a 4% reflector (glass plate) as the output coupler. Two convex lenses and two apertures also are included in the cavity for beam shaping (Fig.6.3b). In this geometry the cuvette is tilted at an angle for preventing internal oscillations within it. This configuration is more efficient than the previous one, since the cavity Q is enhanced by the use of the 100% reflector. The positioning of the cuvette with respect to the focusing lens is found to be critical in determining the energy and divergence of the dye laser beam. Since frequency selective components like gratings and prisms are not used in the cavity, broadband dye laser pulses are obtained along the resonator axis upon proper excitation by the pump laser.

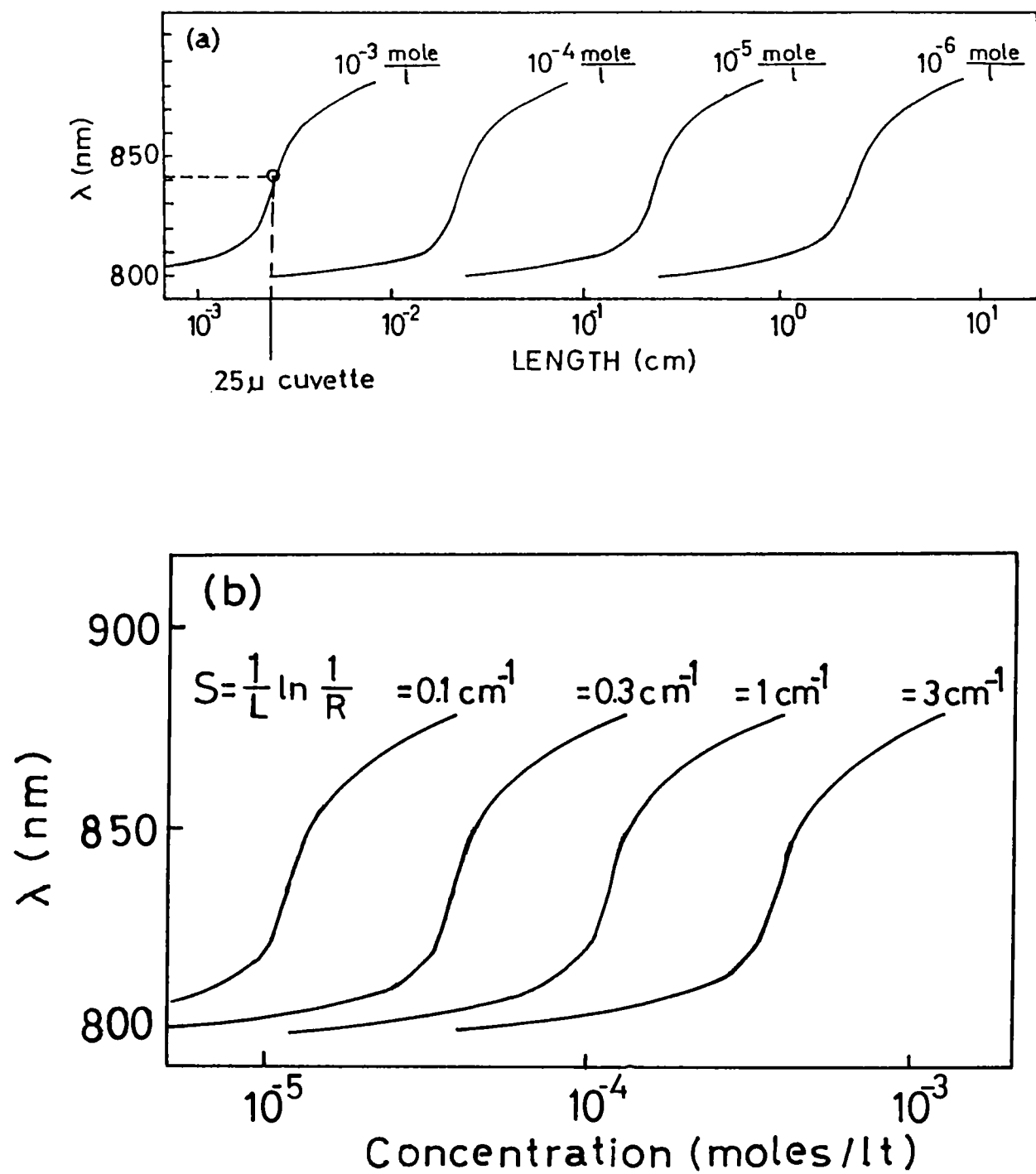


Fig.6.2 : Relationship of the lasing wavelength (λ) to the cuvette length L , dye concentration n , and reflectivity R .

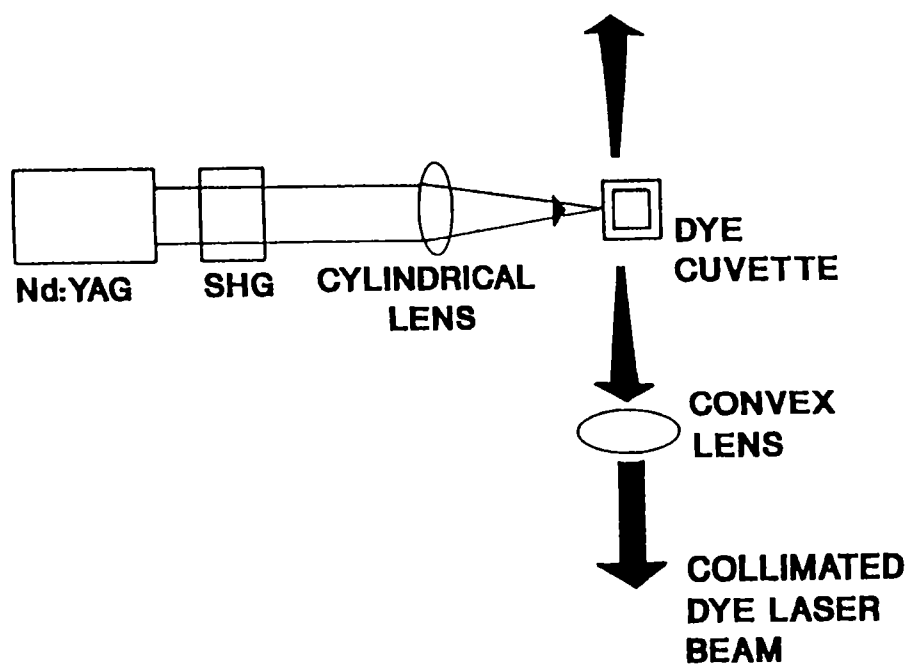


Fig.6.3a : A simple broad band dye laser. A spectrophotometer cuvette forms the resonator cavity.

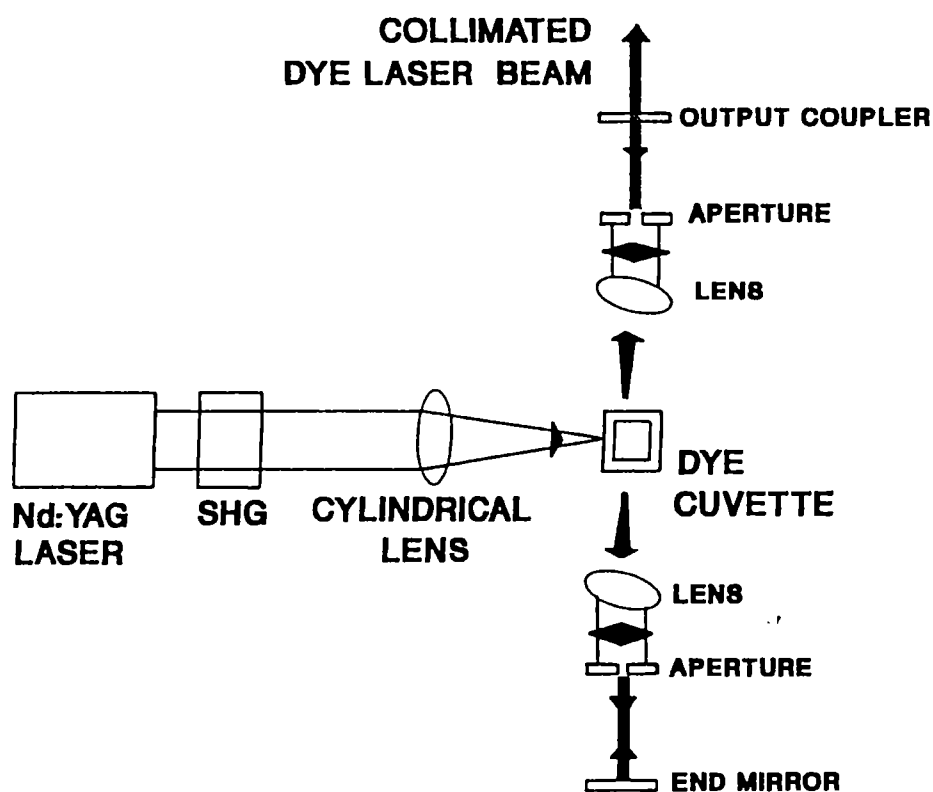


Fig.6.3b : Modified broad band dye laser with an external cavity and beam shaping optics. The cuvette is tilted to prevent internal oscillations.

In the following sections we discuss the results obtained from parametric studies of this broadband dye laser.

6.5 Pump power dependence of the emission

One of our interesting observations has been the occurrence of stimulated emission in test tube samples. Here also the feedback from the curved test tube walls is responsible for this phenomenon, even though the emission is weak and non-directional as compared to the cuvette geometry. This is partly due to geometrical reasons and partly due to the predominance of amplified spontaneous emission (ASE). Fig.6.4a shows the gradual evolution of the lasing band with pump power in a solution of Rhodamine 6G. It may be noted that the lasing peak develops not at the fluorescence peak, but at longer wavelengths, due to the reabsorption effect [42]. However in a solution of DCM in Dimethyl formamide (DMF), lasing action occurs at the fluorescence peak itself, since reabsorption effects are minimal here (Fig.6.4b).

Fig.6.5 shows the increase in dye laser power with pump power. For R6G taken in water at a concentration of 10^{-3} moles/lt, the energy conversion efficiency is found to be around 6%.

6.6 Concentration tuning of the dye laser wavelength

Equation 6.7 shows that the emission wavelength is a function of the length and Q of the cavity, as well as the concentration of the dye. This indicates the possibility of tuning the dye laser wavelength by changing the sample concentration. Fig.6.6 gives the spectrum of laser emission for two concentrations of Rhodamine 6G in water. The peaks are found to be separated by about 40 nm. In Fig.6.7, variation of the lasing peak with concentration in the range of 10^{-3} to 10^{-5} moles/lt is shown. There is good agreement with theory, which is obvious from a comparison with Fig.6.2a. The useful tunable range is found to be from 566 nm to 609 nm, and the maximum bandwidth is observed at 6.5×10^{-4} moles/lt concentration.

Figs.6.8a and 6.8b show the absorption spectrum and laser action in cresyl violet perchlorate solutions prepared in methanol. The

observed tunable range is approximately 22 nm (624 nm - 646 nm) and the highest bandwidth is obtained for the lowest concentration of 4.5×10^{-5} moles/lt (Fig.6.9). Still lower concentrations could not be tried because of the low absorption coefficient of the samples at 532 nm.

Figs.6.10a and 6.10b show the absorption spectrum and the results obtained from the analysis of DCM samples prepared in an ethylene glycol + benzyl alcohol mixture. Tunability is obtained in a range of 17 nm (628 nm - 645 nm), and the highest bandwidth is obtained for a concentration of 4.7×10^{-3} moles/lt (Fig.6.11). In DCM also, because of the low absorption at the pump wavelength, the range of analyzable concentrations is restricted.

6.7 Energy transfer and double band lasing in dye mixtures

It has been known before that since there are spectral regions of weak absorption present in many dyes, considerable losses in absorption will occur on flashlamp pumping, reducing the overall efficiency. Reduced efficiency is to be expected in laser pumping too if the dye absorption is not significant at the pump wavelength. To improve the efficiency of dye lasers, Peterson and Snavely [60] proposed the application of energy transfer in donor-acceptor pairs of organic dyes. Energy transfer is also one of the methods that can be employed for efficient shifting of the dye laser wavelength appreciably relative to the pump wavelength. The basic requirements here are that (a) the fluorescence spectrum of the 'donor' dye overlaps the lowest S-S absorption band of the 'acceptor' dye, and (b) the triplet absorption of the donor dye does not overlap the emission band of the acceptor dye. The donor dye will then strongly absorb a shorter wavelength portion of the flashlamp spectrum converting it into longer wavelength fluorescence light. Now the acceptor dye is excited by the longer wavelength portion of the flashlamp spectrum together with the fluorescence emission from the donor dye, and the pumping efficiency is increased. Peterson and Snavely reported a four fold increase in energy output from a flashlamp pumped Rhodamine 6G (donor)/rhodamine B (acceptor) dye mixture as compared to a solution of pure Rhodamine B. By a proper choice of the dye concentrations it

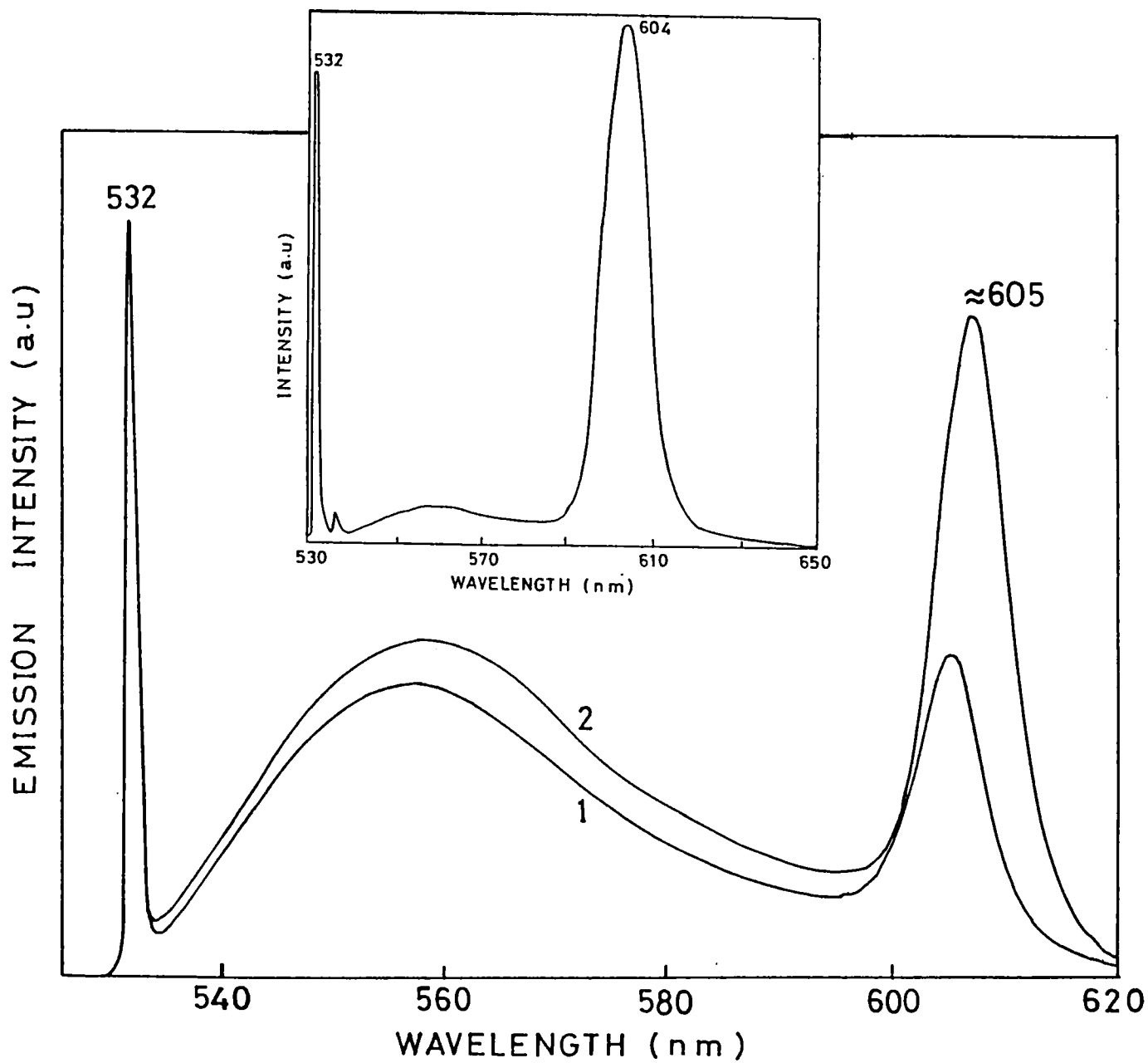


Fig.6.4a : Evolution of the lasing band with pump power in an aqueous solution of Rhodamine 6G, taken in test tube. Concentration - 4.4×10^{-4} moles/lt. The pump power is 2.2 MW for 1, and 3.5 MW for 2. Inset shows strong lasing for a pump power of 7.3 MW.

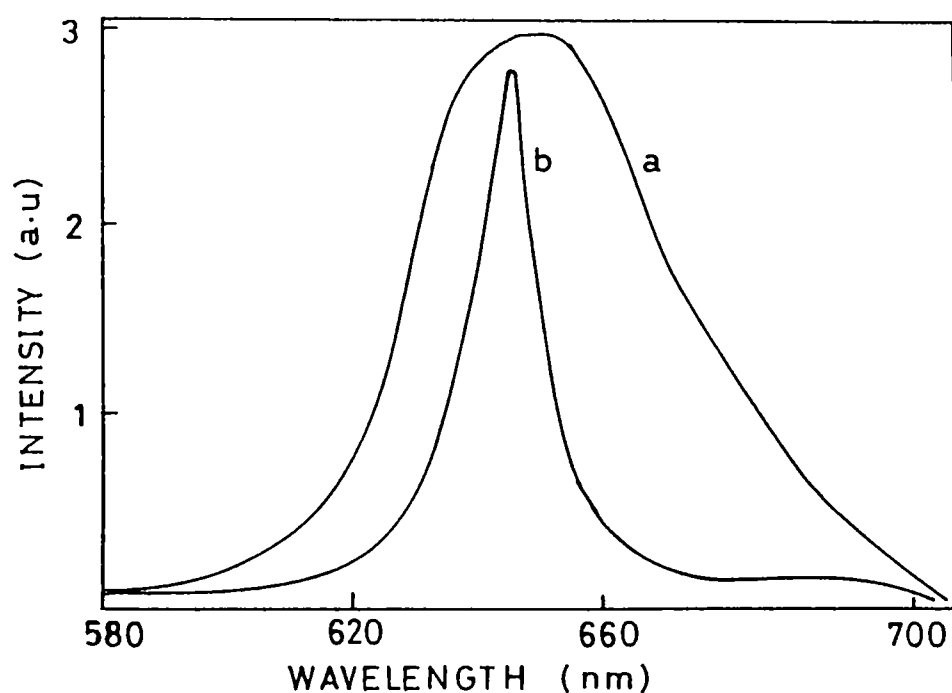


Fig.6.4b : Fluorescence emission (a) evolves to the lasing band (b) at a higher pump power in a solution of DCM prepared in dimethyl formamide. The sample is taken in cuvette.

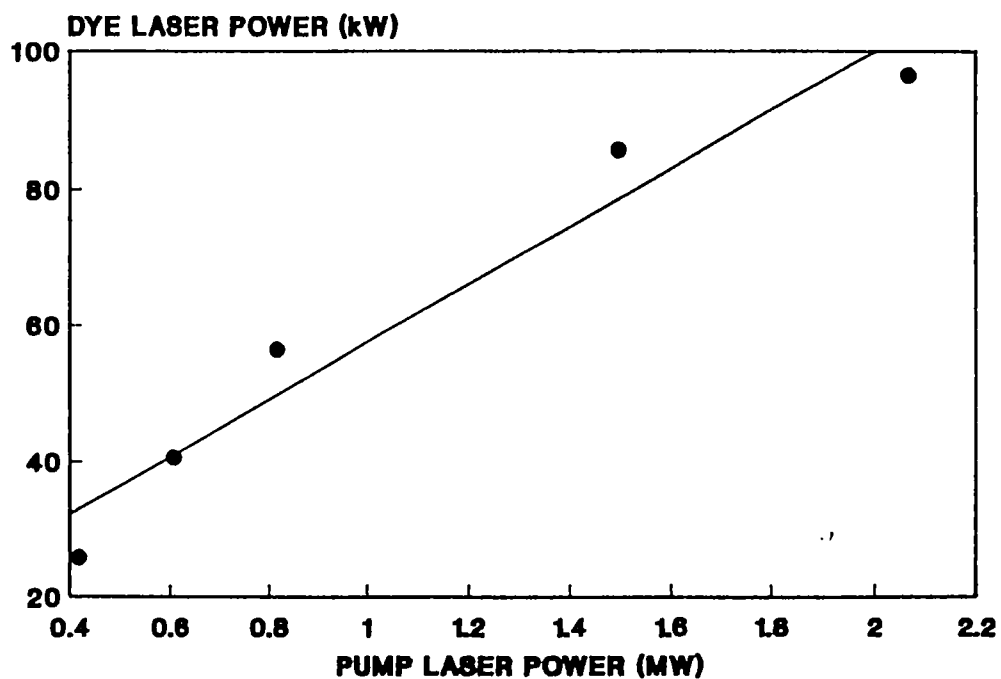


Fig.6.5 : Increase in the dye laser power with pump power for R6G in water, at a concentration of 10^{-3} moles/lit.

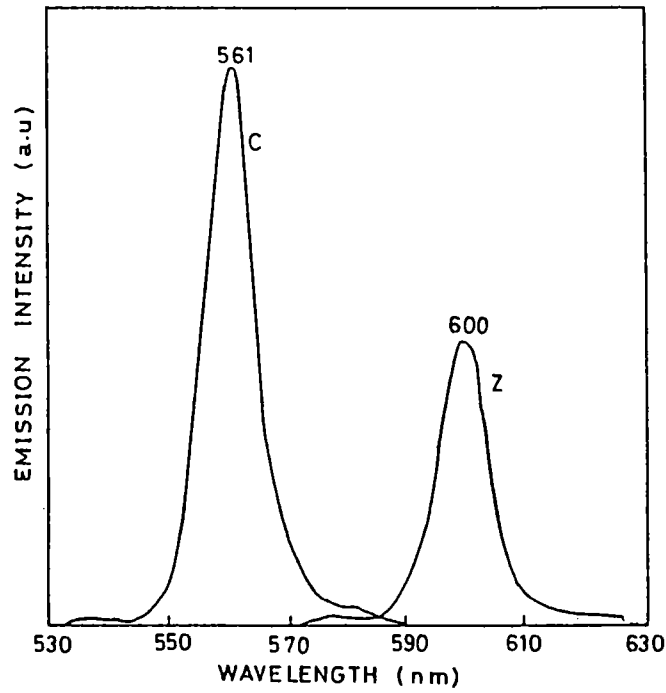


Fig.6.6 : Laser action in aqueous Rhodamine 6G solutions.
 C - 9.6×10^{-5} moles/lt, Z - 1.1×10^{-3} moles/lt.

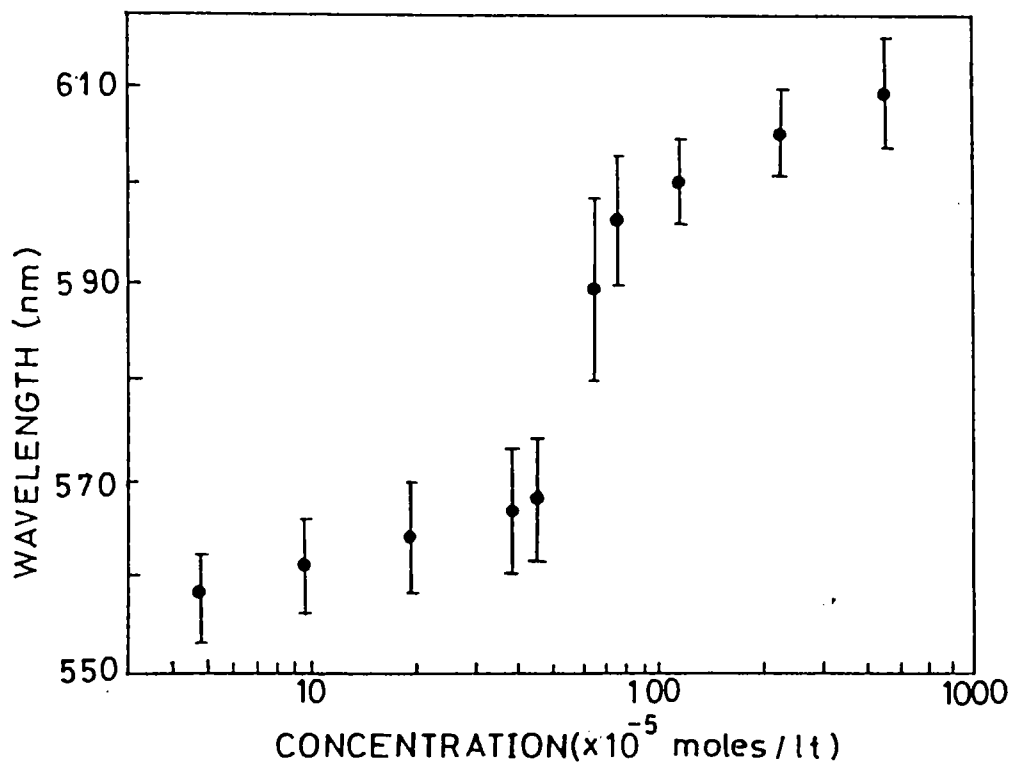


Fig.6.7 : Variation of lasing peak with concentration for Rhodamine 6G dissolved in water. The bars show the bandwidth (FWHM) of laser emission.

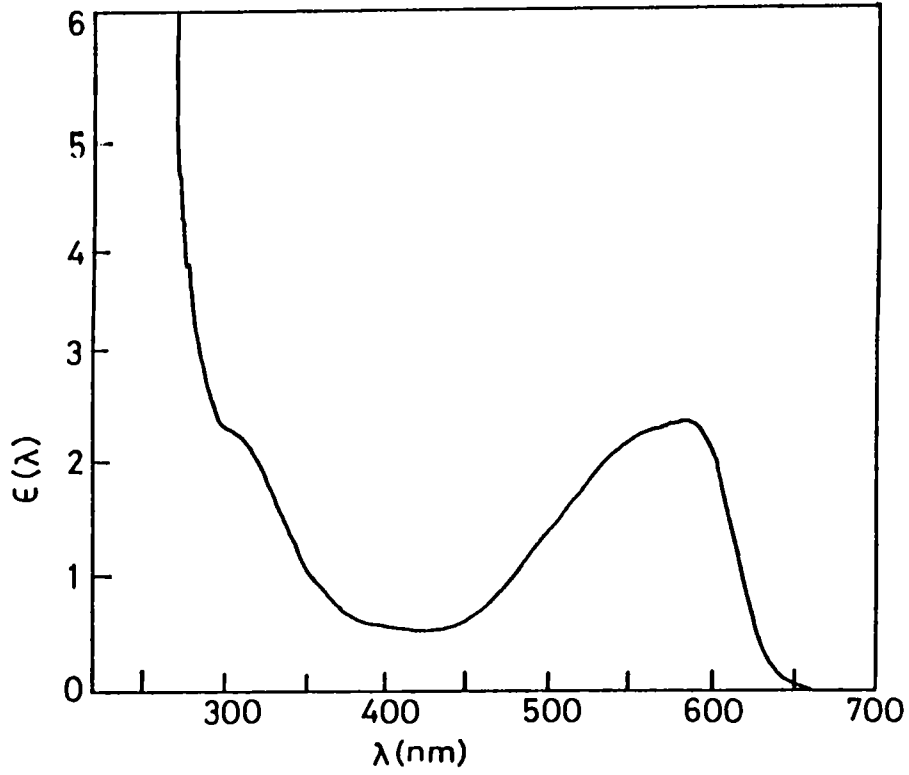


Fig.6.8a : Absorption spectrum of Cresyl violet perchlorate in methanol. Concentration - 4.6×10^{-4} moles/lt.

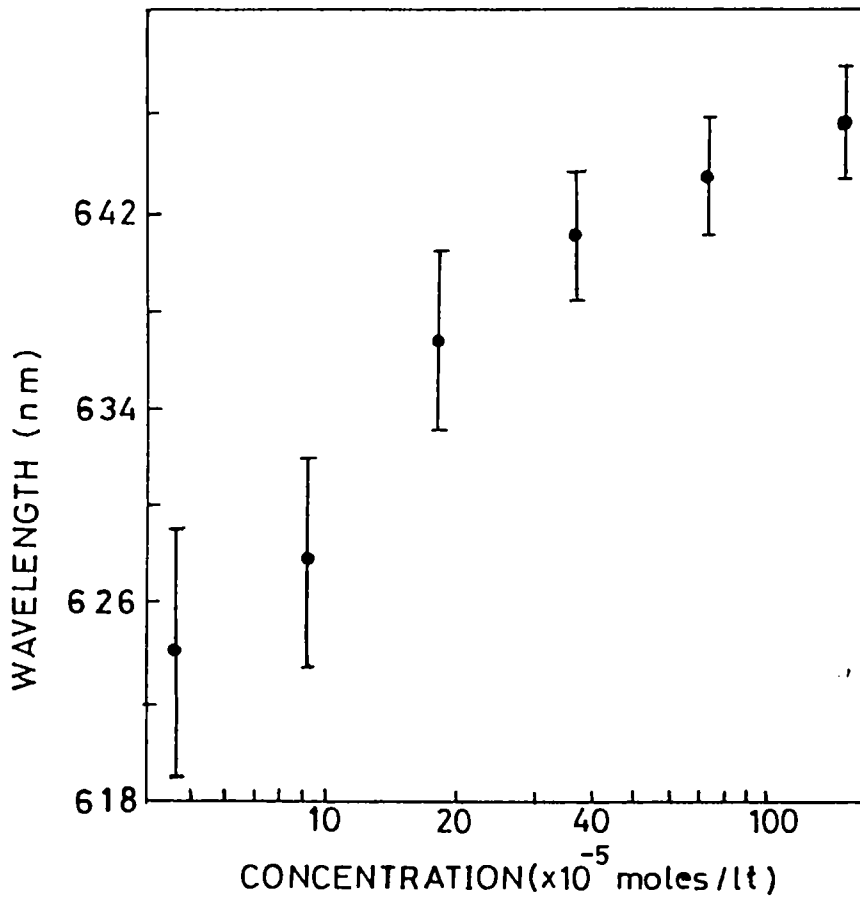


Fig.6.8b : Variation of lasing peak with concentration for Cresyl violet perchlorate dissolved in methanol. The bars show the bandwidth (FWHM) of laser emission.

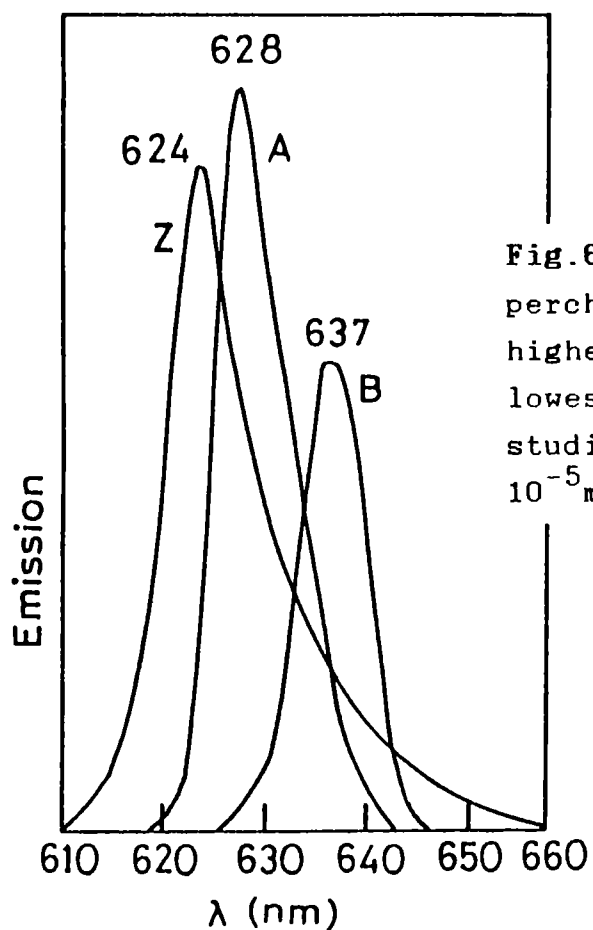


Fig.6.9 : Laser action in Cresyl violet perchlorate + methanol solutions. The highest bandwidth (102 Å) is seen in the lowest concentration (4.5×10^{-5} moles/lt) studied. Z = 4.5×10^{-5} moles/lt, A = 9.1×10^{-5} moles/lt, B = 1.8×10^{-4} moles/lt.

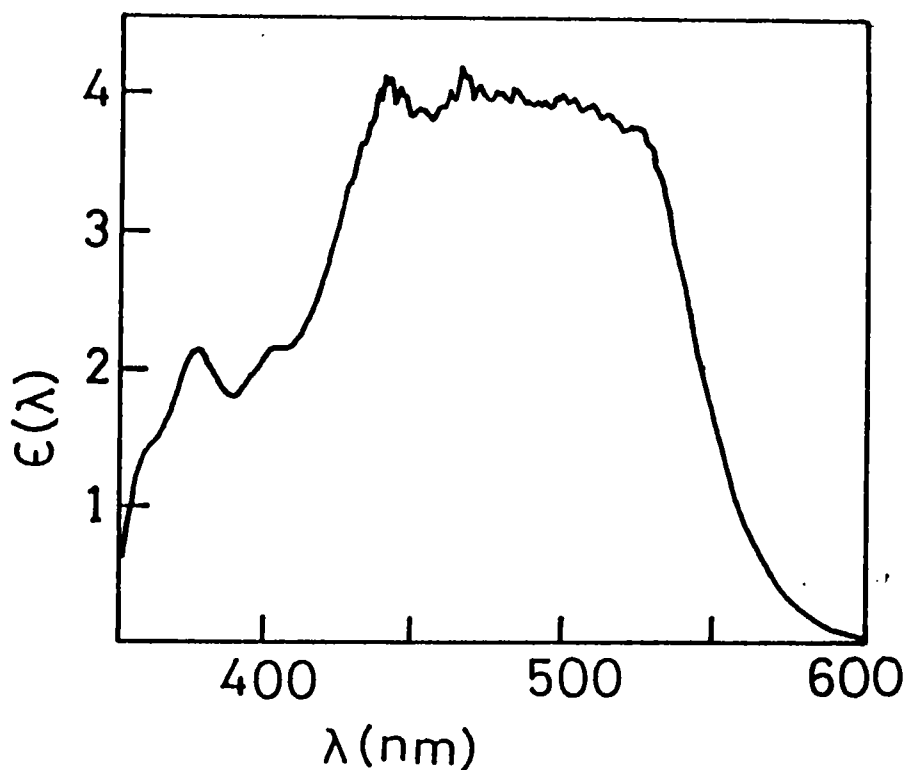


Fig.6.10a : Absorption spectrum of DCM dissolved in an ethylene glycol + benzyl alcohol mixture.

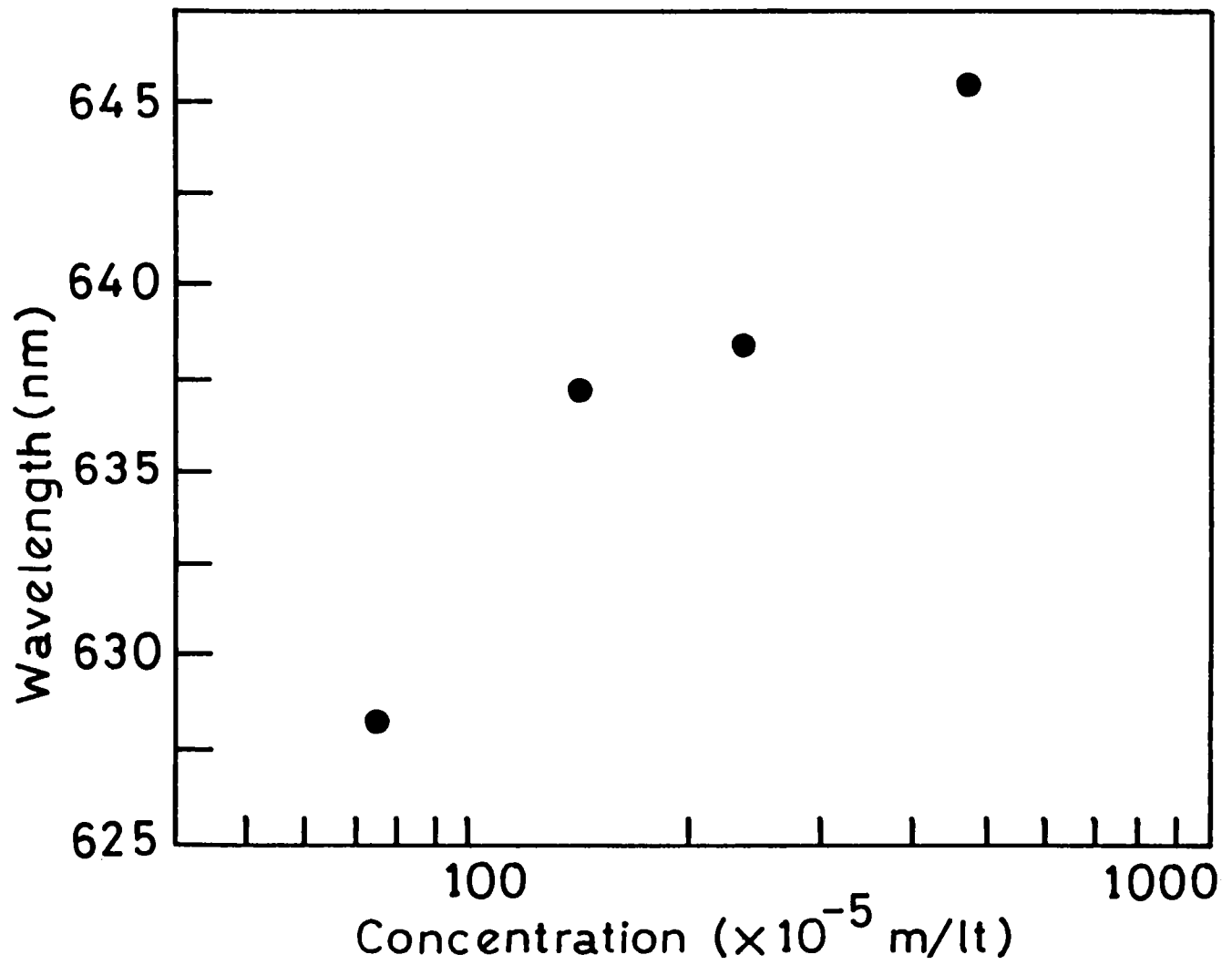


Fig.6.10b : Variation of lasing peak with concentration for DCM dissolved in an ethylene glycol + benzyl alcohol solution. The bandwidths are large, and hence not shown.

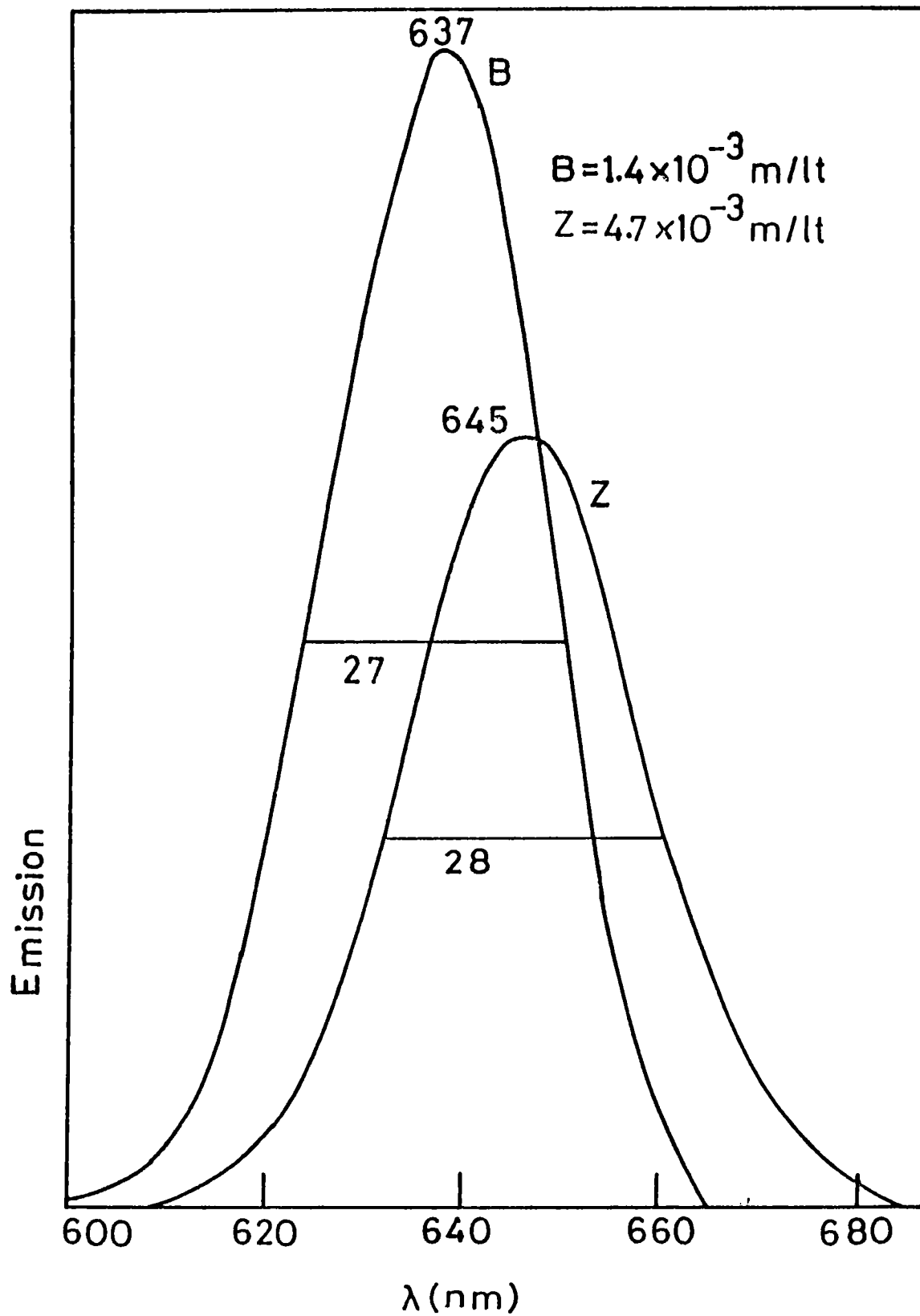


Fig.6.11 : Laser action in DCM + (ethylene glycol + benzyl alcohol) solutions. The highest bandwidth (285 Å) is seen in the highest concentration (4.7×10^{-3} moles/lt) studied.

is also possible to have lasing from both dyes simultaneously. For example, two band lasing of dyes embedded in polymer hosts [61] and simultaneous laser action at the primary colours of blue, green and red from mixtures of three dyes [62] (which the authors used as the source for a multiwavelength LIDAR system) etc. have been reported. It may be noted here that lasing in a second band due to the formation of a protonated excited state form of a single dye species also is possible sometimes [63]. The dye mixture laser is attractive from an instrumentation point of view too, since here only one laser system and one dye cell are required to get multiple wavelengths. Narrowband, widely tunable laser radiation also can be obtained from dye mixture lasers, and a good example is the dye laser reported by Stokes et al [64], that can be tuned in the entire spectral range of 350 to 730 nm, with linewidths ≈ 0.01 nm.

The main mechanisms that have been proposed for energy transfer are (1) radiative transfer, i.e., absorption of donor emission by an acceptor (2) diffusion-controlled collisional transfer and (3) resonance transfer due to long range dipole-dipole interactions [65]. However, radiative transfer is the dominant mechanism in energy transfer dye lasers [66].

To investigate the effects of dye mixing we have studied a Rhodamine 6G (donor)/cresyl violet perchlorate (acceptor) system taken at various concentrations of the acceptor. The R6G concentration has been fixed at 2×10^{-3} moles/lit while the CVP concentration is changed from 2.27×10^{-5} moles/lit to 3.63×10^{-4} moles/lit. The overlap of the relevant absorption and emission bands is shown in Fig.6.12. The evolution and growth of the CVP lasing band around 630 nm is obvious from figures 6.13a and 6.13b. It is seen that by a proper choice of the CVP concentration one can have either double band lasing, or single band lasing of the acceptor molecule. The reduced bandwidth of R6G lasing in the mixture as compared to pure R6G solutions results from the higher concentration used here. The lasing bands are found to vary with CVP concentration as shown in Fig.6.14.

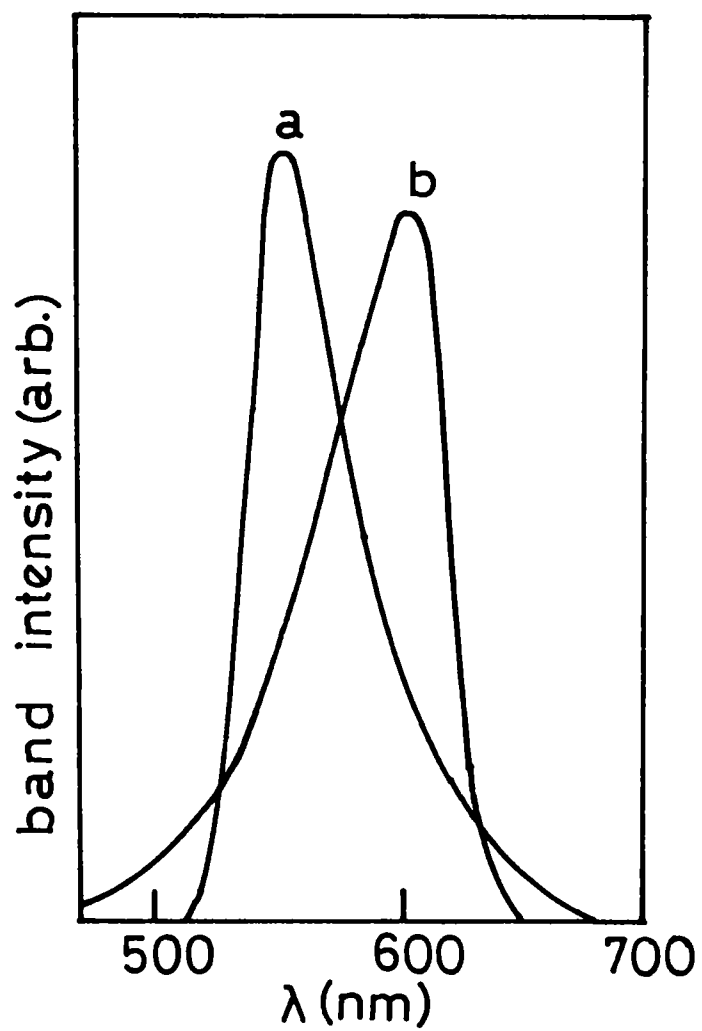


Fig.6.12 : Overlap of the emission band of Rhodamine '6G (curve a) over the absorption band of Cresyl violet perchlorate (curve b).

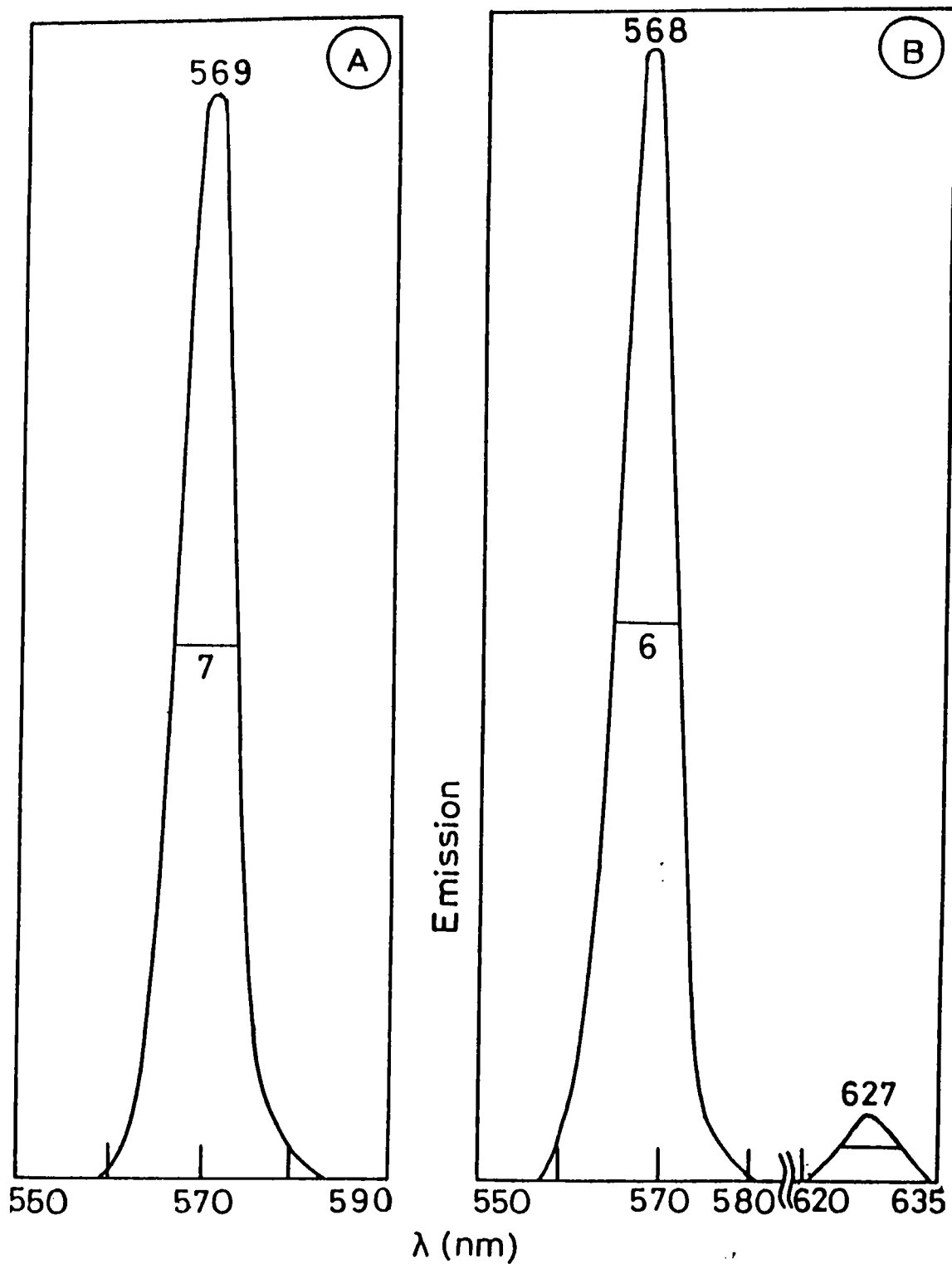


Fig.6.13a : Growth of the CVP lasing band in an R6G + CVP mixture. R6G concentration is fixed at 2×10^{-3} moles/lit, while the CVP concentration is 2.3×10^{-5} moles/lit for A, and 4.5×10^{-5} moles/lit for B. In A only R6G lases, whereas in B the CVP band has just appeared. The emission peaks and halfwidths are marked in nm.

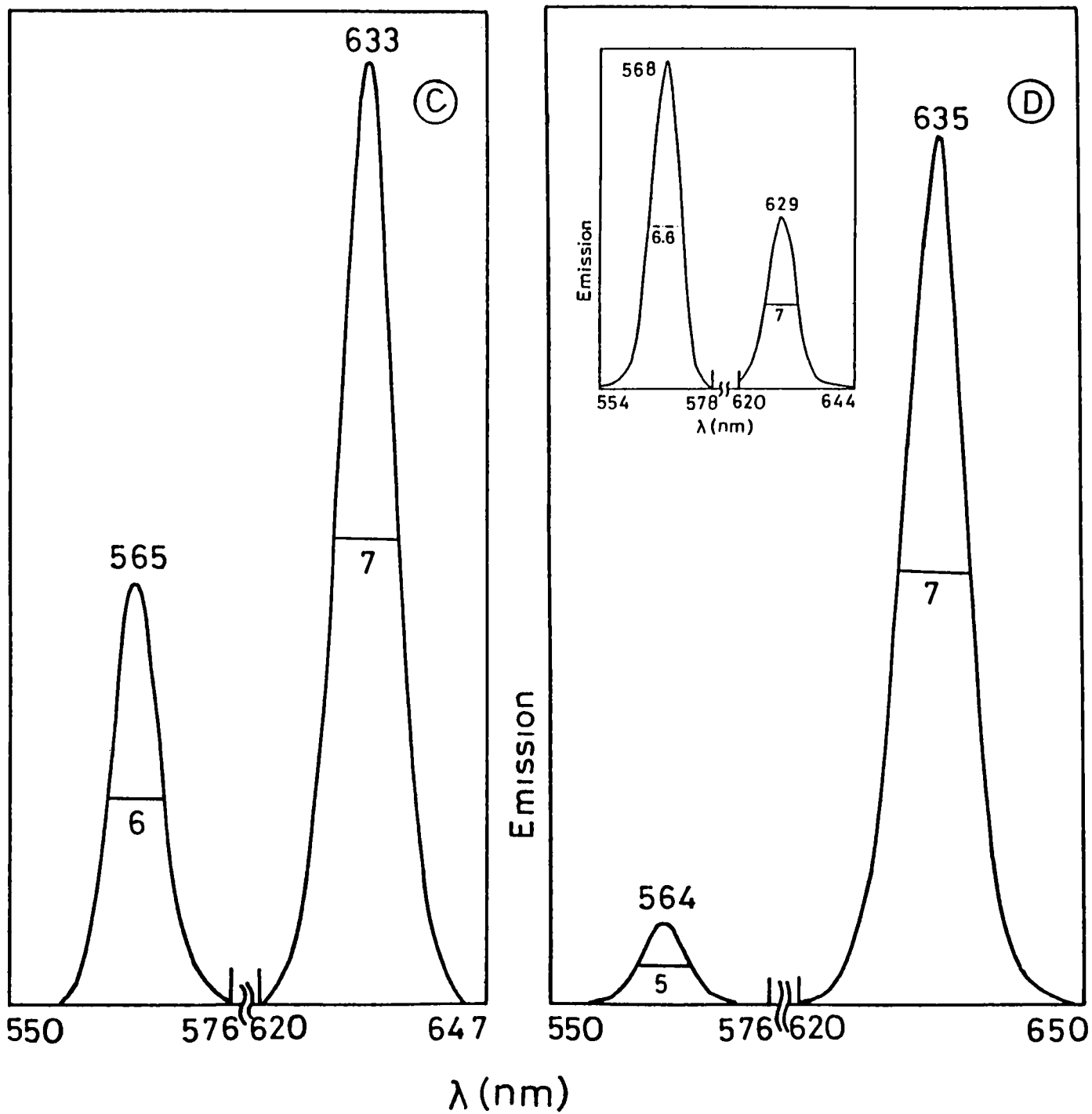


Fig.8.13b : Double band lasing in R6G + CVP mixtures. CVP concentration is 1.8×10^{-4} moles/lit in C, 3.6×10^{-4} moles/lit in D, and 9.1×10^{-5} moles/lit in the inset of D. It is clear that the CVP concentration is very critical in the energy transfer process, which is almost complete in fig.D.

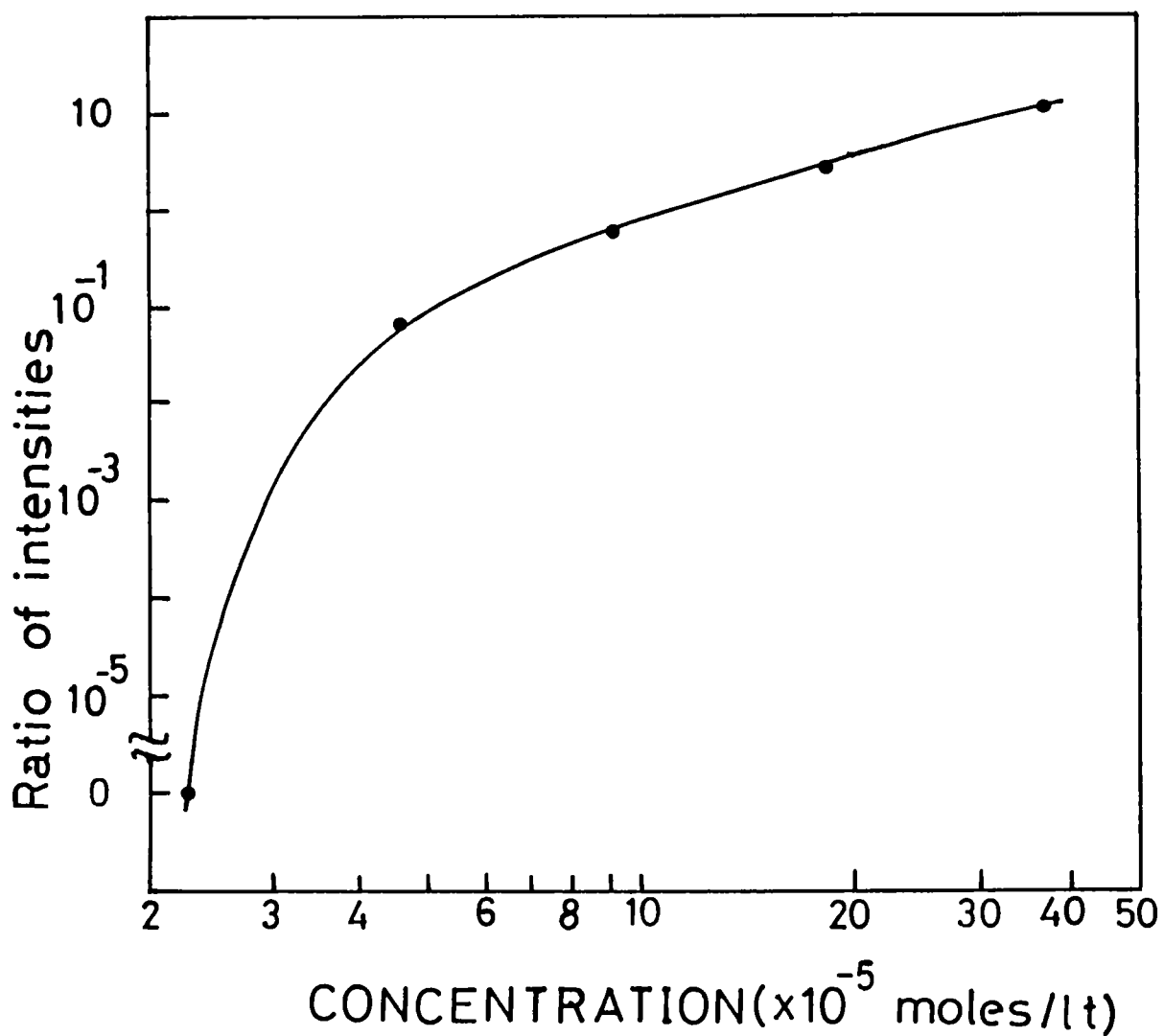


Fig.8.14 : Increase in the relative intensity of CVP lasing band with CVP concentration, in the R6G + CVP mixture. CVP concentration is plotted along the X-axis. Ratio of the CVP lasing band intensity to the R6G lasing band intensity is plotted along the Y-axis.

6.8 Conclusions

The design of a simple broadband dye laser resonator is discussed in this chapter. Observation of stimulated emission and lasing in an unconventional test tube geometry is reported. Details of concentration tuning of the emission wavelength in Rhodamine 6G, DCM and Cresyl violet solution lasers are given. Double band lasing in R6G/CVP mixtures is investigated, and the energy transfer mechanism is studied at various concentrations of the acceptor molecule. Tunability of broadband laser radiation is achieved over a range of about 73 nm collectively from R6G, DCM and Cresyl violet samples. The good spatial coherence, controllable spectral width, moderate power levels and wide tunability of these broadband lasers make them useful in several applications like ultrafast technology [67], incoherent spectroscopy [68], white light fourier optical processing [69], all-optical image transfer [70] etc.

CHAPTER 6 - REFERENCES

- [1] Rautian S G and I I Sobel'Mann, *Opt.Spectrosc.* **10**, 65 (1961)
- [2] Brock E G, P Czavinsky, E Hormats, H C Nedderman, D Stripe, and F Unterleitner, *J.Chem.Phys.* **35**, 759 (1961)
- [3] Broude V L, V S Mashkevich, A F Prikhotko, N F Prokopyuk, and M S Soskin, *Sov.Phys.Solid State* **4**, 2182 (1963)
- [4] Stockman D L, W R Mallory, and F K Tittel, *Proc. IEEE* **52**, 318 (1964)
- [5] Stockman D L, *Proc. ONR Conference on organic lasers, Cameron Station, Alexandria, USA* (1964)
- [6] Sorokin P P and J R Lankard, *IBM J.Res.Develop.* **10**, 162 (1966)
- [7] Schäfer F P, W Schmidt, and J Volze, *Appl.Phys.Lett.* **9**,306 (1966)
- [8] Schäfer F P, W Schmidt, and K Marth, *Ber.Bunsenger.Phys.Chemio.* **72**, 328 (1968)
- [9] Spaeth M L and D P Bortfeld, *Appl.Phys.Lett.* **9**, 179 (1966)
- [10] Stepanov B I, A N Rubinov, and V A Mostovnikov, *JETP Lett.* **5**, 117 (1967)
- [11] Sorokin P P and J R Lankard, *IBM J.Res.Develop.* **11**, 148 (1967)
- [12] Macfarland B B, *Appl.Phys.Lett.* **10**, 208 (1967)
- [13] Kotzubanov V D, L Ya Malkes, Yu V Naboikin, L A Ogutsova, A P Podgornyi, and F S Pokrovskaya, *Bull.Acad.Sci.USSR, Phys.Ser.* **32**, 1357 (1968)
- [14] Kotzubanov V D, L Ya Malkes, Yu V Naboikin, L A Ogutsova, A P Podgornyi, and F S Pokrovskaya, *Opt.Spectrosc.* **25**, 406 (1968)
- [15] Soffer B H and B B Mcfarland, *Appl.Phys.Lett.* **10**, 266 (1967)
- [16] Jarrett F M and J F Young, *Opt.Lett.* **4**, 176 (1979)
- [17] Kowalski F W, P D Hale, and S J Shattil, *Opt.Lett.* **13**, 622 (1988)
- [18] Telle J M and C L Tang, *Appl.Phys.Lett.* **26**, 572 (1975)
- [19] Jethwa J, S St.Anufrik and F Docchio, *Appl.Opt.* **21**, 2778 (1982)
- [20] Danailov M B and I P Christov, *Opt.Commun.* **73**, 235 (1989)
- [21] Snavely B B and F P Schäfer, *Phys.Lett.* **28 A** 728 (1969)
- [22] Marling J B, D W Gregg, and S J Thomas, *IEEE J Quant.Electron.* **QE-6**, 570 (1970)
- [23] Marling J B, D W Gregg, and L Wood, *Appl.Phys.Lett.* **17**,527 (1970)
- [24] Pappalardo R, H Samelson, and A Lempicki, *Appl.Phys.Lett.* **16**, 267 (1970)

- [25] Peterson O G, S A Tuccio, and B B Snavely, Appl.Phys.Lett. **17**, 245 (1970)
- [26] Glenn W H, M J Brienza, and A J DeMaria, Appl.Phys.Lett.**12**, 54 (1968)
- [27] Bradley D J and A J E Durrant, Phys.Lett. **27 A** 73 (1968)
- [28] Sotter B H and J W Linn, J.Appl.Phys. **39**, 5859 (1968)
- [29] Mack M E, Appl.Phys.Lett. **15**, 81 (1969)
- [30] Bradley D J, G M Gale, and P D Smith, J.Phys.B **3**, 11 (1970)
- [31] Ruddock I S and Bradley D J, Appl.Phys.Lett. **29**, 296 (1976)
- [32] Shank C V, Paper WE 3 presented at the XIIth Int.Quantum Electronics Conf., Munich, Germany, June 22 (1982)
- [33] Valdmanis J A, Fork R L, and Gordan J P, Opt.Lett. **10**, 131 (1985)
- [34] Fork R L, Cruz C H, Becker P C, and Shank C V, Opt.Lett. **12**, 483 (1987)
- [35] Penzkofer A, Lecture 1, SERC School on Ultrafast Phenomena in Lasers and Optics, Dharwad, 16 Nov.- 4 Dec., 1992
- [36] Kogelnik H and C V Shank, Appl.Phys.Lett. **18**, 152 (1971)
- [37] Shank C V, J E Bjorkholm, and H Kogelnik, Appl.Phys.Lett. **18**, 395 (1971)
- [38] Owen J F, P W Barber, P B Dorain, and R K Chang, Phys.Rev.Lett. **47**, 1075 (1981)
- [39] Lin H B, A L Huston, B L Justus, and A J Campillo, Opt.Lett. **11**, 614 (1986)
- [40] Biswas A, H Latifi, R L Armstrong, and R G Pinnick, Opt.Lett.**14**, 214 (1989)
- [41] Morantz D J, B G White, and A J C Wright, Phys.Rev.Lett.**8**, 23(1962)
- [42] Schäfer F P (ed.), "*Dye Lasers*", Springer-Verlag, Berlin (1977)
- [43] Sorokin P P, J R Lankard, V L Moruzzi, and E C Hammond, J.Chem.Phys. **48**, 4726 (1968)
- [44] Bjorkholm J E, F C Damen, and J Shah, Opt. Commun. **4**, 283 (1971)
- [45] Yamaguchi G, F Endo, S Murakawa, S Okamura, and C Yamanaka, Jpn.J.Appl.Phys. **7**, 179 (1968)
- [46] Strome F C Jr. and J P Webb, Appl.Opt. **10**, 1348 (1971)
- [47] Schäfer F P and H Miller, Opt.Comm. **2**, 407 (1971)
- [48] Nair L G and K Dasgupta, IEEE J Quant.Electron. **QE-16**, 111(1980)
- [49] Littman M G, Opt.Lett. **3**, 138 (1978)

- [50] Littman M and Metcalf, Appl.Opt. 17, 2224 (1978)
- [51] Shoshan I, N Danon, and U Oppenheim, J.Appl.Phys. 48, 4495 (1977)
- [52] Hansch T W, Appl.Opt. 11, 895 (1972)
- [53] Soep B, Opt.Comm. 1, 433 (1970)
- [54] Kato D and T Sato, Opt.Comm. 5, 134 (1972)
- [55] Sorokin P P and J R Lankard, Phys.Rev. 186, 342 (1969)
- [56] Bass M and T F Deutsch, Appl.Phys.Lett. 11, 89 (1967)
- [57] Hansch T W, F Varsanyi, and A L Schawlow, Appl.Phys.Lett. 18, 108 (1971)
- [58] Erickson L E and A Szabo, Appl.Phys.Lett. 18, 433 (1971)
- [59] Vrehen Q H F and A J Breimer, Opt.Comm. 4, 416 (1972)
- [60] Peterson O G and B B Snavely, Bull.Am.Phys.Soc. 13, 397 (1968)
- [61] Belega E D, LK Denisov, and V A Sivovolov, Sov.J.Quantum Electron. 17, 1392 (1987)
- [62] Saito Y, M Kato, A Nomura, and T Kano, Appl.Phys.Lett.56, 811 (1990)
- [63] Maslov V V, M I Dzyubenko, S N Kovalenko, V M Nikitchenko, and A I Novikov, Sov.J.Quantum Electron. 17, 998 (1987)
- [64] Stokes E D, F B Dunning, R F Stebbings, G K Walters, and R D Rundel, Opt.Comm., 5, 267 (1972)
- [65] Birks J B, J.Phys.B 1, 946 (1948)
- [66] Mohamed Ali, S A Ahmed, and Kahil Mitwally, Appl.Opt.28, 3708 (1989)
- [67] J C Diels, in "*Dye laser principles with applications*", (ed.) F J Duarte and L W Hillman, Academic press (1990)
- [68] Morita N and T Yajima, Phys.Rev.A 30, 2525 (1984)
- [69] Stark H, (ed.) "*Applications of Optical Fourier transforms*", Academic press (1982)
- [70] Tagliaferri A A, J Calatrni, and C Froehly, Opt.Comm.67, 180(1988)

CHAPTER - 7

GENERAL CONCLUSIONS

Dye lasers are perhaps the most versatile and one of the most successful laser sources known today. Indeed, at the time of the discovery of this class of lasers by Sorokin and Lankard, few could have anticipated the spectacular diversification and their significant contribution to basic physics, chemistry, biology, and additional fields. For dye lasers, high pulse energies at conversion efficiencies exceeding 50% have been obtained, cw and pulsed single-longitudinal-mode operation at linewidths less than 1 kHz is possible, and ultrashort pulses (\approx fs) and high pulse repetition frequencies are achievable. The wavelength region covered by dyes so far is very broad, extending from 320 nm to 1200 nm. This unique flexibility furnishes many economic and engineering design advantages, providing numerous alternatives in the dye laser system integration. The several applications of dye lasers include industrial, medical, and military purposes, as well as in large-scale laser isotope separation, the study of fundamental physics, various types of spectroscopy techniques, laser radar and LIDAR etc. It is in this perspective that investigations of the optical properties of laser dyes become significant.

Several workers have shown that multiphoton and Excited state absorptions become strong in laser dyes at typical pump beam intensities leading to the population of higher energy levels. The study of these processes has been mostly based on the observation of antistokes fluorescence (ASF) emitted by these states, usually at a shorter wavelength than the pump wavelength. Different variations of the ASF technique have been applied before to characterize two-photon absorptions in dye solutions. However, a serious drawback of the ASF technique is its low sensitivity, arising from the fact that higher energy levels are nonradiatively coupled to the first excited singlet state in organic dyes, thereby reducing the ASF quantum yield significantly. Hence the detection of ASF and its discrimination from the strong stokes fluorescence is often problematic. Due to the low

sensitivity, in general a radiometric estimate of multiphoton processes can lead to highly erroneous results, particularly in weakly absorbing media. Further, ASF resulting from different orders of multiphoton excitation (two photon, three photon etc.) can cover a broad wavelength region necessitating the need of broadband detectors, thus making the instrumentation quite expensive. We have proposed and successfully demonstrated the application of Pulsed photoacoustic (PA) technique to the investigation of higher order absorptions in fluorescing compounds, taking the dyes DCM and cresyl violet perchlorate as typical samples. An additional advantage of this technique is that the PA signal becomes stronger when ASF is weaker, due to the complementary nature of the underlying effects. The same acoustic transducer can be used with the same sensitivity for probing de-excitations from various higher energy levels, and a change of detector and/or spectral response normalization is not required.

However, the PA technique is not without its limitations: We have ensured from experiments that the PA technique fails to observe a nonlinear absorption that leads to a transition which is strongly radiative in nature, for example, the $S_1 \rightarrow S_0$ fluorescence channel in dyes. Here ASF is quite strong, and is of course the better choice.

Our investigations of the asymmetry in the intensities between the forward and backward Stimulated Raman scattered radiations in an organic compound (acetone) have shown that the intensity ratio can be controlled by the addition of trace quantities of an absorbing species, for example, a dye. Optical pulse narrowing in stimulated Raman and Brillouin scattering, and feedback enhancement of SRS also have been investigated.

The narrow spectrum is usually considered as an intrinsic laser feature and is exploited in numerous applications. However there are situations where a broad spectral source with good spatial coherence and controllable spectral width is needed, examples of which are coherent transient spectroscopy with incoherent light, white light Fourier optical processing, all optical image transfer etc.. Some

broadband sources that have been proposed and examined in recent years utilize amplified spontaneous emission, picosecond continuum, incompletely mode-locked dye laser and transversal shifting of the frequency components in the dye. We have investigated the broadband laser action from various dye solutions, and double band lasing by energy transfer in a Rhodamine 6G + Cresyl violet perchlorate solution. Good spatial coherence, controllable spectral width and concentration tuning of the emission wavelength have been achieved in the reported configuration.

- G 530A -